UNIVERSITY OF OKLAHOMA

GRADUATE COLLEGE

# THE IMPACT OF OKLAHOMA'S WINTER WHEAT BELT ON THE MESOSCALE ENVIRONMENT

A Dissertation

SUBMITTED TO THE GRADUATE FACULTY

in partial fulfillment of the requirements for the

degree of

Doctor of Philosophy

By

**RENEE ANN MCPHERSON**

Norman, Oklahoma

2003

UMI Number: 3082929



ProQuest Information and Learning Company
300 North Zeeb Road
P.O. Box 1346
Ann Arbor, MI 48106-1346

# THE IMPACT OF OKLAHOMA'S WINTER WHEAT BELT ON THE MESOSCALE ENVIRONMENT

A Dissertation APPROVED FOR THE
SCHOOL OF METEOROLOGY

BY

# ACKNOWLEDGMENTS

Funding for this research was made possible by Grant No. NSF-0074852 of the National Science Foundation. Computer and data resources were provided by the Oklahoma Climatological Survey and the Scientific Computing Division of the National Center for Atmospheric Research.

This document is dedicated to the series of scientific mentors who most influenced my career path: Dr. Charles Pruett, Dr. Lyle Horn, Dr. Patricia Pauley, Dr. Kelvin Droegemeier, and Dr. Kenneth Crawford. Dr. Pruett (also known to my brother and I as "Dad") was a research physicist at the Physical Sciences Laboratory and Synchrotron Radiation Center at the University of Wisconsin – Madison. Although Dad did relinquish his 50-yard-line seats at Camp Randall Stadium during the bad years of Wisconsin football, he provided me vast opportunities to learn astronomy, chemistry, physics, and other sciences. His encouragement, patience, and love are appreciated more than he will ever know.

Dr. Horn and Dr. Pauley helped to focus my love of science and mathematics into a love of the atmospheric sciences. Dr. Horn and his plastic bag of Kix™ cereal were my unfailing companions during my undergraduate days in the Meteorology program at UW – Madison. His dynamics class was the first opportunity for me to understand what I could do with my mathematics background. I am a meteorologist today because of his counsel, teaching, and time. Dr. Pauley supported my proposal to spend two weeks in Oklahoma "chasing" storms as the basis of my senior honors project. She spent what must have been grueling hours editing my first, substantial research paper. Even so, she found the time and energy to keep laughing.

It is true that my writing skills were sharpened by the points of Dr. Droegemeier's and Dr. Crawford's pens; however, their greatest gifts to me were the opportunities that they provided at the University of Oklahoma. Dr. Droegemeier encouraged me to edit the original proposal for the Center for the Analysis and Prediction of Storms. From this task, I learned how proposals were written and how to obtain funding. He also supported my desire to lead the instruction of Dynamics I, which enhanced my learning experiences while working toward my Masters degree. As my boss, mentor, and friend for the past decade, Dr. Crawford taught me how to apply my scientific knowledge to serve my community. In innumerable ways, he showed me how to lead and how to follow, when to bend and when to stand ground, and what to pursue and what to release. I am honored and deeply grateful to be a recipient of his wisdom and mentorship.

Without many other supporters, this manuscript would not have been completed. When I wondered if I would ever finish, the faces of colleagues, teachers, friends, and family would appear in my mind as a source of encouragement. Thank you.

I thank the employees of the Oklahoma Climatological Survey who have invested their energies and talents in creating and maintaining the Oklahoma Mesonet and its related programs. In particular, I personally acknowledge those who rarely see the limelight (or any natural light, in some cases): Mr. Derek Arndt, Mr. Stdrovia Blackburn, Mr. Jared Bostic, Ms. Leslie Cain, Mr. Thomas Cannon, Ms. Amy Cameron, Mr. J. D. Carlson (at Oklahoma State University), Mr. David Demko, Mr. Gavin Essenberg, Mr. Christopher Fiebrich, Mr. Justin Greenfield, Mr. David Grimsley, Mr. John Humphrey, Mr. Rafal Jambreski, Ms. Shaye Johnson, Mr. Kris Kesler, Mr. James Kilby, Mr. Sridhar Kulasekharan, Ms. Cerry Leffler, Ms. Janet Martinez, Mr. Gary McManus, Mr. William McPherson, Ms. Andrea Melvin, Mr. Kenneth Meyers, Mr. Dale Morris, Mr. Gary Reimer, Mr. Putnam Reiter, Mr. Mark Shafer, Mr. Thomas Smith, Mr. Bradley Stanley, Ms. Kelly Stokes, Ms. Jessica Thomale, Ms. Sue Weygandt, Mr. Michael Wolfinbarger, Mr. William Wyatt, Mr. Qingping Xu, and Mr. Robb Young. These individuals spent years serving the leadership of the Oklahoma Mesonet and played critical roles in the success of the network. In addition, dozens of undergraduate and graduate students participated in maintaining the Mesonet and examining its data. I appreciate your dedication.

To my doctoral committee, I offer gratitude for your patience and perseverance. Dr. David Stensrud was my guide for the statistical analysis and numerical modeling effort, and he helped me win the battle between computer and human. Every time I saw him, I was reminded that I needed to finish my degree, although other interests pursued my time. I greatly value both his guidance and his friendship. Dr. Kenneth Crawford was my constant encourager, valued editor, and mentor. Dr. May Yuan, Dr. Claude Duchon, Dr. Kelvin Droegemeier, and Dr. Peter Lamb provided me valuable insight and questions that challenged my thinking.

I eagerly employed programs written by Mr. Derek Arndt, Mr. Justin Greenfield, and Mr. William McPherson to process millions of observations into output that suited my needs. I appreciate the discipline, consistency, and quality workmanship of Mr. Michael Wolfinbarger, whose software visualized data for me that it never was meant to visualize.

I lavish my greatest thanks to Billy, my husband, and to Jesus Christ, my Lord and Savior. Billy's programming skills saved my sanity on countless occasions; his questions challenged my presumptions; and his support carried me through. My joys are greater and my trials less painful because you are with me.

When the research herein is forgotten, this truth shall remain:

*"For God so loved the world that He gave His only begotten Son,*
*that everyone believing into Him should not perish,*
*but have everlasting life.*
*For God did not send His Son into the world that He might judge the world,*
*but that the world might be saved through Him."*
*– John 3:16,17*

## TABLE OF CONTENTS

## ABSTRACT

The research documented in this manuscript demonstrates that Oklahoma's winter wheat belt has a significant impact on the near-surface, mesoscale environment during growth and after harvest. Differences in near-surface atmospheric variables across the wheat belt and its adjacent lands are documented using the following methods: (1) observational analyses of monthly averaged daily statistics (e.g., daily maximum or minimum) during Crop Year 2000, (2) observational analyses of daily averages and instantaneous measurements for several case study days during Crop Year 2000, (3) statistical analyses of daily statistics from 1994 through 2001, and (4) numerical simulations of case study days during Crop Year 2000 that applied two different land uses over the wheat belt region for comparison.

Analysis results from these different methods are consistent and establish a convincing case that the crop belt modifies both the mesoscale climatology and, on many days, the daily weather of Oklahoma. Consequently, it is imperative that mesoscale forecasts, whether produced objectively or subjectively, account for the vegetation-land-air interactions that occur across western Oklahoma and, presumably, across other crop regions in the U.S. and around the globe.

# CHAPTER 1: INTRODUCTION

The earth's surface, the water that pauses upon or drains over it, and the vegetation that grows from and above it are joined irrevocably to the overlying atmospheric boundary layer through fluxes of energy, momentum, moisture, and gases. The interwoven nature of this demarcation between solid or liquid and the gaseous air above is a topic of heightened interest in the meteorological community (e.g., National Research Council 1998). In particular, the impact of vegetation on the atmosphere — from germination to maturity to senescence[1] to death or dormancy — has been studied across a spectrum of temporal and spatial scales (e.g., Bonan 2001; Freedman 2001; Cihlar et al. 1992; Rabin et al. 1990). The understanding of these vegetation-air interactions is critical to the maturation of atmospheric numerical models (e.g., Emanuel et al. 1995; Pleim and Xiu 1995; Betts et al. 1998; Schultz et al. 1998; Chen and Dudhia 2001a, 2001b; Lu et al. 2001; Nagai 2002).

The quantity, type, and condition of vegetation strongly influence the fluxes of energy, momentum, and moisture in the atmospheric boundary layer (Taylor and Lebel 1998). Vegetation affects the surface albedo and, hence, the amount of net radiation entering the surface energy budget. The partitioning of this incoming energy into latent and sensible heat fluxes is determined, in part, by the amount of evapotranspiration from plants (Mahfouf et al. 1987; Collins and Avissar 1994). These fluxes, in turn, influences the temperature and moisture profiles in the lower atmosphere. In addition, evapotranspiration and photosynthesis affect the exchange of water vapor and carbon dioxide near the land surface (Cihlar et al. 1992).

[1] Senescence is the period from full maturity of the plant until its death.

At the mesoscale, the differences in surface fluxes over vegetation and over dry, bare soil can result in differential heating that generates a sea breeze-like circulation, or a "vegetation breeze" (Mahfouf et al. 1987; Segal et al. 1988). Observations indicate that vegetation breezes and other "inland breeze" circulations can have an appreciable effect on the formation of shallow cumulus clouds (Garrett 1982; Cutrim et al. 1995). Numerical simulations denote that these circulations can provide preferred regions for focusing atmospheric instabilities and initiating convective development (Sun and Ogura 1979; Garrett 1982; Mahfouf et al. 1987; Chang and Wetzel 1991; Chen and Avissar 1994).

Vegetation influences the diurnal range of temperatures, depth of the convective boundary layer, and amount of cloud cover for a region (Segal et al. 1989; Rabin et al. 1990; Bonan 2001; Durre and Wallace 2001; Freedman et al. 2001). Although feedbacks between vegetation and rainfall are not well established, evidence exists that vegetation may enhance or mitigate extreme climatological conditions such as droughts (Dirmeyer 1994; Sud et al. 2001).

These studies and others highlight that mesoscale areas of vegetation can alter the mesoscale environment. Nevertheless, many previous studies are limited in their real-world applicability. Past observational studies have focused on specific events or case studies (e.g., Segal et al. 1989), relatively short time periods (e.g., LeMone et al. 2000), or small regions (e.g., Smith et al. 1994). Past numerical studies have modeled highly idealized environments (e.g., Mahfouf et al. 1987) or have lacked an extended set of regional observations for model initialization and verification (e.g., Hong et al. 1995). The authors have acknowledged these restrictions and have attributed them to a dearth of long-term, mesoscale observations across a large area. This study helps to fill this void in adequate measurements by using surface data from the Oklahoma Mesonet in both observational and numerical experiments. Consequently, this research further delineates the magnitude and scale (in both space and time) whereby a crop belt can alter the near-surface environment.

Winter wheat, which accounts for about three-fourths of U.S. wheat production, is sown in the fall and harvested in the late spring or early summer. During early spring, a mature wheat crop forms a swath about 150 km wide that extends from southwest Oklahoma into north-central Oklahoma and southern Kansas (Rabin et al. 1990; Markowski and Stensrud 1998). The density of the wheat fields increases from the Oklahoma-Texas border, where summer crops or grasslands are interspersed with wheat crops, to the Oklahoma-Kansas border, where about 90% of the land is used for growing wheat. On either side of this band of non-irrigated cropland is sparse or dormant vegetation, especially across extreme western Oklahoma and the Panhandle. During the late spring or early summer, after growers harvest the wheat, previously dormant grassland grows. The result is a band of short stubble and bare soil surrounded by mature prairie grasses. Hence, Oklahoma's wheat belt affords scientists the unique opportunity to study the impact of a band of either abundant or sparse vegetation when compared to adjacent lands. Just as important, the width of this band is consistent with the preferred scale for mesoscale vegetation breeze circulations – the local Rossby radius of deformation (Anthes 1984; Pielke et al. 1991; Avissar and Chen 1993; Lynn et al. 1995; Chen and Avissar 1994). Thus, Oklahoma is an optimal real-world environment for examination of mesoscale vegetative impacts on the atmosphere.

The following hypotheses are investigated in this study:

1. *Monthly averaged, daily averaged, and instantaneous surface temperature and moisture fields are affected by the evolution (e.g., during growth and after harvest) of Oklahoma's winter wheat crop.*

2. *The impact of Oklahoma's winter wheat belt on monthly climatic patterns is statistically significant.*

3. *Surface fluxes from Oklahoma's winter wheat belt modify the depth of the planetary boundary layer.*

Results from validating these hypotheses will extend the current state of knowledge in the atmospheric sciences by providing evidence of the extent to which a large (25,000 $km^2$), mesoscale crop belt can influence the mesoscale environment. Because the Oklahoma Mesonet provides a statewide, mesoscale, multiyear data set, the documentation of the impact from the winter wheat belt on mesoscale climate and weather using these data will distinguish this study from past research.

To provide a background for this research, Chapter 2 overviews pertinent literature that describes the primary interactions between vegetation and the atmosphere, details several of these interactions, and discusses the impact of vegetation on the mesoscale atmosphere. Chapter 3 describes the data used in this study, including Oklahoma Mesonet observations, measurements from the Atmospheric Radiation Measurement (ARM) Program, land cover information, spectral vegetation index products, and county wheat production statistics for Oklahoma. Chapter 4 reviews the numerical model that was employed and lists selected parameters for operation. Chapter 5 overviews the development of winter wheat in Oklahoma and presents the results of the observational study, including monthly, daily, and instantaneous anomalies in measured fields. Chapter 6 outlines the design of the numerical experiments and provides results from six simulations. Conclusions are reviewed and discussed in Chapter 7.

# CHAPTER 2: OVERVIEW OF SELECTED PERTINENT STUDIES

## 2.1 Overview of Vegetation-Atmosphere Interactions

Interactions among the lithosphere, biosphere, and atmosphere are abundant and complex. Consequently, an exhaustive review of these interactions is not practical. The principal contributors to the near-surface exchange of energy and moisture, however, are well documented and salient to this study. One conventional method to describe these fluxes is to identify components of the Simple Biosphere (SiB) model (Sellers et al. 1986). In Fig. 2.1, a schematic of boundary layer processes is drawn as a circuit diagram. With respect to Ohm's Law (V=IR), sensible and latent heat fluxes are analogous to the current, I; air temperature or vapor pressure differences are analogous to the electric potential difference, V. Hence, fluxes in "parallel" are additive and fluxes in "series" are equal. Only changes in potential, not its specific value, are important. In addition, as any "resistance" to energy or moisture transfer increases (e.g., the soil dries or plant stomata close), the corresponding flux decreases.

According to the physics of SiB (Fig. 2.1), the exchange of water from the land to the atmospheric boundary layer is accomplished via three pathways. The first pathway transfers water through the soil to ground cover above (represented by the resistance $r_{soil_g}$), through the ground cover (i.e., roots, stems, and leaves) to the air-plant interface ($r_{plant_g}$), from that interface to the air above ($r_g$), through the air inside the canopy to the top of the canopy ($r_d$), and from the canopy top through the atmospheric surface layer ($r_a$). The second pathway transfers water directly from bare soil to the air above ($r_{surf}$), through the air inside the canopy to the top of the canopy ($r_d$), and from the canopy top through the atmospheric surface layer ($r_a$). The third pathway transfers water through the soil to the roots of the canopy plants ($r_{soil_c}$), through the canopy plants ($r_c$), from these plants to the air at the top of the canopy ($r_b$), and from the canopy top through the atmospheric surface layer ($r_a$).

The exchange of thermal energy from the land to the boundary layer is accomplished by two pathways: (1) the transfer from ground cover or bare soil through the canopy ($r_d$), and from the canopy through the atmospheric surface layer ($r_a$); and (2) the transfer from canopy plants to the air at the top of the canopy ($r_b$), and from the top of the canopy through the atmospheric surface layer ($r_a$).

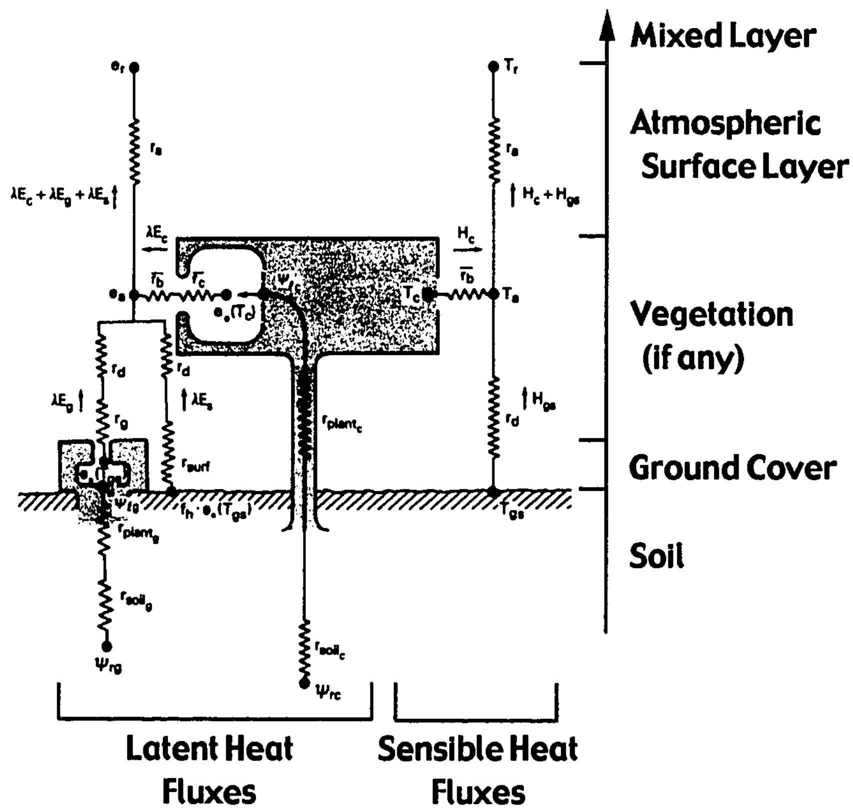


FIGURE 2.1. Framework of the Simple Biosphere (SiB) model from Sellers et al. (1986). The transfer pathways for latent and sensible heat fluxes are shown on the left and right sides of the diagram, respectively.

In addition to the vegetative impact on latent and sensible heat fluxes noted in SiB, plants intercept water during rainfall and provide a surface on which dew or frost may form. Vegetation also may drip water to the ground and evaporate water directly to the atmosphere, and it regulates net incoming radiation via albedo differences, absorption of short- and long-wave radiation, and emission of long-wave radiation (Lakhtakia and Warner 1994; Segal et al. 1988). As a result, the quantity, type, and condition of vegetation strongly influence the surface energy balance and, in particular, the fluxes of energy, momentum, and moisture in the atmospheric boundary layer (Taylor and Lebel 1998).

Past studies indicate that an *increase* in living vegetation coverage[2] across an area *increases* the following physical variables: albedo for near-infrared wavelengths, absorption of solar radiation, roughness length, turbulence, evapotranspiration, relative and specific humidities, equivalent potential temperature, moisture retention, and minimum temperatures (Anthes 1984). In addition, an increase in coverage *decreases* the following variables: albedo for visible wavelengths, infrared emission, surface winds, runoff and erosion, Bowen ratio, and maximum temperatures (Anthes 1984). There also is evidence that an increase in vegetation may increase clouds, rainfall, and upward motion (Schickedanz 1976; Freedman et al. 2001).

Senescent, irrigated, grazed, and dead vegetation may reinforce, negate, or have no impact on the physical properties and processes mentioned above (Otterman 1981; Turner et al. 1992; Walthall and Middleton 1992; Otterman 1976; Schwartz 1992). Indeed, even the *type* of vegetation causes different impacts, including the generation of different transpiration rates (Segal et al. 1988; Doran et al. 1992; Carleton et al. 1994; Bonan 2001).

[2] Vegetation coverage is the percentage of a given area covered by vegetation.

## 2.2 Mechanisms of Vegetation-Atmosphere Interactions

A better understanding of the physical mechanisms of these vegetation-atmosphere interactions will help in the analysis of the observational and numerical simulation results from the current study. The primary physical attributes of plants that cause interactions with the atmosphere are (1) the vegetation's response to incoming radiation and its emission of longwave radiation, (2) the vegetation's physical presence, which relates to its roughness length, (3) the plant's transpiration, which regulates the latent heat flux portion of the surface energy budget, and (4) the plant's photosynthesis, which generates $CO_2$. $CO_2$ flux is not germane to this study; hence, further discussions will exclude this flux.

### *2.2.1 Radiative Effects*

Through the plant's albedo, vegetation coverage modifies net incoming solar radiation – the source for surface energy exchanges. The partitioning of incident radiant energy into reflected, scattered, transmitted, or absorbed radiation depends on leaf, plant, and substrate characteristics, including variations in vegetation type, structure, coverage, and condition (Matthews and Rossow 1987). A host of field experiments has been conducted to better understand the interactions between radiation and plants.

Using three native grasses from the study region of the First International Satellite Land Surface Climatology Project (ISLSCP) Field Experiment (FIFE), Walter-Shea et al. (1992) determined that healthy green grass reflected and transmitted weakly in the visible and strongly in the near-infrared. These results were attributed to physical properties of the plant. Pigments in a healthy green leaf absorbed strongly in the visible. Conversely, the leaf mesophyll scattered most of the incident near-infrared radiation (NIR). In addition, optical properties of leaves caused attenuation in the middle infrared band when the water content of leaves increased. Mild water stress decreased the turgor pressure in the cell and created a decrease in the cell volume and intercellular space.

In an analysis of surface reflectances from visible wavelengths, Matthews and Rossow (1987) resolved that the primary factor controlling surface reflectance at 0.6 μm was the density of vegetation cover. Because vegetation appeared darker at this wavelength than most soils, a stratification of reflectance values was evident from dense forest to steppe or from grassland to desert. The spectral variation within forests, either locally or between ecosystems, was less than that within shrubs or grasslands.

Matthews and Rossow (1987) also ascertained that snow cover amplified the stratification of reflectance values over vegetation. This conclusion was supported by Betts and Ball (1997), who examined the annual cycle of albedo over grassland, aspen forest, and coniferous forest using data from the Boreal Ecosystem-Atmosphere Study (BOREAS) in Saskatchewan and Manitoba, Canada. During the summer, without snow cover, daily average albedos were approximately 0.2 over grass, 0.15 over aspen forest, and 0.083 over coniferous forest. During the winter, with snow on the ground or in the canopy, analogous values were 0.75 for grasses, 0.21 for aspens, and 0.13 for conifers.

Ba et al. (2001) documented differences in the albedo - vegetation relationship between wet and dry regions. Monthly albedos calculated from Meteosat satellite data over Africa during 1983-1988 were compared to values of the normalized difference vegetation index (NDVI[3]). Over wetter regions, there was a relatively small range of albedos (from 0.10 to 0.20) yet a large range of NDVI

[3] NDVI = (*NIR* – *red* ) / (*NIR* + *red* ), where *NIR* is the amount of energy measured in the near-infrared spectral band and *red* is the amount of energy measured in the red portion of the spectrum.

values (0.1 to 0.5) and an evident seasonal cycle of albedo. Over drier regions, there was a larger range of albedos (from 0.10 to 0.35), a similar range of NDVI values (0.1 to 0.5), but little evidence of a seasonal cycle of albedo. The authors hypothesized that vegetation in wet regions adequately concealed the soil; hence, seasonal changes in foliage (and the corresponding changes in NDVI values) did not impact albedo considerably. In dry regions, however, where vegetation was sparse and bare soil was exposed, the soil moisture influenced the albedo significantly.

Changes in the radiative effects of vegetation occur as plants mature during their growing season. Turner et al. (1992) discovered that, across all wavelength bands except NIR, reflectance values from tallgrass canopies increased as the plants matured and senescent material increased. Walthall and Middleton (1992) documented that after senescence commenced, leaf pigments began to absorb more strongly in the blue region than in the red region of the visible spectrum. The sensitivity of the red and blue spectral bands appeared to be related to alterations in vegetative pigment concentrations. As the plant matured, chlorophylls dominated; by senescence, carotenoids dominated.

Moore et al. (1996) examined the growing season cycle of albedo in a deciduous forest canopy at the Environmental Monitoring Site in Harvard Forest. They detected forest canopy leaf-out and leaf-drop from an increase and decrease, respectively, of the global albedo. After the albedo initially increased at leaf-out, an 11% decrease in global albedo was recorded during the growing season; the albedo decrease principally resulted from a significant decrease of near-infrared reflectance. The decreasing values of NIR reflectance were attributed to phenological changes in the canopy, including water stress, a change in thickness of the mesophyll layer, or a change in the canopy structure (e.g., leaf-area density or leaf-angle distribution).

Otterman (1981) demonstrated the effect of both living and dead vegetation on radiation absorption. Albedos computed using Landsat images of naturally vegetated land in the Sinai-Negev, Afghanistan-USSR, and the Sahel were compared to those from nearby anthropogenically modified regions. The data indicated that the albedo over the protected land was significantly lower (by almost 0.2) than that over the modified land. Consequently, native plants increased their absorption of solar radiation. Moreover, absorption was higher in both the visible and infrared even though the living vegetation had a high albedo in the infrared. This result led Otterman (1981) to conclude that, because of its low albedo in the infrared, dead plant matter (underlying the living vegetation) in the protected area increased the total energy absorption of the region. Similarly, Otterman (1976) determined that the significant emission of infrared radiation by forest debris resulted in warmer surface temperatures over densely vegetated areas as compared to nearby sparsely vegetated regions.

Field management practices that modify the density of vegetation also have been shown to change the reflective characteristics of the surface, thus affecting the surface energy budget. During FIFE in 1987, Turner et al. (1992) studied reflectance values over grassland at the Konza Prairie Research Natural Area. Radiation measurements were compared among sites characterized by these grassland field management practices: mowed, grazed, burned and grazed, burned and ungrazed, and natural (unmanaged). During the growing season, shortwave reflectance averaged about 8% higher on grazed sites than on burned, ungrazed sites; it ranged from 4% to 27% higher on mowed sites than on unmowed control plots. Near-infrared reflectance averaged about 15% lower on grazed sites than on burned plots and 18% lower on mowed sites than on unmowed plots. Because of the soil's higher albedo in the visible and lower albedo in the near-infrared, defoliation severe enough to expose the soil tended to increase reflectance of visible light and decrease reflectance of NIR.

### 2.2.2 *Roughness Length*

As objects extend farther above the surface, the roughness length[4] increases. The structure of most plants extends above the ground from a few centimeters for short ground covers to tens of meters for tall trees. The heightened roughness length associated with vegetation (contrasted with bare soil) weakens near-surface wind speeds and intensifies low-level turbulence (Anthes 1984; Lee 1992). On the small scale, this enhanced low-level turbulence may accelerate the initiation of convection (Garrett 1982); on the synoptic scale, frictional inflow into extratropical cyclones may increase, possibly resulting in enhanced precipitation.

Doran et al. (1995) attributed differences in the roughness length to causing weaker 9-m winds over cropland than over steppe. During a field experiment in Washington early in June 1992, these researchers observed winds over the farm (roughness length ~0.1 m) to be weaker than winds over the steppe (roughness length ~0.02 m) on all days. Similarly, Rosenan (1963) observed an increase in autumn precipitation near Tel Aviv, Israel following irrigation of nearby land. Rosenan hypothesized that the taller, irrigated vegetation had increased the surface roughness length and associated turbulent mixing, resulting in more convection.

Bechtold et al. (1991) used a two-dimensional version of the meso-β model of Nickerson et al. (1986) to examine, in part, the impact of vegetation on turbulent mixing. In a simulation that compared the turbulent activity over adjacent areas of bare land and ocean, significant turbulence developed over land but little or none occurred over the water. To determine if the lack of turbulence over water simply resulted from stability associated with the cool water surface, the authors also ran a simulation with contiguous areas of transpiring crop and forest.

[4] Roughness length is a measure of the roughness of the surface based on the logarithmic wind profile.

Results indicated that turbulent mixing occurred over both the cropland and the forest, with vertical mixing predominant over the forest. The authors attributed the presence of turbulence over both foliages to the roughness lengths of the vegetation.

*2.2.3 Latent and Sensible Heat Fluxes*

Transpiration, regulated by the aperture of plant stomata, governs the partitioning of radiant energy absorbed by vegetation. When vegetation is unstressed, stomata open and the plant transpires freely. Large latent heat fluxes can result from abundant insolation. When vegetation is stressed, the stomata close and transpiration stops. As a result, abundant insolation is converted mostly to sensible heat flux (Chen and Avissar 1994; Avissar and Pielke 1989). Hence, the Bowen ratio[5] is a good indicator of both environmental stress at the surface and the condition of the vegetation. Bowen ratio values range from infinity in extremely dry conditions to near zero over wet regions. Negative values can occur over strongly transpiring vegetation for certain atmospheric conditions (Avissar and Pielke 1989).

Observations from warm season crops indicate that more than 70% of the net radiation can be converted to latent heat flux, leaving less than 30% available for sensible heat flux (Segal et al. 1988). For example, Aase and Siddoway (1982) measured evapotranspiration over wheat in a semiarid region near Sidney, MT during two growing seasons: (1) 4 April to 16 August 1978 and (2) 5 May to 17 August 1979. The average evapotranspiration rate was 4.7 mm day$^{-1}$ and 5.5 mm day$^{-1}$ for the 1978 and 1979 warm seasons, respectively. Given approximated values of net radiation for this location and dates, Segal et al. (1988) determined that, if the net radiation were converted entirely into evaporation, these rates would have been 6.0 and 6.2 mm day$^{-1}$, respectively.

[5] The Bowen ratio is the ratio of sensible heat flux to latent heat flux at the surface.

Hence, between 78% and 89% of the available energy was partitioned into latent heat flux by the wheat.

From 20 June to 17 August 1979, Aase and Siddoway (1982) measured evapotranspiration over both wheat and nearby bare soil and discovered rates of 4.5 and 0.9 mm day$^{-1}$, respectively. In other studies (Reddy 1983; Rogerson 1976), an examination of observations likewise indicated that the typical evapotranspiration rate over wheat was at least 2 mm day$^{-1}$ higher than that over bare soil. In contrast, the evapotranspiration from forest canopies was found to be 1–2 mm day$^{-1}$ *less* than that over well-irrigated crops (Segal et al. 1988). Values of latent heat flux also were lower for nonirrigated crops than for irrigated crops.

Doran et al. (1992) documented results from a regional flux field campaign near Boardman, OR during early June 1991. Using both surface and aircraft measurements, sensible and latent heat fluxes were compared between steppe, shrub, grass, and irrigated crops of wheat, alfalfa, corn, and potatoes during a span when almost no rainfall occurred. The average daily maxima of latent heat flux for the shrub and grass sites ranged between 45 and 80 W m$^{-2}$, those over the steppe were around 50 W m$^{-2}$, and those over irrigated cropland were between 350 and 425 W m$^{-2}$. Flying between 12 and 14 m above ground level over the steppe and irrigated cropland on 15 June, aircraft measured minimal fluctuations in mixing ratios over the steppe but significant fluctuations in mixing ratios over the farm. Mixing ratios were 0.4 g kg$^{-1}$ higher over the farm than over the steppe. On the same day, air temperatures and temperature fluctuations were larger over the steppe than over the farmland, indicating that sensible heat flux was enhanced over the steppe relative to the crops.

Results from similar experiments the following year were reported in Doran et al. (1995). On a mid-June day, when winds ranged from 3 to 7 m $s^{-1}$, surface fluxes of sensible heat over the steppe peaked at 300 W $m^{-2}$ or more while those over the farm were 80 W $m^{-2}$ or less. Latent heat fluxes over the steppe averaged less than 100 W $m^{-2}$ whereas those over the farm ranged from 400 to 500 W $m^{-2}$. On another day, when winds ranged from 4 to 11 m $s^{-1}$, latent heat fluxes over the crops reached values greater than 700 W $m^{-2}$. During windy days, latent heat fluxes over both land use types increased while sensible heat fluxes slightly increased over the steppe and decreased over the farm.

Eaton et al. (2001) studied the summer-season energy balance for 10 sites across the western and central Canadian subarctic. Sites were characterized as one of the following terrain types: lake, wetland, shrub tundra, upland tundra, or coniferous forest. Results demonstrated that, except for the two lake sites, sites belonging to the same terrain type partitioned surface energy in similar manners. [The two lakes in the study had vastly different depths and thermal masses; hence, each lake distributed energy differently.] The lake and wetland sites averaged Bowen ratios less than 0.5 as a result of the high availability of moisture and low resistance to evaporation. The shrub tundra sites, with adequate moisture availability but higher stomatal resistance, had Bowen ratios near 0.55. With less soil moisture available and a higher vegetative resistance, the upland tundra averaged about 0.8 for the Bowen ratio. Finally, Bowen ratios from coniferous forest ranged from 0.04 to 0.10 over the well-drained soil. The forest sites primarily contained spruce, which has a closed canopy that suppresses evaporation from the understory.

The development of the plant itself influences latent heat fluxes. Moore et al. (1996) measured the Bowen ratio over a deciduous forest canopy during a growth cycle. After leaves first emerged, transpiration slowly increased. As leaves matured fully, transpiration increased substantially until midsummer, when it reached a plateau (also Fitzjarrald et al. 2001; Yi et al. 2001). During August, however, transpiration began to decline, as woody tissue[6] became more prevalent. Measurements of latent heat flux above the canopy and in the subcanopy (understory) mirrored these changes. During winter, the subcanopy accounted for almost all of the above-canopy water vapor flux. By midsummer, the subcanopy evapotranspiration accounted for only about 10% of the above-canopy flux of water vapor. The sensible heat flux in the subcanopy was maximized during the spring and fall, when the canopy was leafless and insolation was greater compared to winter.

Vegetation density alters the distribution of surface heat fluxes across a region. Smith et al. (1994) examined surface fluxes across tallgrass prairie using data from the fifth FIFE intensive field campaign (23 July – 12 August 1989). During the period studied, a northwest-to-southeast foliage gradient was observed across the Konza Prairie, with greener and more dense vegetation located in the southeast (SE) quadrant. Rainfall received within the SE quadrant was twice that measured within the other three quadrants, thus enhancing the vegetation gradient throughout the study period. Although net radiation was nearly constant across all quadrants, the SE quadrant was characterized by higher latent heat fluxes and lower sensible heat fluxes during the day than the other quadrants. Values of latent flux in the SE quadrant were more than twice those for the northwest quadrant.

As discussed earlier, net radiation measured above the canopy differs among plant types; hence, the amount of energy available for transpiration and the magnitude of transpiration differ among plant types. Using preliminary data

[6] Woody tissue, or xylem, is the supporting and water-conducting tissue of vascular plants.

from field experiments on 10 May 1997 and 20 May 1997 obtained via the Cooperative Atmosphere Surface Exchange Study (CASES; hereafter referred to as CASES-97), LeMone et al. (2000) documented relationships between surface fluxes and vegetation type on days with weak surface winds (5–6 m $s^{-1}$ from the south-southwest on 10 May, and 6–7 m $s^{-1}$ from the east to east-northeast on 20 May). Soil moisture values were greater and more uniform on 20 May than on 10 May because of a recent, widespread rainfall event. Three types of surface coverage were compared: growing winter wheat, short grass prairie, and bare soil. Data from CASES-97 indicated that, as a result of evapotranspiration, the latent heat flux (LE) was greater than the sensible heat flux (H) on both days over the growing winter wheat. In contrast, LE $\approx$ H over the grassland and LE < H over the bare soil on 10 May. On 20 May, however, LE > H above all three coverage regimes and, significantly, LE was fairly uniform across the coverages. The authors hypothesized that this uniformity resulted from three separate effects: (1) substantial evaporation from wet soil at the bare soil site, (2) enhanced evapotranspiration from greener grassland, and (3) reduced evapotranspiration from wheat reaching maturity and becoming senescent.

Analyses of CASES-97 data disclosed other contrasts between variables measured across different vegetative regimes (LeMone et al. 2000). Throughout the day on both 10 and 20 May, values of soil heat flux were largest at the bare ground site and smallest at the grassland site. Sensible heat fluxes were lower and more uniform on 20 May, the day with wetter surfaces. On 10 May, the drier day, larger values of sensible heat flux were associated with lower values of NDVI (i.e., less green vegetation) and with a decreased downward $CO_2$ flux (i.e., less photosynthesis). In addition, infrared radiometric surface temperatures were cooler, warmed more slowly, and heated more uniformly on 20 May than on 10 May. Temperatures at 2 m, however, warmed more rapidly on 20 May than on 10 May, presumably because the boundary layer was shallower on 20 May. Thus, the heating was constrained within a shallower layer. On 10 May, the daytime mixing ratio (between 1000 and 1800 CST) was 1.5 g $kg^{-1}$ larger over winter wheat than over either grassland or bare soil.

Yates et al. (2001) used data from the full CASES-97 field experiment – ranging from 21 April to 22 May 1997 – to determine additional information about fluxes over varying land covers. First, the authors noted that cloud cover increased the variability of latent heat flux more at sites with growing winter wheat than at sites with grassland or pasture. In contrast, cloud cover did little to change the variability of sensible heat flux over either vegetation type. Second, on clear days, mean latent heat fluxes, based on 6-h averages centered at solar noon, were about 300 W $m^{-2}$ over winter wheat, 210 W $m^{-2}$ over grassland/pasture, and about 180 W $m^{-2}$ over bare soil/sparse vegetation. Using these same days, the mean sensible heat flux averaged 250 W $m^{-2}$, 180 W $m^{-2}$, and 160 W $m^{-2}$ over wheat, grassland, and sparse vegetation, respectively. Third, data from clear days also established that latent heat fluxes increased over the grassland throughout the course of the field experiment, as grass green-up occurred and the vegetation gradually became more photosynthetically active.

Clark and Arritt (1995) used the one-dimensional primitive equation model by Heim (1993) and Segal et al. (1995) to examine the effects of vegetation and soil moisture on the development of deep convection. The authors conducted 54 independent simulations out to 12 hours. The parameter space spanned from 0.075 to 0.450 for volumetric soil moisture content and from 0 to 100% for vegetation coverage. Using a representative midsummer sounding from Topeka, KS, Clark and Arritt (1995) ascertained that sensible heat flux decreased with increasing foliage for relatively dry soils and was relatively constant or slightly increased with increasing foliage for saturated soils. In particular, at solar noon, the sensible heat flux was 430 W $m^{-2}$ over dry, bare soil but was only about 100 W $m^{-2}$ over saturated bare soil. Above the fully vegetated surface, values of sensible heat flux ranged from 270 W $m^{-2}$ for dry soil to 130 W $m^{-2}$ for saturated soil. In these same experiments, at solar noon, the latent heat flux was 90 W $m^{-2}$ over dry, bare soil and 450 W $m^{-2}$ over saturated, bare ground. Over the fully vegetated surface, values of latent heat flux ranged from 450 W $m^{-2}$ for dry soil to ~600 W $m^{-2}$ for saturated soil. Hence, vegetation moderated the impact of variations in soil moisture.

## 2.3 The Mesoscale Impact of Vegetation

For the current study of the atmospheric impact of winter wheat, local influences of vegetation on the atmosphere are not pertinent unless they extend their impact to the meso-β scale[7]. Vegetation must be of sufficient density and extent to alter significantly the partitioning of net radiation across a region. As a result, the atmospheric boundary layer and the free atmosphere above can be changed in a measurable way, including the diurnal temperature range, cloud cover, rainfall, heating patterns, or circulations.

### *2.3.1 Impact on the Diurnal Temperature Range*

Using daily maximum and minimum temperature data from the U.S. Historical Climatology Network (Easterling et al. 1996), Bonan (2001) created a monthly climatology of diurnal temperature range across the Midwest and Northeast United States for the period 1986-1995. Land cover across the Midwest was characterized by cropland; that of the Northeast was characterized by deciduous forests. Linear correlations between monthly diurnal temperature range and longitude denoted that the former *increased* with eastward longitude during May, June, and July. No correlation between diurnal temperature range and longitude existed during August.

[7] Meso-β scale, as defined by Orlanski (1975), encompasses a spatial extent of 20 - 200 km.

These results were contrary to those expected from a documented eastward increase in cloud cover during those four months (Dai et al. 1999). If cloud cover were the predominant cause of a longitudinal change in temperature, then the longitudinal decrease of the maximum temperature should exceed that of the minimum temperature. Bonan (2001), however, observed the opposite: the minimum temperature cooled at a greater rate toward the east than did the maximum temperature. These results were consistent with a moderation of maximum temperatures by the Midwestern cropland as compared with the forested Northeast.

Similarly, observations of moderated maximum temperatures were measured at an Oklahoma Mesonet site in southwestern Oklahoma (Fiebrich and Crawford 2001). Growing, irrigated cotton surrounds the Altus Mesonet site during the summer months. Measurements during August 1998 indicated that during clear days when average winds exceeded 5 m $s^{-1}$, the maximum temperature at Altus could be 4°C cooler than those measured in adjacent counties. The authors attributed the cool anomaly to increased evapotranspiration from the cotton crops.

Durre and Wallace (2001) applied daily climatologies from the National Climatic Data Center (1999) to examine the diurnal temperature range for the eastern United States. As a result of an increase in both the length of the day and the daily net incoming solar radiation, the authors expected that the largest diurnal range of temperatures would occur around the summer solstice. Instead, they documented a seasonal minimum in the diurnal temperature range during the summer growing season. This summer minimum was more prominent when only clear days were considered, leading the authors to exclude seasonal changes in cloud coverage as the causal ingredient. In addition, the amplitude and seasonal length of the minimum were greater for southern latitudes than for northern latitudes. These observations were congruent with a lengthening of the growing season from north to south. Finally, a comparison of diurnal temperature range with weekly NDVI demonstrated that the maximum in the former occurred only one to two weeks after the onset of a rapid increase in weekly NDVI values. As vegetation rapidly matured, the diurnal temperature range decreased.

### *2.3.2 Impact on the Boundary Layer*

In numerical studies, the depth of the planetary boundary layer (PBL) was shallowest over an irrigated area of vegetation and deepest over dry, bare land (Segal et al. 1989). Hence, the mixing ratio throughout the PBL was largest over vegetated surfaces, where evapotranspiration was enhanced, dry air entrainment was reduced, and air was mixed within a shallower layer (Segal et al. 1995). As a result, given a vertical profile of temperature and moisture that already was favorable for thunderstorms, growing vegetation could greatly enhance the development of convective clouds. An initially stable environment would reduce turbulence and thus support a gradual increase in moist static energy over vegetation. Although convection might initiate later, clouds could persist longer within this initially stable environment than within initially neutral or unstable environments (Hong et al. 1995).

Because upwind conditions may influence measurements at a given location, the PBL over vegetation must be examined relative to its nearby environment. For example, on days when winds blew perpendicular to a land use boundary between steppe and farmland, Doran et al. (1995) noted that growth of the mixed layer over the farm was modified considerably by the surface flux of sensible heat over the steppe. Conceptually, the authors determined that the air was heated over the steppe and advected over the farm, where it became part of the boundary layer structure. As a result, the mixed layer depth was comparable between steppe and farm. Because strong surface heating ceased when the air moved over the irrigated crops, temperatures of the mixed layer generally were about 1°C cooler over the farm than over the steppe. A simple thermodynamic model confirmed that the advection of the mixed layer from above the steppe to over the farmland could account for the PBL observations over the farm.

### 2.3.3 *Impact on Clouds*

Observational evidence suggests that, during fair weather, vegetation modifies the development of cumulus clouds. Cutrim et al. (1995) examined the impact of deforestation on cumulus cloud fields across parts of Amazonia during the end of the dry season (July through October). Using visible satellite images at 1800 UTC, the authors detected imprints of land-surface features, including rivers, a natural savanna, and a deforested region. The latter two features were indicated by denser fields of cumulus. Similarly, Carleton et al. (1994) documented an increase in convective clouds over forested areas as compared to cropland.

Rabin et al. (1990) observed that clouds first initiated over a region of harvested wheat that was adjacent to growing vegetation; clouds were suppressed over forested areas. The authors conducted their observational study during late June 1988 – after the wheat harvest reduced vegetation across the Oklahoma wheat belt to stubble. This harvested area displayed albedos 10–20% higher than the adjacent grassland or forest, and the absence of growing vegetation reduced the transport of soil moisture from root level into the atmosphere. As a result, the incoming solar energy was partitioned primarily into sensible heat flux, creating a region of locally warmer temperatures over the wheat belt during the daytime. In a dry environment, this surface heating (and its mixture through the PBL) caused the convective temperature to be attained about two hours earlier over the wheat stubble than over adjacent vegetated areas. Clouds were noticeably absent, on the other hand, at midday over areas with dense vegetation, such as forested regions to the east and southeast of Oklahoma City. Across those densely vegetated areas, as much as 70% of the insolation was partitioned into latent heat flux; thus, less energy remained for sensible heating and PBL warming.

The observational results of Rabin et al. (1990) were consistent with those modeled by Rabin (1977). Using a surface energy-budget model, Rabin (1977) documented that, when the lower atmosphere was relatively dry, less energy was required to form clouds over regions with high Bowen ratios; hence, convection first initiated over drier, hotter surfaces. When the lower atmosphere was relatively moist, less energy was required to form clouds over regions with low Bowen ratios; hence, convection first initiated downwind of moist surfaces. The conditions necessary to obtain these results were minimal topography, calm winds, landscape features of sufficient size to modify an air mass, and about $200 \times 10^4$ J m$^{-2}$ of combined sensible and latent heat fluxes for use in modifying the air mass.

Freedman et al. (2001) used National Weather Service observations from the eastern U.S., a boundary-layer cloud analysis, and a variety of atmospheric turbulence and trace gas measurements in Harvard Forest (in north-central Massachusetts) to study the impact of boundary layer cumulus on vegetation-atmosphere feedbacks. The region studied was predominantly temperate deciduous, broadleafed evergreen, and boreal forests. Results indicated that, across the eastern United States, the occurrence of boundary layer cumulus (BLcu) increased rapidly with the development of transpiring vegetation. As BLcu developed during the growing season, observations that the afternoon lifted condensation level (LCL), relative humidity, and mixed-layer height remained relatively constant from late spring through summer implied that a coupling of the vegetation and atmosphere occurred. In addition, after BLcu appeared, a measured increase of $CO_2$ uptake (indicating increased photosynthesis) occurred along with lower values of evapotranspiration, maximum temperature, and vapor pressure deficit as compared to clear days. In other words, BLcu tended to ameliorate the abundant summer insolation and high surface temperatures, allowing plants to recover from the environmental stress.

Jarvis et al. (1985) determined that BLcu and forest developed a positive feedback. As clouds initially shaded direct sunlight from vegetation, diffuse radiation increased. Because diffuse radiation penetrated deeper into the forest canopy, enhanced photosynthesis and transpiration efficiency resulted. As evapotranspiration within the forest increased the low-level moisture, the vapor-pressure deficit diminished and facilitated the continued formation of BLcu. In turn, BLcu further reduced environmental stresses and thus promoted stomata to remain open, enhancing evapotranspiration. The authors suggested that the increased extent and density of eastern forests across the U.S. during the past century contributed to the documented increase in relative humidities and cloudiness across this region during that period.

Environmental stress can be imposed not only by the atmosphere, but also by the soil. In a modeling study, Garrett (1982) examined the onset of convection between two identical forested regimes, one with adequate soil moisture for transpiration and one without. The simulation that used insufficient soil moisture for transpiration exhibited higher surface temperatures, faster growth of the boundary layer, an earlier onset of convection, and an earlier end to rainfall than did the simulation that used adequate soil moisture. Other simulations indicated that denser vegetation served to increase transpiration, maintain cooler and more moist low-level air, reduce boundary layer depth and entrainment of dry air aloft, and decrease convective precipitation. [Because these simulations were conducted using a one-dimensional model, the impact of solenoidal circulations created by surface gradients was not considered.]

Hong et al. (1995) used the two-dimensional PBL model of Huang (1990) and Huang and Raman (1991a,b) to investigate the effectiveness of vegetation to initiate clouds under different atmospheric stabilities. The experiments modeled two 80-km-wide irrigated areas of vegetation that were located on opposing sides of an 80-km-wide area of dry bare soil. Thermal contrasts that resulted from gradients in sensible heat flux across the different land surfaces caused model convection to develop. Numerical simulations indicated that, within a convectively unstable PBL, these convective clouds initiated earlier (i.e., earlier existence of turbulence), dissipated sooner (i.e., more vertical mixing that entrained dry air aloft), and had stronger vertical velocities than did clouds that developed within an absolutely stable atmosphere.

### *2.3.4 Impact on Rainfall*

Rain that falls onto vegetation affects the region for a longer period of time than that which falls onto bare land. Plants transport soil moisture from root depth to the leaves and evaporatively lose water through open stomata. The increased evapotranspiration decreases the vapor pressure deficit, which, in turn, may enhance clouds and rainfall. The positive feedback that results can help the environment mitigate or recover from drought conditions. Observational and modeling studies indicate that regional-scale irrigation practices can alter convective rainfall patterns (Barnston and Schickedanz 1984; Lanicci et al. 1987) and that forests may enhance convection and rainfall in the Tropics (Mahfouf et al. 1987; Segal and Arritt 1992; Woodcock 1992; Blyth et al. 1994; Trenberth 1999).

Simulations also have demonstrated that total rainfall increases as the vegetation density increases, regardless of the soil moisture content, and that rainfall maximizes over saturated, fully vegetated soil (Clark and Arritt 1995). Mintz (1984) concluded that precipitation increased over land when evaporation increased. Clark and Arritt (1995) noted that, when using an average thermodynamic profile during the summer at Topeka, KS, convection occurred earlier and rainfall amounts increased as the foliage increased. Their model results did not vary even when moderate changes were applied to the initial moisture and temperature profiles. Garrett's (1982) simulations, however, provided contrasting results. Given an initial atmosphere with sufficient low-level moisture and in the absence of mesoscale circulations, Garrett concluded that soil evaporation and plant transpiration had negligible impacts on the amount of rainfall. In addition to model sensitivities, differences between the results of Garrett (1982) and Clark and Arritt (1995) likely resulted from boundary-layer temperature and moisture profiles; the environment of the former study favored convective development when surface temperatures increased whereas that of the latter study favored convective development when surface moisture increased.

Taylor and Lebel (1998) investigated persistent convective-scale rainfall patterns using observational data (station spacing of 7.5 – 15 km) from the Hydrological – Atmospheric Pilot Experiment in the Sahel (HAPEX–Sahel) in southwest Niger. They observed that during the wet months of July and August, antecedent precipitation influenced rainfall patterns, particularly when intense, large-scale storms moved over strong gradients in surface evapotranspiration. When the time interval between events was one or two days, then surface evaporation rates from wet soil were relatively uniform and the rainfall pattern from a subsequent event was not strongly influenced by the preceding rainfall.

When the time interval extended to three or four days, variability in root-level soil moisture caused vegetation to transpire in a pattern similar to the preceding rainfall event. This heterogeneity allowed rainfall patterns to persist from one event to another. In fact, when the gradient in deep soil moisture was strong, vegetation density could be influenced to provide an even stronger feedback and a more persistent condition that might continue for several weeks (Taylor et al. 1997). Secondary rainfall events that moved over a heterogeneous surface when heat flux gradients were weak (e.g., windy or cloudy days) did not enhance the persistence of a previous rainfall pattern. Instead, the secondary rainfall homogenized the surface moisture.

Similarly, Rind (1982) used a general circulation model to ascertain that the amount of soil moisture across the U.S. on June 1 was related to the subsequent convective precipitation during July and August. These results contrasted with a similar study by Fowler and Helvey (1974) who examined July and August rainfall over eastern Washington. The authors did not uncover a statistically significant relationship between rainfall amount and soil moisture. The atmosphere over eastern Washington, however, regularly undergoes large-scale subsidence in the rain shadow of the Cascades. In contrast, during the summer months across the Great Plains, weak synoptic-scale conditions prevail and abundant convection can develop.

Other studies suggest that the irrigation of crops in arid or semiarid regions enhances local cloudiness and rainfall (Stidd 1967 and 1975; Joos 1969; Changnon 1973). In a study of the effect of irrigation on rainfall, Schickedanz (1976) observed statistically significant increases in warm-season rainfall over irrigated areas across the southern and central Great Plains. When irrigated years (1946-1970) were compared with nonirrigated years (1931-1945), rainfall over irrigated regions increased 14–26% in June, 57-91% in July, and 15–26% in August. The author hypothesized that the increased rainfall resulted from the presence of a relatively cool, moist dome over the irrigated regions.

Barnston and Schickedanz (1984) indicated that any enhancement to the low-level moisture field from irrigation required synoptic-scale uplift (e.g., fronts, surface low-pressure systems) to increase cloud development and rainfall. Moore and Rojstaczer (2001) expanded upon the research of Barnston and Schickedanz (1984) and Schickedanz (1976) by examining precipitation patterns across the High Plains from 1957 to 1997. Three regions were examined: the Texas Panhandle (similar to the Schickedanz studies), eastern Colorado – western Kansas, and eastern Nebraska. In contrast to the previous studies, Moore and Rojstaczer (2001) did not find convincing evidence that irrigation induced increased rainfall within any of these regions. The authors hypothesized that climatological changes provided a greater influence on warm season rainfall than did regional irrigation; they believed that the Schickedanz results were affected by droughts during the 1930s.

Using crop insurance loss-cost data from Texas, a hail maximum was located near a region of maximum irrigation in the Lubbock-Plainview area (Schickedanz 1976; Henderson and Changnon 1972; Beebe 1974). Similarly, using Vertically Integrated Liquid (VIL) values from the Twin Lakes (KTLX) weather radar during the eight months between March and June for 1997 and 1998, Pugh (1999) discovered a maximum number of possible occurrences of hail (VIL $\geq$ 20 $kg/m^2$) in Grant County, OK, where winter wheat production was maximized. Likewise, Beebe (1974) determined that the seasonal peak in tornado frequency across irrigated counties of the Texas Panhandle coincided with the timing of a maximum increase in regional crop irrigation. Notably, this peak in tornado frequency occurred later than it did across regions immediately surrounding the irrigated area.

Using a single-column model that linked state-of-the-art soil, land, and cloud models, Sud et al. (2001) examined the influence of vegetation on rainfall in the U.S. Southern Great Plains. They performed 600 simulations over four case-study days during June, July, and September using data from the Atmospheric Radiation Measurement Cloud and Radiation Testbed (ARM CART) site in the U.S. Great Plains. The parameter space spanned six vegetation densities, five soil types, and four soil moisture profiles. Results showed a strong, positive feedback between evapotranspiration and precipitation for wet conditions and little or no feedback for drought conditions. Under wet conditions, increased vegetation led to the production of more rainfall; however, under dry conditions, the biosphere did little to relieve the drought. Trenberth and Guillemot (1996), in an analysis of the 1993 floods across the U. S. Midwest, also documented that much of the precipitation during the summer floods appeared to result from local evapotranspiration, which produced a positive feedback.

Dirmeyer (1994) documented results similar to those for the dry conditions in Sud et al. (2001). Using a general circulation model with a simplified version of the Simple Biosphere (SiB) Model (Sellers et al. 1986; Xue et al. 1991), yearlong simulations were conducted to determine if changes in grassland that occur during a drought (e.g., dormancy) could feedback on the drought itself. Three cases were compared to a control case and were initialized with the following springtime conditions: (1) low initial soil moisture, (2) dormant vegetation settings, and (3) both minimal soil moisture and dormant vegetation. The former two simulations produced moderate drought during part or all of the summer season. The latter case resulted in a severe and extended drought, marked by changes in most variables that were greater than the sum of those for the former two cases. Of interest, although dormant vegetation might have intensified the meteorological drought, it served to protect the soil from being increasingly depleted of moisture.

### 2.3.5 *Impact on Differential Heating*

Several observational studies indicated that near-surface air temperatures were cooler over irrigated regions when compared to bare soil areas exposed to similar conditions. Reported temperature gradients include 1-2°C across 8 km (De Vries and Birch 1961), 1.5°C across 17 km (Davenport and Hudson 1967), and 3.1°C across about 10 km (Burman et al. 1975). Over irrigated cotton, Voronstov (1963) observed a significant cold pool that extended ~400 m above ground, with the horizontal temperature gradient weakening around 700 m. Dzerdzeevskii (1963) measured a similar cold pool above irrigated areas compared to nearby steppe. Observations detected that the cold pool extended to about 1 km when the surface was dry and to about 600 m during saturated conditions.

Segal et al. (1989) used satellite imagery, surface observations, and aircraft measurements of the PBL over northeast Colorado during CINDE (Convective Initiation and Downburst Experiment) in 1987 to examine differential heating between irrigated crops and dry, sparsely vegetated land. Satellite infrared temperatures of surface conditions indicated that a pool of air over irrigated regions was ~10°C cooler than that across the nearby dry land. Surface and aircraft measurements verified the existence of the cold pool, though its gradient was less than that measured by satellite. The cold pool was determined to extend at least 445 m above ground (the highest aircraft measurement). Radiosonde measurements on 28 July 1987 around 1315 LDT indicated that the shallowest PBL existed over the irrigated land, the warmest potential temperature within the PBL was over the dry land, and the highest mixing ratio overlaid the irrigated land. All aircraft flights observed notably higher equivalent potential temperatures over the irrigated plots.

The spatial variation of vegetation and the associated gradients created in sensible heat flux can change the evolution of surface baroclinic zones, especially when a variation of vegetation density or type is accompanied by substantial soil moisture in the root zone. Even though surface evaporation over bare, moist soil can be substantial, latent heat fluxes are enhanced over a longer period of time when moist soil underlies vegetation, allowing roots to access moisture through an extended soil depth (Chang and Wetzel 1991; Wetzel and Woodward 1987; Rabin et al. 1990). Focusing on the development of severe storms, Chang and Wetzel (1991) modeled the impact of spatial variations of soil moisture and vegetation on boundary layer evolution. They determined that vegetation discontinuities on the meso-$\alpha$ scale either created new or enhanced existing surface gradients both by compacting the spatial rate of temperature change into mesoscale regions and by accumulating moisture within a shallower boundary layer. The differential heating intensified the surface pressure gradient, which, in turn, enhanced both warm advection and convergence across the weak surface boundary. By destabilizing the local environment, these foliage gradients became preferred regions for convective initiation in conditionally unstable environments. Without vegetation, surface evaporation alone was insufficient to establish strong thermal gradients at the surface.

### *2.3.6 Impact on Mesoscale Circulations Simulated by Numerical Models*

On the mesoscale, variations in soil moisture or soil texture have been shown to significantly influence PBL characteristics and mesoscale circulations (Zhang and Anthes 1982; Ookouchi et al. 1984; Mahfouf et al. 1987; Yan and Anthes 1988; Schadler 1990; Lynn et al. 1998). These mesoscale circulations can produce mesoscale fluxes greater than their associated turbulent fluxes, and they do so predominantly in narrow zones a few hundred meters wide (Mahrt et al. 1994; Lynn et al. 1995). As a result, well-defined mesoscale circulations aid the transport of heat and moisture throughout the PBL and advance the potential erosion of any capping inversion. Sea-breeze-like fronts moving from opposing wet patches toward the center of a dry patch may collide and enhance the solenoidal circulation, particularly if the dry patch is wide enough for the collision to occur shortly after moist convection initiates (Lynn et al. 1998).

Differential heating caused by sensible heat gradients across adjacent regions of active vegetation and dry, bare soil also can generate a sea breeze-like circulation (Purdom and Gurka 1974; Segal et al. 1988; Mahfouf et al. 1987; Hong et al. 1995; Lee and Kimura 2001). This circulation has been labeled by various scientists as a "land breeze", a "land-land breeze", an "inland breeze", a "vegetation breeze", and a "nonclassical mesoscale circulation". For the current wheat study, Segal and Arritt's (1992) terminology – "vegetation breeze" – will be adopted and will denote that the resulting surface wind blows *from* a vegetated region. Similar circulations have been modeled across boundaries of distinct vegetation types (Pielke et al. 1991). Observations indicate that vegetation breezes have an appreciable effect on the formation of shallow cumulus clouds (Rabin et al. 1990; Garrett 1982). Numerical simulations demonstrate that these circulations can provide preferred regions to focus atmospheric instabilities and to initiate convective development (Sun and Ogura 1979; Chen and Avissar 1994; Chang and Wetzel 1991; Mahfouf et al. 1987; Garrett 1982).

Anthes (1984) authored the landmark study on mesoscale circulations that result from alternating bands of dense vegetation and bare soil. Given marginally unstable atmospheric conditions and the differential heating generated by these bands, mesoscale circulations of similar intensity to sea-breeze circulations were hypothesized to be generated in a semiarid region. Anthes (1984) applied linear theory to demonstrate analytically that, as a result of these circulations, convective rainfall would be significantly greater when generated by vegetation/bare land contrasts than by either uniformly vegetated or uniformly bare surfaces. In addition, a length scale between 50 and 100 km was deemed to be the most effective to generate circulations deep enough to initiate moist convection. Similarly, Chen and Avissar (1994) and Lynn et al. (1995) noted that heterogeneities must be at least 10 km wide to establish mesoscale fluxes. At scales smaller than 10 km, turbulent mixing overpowered horizontal pressure gradient forces.

Mahfouf et al. (1987) used a two-dimensional numerical model (Nickerson et al. 1986) to verify Anthes' hypothesis. In one experiment, a bare, relatively dry, loamy soil was positioned adjacent to a dense grass surface. At 1400 LST in their simulation, the sensible heat flux over the bare soil was 400 W $m^{-2}$ while that over the vegetative cover was 170 W $m^{-2}$. By 1800 LST, a horizontal wind of 2.7 m $s^{-1}$ flowed from the foliage toward the bare soil. Concurrently, at 1200 m above ground, an upward vertical velocity of 5 cm $s^{-1}$ was simulated over the bare soil and a downward vertical velocity of 3 cm $s^{-1}$ was simulated over the vegetation. In other experiments, the authors noted that dense forest shielded discontinuities in soil moisture from strongly influencing atmospheric circulations. In their study, a horizontal wind of less than 0.5 m $s^{-1}$ was observed over the forest at 1800 LST across the moisture gradient as compared to 6 m $s^{-1}$ for the same moisture discontinuity without the forest. With respect to the horizontal gradient of sensible heat flux, which Pielke (1984) indicated must be at least 100 W $m^{-2}$ per 30 km to alter local wind patterns, Mahfouf et al. (1987) demonstrated that significant discontinuities in soil moisture over bare plots, in soil moisture over sparsely vegetated plots, or in the density of foliage over uniform soil moisture had the potential to produce measurable local circulations.

Pinty et al. (1989) employed the methodology of Mahfouf et al. (1987) to examine the influence of variations in vegetation type on mesoscale circulation development. Measurements from the HAPEX-MOBILHY field experiment

(André et al. 1986, 1988) in southwest France were used to prescribe realistic soil and vegetation characteristics in a two-dimensional model. Simulations were conducted with the numerical model (Nickerson et al. 1986) used by Mahfouf et al. (1987). A new soil-vegetation package, which applied measurements from HAPEX-MOBILHY, was implemented to provide more realistic model physics for land-air interaction studies. Simulations were conducted on flat terrain with clear sky conditions and no synoptic-scale flow. An agricultural crop was located on the western half of the domain; a sparse pine forest with dense understory was positioned on the eastern half of the domain. The authors conducted two simulations: (1) moist soil below both foliages and (2) dry soil below the crop and moist soil below the forest. In the first experiment, where sufficient moisture was available and both vegetation regimes were unstressed, a significant mesoscale circulation developed. The circulation resulted from a thermal contrast between the higher sensible heat flux over the forest as compared to that over the agricultural crop. This contrast was eliminated, however, in the second experiment because the crop was stressed by dry soil conditions and, thus, evapotranspiration was reduced substantially.

In contrast, Pielke et al. (1991) documented a circulation in the opposite direction using the Regional Atmospheric Modeling System (RAMS; Tremback et al. 1986; Schmidt and Cotton 1990) developed at Colorado State University (CSU). In their two-dimensional simulation, forest (LAI = 5.8, $z_0$ = 2 m, and albedo = 0.15 at local noon) covered one half of the domain and irrigated wheat (LAI = 4.7, $z_0$ = 2 cm, and albedo = 0.25 at local noon) covered the other half. Sufficient moisture existed in the root zones for evapotranspiration to occur near its potential rate. In this case, evapotranspiration over the forest was more abundant than that over the cropland; hence, the PBL was cooler and shallower over the forest. A thermally direct circulation was generated during the late afternoon, with the upward branch of the circulation developing over the cropland.

Using two-dimensional mesoscale simulations (Pielke 1974) under clear sky conditions and weak synoptic flow, Segal et al. (1988) verified the results of McCumber (1980) that indicated that the addition of vegetation on land would lead to a suppression of the modeled sea-breeze circulation as compared to a simulation without vegetation. The added vegetation caused a decrease in the sensible heat flux, thus decreasing the PBL height, turbulent motion, and upward vertical velocity over the land. Observations by Alpert and Mandel (1986) seemed to verify this weakened sea breeze. Measurements of inland flow, predominantly from the sea breeze, on the coast of Israel indicated a decrease in wind speed during a 40-year period when increased planting and irrigation slowly enhanced the coastal foliage density.

Additional simulations of Segal et al. (1988) demonstrated that only weak circulations developed when bare, wet soil was adjacent to nonstressed vegetation or when nonstressed vegetation was adjacent to water. Weak circulations resulted because the amount of evaporation from bare, wet soil or water was similar to that from nonstressed vegetation. Thermal circulations comparable in intensity to a sea breeze, however, were generated by covering half of the mesoscale domain with dense, unstressed vegetation and the other half of the domain with dry, bare soil. In particular, a strong vegetation breeze was established when simulating an event whereby a heavy uniform rainfall was followed by several dry days. In this case, the surface of the bare soil became dry whereas the vegetation accessed its substantial supply of root-level moisture for evapotranspiration.

Four additional experiments by Segal et al. (1988) are salient to the current study. First, as foliage density decreased, circulation intensity reduced. Second, when simulated environmental stresses were imposed, latent heat flux over the vegetation reduced and the vegetation breeze decreased. Third, when swaths of dry, bare soil flanked a swath of nonstressed vegetation, two circulation cells were established, with upward vertical velocities evident over both bare soil patches. And fourth, when a weak easterly crosswind (3 m $s^{-1}$) was imposed on this last simulation, a distortion of the two-cell circulation occurred. In particular, significant vertical motion was noted only over the eastern swath of bare soil, and convergence at the windward edge of the vegetation belt was enhanced. This final simulation perhaps was the most realistic for the current study focused on the winter wheat belt of Oklahoma.

Chen and Avissar (1994) examined mesoscale and turbulent heat fluxes over heterogeneous and homogeneous land uses employing the RAMS model from CSU (Pielke et al. 1992). In their first experiment, the authors alternated patches of irrigated land and dry land, comparing their results to simulations with uniformly dry land and uniformly wet land. The mesoscale circulations that were generated over the patchy landscape caused the total mesoscale heat flux within the model domain to dominate the total turbulent heat flux. Thus, the total heat flux was greater for the patchy landscape than for either homogeneous landscape.

### *2.3.7 Observational Evidence of Vegetation-Induced Mesoscale Circulations*

Segal and Arritt (1992) noted that regions where vegetation breezes might be observed in nature typically were smaller in areal extent than were their numerically simulated counterparts (because of the idealized nature of the simulations). In particular, past observational studies were characterized by nonuniform regions (e.g., in size, soil moisture, vegetation density), small zones where the sensible heat flux was suppressed, and periods when moderate synoptic or mesoscale flows obscured the land-atmosphere interactions. Evaluating several real-world studies of possible vegetation breezes, Segal and Arritt (1992) documented that vegetated areas used in these studies typically were 10-100 km wide, with a band of decreasing foliage that extended 1-10 km beyond the area's defined boundary. In addition, these vegetated regions had foliage that averaged 50% to 90% coverage and sensible heat fluxes measured to be 20% to 50% of those over the surrounding area.

Three observational case studies from Segal et al. (1989) provided little evidence of a vegetation breeze, although a cold pool was measured over irrigated crops as compared to neighboring dry land. The authors noted, however, that both the imposed synoptic flow and the thermally induced upslope flow along the Front Range of the Rockies might have obscured any mesoscale circulation induced by a contrast in land use. Even so, low-level horizontal temperature gradients were of comparable intensity to those associated with moderate sea breezes.

Souza et al. (2000) did measure a vegetation-induced circulation across sloping terrain in the state of Rondônia, Brazil (10°S, 62°W). Using near-surface and upper-air data for a 10-day period during mid-August 1994, the authors documented a perturbation wind (observed, ensemble-averaged wind minus mean synoptic, ensemble-averaged wind) within the lowest 3 km of the atmosphere that was directed from the forest toward the deforested pasture. A perturbation wind in the opposite direction was measured between 3 and 5 km above ground. The measured circulation was strongest between 1100 and 1400 local time, when maximum surface heating occurred.

Doran et al. (1995) documented a possible "farm breeze" circulation across a boundary between steppe and irrigated cropland near Boardman, WA on 11 June 1992. Throughout that day, winds over the steppe were from the southwest or west, perpendicular to the steppe-cropland boundary and blowing from steppe to farmland. Over the farm, however, southwest or west winds during the morning veered to the north and northeast during the early afternoon. The wind shift over the farm was measured both by surface stations and by three sodars that measured winds at 60 m above ground. With no change in the large-scale wind pattern nor a terrain-related change in the wind field, the authors attributed this wind shift to a farm breeze circulation. Sensible heat fluxes between 1000 and 1530 PDT averaged about 300 W $m^{-2}$ over the steppe yet only 60 W $m^{-2}$ over the farm. A component of the wind that opposed the larger-scale flow over the steppe became evident by late morning, when wind speeds over the farm decreased and winds began to veer to the north-northeast. Surface stations west of the steppe-farm boundary also measured wind shifts; however, no "farm breeze front" was detected. These observations seemed consistent with the numerical modeling study of Bechtold et al. (1991) whereby a crosswind up to 6 m $s^{-1}$ from crop to forest did not significantly disrupt a simulated inland breeze circulation. Similarly, modeling studies by Chen and Avissar (1994) indicated that a 5 m $s^{-1}$ background wind did little to alter mesoscale circulations generated by inland breezes. A 10 m $s^{-1}$ wind, however, did reduce mesoscale circulations significantly.

Inspecting 21-day ensemble-averages of the perturbation wind field (observed surface wind minus daily mean surface wind), Smith et al. (1994) discovered perturbation winds blowing across a vegetation gradient at 1515 LDT during the fifth FIFE intensive field campaign. The perturbation winds were directed from an area of dense, green vegetation (and low sensible heat fluxes) toward an area of sparser, drier vegetation (and high sensible heat fluxes). A three-day ensemble average depicted even more intense perturbation winds. The authors attributed these winds to a local, direct circulation that was established by the sensible heat gradient between the dense and sparse vegetation areas. Wai and Smith (1998) studied upper-air observations for this same experiment and found that the secondary circulation had a vertical extent of at least 500 m. In addition, the circulation was not weakened substantially by convective clouds, provided that the horizontal temperature gradient at the surface was maintained. Substantial rainfall and cold-air advection, however, did disrupt the direct circulation.

Mahrt et al. (1994) examined the horizontal structure of vegetation breezes using aircraft observations from the California Ozone Deposition Experiment (CODE). An irrigated area 10-15 km across was compared to its drier and warmer surroundings. The aircraft flight track was divided into an intensely irrigated section about 12 km across, a 7-km wide swath of mixed land use on both sides of the irrigated region, and, beyond that, a dry region with little transpiring vegetation. Results indicated that on a day with 2 m $s^{-1}$ ambient winds, a cool vegetation breeze was generated, moving outward from the irrigated area. Vegetation breeze fronts formed about 1.5 km to the east and to the west of the edge of the intensely irrigated region. An additional vegetation breeze flowed from the mixed vegetation area to the warm bare soil and also created an inland breeze front. The breeze fronts were well defined from 1045 to 1245 solar time and were accompanied by sharp horizontal moisture gradients, a moderate temperature gradient, and horizontal convergence. On a day with 4 m $s^{-1}$ ambient winds, well-defined vegetation breezes did not exist.

Shaw and Doran (2001) found little observational evidence of vegetation breezes over the ARM CART site in the U.S. Great Plains. Divergence fields from the ARM CART surface network were composited for 23 "dry days" (days with no rain for that day or the preceding 18 hours) and 23 "wet days" (days not classified as "dry days") during the spring of 1995, and for 14 dry days and 32 wet days during the summer of 1995. Even with strong thermal contrasts between regions of grassland and adjacent wheat cropland (either maturing or harvested), no divergence pattern, save one case, seemed related to any surface temperature gradient. The single case was a persistent region of convergence across the north-central portion of the ARM/CART region and used the data representing composited summer dry days. This region of convergence was associated with a strong temperature gradient between harvested wheat and grassland. The authors believed this convergence to be evidence of a mesoscale circulation resulting from land use differences. In most other cases, however, divergence patterns were aligned closely with local, but small, changes in topography.

One factor that may have masked the divergence signature of a thermally driven mesoscale circulation in Shaw and Doran's (2001) study was the intensity of the winds. Only one spring dry day and two summer dry days experienced wind speeds frequently below 2.5 m $s^{-1}$. Pielke et al. (1991) noted that a prevailing wind would diffuse the horizontal temperature gradient and reduce the accompanying mesoscale circulation. In their numerical simulations, the authors determined that a moderate prevailing wind acted to increase the domain-averaged subgrid-scale vertical heat fluxes and to decrease domain-averaged mesoscale vertical heat fluxes compared to the simulations with calm prevailing flow. Except for moderately weak winds (5 m $s^{-1}$) and large-width land strips (at least 16 km wide), the subgrid-scale fluxes dominated the mesoscale fluxes, and the mesoscale circulations were reduced substantially.

## 2.4 Relevance of Past Studies to Current Research

Past studies provide a foundation to better understand the physical mechanisms that cause differences in near-surface temperature and moisture fields across regions of distinct land use types. In particular, the research suggests that gradients in near-surface temperature and moisture fields across Oklahoma's winter wheat belt and its adjacent grasslands should be evident, quantifiable, and dependent on near-surface winds, boundary-layer structure, and the stage of the growing season. The following research will build upon this foundation to document the spatial and temporal extent to which Oklahoma's wheat belt influences weather and climate across the state.

# CHAPTER 3: THE STUDY REGION AND OBSERVATIONAL DATA USED

To better interpret the results within Chapters 5 and 6, overviews of both the climatology of the study region and the observational data sources are provided here. For the current study, the *winter wheat belt* was defined as the swath of land across Oklahoma and Kansas that was characterized by either winter wheat or a winter wheat/grassland mix as the land use type designated by the U.S. Geological Survey (USGS). *Oklahoma's wheat belt* was defined as that subset of the winter wheat belt located solely within Oklahoma. The location and extent of Oklahoma's wheat belt is depicted in Fig. 3.1. Only the impact of Oklahoma's wheat belt was analyzed in the observational study.

FIGURE 3.1. Map of the measurement sites of the Oklahoma Mesonet (dots). The shaded region (violet) represents Oklahoma's winter wheat belt, as defined for this study.

## 3.1 Description of the Study Region

The topography of Oklahoma influences the state's climate, which, in turn, governs the natural vegetation of the region. In general, the land slopes downward west-to-east, from 1500 m above sea level in the far western

Panhandle[8] to 90 m in southeastern Oklahoma (Fig. 3.2). Just north of Oklahoma's lowest elevation, the Ouachita Mountains extend about 600 m above the surrounding landscape. In southwestern Oklahoma, the Wichita Mountains provide 350 m of additional relief above the plains.

Thirty-year climatologies of precipitation have not changed substantially during the decades of the 20th century. Figures 3.3 and 3.4 display the normal annual total precipitation for the periods 1971 - 2000 and 1931-1960, respectively. The climatological rainfall pattern across Oklahoma reflects the state's topography. The meridional gradient of precipitation across Oklahoma also reflects the prevailing winds that result from the mid-latitude, synoptic-scale weather patterns of the region (Johnson and Duchon 1995). Southerly and southeasterly winds across eastern Oklahoma advect moisture from the Gulf of Mexico into the state; southerly and southwesterly winds across western Oklahoma advect drier air from the Mexican Plateau and the Texas Plains.

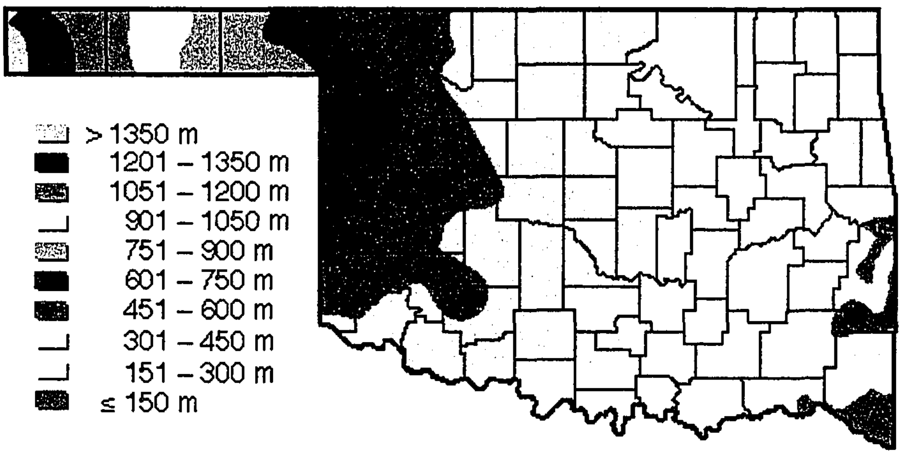




FIGURE 3.2. Topographical map of Oklahoma. (Courtesy of the Oklahoma Climatological Survey.)

[8] The three counties farthest to the northwest (see Fig. 3.1) define the *Panhandle* of Oklahoma.

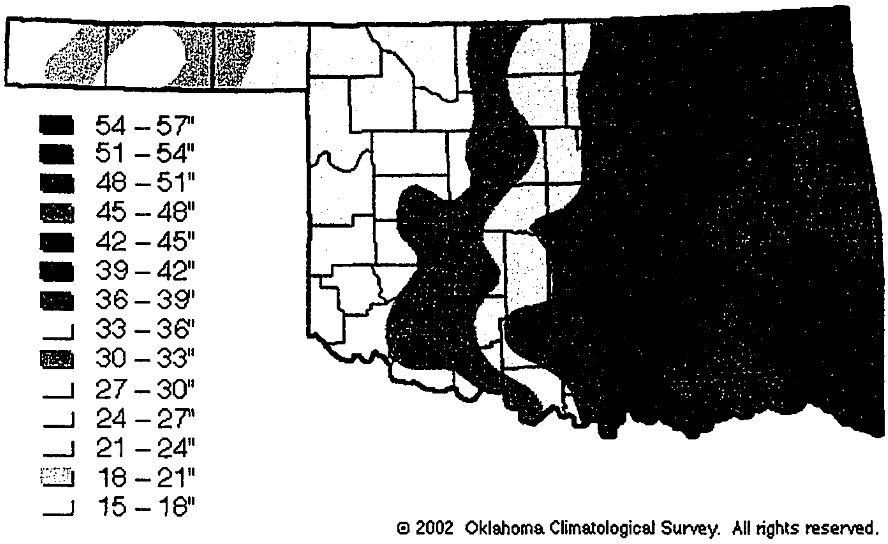


FIGURE 3.3. Normal annual total precipitation (in inches) across Oklahoma for 1971 – 2000. (Courtesy of the Oklahoma Climatological Survey.)

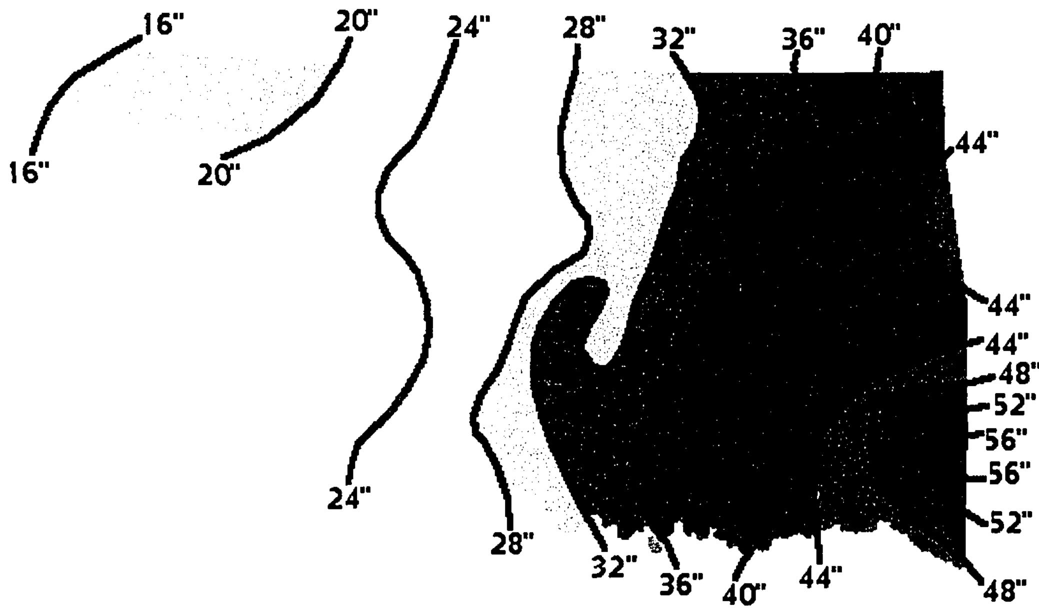


FIGURE 3.4. A digital representation of the normal annual total precipitation (in inches) for 1931–1960 across Oklahoma (digitized from NOAA 1977).

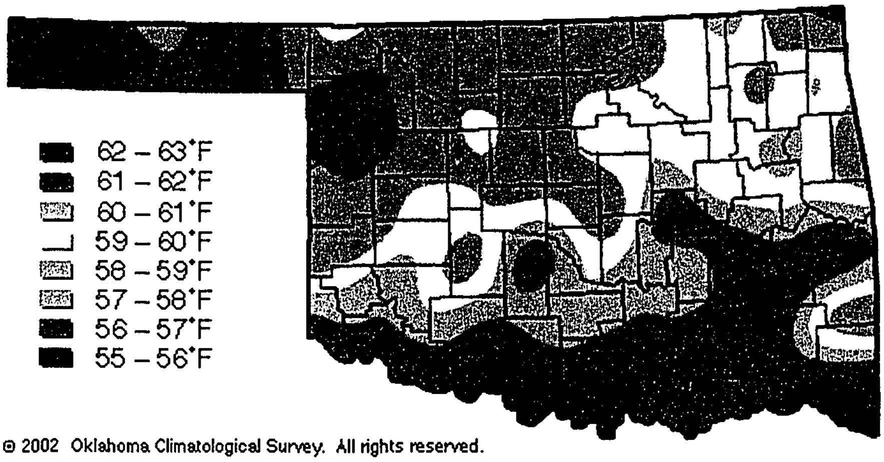


FIGURE 3.5. Mean annual air temperature (in degrees Fahrenheit) across Oklahoma for 1971 – 2000. (Courtesy of the Oklahoma Climatological Survey.)

Normal annual rainfall (Fig. 3.3) and mean annual air temperature (Fig. 3.5), as well as substantial hydrologic features, greatly influence the type of vegetation that grows naturally across the region. Through land surveys conducted subsequent to the "dust bowl" years of the 1930's, Duck and Fletcher (1943) developed a map of the potential natural vegetation[9] of Oklahoma. They documented that the three most prominent vegetation regimes related to the current study were mixed-grass – eroded plains, tallgrass prairie, and postoak – blackjack oak forest. The mixed-grass – eroded plains regime resided predominantly to the west of Oklahoma's wheat belt and was characterized by moisture deficiency during all seasons. Most of the land area occupied by today's wheat belt originally was tallgrass prairie. Although the tallgrass prairie regime was more humid than the mixed-grass – eroded plains, it again featured deficient moisture during all seasons. The post oak – blackjack oak regime was characterized by adequate moisture during all seasons and resided mostly to the east of the wheat belt.

Significant to the location of today's wheat belt, Duck and Fletcher (1943) remarked that "climatic peculiarities do not characterize the Tallgrass Prairie

[9] Potential natural vegetation is a term used in the biological sciences to describe a well-founded estimate of the type and location of natural vegetation across a region.

Game Type insofar as Oklahoma is concerned." Thus, *substantial anomalies in the atmospheric measurements across this region were not expected, and results to the contrary found in this study were considered significant.*

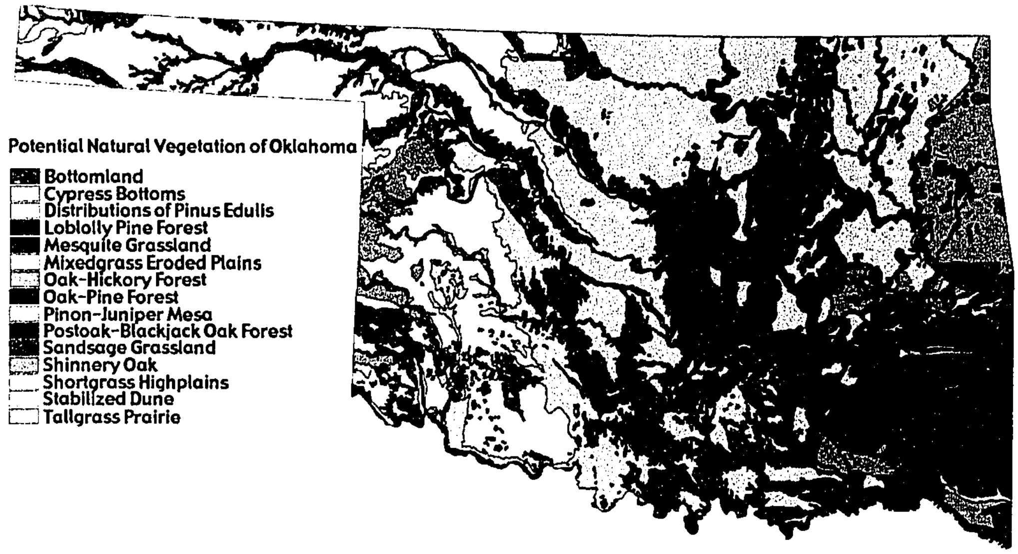


FIGURE 3.6. The potential natural vegetation of Oklahoma, as published by Duck and Fletcher (1943). Note that tallgrass prairie once dominated the landscape that now comprises Oklahoma's winter wheat belt.

## 3.2 Oklahoma Mesonet Observations

The primary source of observational data for this study is the Oklahoma Mesonet (Brock et al. 1995), a statewide surface network comprised of more than 110 stations. Data from the Oklahoma Mesonet will be referred to as "Mesonet data". The Mesonet dataset extends from 1994 to the present and includes the following variables at every station: air temperature at 1.5 m, relative humidity at 1.5 m, wind speed and direction at 10 m, rainfall, station pressure, incoming solar radiation, and soil temperature at 10 cm under both bare soil and natural sod cover. Additionally, 9-m air temperature, 2-m wind speed, 5–cm soil temperature under both bare soil and sod, and 30-cm soil temperature under sod have been measured by more than half of the Mesonet sites since 1994. All above ground measurements are recorded every five minutes; soil temperature measurements are recorded every 15 minutes.

Upgrades to the Oklahoma Mesonet during 1999 added measurements of soil moisture at 5 cm, 25 cm, 60 cm, and 75 cm below natural sod, net radiation, and ground heat flux at about 100 Mesonet sites. Sensors also were added to calculate sensible heat flux using the profile method described in Brotzge and Crawford (2000). Latent heat flux were calculated as a residual using the surface energy balance equation. Brotzge and Crawford (2000), Crawford and Bluestein (1996), and others have demonstrated the utility of the Oklahoma Mesonet for surface energy budget studies.

Quality control of the data is accomplished in several steps. First, laboratory personnel calibrate all Mesonet sensors prior to their deployment in the field. Second, field technicians visit each site at least three times per year to clean equipment, mow vegetation, and conduct sensor intercomparisons. Third, the Mesonet central computer system operates an extensive set of automated quality assurance routines. These routines are detailed by Shafer et al. (2000) and include step, range, persistence, like-sensor, and nearest neighbor tests. Finally, a quality assurance meteorologist examines the data and manually "flags" any suspect data or removes automated flags from data deemed to be consistent with atmospheric conditions (e.g., heatburst, thunderstorm outflow). The quality-assured data archive contains 99% of the observations possible.

Monthly averages computed for Crop Year 2000 in Chapter 5 were based on more than 3000 daily maxima or minima each month. A given daily extreme represented a 5-min observational period. Statistical analyses discussed in Chapter 5 were founded upon more than 20 million Mesonet observations over eight distinct years. These observations spanned crop years with annual wheat production for Oklahoma ranging from 93 million to 199 million bushels.

## 3.3 Extent of the Winter Wheat Belt

Winter wheat is sown in the fall and harvested in the late spring or early summer. The winter wheat belt extends across portions of western Oklahoma for several reasons. First, because the natural vegetation was grassland, a grass crop (such as wheat) is well-supported by the land. Second, water for irrigation is scarce; hence, the crop must grow using precipitation alone. Third, and related to the second point, the two vital times when the wheat crop requires water – at initial growth and during plant maturity – coincide with early autumn and late spring climatological peaks in monthly precipitation across the region.

The boundary of Oklahoma's winter wheat belt, as defined for this research and as outlined in Fig. 3.1, was designated using a land cover data base, aerial photographs, and Mesonet field technician reports. The land cover characterization was from the North America Land Cover Data Base from the USGS. The data base was constructed from Advanced Very High-Resolution Radiometer (AVHRR) data spanning April 1992 through March 1993. It has a 1–km nominal spatial resolution and is georeferenced in a Lambert Azimuthal Equal Area projection (Loveland et al. 1999). Figure 3.7 displays a subset of this data base. Land cover that was categorized as either winter wheat or a mix of winter wheat and grassland has been colored in Fig. 3.7 to emphasize the location and extent of the winter wheat belt.

Digital Orthophoto Quadrangles supplied by the Oklahoma GIS Council (ftp://okmaps.onenet.net), in cooperation with the USGS, Natural Resources Conservation Service (NRCS), and U.S. Department of Agriculture, were georeferenced with Oklahoma Mesonet site locations. Because these photographs were captured primarily during February 1995, a month when grassland and summer crops are dormant, winter wheat fields were straightforward to distinguish. The aerial photographs were centered on Mesonet sites within and nearby the wheat belt. Information gathered from visual inspections of the images aided data interpretation. Figures 3.8 and 3.9 show examples of a 1:500 map scale image of the Kingfisher and Guthrie Mesonet sites, respectively.

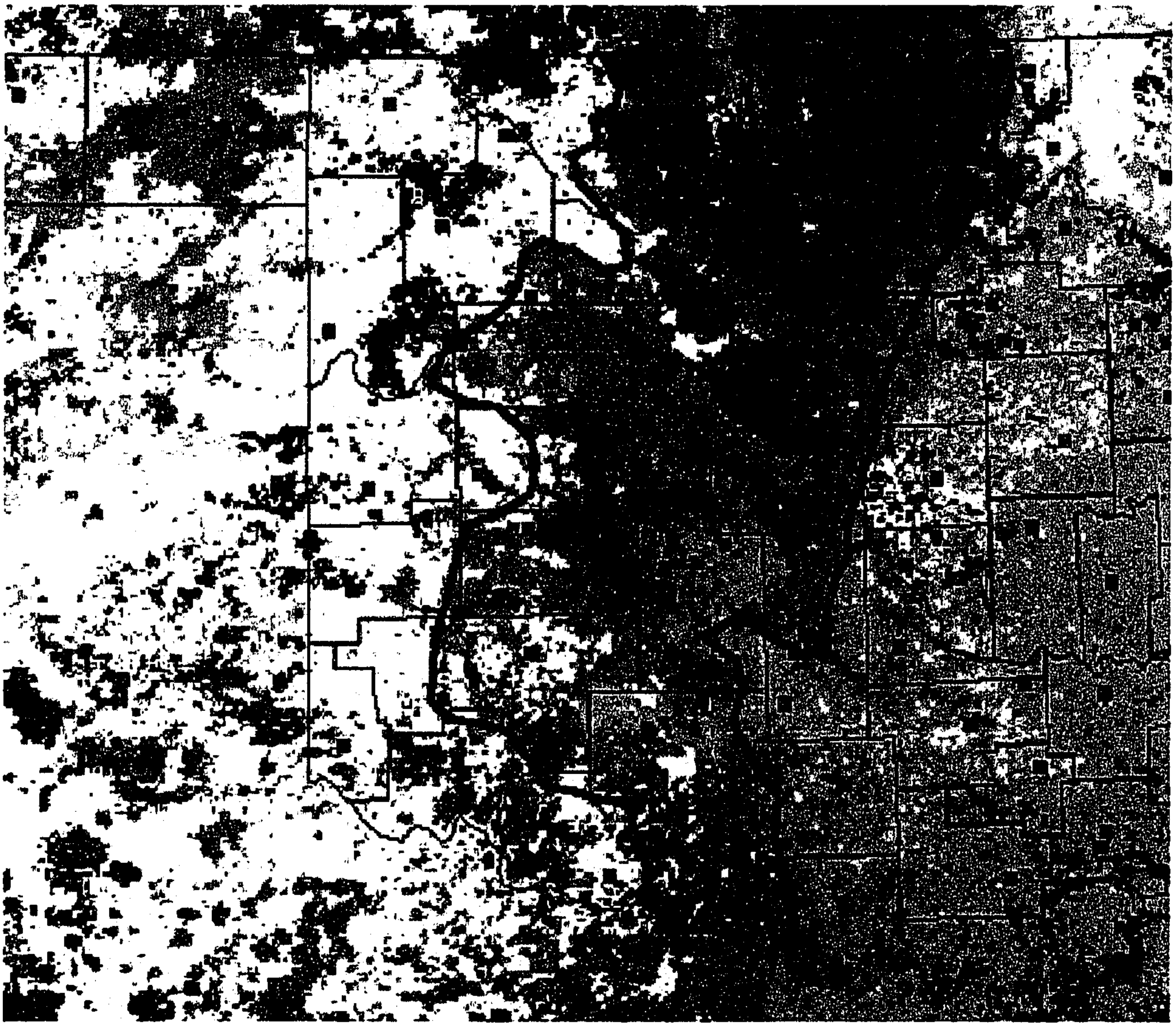

FIGURE 3.7. Land cover characterization from the North America Land Cover Characteristics Data Base 2.0 of the U.S. Geological Survey. Dark red pixels represent winter wheat, and nearby light orange pixels represent a mix of winter wheat and grassland. The thick, dark line outlines Oklahoma's winter wheat belt, as defined for this study. Black squares are locations of Oklahoma Mesonet sites. Oklahoma counties are outlined with thin, solid black lines.

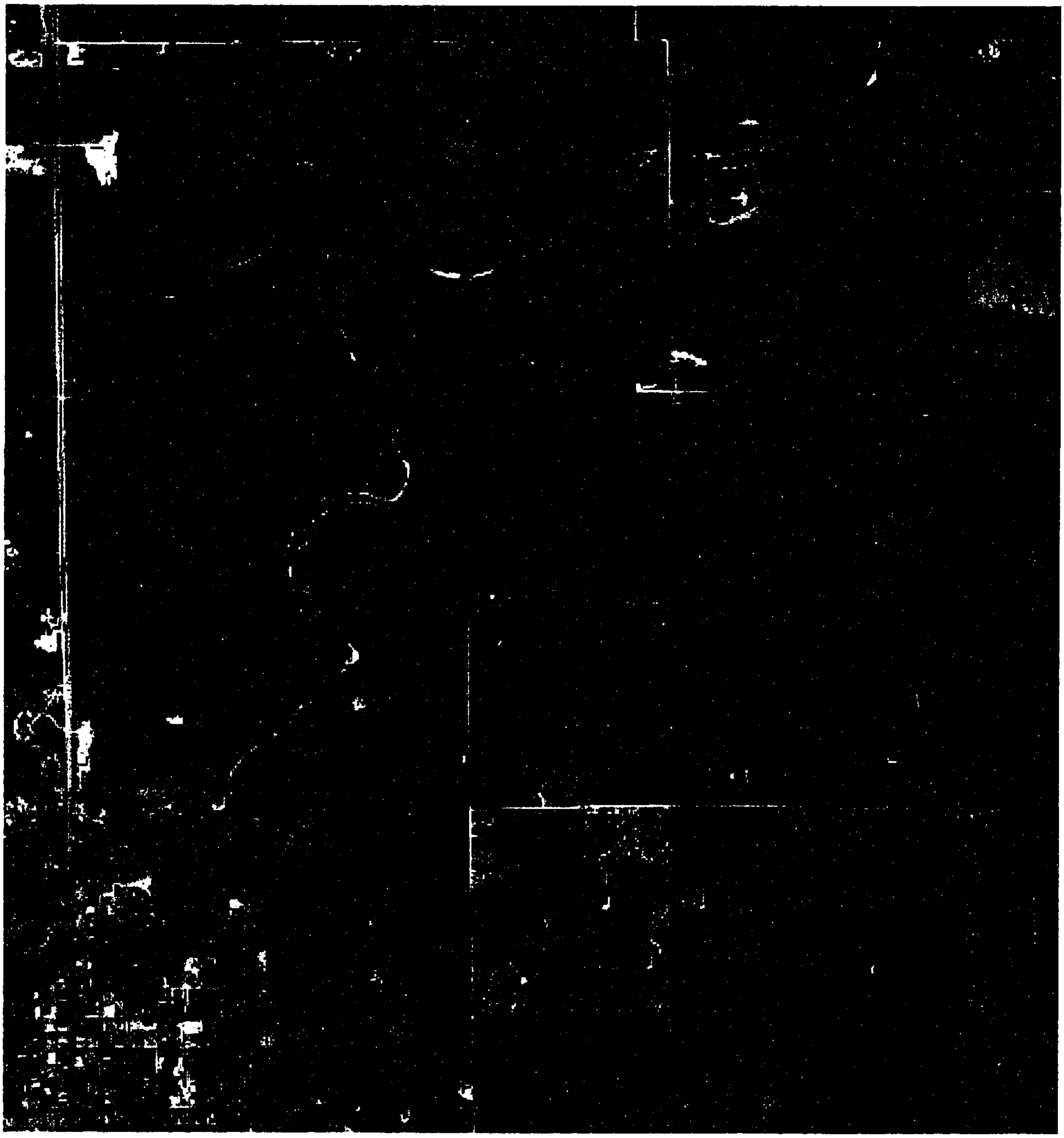

FIGURE 3.8. An aerial view of the Kingfisher Mesonet site, with North at the top of the image. The site is located at the center of the image. The dominant land cover is winter wheat, seen as dark cropland covering about three-fourths of the image. A riverbed snakes from southwest to northeast and forks around the town of Kingfisher, which is located in the lower left corner of the image. This photograph is a portion of a Digital Orthophoto Quadrangle from February 20, 1995 and is courtesy of the Oklahoma GIS Council (ftp://okmaps.onenet.net).

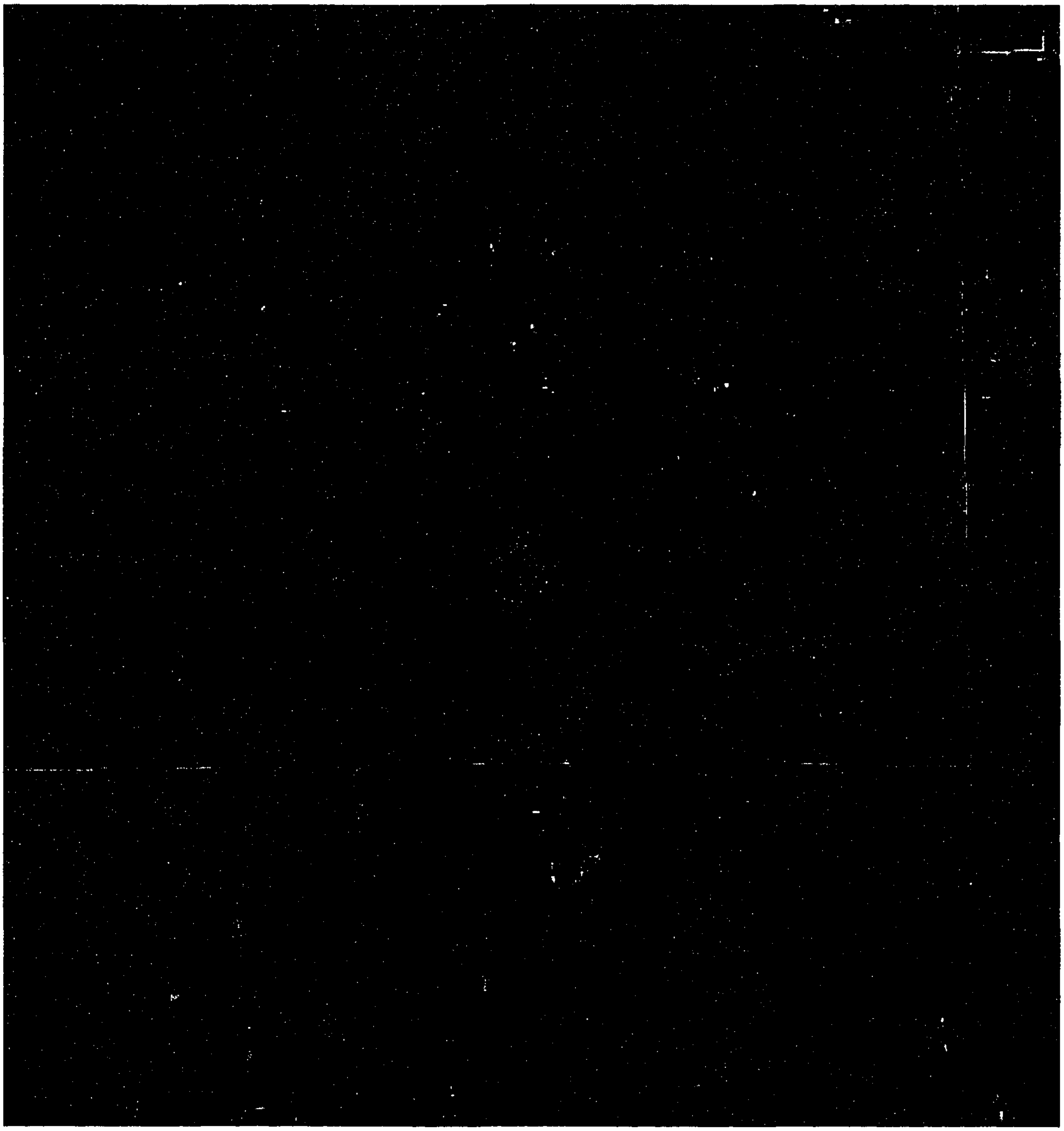

FIGURE 3.9. An aerial view of the Guthrie Mesonet site, with North at the top of the image. The site is located at the center of the image. The dominant land cover is grassland and summer cropland. A few dark areas of growing winter wheat stand out amid the dormant vegetation. Ribbons of conifers, most likely Eastern Red Cedar, are evident along river beds. This photograph is a portion of a Digital Orthophoto Quadrangle from February 20, 1995 and is courtesy of the Oklahoma GIS Council (ftp://okmaps.onenet.net).

Using the aerial images and firsthand reports from Mesonet field technicians, several Mesonet sites were identified as unrepresentative of their region based on the extent of the wheat belt defined for this study. Three sites located within the wheat belt — Altus, Butler, and Fort Cobb — measure data influenced by nearby evaporation sources. The Altus site was installed at an irrigation research station operated by Oklahoma State University, whereas Butler and Fort Cobb are near lakes. Two sites — Grandfield and Tipton — are situated near fields of crops that have growing seasons different from that of winter wheat. Three sites — Buffalo, Medicine Park, and Perkins — are in a landscape setting that is not representative of the defined wheat belt. Although there are wheat fields nearby, Buffalo and Perkins are located more than 25 km from the defined wheat belt. Medicine Park is located within the defined wheat belt but is surrounded by grasslands alone. Finally, Ninnekah and Freedom reside in grassland landscapes but have several wheat fields that grow adjacent to one quadrant of the site; hence, the wind direction directly influences air temperature and moisture measurements at these two sites. Even with these caveats, to maintain adequate site distribution for objective analyses, all of these stations are used in the monthly and daily observational studies unless otherwise noted.

## 3.4 Spectral Vegetation Observations

The growth and condition of the winter wheat crop was monitored through the use of a spectral vegetation index. Satellite reflectances are used to produce spectral vegetation indices, or SVIs, which describe some aspects of the vegetative state. SVIs are surrogates for the amount and condition of vegetation and for estimates of surface fluxes (Deering et al., 1992). Currently, SVIs rely on the fact that vegetation absorbs strongly in the red portion of the spectrum and scatters in the near-infrared. For this study, products derived from the normalized difference vegetation index (NDVI), a common SVI generated from

AVHRR data, were employed. NDVI is defined as follows:

$$\text{NDVI} = (NIR - red) \;/\; (NIR + red)\,,$$

where *NIR* is the amount of energy measured in the near-infrared spectral band and *red* is the amount of energy measured in the red portion of the spectrum (Tucker 1979).

The primary NDVI-derived product used was visual greenness, as defined by the Forest Service Intermountain Fire Sciences Lab of the U.S. Department of Agriculture (Burgan and Hartford 1993). Visual greenness depicts the state of greenness of the vegetation compared to a very green reference, such as an alfalfa field. Wet or densely vegetated areas appeared green, and dry or sparsely vegetated areas appeared red to tan. Values ranged from 0 to 100 percent. To generate this product for each week of Crop Year 2000, seven days of NDVI observations were composited at each pixel; the highest value of NDVI during each week was used. The visual greenness product also was implemented within the Oklahoma Fire Danger Model (Carlson et al. 2002).

A relationship between visual greenness and the extent and maturity of the winter wheat crop was demonstrated by comparing a visual greenness map from late in the growing season (April) with the winter wheat production from Crop Year 2000. Figure 3.10 displays visual greenness for the week ending 20 April 2000. Oklahoma's winter wheat belt is distinguished by dark green and is surrounded by yellow and reds that, in this case, represent dormant grassland. By visual inspection of Fig. 3.10, the counties that had the greatest percentage of dark green pixels (representing high vegetative greenness) are Alfalfa, Canadian, Grant, Garfield, Kingfisher, Kiowa, and Washita. For comparison, Fig. 3.11 displays the Oklahoma Wheat County Estimates for Crop Year 2000, which ended June 2000 (Oklahoma Agricultural Statistics Service 2001). County wheat production (in bushels) is displayed, with purple and dark red representing high production and light yellow representing low production. The counties that recorded the greatest wheat production during Crop Year 2000 are Grant (11,550,000 bushels), Garfield (9,820,000), Alfalfa (8,920,000), Texas (7,700,000), Kiowa (7,030,000), Kay (6,390,000), Kingfisher (6,300,000), Custer (6,210,000), Canadian (6,100,000), Woods (5,770,000), and Washita (5,200,000). [Figure 3.12 displays Oklahoma county names for reference.] Conversely, counties that recorded relatively low wheat production during 2000 include Woodward (2,100,000 bushels), Comanche (1,790,000), Roger Mills (1,160,000), Harmon (750,000), and Osage (435,000). These counties do not contain substantial acreages of winter wheat (denoted by dark red pixels in Fig. 3.7) and are associated with lower visual greenness values, as evidenced by few dark green pixels in Fig. 3.10. This strong, subjective interconnection indicated that maps of visual greenness could be used to define the spatial extent and general maturity of the Oklahoma wheat belt during Crop Year 2000.

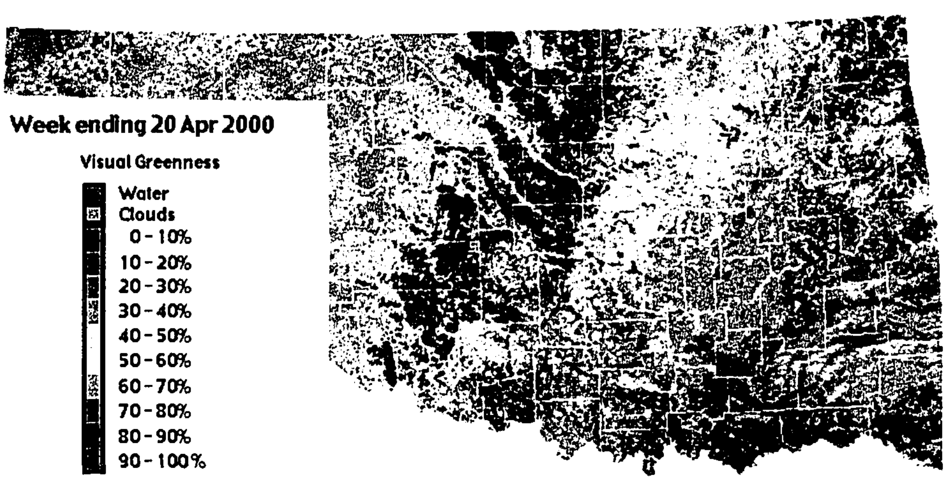


FIGURE 3.10. Visual greenness map from NDVI imagery for the week ending 20 April 2000. Wet or densely vegetated areas appear green, and dry or sparsely vegetated areas appear red to tan. A dark green swath across western and north-central Oklahoma distinctly reveals the extent of Oklahoma's wheat belt.

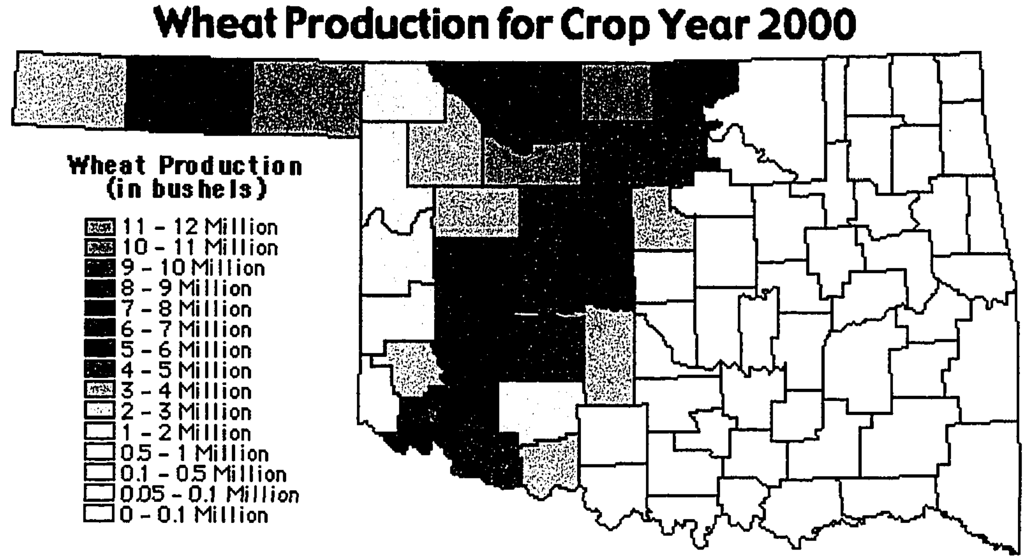


FIGURE 3.11. Map of Oklahoma Wheat County Estimates for Crop Year 2000, based on data from the Oklahoma Agricultural Statistics Service (2001). Purples and dark reds indicate high wheat production; light yellows denote low wheat production.

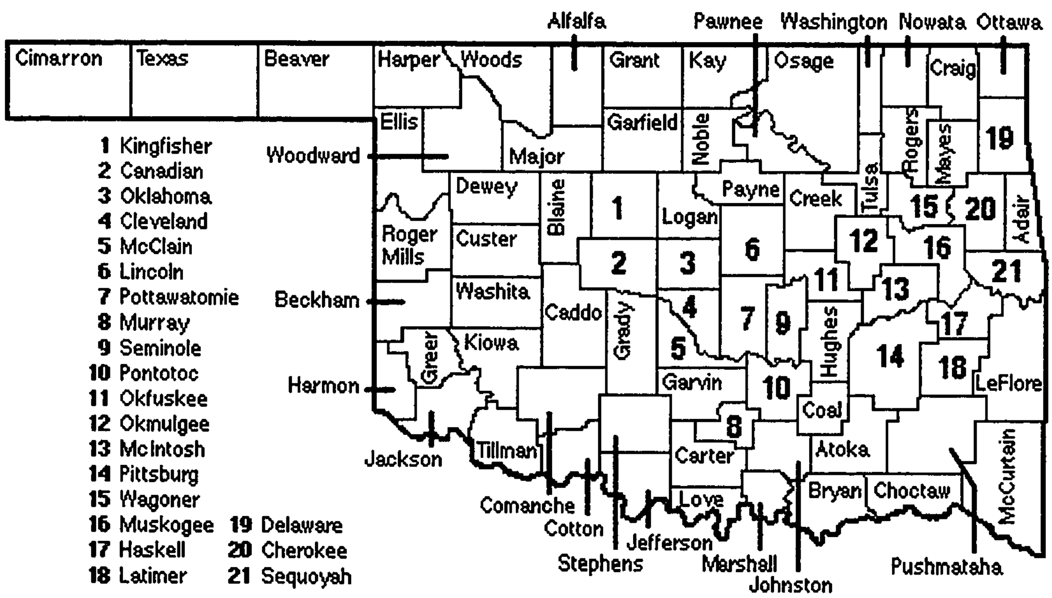


FIGURE 3.12. Oklahoma county names. (Courtesy of the Oklahoma Climatological Survey.)

### 3.5 Other Data Sources

In addition to data from the Oklahoma Mesonet, this study employed thermodynamic vertical profiles of the atmosphere from the Atmospheric Radiation Measurement (ARM) Program (Ackerman and Stokes 2003; Stokes and Schwartz 1994). Part of Oklahoma's winter wheat belt is located within ARM's Cloud and Radiation Testbed, sponsored by the U.S. Department of Energy. As input to the numerical model (discussed in Chapter 4), surface and upper-air observations were utilized from the National Weather Service, an agency of the National Oceanic and Atmospheric Administration.

Surface flux measurements or estimates from the Oklahoma Mesonet and ARM Program, though valuable, were not used in this research. Because Mesonet latent heat fluxes are calculated as residuals in a surface energy balance equation, their magnitudes are influenced significantly by the measured net radiation. Net radiation at Mesonet sites within the wheat belt is measured over natural sod, not growing or harvested wheat. Hence, the residual values of latent heat flux do not represent growing wheat, which is the focus of this work. Similarly, Bowen ratio measurements at ARM facilities represent values over the land use at those particular sites. Because stations are situated primarily on grassland, even within the wheat belt, measurements of Bowen ratio do not represent adequately either the growing or harvested wheat.

# CHAPTER 4: THE NUMERICAL MODEL

Numerical simulations were conducted to investigate which physical processes might generate horizontal differences between the atmosphere over the wheat belt and that over adjacent lands. In addition, simulations were employed to provide insight into how the atmosphere across western Oklahoma differed if the wheat belt were replaced by grasslands.

## 4.1 Overview of the Numerical Model

The National Center for Atmospheric Research (NCAR) – Pennsylvania State University (PSU) mesoscale model was used because of its well established history, its incorporation of land surface parameterizations, and its documented ability to simulate both mesoscale phenomena and land-atmosphere interactions. The Fifth-Generation NCAR / PSU Mesoscale Model (hereafter termed MM5) is a community mesoscale model that has been upgraded from that documented by Anthes and Warner (1978). MM5 is a three-dimensional, limited-area, nonhydrostatic model devised to simulate atmospheric circulations on the mesoscale and regional-scale.

The vertical coordinate, sigma ($\sigma$), is terrain-following and is defined as

$$\sigma = (p - p_{top}) / (p_{sfc} - p_{top}),$$

where p is the pressure, $p_{top}$ is a specified constant pressure at the top of the model domain, and $p_{sfc}$ is the surface pressure. An Arakawa-Lamb B-staggered grid (Arakawa and Lamb 1977) is used in the horizontal. In the vertical, sigma, the horizontal velocity components, and all scalars are defined on each sigma level whereas vertical velocity is defined halfway between sigma levels. A thorough discussion of the model's governing equations is presented by Grell et al. (1994).

MM5 features two-way nesting and can support up to nine interacting domains. Lateral boundary conditions for a given sub-domain are supplied by its mother domain[10]. The boundary values for the main domain are provided by either an analysis, a previous coarser-mesh simulation, or another model's forecast. In this case, boundary values were prescribed by Eta model analyses at 3 h intervals provided by the National Centers for Environmental Prediction (NCEP; NCEP 2000).

Two domains were defined: (1) a mother domain with 175 and 250 grid points in the north/south and east/west directions, respectively, and a 12–km grid spacing and (2) a nested domain with 181 and 151 grid points in the north/south and east/west directions, respectively, and a 4–km grid spacing. Forty sigma levels defined the vertical resolution for both domains, and $p_{top}$ was set to 10000 Pa. To minimize the impact of the lateral boundary of the nested domain, the wheat belt was centered within the higher-resolution domain.

The NCEP Eta model analyses were interpolated to model levels to serve as initial and boundary conditions. NCEP Eta model analyses also provided the initial soil moisture (at 10 and 200 cm) and soil temperature (at 10, 200, and 400 cm) fields. NWS surface and upper air observations and hourly Oklahoma Mesonet data were assimilated into the model to enhance the gridded, first-guess field. All atmospheric analyses and observations were input in pressure coordinates prior to a preprocessing step that converted the pressure-level fields into sigma coordinates.

A suite of physics options is available in MM5. For the mother domain, this study used the Grell cumulus parameterization, which was designed for

[10] The mother domain is the smallest domain in which a given sub-domain is completely embedded.

horizontal grid sizes on the mesoscale (e.g., 10-30 km) and balances explicit and parameterized rainfall. Cumulus parameterization was not permitted within the nested domain. Cloud water, rain water, and ice fields were predicted explicitly with microphysical processes on both domains. Parameterization of the PBL used nonlocal closure from Hong and Pan (1996), a scheme appropriate when high vertical resolution defines the PBL. Longwave and shortwave interactions between cloud and clear-air were computed explicitly. For longwave interactions, the Rapid Radiative Transfer Model of Mlawer et al. (1997) accounted for the absorption spectra of water vapor, carbon dioxide, and ozone.

## 4.2 The Land Surface Module and Surface Characteristics

MM5's version of the Eta Land-Surface Model (LSM; Chen and Dudhia 2001a,b) from Oregon State University and NCEP was activated for all simulations. It provided enhancements to depict land-atmosphere interaction more realistically. The MM5 LSM couples three representations of surface physics: a Penman potential evaporation approach that is diurnally dependent (Mahrt and Ek 1984), a multilayer soil model (Mahrt and Pan 1984), and a primitive canopy model (Pan and Mahrt 1984). Calculations within the canopy are enhanced by the canopy resistance approach of Noilhan and Planton (1989) and Jacquemin and Noilhan (1990). Prognostic variables include soil moisture, soil temperature, and water stored on the canopy. The soil variables are calculated for four soil layers (surface to 10 cm, 10–30 cm, 30–60 cm, and 60–100 cm). Figure 4.1 displays a schematic representation of the model.

For the current study, evaporation of precipitation from canopy plants is negligible; thus, total evaporation is the sum of the direct evaporation from the top soil layer and the transpiration from the plants. A green vegetation fraction partitions the total evaporation between these components. Transpiration is proportional to the vegetation fraction, the potential evaporation, and the inverse of the canopy and air resistances.

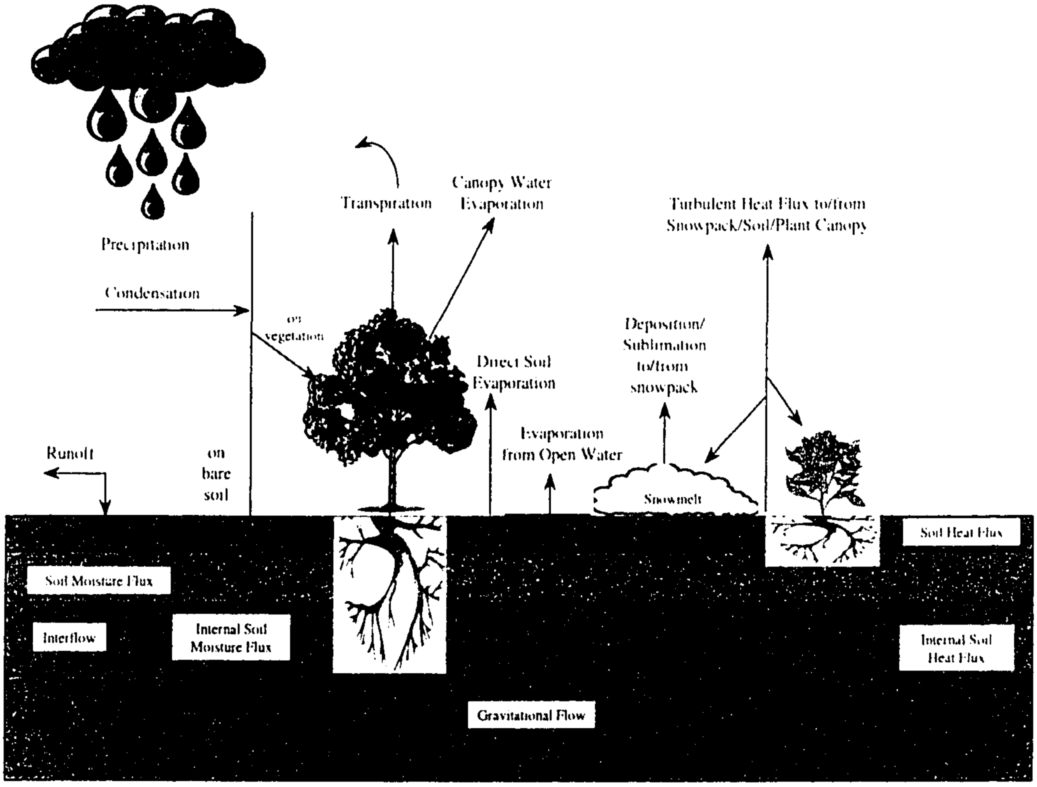


FIGURE 4.1. A schematic representation of the Oregon State University Land Surface Model in the coupled MM5 model (from Chen and Dudhia 2001*a*).

The spatial distribution of land use and soil types prescribed the secondary vegetation and soil parameters, such as albedo, minimum stomatal resistance, thermal inertia, and roughness length. The LSM used an annual-mean surface temperature adjusted to the elevation of the model terrain, a monthly climatological vegetation fraction, and a dominant soil type in each model grid cell. USGS 5-minute (~9 km) and 2-minute (~4 km) gridded data for elevation and land use defined these static fields for the mother domain and the nested domain, respectively. The USGS land use data set had categories for water bodies, snow or ice, urban, and 21 general types of vegetation, including cropland and mixed vegetation. Parameter values depended on only two seasons: winter (15 October – 15 April) and summer (15 April – 15 October).

A 16-point, two-dimensional parabolic fit was employed to interpolate land use, soil type, and vegetation fraction from the latitude/longitude data sets to the mesoscale grid. The parabolic interpolation directly computed the vegetation fraction at the grid point. For land use and soil type, defined by categories, the interpolation calculated the percentage of each category on the grid. When water coverage was greater than 50% at a given grid point, then water was assigned to that point. Otherwise, the category with the largest percentage (excluding water) was assigned to the grid point.

Figures 4.2, 4.3, and 4.4 illustrate the model's initial configuration, using a Lambert Conformal map projection. The location and size of the two model domains are displayed in Fig. 4.2. Figures 4.3 and 4.4 show the gridded terrain and gridded vegetation data, respectively, used for the nested domain. Note that grassland defines a substantial portion of the wheat belt. In addition, the vegetation type for the corn belt across southern Iowa (not shown) is identical to that of Oklahoma's winter wheat belt even though the two crops have remarkably different growing seasons. Section 6.2 will discuss how this region was redefined for this study. Vegetation fraction maps also are shown in Chapter 6.

Mother and Nested Domains for Simulations

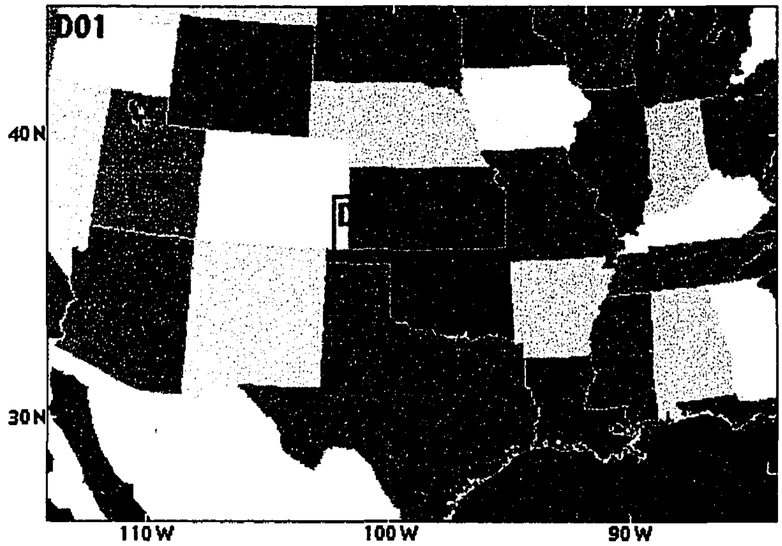


FIGURE 4.2. Map of the mother domain (D01) and nested domain (D02) used in this study. The mother domain comprised 175 and 250 grid points in the north/south and east/west directions, respectively, and a 12-km grid spacing. The nested domain contained 181 and 151 grid points in the north/south and east/west directions, respectively, and a 4-km grid spacing. Color solely delineates state boundaries.

Terrain Height (m)
Above Mean Sea Level

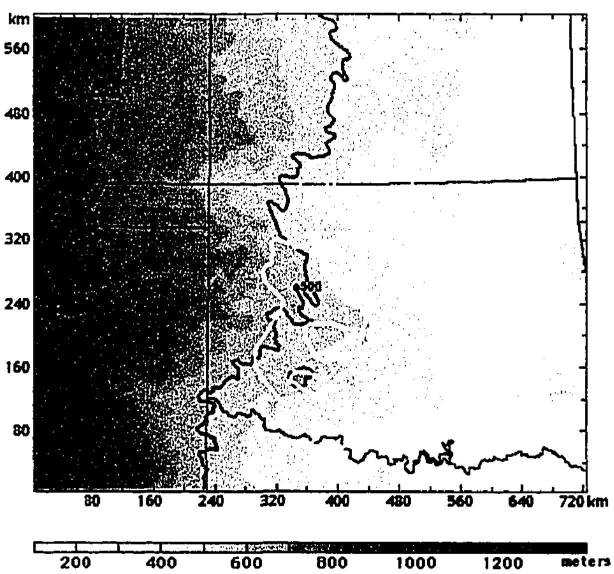


FIGURE 4.3. Representation of the U.S. Geological Survey terrain elevation for the nested domain. Solid black contours denote elevation at intervals of 500 m.

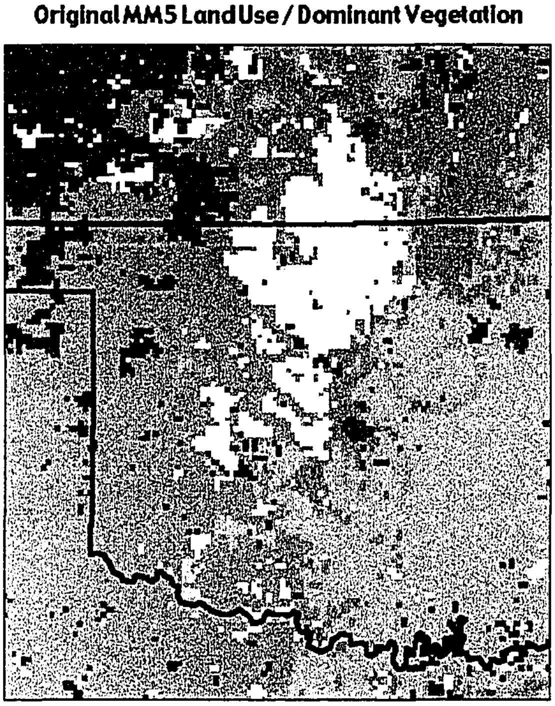


FIGURE 4.4. Representation of the U.S. Geological Survey dominant vegetation categories within the nested domain. Land use categories of interest to this study included "mixed dry/irrigated cropland/pasture" (light yellow), "grassland" (green), and "savanna" (pink). The dataset was derived from satellite measurements and categorized water bodies, snow or ice, urban, and 21 general types of vegetation, including cropland and mixed vegetation.

# CHAPTER 5: RESULTS FROM OBSERVATIONS

Evidence that Oklahoma's winter wheat crop modified the surface layer was noted by scientists at the Oklahoma Climatological Survey during manual quality assurance procedures for Oklahoma Mesonet data. Quality assurance meteorologists reported a swath of anomalously moist, monthly averaged dew points across the growing wheat belt during November and April (Fiebrich and Crawford 2001). A corresponding swath of anomalously warm, monthly averaged air temperatures was noted during July across the harvested wheat belt. Although these anomalies did not occur every year between 1996 and 2001, they pointed to the probability that Oklahoma's wheat belt modified its mesoscale environment.

The following observational analyses of monthly, daily, and instantaneous (i.e., during a given five-minute measurement period) anomalies in the variable fields measured at Oklahoma Mesonet sites were used to quantify the impact of the winter wheat belt on the mesoscale environment. A brief discussion will follow the analyses to condense and overview the results.

## 5.1 Winter Wheat Development

Although wheat was grown across portions of the southern Great Plains during the 1840s, Paulsen (2000) noted that yields typically were poor because the wheat seedlings had been derived from those for mild climates. During the 1870s, however, German Mennonites introduced a hardy variety of wheat to the region. The spread of this hardy wheat ("Turkey Red") advanced during the 1890s as a result of severe winters that killed other wheat varieties. Yet, rapid expansion of the wheat belt across the southern Great Plains did not occur until after the 1920s. By that time, techniques had improved to farm wheat in low moisture soils. In addition, grain drills, reapers, tractors, and the self-propelled combine had been introduced (Paulsen 2000).

The growth stages of winter wheat are as follows: germination (plant development begins), seedling (the first leaf appears), tillering (tillers and secondary root system appear), stem elongation (shoots and tillers stop initiating from the main stem and the stem elongates), booting (the developing head enlarges), heading (the head emerges from under the last leaf), flowering (the head flowers), milk (kernel formation begins), dough (kernel formation ends), and ripening (the seed loses moisture). Tillers present the opportunity for a plant to develop additional stems, with their associated leaves, roots, and head. Germination, seedling, and tillering occur during the autumn, though tillering may continue throughout the winter and early spring for some varieties of wheat. The remaining stages occur during the spring.

The development of winter wheat occurs with a systematic progression that is dependent on the number of heat units, or growing degree days[11], experienced by the plant. The heat units for a given day are calculated using an average of the day's maximum and minimum temperatures from a site nearby the wheat fields. The crop's stage of growth can be determined from the accumulated heat units. For example, between 80 and 100 heat units (depending on the cultivar) are required to produce each leaf on the main stem, 650 heat units are needed to complete the heading and maturation stages, and a total of 2200 heat units are required for winter wheat to reach maturity from planting (Fowler 1993). The development of wheat may be augmented by warmer temperatures, but the risk of damage to the plant also can increase, depending on the growth stage of the crop. For example, heat stress during the stem

[11] Growing degree days are accumulated daily from the date of planting and are computed using the average of the daily maximum and minimum temperatures (in degrees Fahrenheit) minus a base temperature, which is crop dependent.

elongation and booting stages increases the rate of tiller mortality, thus removing the possibility of increased transpiration (Fowler 1993). Similar environmental stress prior to flowering decreases the number of heads and kernels that ripen. In addition, water stress can reduce transpiration (Segal et al. 1988).

During the growing season, evapotranspiration (ET) from wheat does not increase linearly as potential evapotranspiration increases (Musick and Porter 1990). The maturity of the wheat crop has a pronounced effect on the transpiration rate (Segal et al. 1988). The ratio of actual ET to potential ET is greater prior to wheat maturity (i.e., before 2200 heat units have been accumulated), when the plant is developing internal structure. As the formation of wheat kernels ends and leaves become senescent, the ET ratio declines, especially as the plant loses greenness.

The Oklahoma Irrigation Guide (NRCS 1998) of the Natural Resource Conservation Service (NRCS) documents the seasonal cycle and latitudinal variation of evapotranspiration from winter wheat across the state. Table 5.1 outlines the monthly consumptive use of water (i.e., average evapotranspiration by month) in inches at three locations in or near Oklahoma's wheat belt. Altus (34° 38′ N, 99° 20′ W) is located in far southwest Oklahoma, Elk City (35° 25′ N, 99° 24′ W) resides in west-central Oklahoma, and Woodward (36° 26′ N, 99° 24′ W) is in northwest Oklahoma. Plant and harvest dates are averages for the local area.

Note that a fall peak in ET occurs during either October or November, depending on latitude (Table 5.1). The spring peak in ET occurs during April, with ET still significant during May for the two northern locations. By July, all winter wheat has been harvested.

TABLE 5.1. Monthly consumptive use of water (in inches) for winter wheat.

| *Month* | *Altus, OK* Plant Date: Oct. 1 Harvest: Jun. 1 | *Elk City, OK* Plant Date: Oct. 1 Harvest: Jun. 10 | *Woodward, OK* Plant Date: Sep. 15 Harvest: Jun. 15 |
|---|---|---|---|
| September | – | – | 0.98 |
| October | 1.92 | 1.71 | 2.35 |
| November | 2.01 | 1.71 | 1.74 |
| December | 0.80 | 0.67 | 0.62 |
| January | 0.80 | 0 | 0 |
| February | 1.90 | 1.53 | 0.68 |
| March | 3.37 | 2.93 | 2.77 |
| April | 4.26 | 4.52 | 4.78 |
| May | 1.94 | 3.14 | 4.19 |
| June | – | 0.22 | 0.55 |
| Seasonal Totals | 17.01 | 16.43 | 18.67 |

## 5.2 Wheat Development as Inferred from Visual Greenness Maps

As noted earlier, visual greenness maps were employed to infer the extent and maturity of winter wheat across Oklahoma. To coincide with monthly and daily investigations detailed in Sections 5.3 – 5.5, visual greenness maps from the 1999-2000 winter wheat crop year were examined.

Figure 5.1 displays a subset of weekly maps of visual greenness from Winter 1999 through Summer 2000. "Green-up" of the winter wheat fields commenced at the end of October 1999 (Figs. 5.1*a*,*b*) and was followed by rapid crop growth during November (Fig. 5.1*c*). Crop dormancy began during December (Fig. 5.1*d*); the crop's visual greenness slowly decreased from December 1999 through February 2000 (Figs. 5.1*d*,*e*,*f*). Green-up rapidly recommenced during early March (Fig. 5.1*g*); visual greenness values steadily increased to a maximum during mid-April (Fig. 5.1*h*). By early May, wheat became senescent and other species of vegetation started to grow (Fig. 5.1*i*), masking the boundaries of the wheat belt. A minimum in visual greenness values across the wheat belt became noticeable during late May (Fig. 5.1*j*), coincident with the onset of the harvest of

Oklahoma's winter wheat. By June, the disappearance of growing wheat was manifest by a distinct minimum in visual greenness (not shown). Except for the growth of other species near several river beds that cross the wheat belt, growing vegetation within the wheat belt remained sparse throughout the summer (Figs. 5.1*k*,*l*).

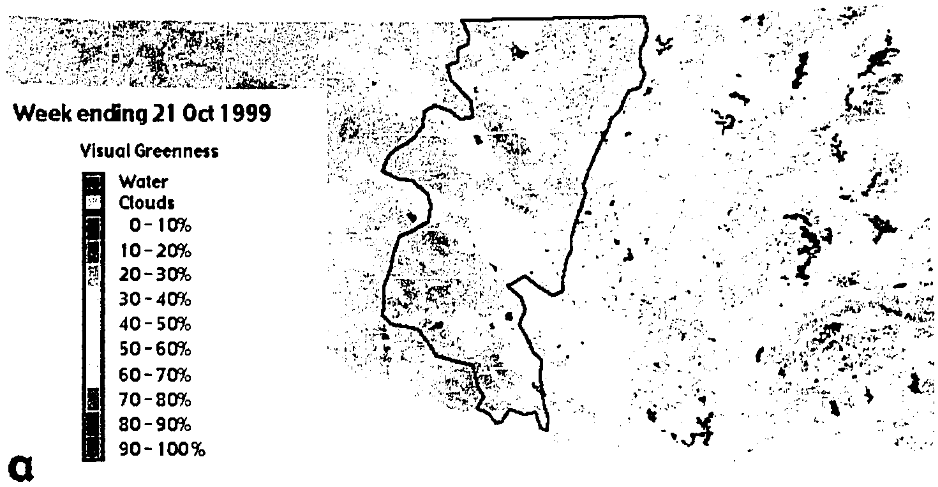


FIGURE 5.1*a*. Map of visual greenness for the week ending 21 October 1999. Wet or densely vegetated areas appear green, and dry or sparsely vegetated areas appear red to tan. The black outline represents the boundary of Oklahoma's winter wheat belt.

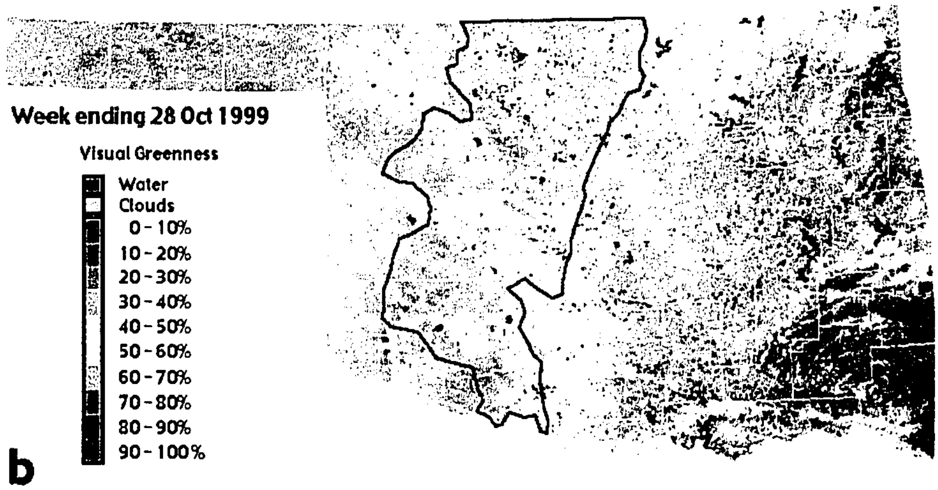


FIGURE 5.1*b*. Same as Fig. 5.1*a* except for the week ending 28 October 1999.

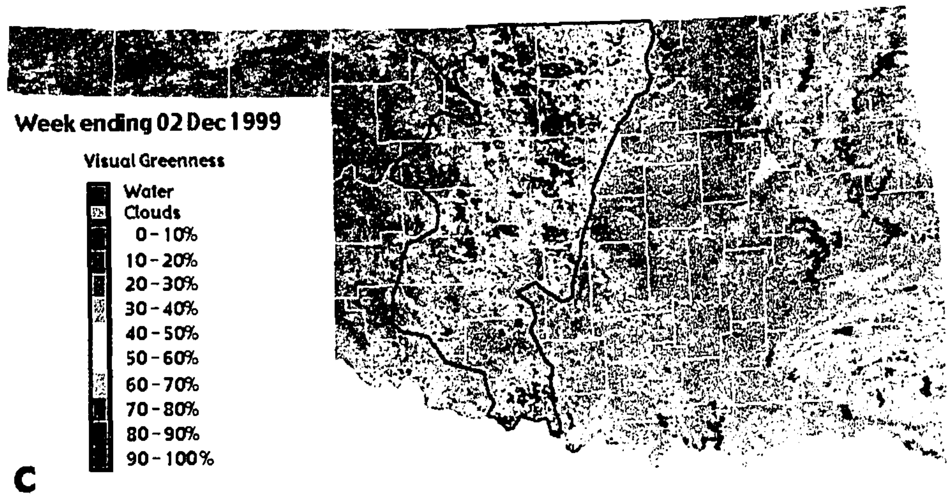


FIGURE 5.1*c*. Same as Fig. 5.1*a* except for the week ending 2 December 1999. The black outline represents the boundary of Oklahoma's winter wheat belt.

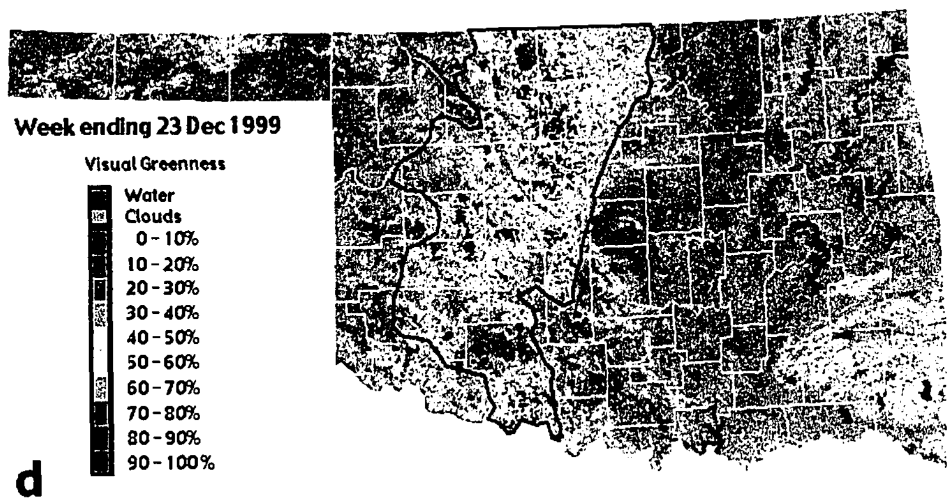


FIGURE 5.1*d*. Same as Fig. 5.1*a* except for the week ending 23 December 1999.

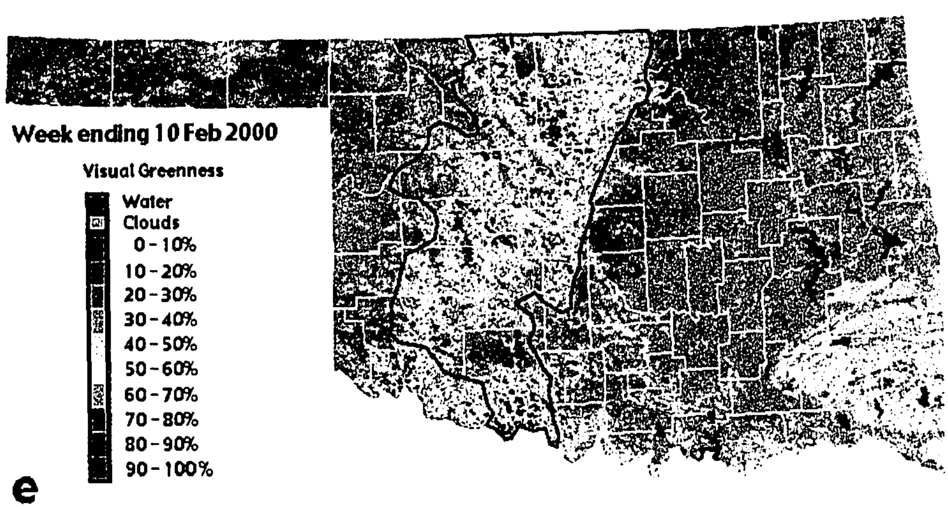


FIGURE 5.1*e*. Same as Fig. 5.1*a* except for the week ending 10 February 2000.

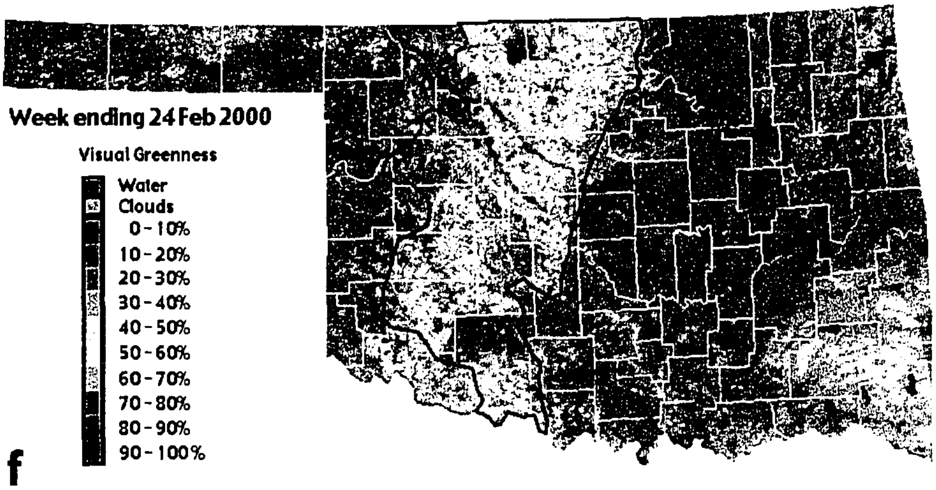


FIGURE 5.1*f*. Same as Fig. 5.1*a* except for the week ending 24 February 2000. The black outline represents the boundary of Oklahoma's winter wheat belt.

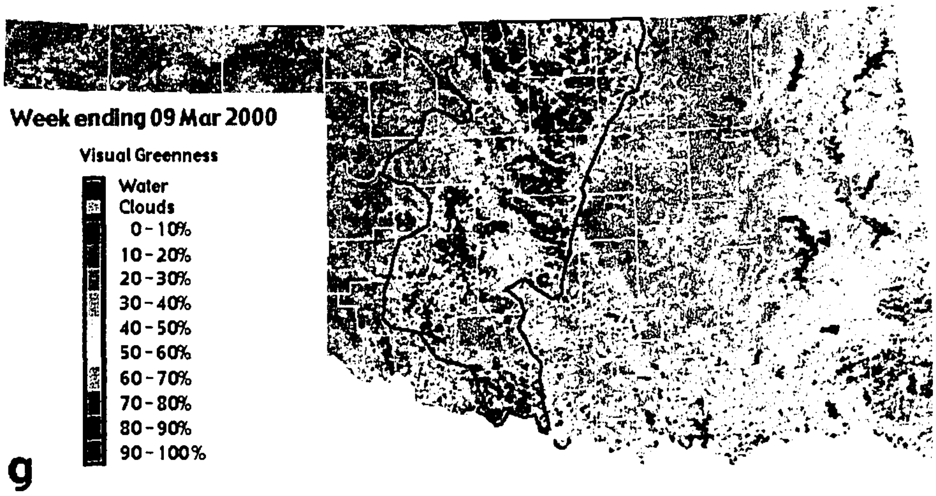


FIGURE 5.1*g*. Same as Fig. 5.1*a* except for the week ending 9 March 2000.

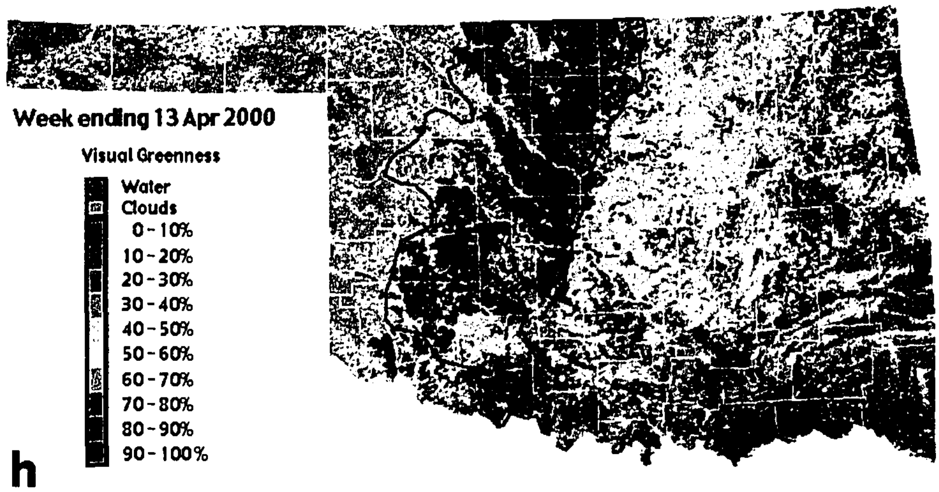


FIGURE 5.1*h*. Same as Fig. 5.1*a* except for the week ending 13 April 2000.

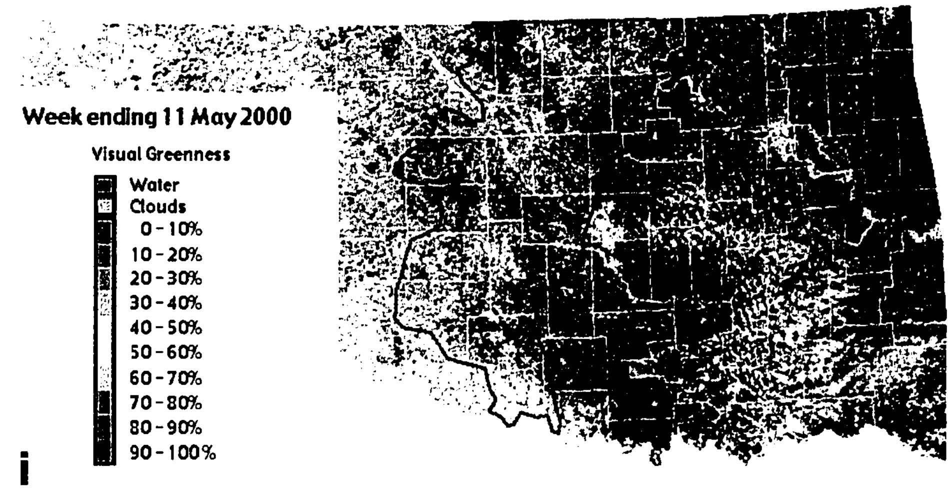


FIGURE 5.1*i*. Same as Fig. 5.1*a* except for the week ending 11 May 2000. The black outline represents the boundary of Oklahoma's winter wheat belt.

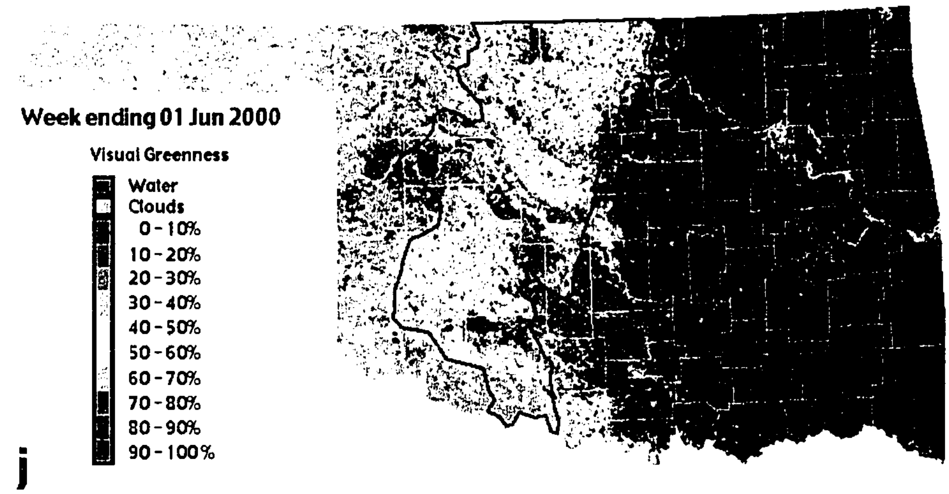


FIGURE 5.1*j*. Same as Fig. 5.1*a* except for the week ending 1 June 2000.

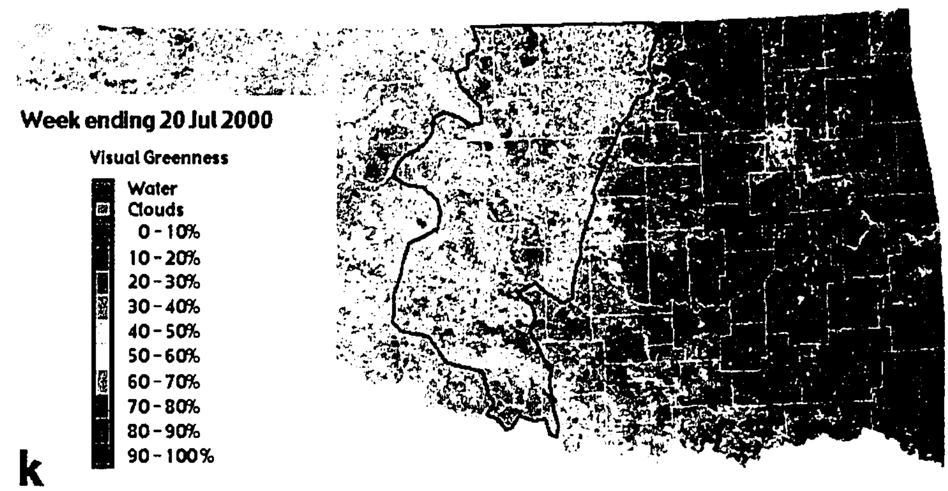


FIGURE 5.1*k*. Same as Fig. 5.1*a* except for the week ending 20 July 2000.

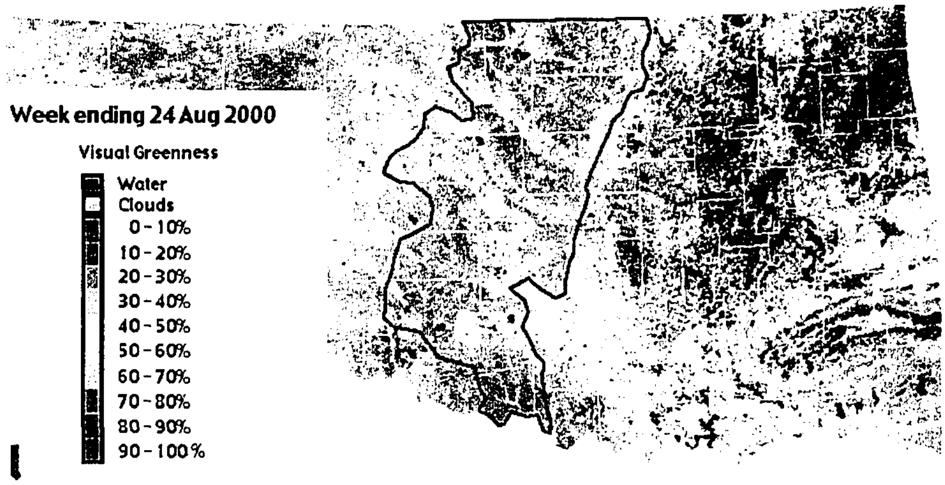


FIGURE 5.1*l*. Same as Fig. 5.1*a* except for the week ending 24 August 2000. The black outline represents the boundary of Oklahoma's winter wheat belt.

## 5.3 Monthly Anomalies

To determine whether Oklahoma's wheat belt significantly altered the mesoscale environment, monthly averages of several variables were calculated at every Mesonet site. If the wheat belt's influence occurred rarely (e.g., on days with unusual environmental conditions), then monthly averages should not reveal a distinct pattern of change across the wheat belt. If, however, the wheat belt frequently or continually affected its environment, then its location should be evident in the monthly averaged data.

### *5.3.1 Monthly Averaged Data from the Oklahoma Mesonet*

For this study, TMAX, TMIN, and TAVG were defined as the maximum, minimum, and average daily air temperatures (in °C), respectively. Similarly, DMAX, DMIN, and DAVG were the maximum, minimum, and average daily dew points (in °C), respectively. In addition, HMAX was the maximum daily relative humidity (in percent), and VDEF was the average daily vapor deficit (in hPa). All derived variables were applicable at 1.5 m above ground and were calculated for midnight to midnight Central Standard Time (CST; CST = UTC – 6 h). A one-pass Barnes analysis (Barnes 1964) was employed to obtain gridded data for contour maps (e.g., Figs. 5.2 – 5.6).

A distinct minimum (i.e., thermal trough) in the values of monthly averaged TMAX was colocated with the winter wheat belt during November (Fig. 5.2*a*), a month previously noted to be a period of rapid wheat growth. From 1994 through 2001 (not shown), a minimum consistently appeared in maps of monthly averaged TMAX for November. Monthly averaged values of TMAX for the period of December 1999 through April 2000 (Figs. 5.2*b–f*) displayed a similar cool bias over the dormant or growing wheat. The most pronounced latitudinal gradient of TMAX values across the wheat belt (about 1-1.5°C over 80-100 km) occurred across north-central Oklahoma, including Grant, Garfield, and Alfalfa counties. These same counties recorded the highest wheat production during Crop Year 2000 (Fig. 3.11).

During May 2000, TMAX values across Oklahoma no longer exhibited a distinct cool anomaly (Fig. 5.2*g*). As demonstrated earlier, May was identified as the month when other vegetative species greened rapidly statewide (Fig. 5.1*i*). By June 2000, the month when the wheat harvest concluded (Fig. 5.1*j*), a warm anomaly had developed (Fig. 5.2*h*) and remained evident in the data through July (Fig. 5.2*i*) and August (Fig. 5.2*j*). Although the July warm anomaly persisted from year to year, the TMAX pattern during August typically was disorganized (not shown). During August, vegetation became senescent or was consumed by cattle across the western half of Oklahoma. Monthly averaged values of TMAX during September and October 2000 (not shown) did not reveal any definitive anomaly across the wheat belt.

The characteristic patterns indicated by the maps of monthly averaged TMAX also were apparent in maps of monthly averaged TAVG for Crop Year 2000 (not shown), though the magnitude of all anomalies was reduced for the monthly averages of TAVG. Monthly averaged values of TMIN (not shown) exhibited the marriage of a latitudinal temperature gradient (i.e., temperature increased as latitude decreased) and an elevation gradient (i.e., temperature increased as elevation decreased). Hence, the warmest monthly averaged values of TMIN occurred across southeast Oklahoma, corresponding to the lowest elevation and the most southern latitude in Oklahoma.

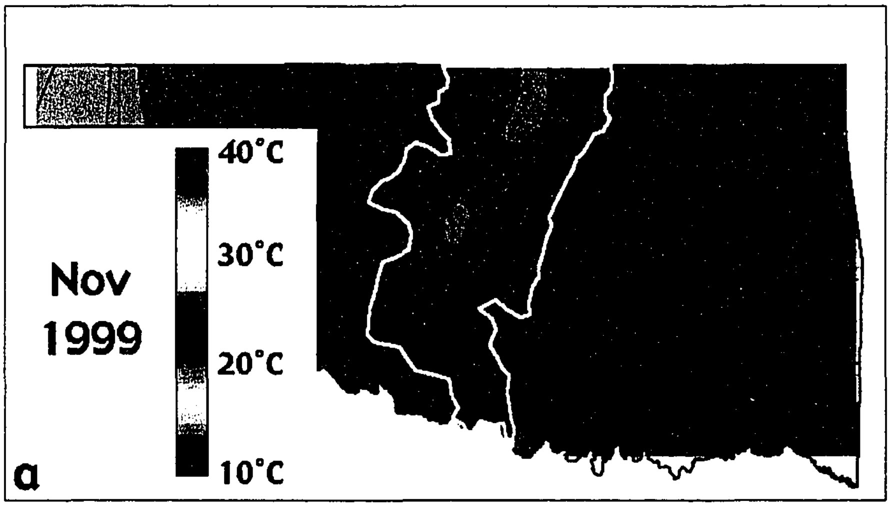


FIGURE 5.2*a*. Map of the monthly averaged values of TMAX (maximum daily air temperature) during November 1999. The white outline represents the boundary of Oklahoma's winter wheat belt. Thick black lines denote isotherms at intervals of 1°C.

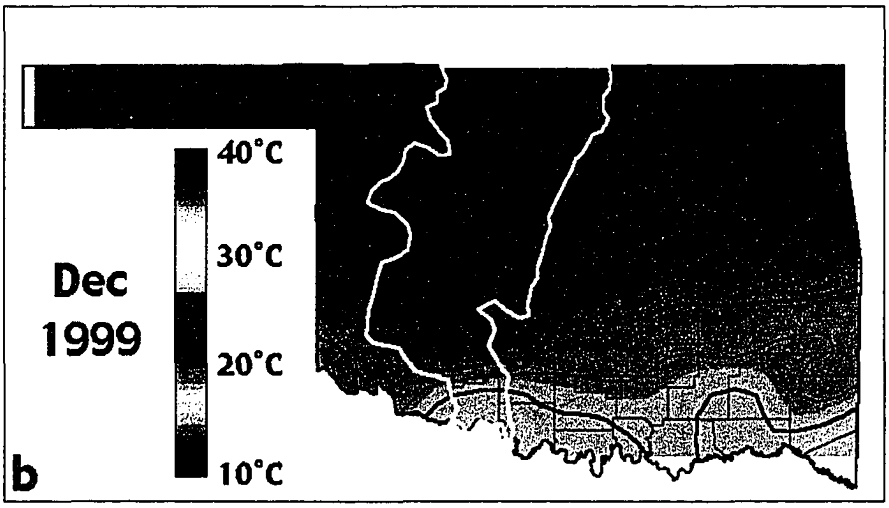


FIGURE 5.2*b*. Same as Fig. 5.2*a* except for December 1999.

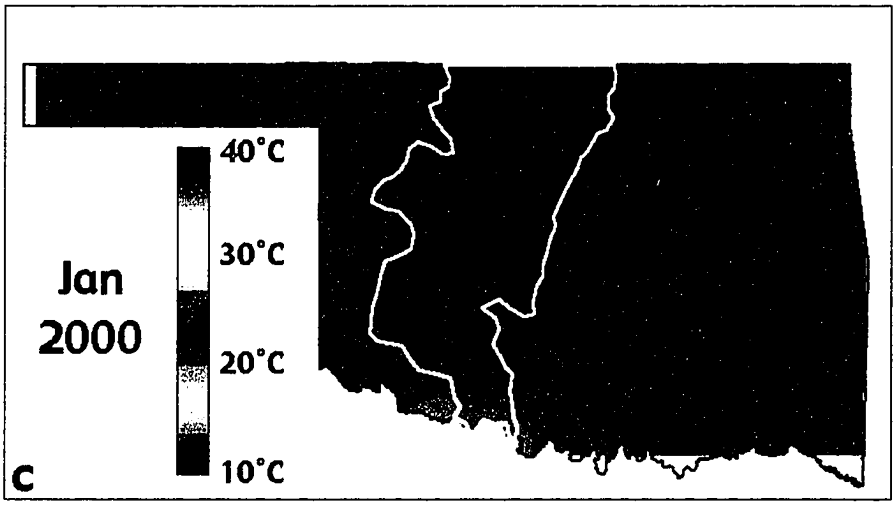

FIGURE 5.2*c*. Same as Fig. 5.2*a* except for January 2000. The white outline represents the boundary of Oklahoma's winter wheat belt.

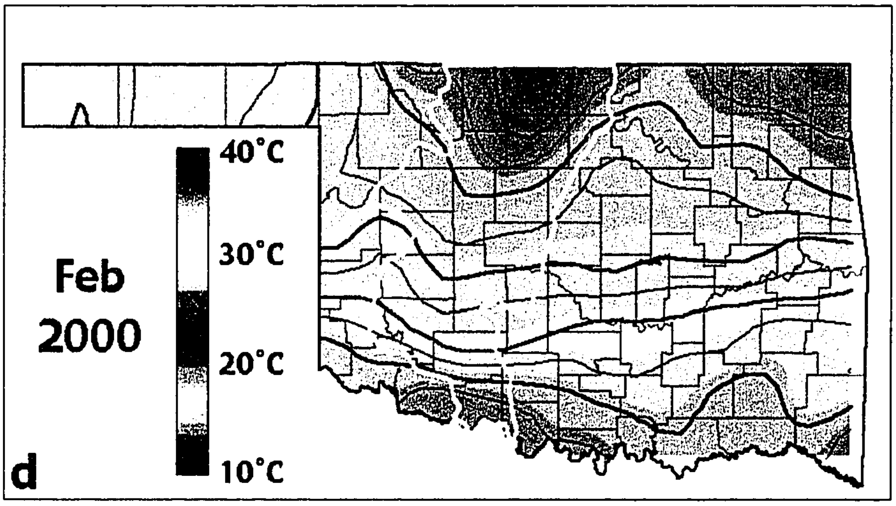

FIGURE 5.2*d*. Same as Fig. 5.2*a* except for February 2000.

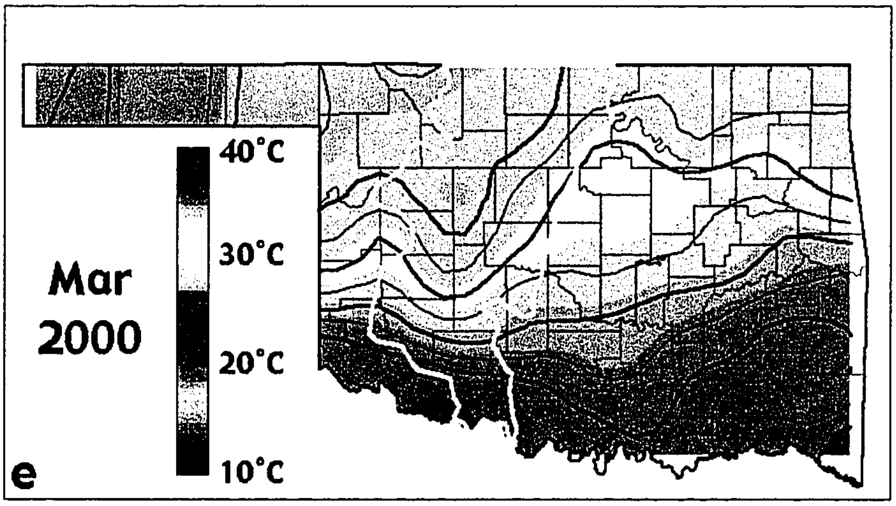

FIGURE 5.2*e*. Same as Fig. 5.2*a* except for March 2000.

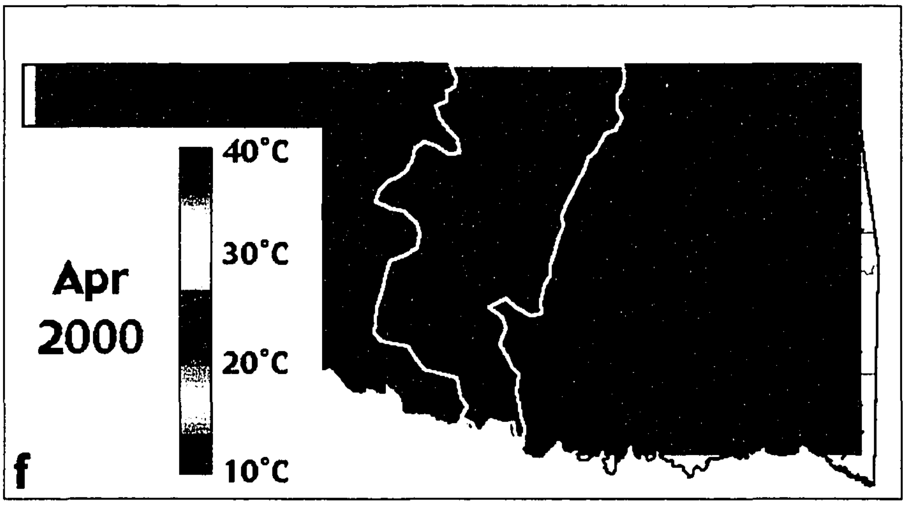

FIGURE 5.2*f*. Same as Fig. 5.2*a* except for April 2000. The white outline represents the boundary of Oklahoma's winter wheat belt.

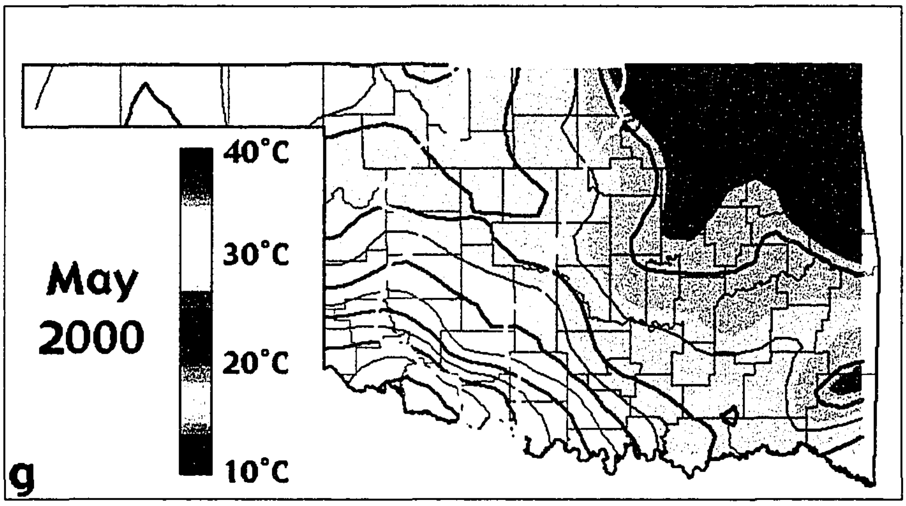

FIGURE 5.2*g*. Same as Fig. 5.2*a* except for May 2000.

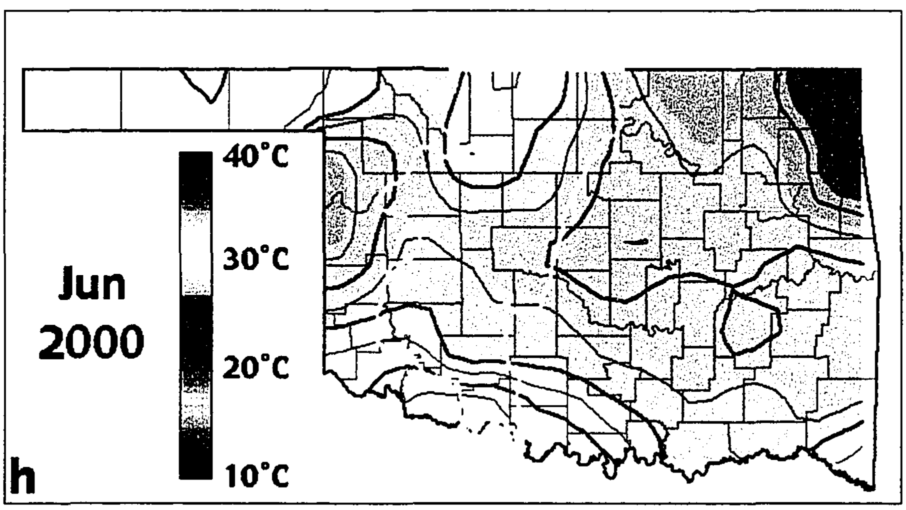

FIGURE 5.2*h*. Same as Fig. 5.2*a* except for June 2000.

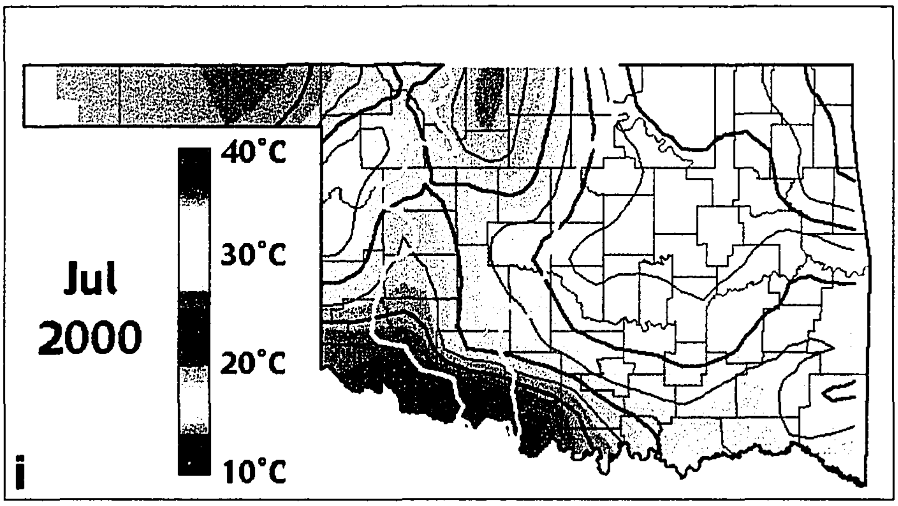

FIGURE 5.2*i*. Same as Fig. 5.2*a* except for July 2000. The white outline represents the boundary of Oklahoma's winter wheat belt.

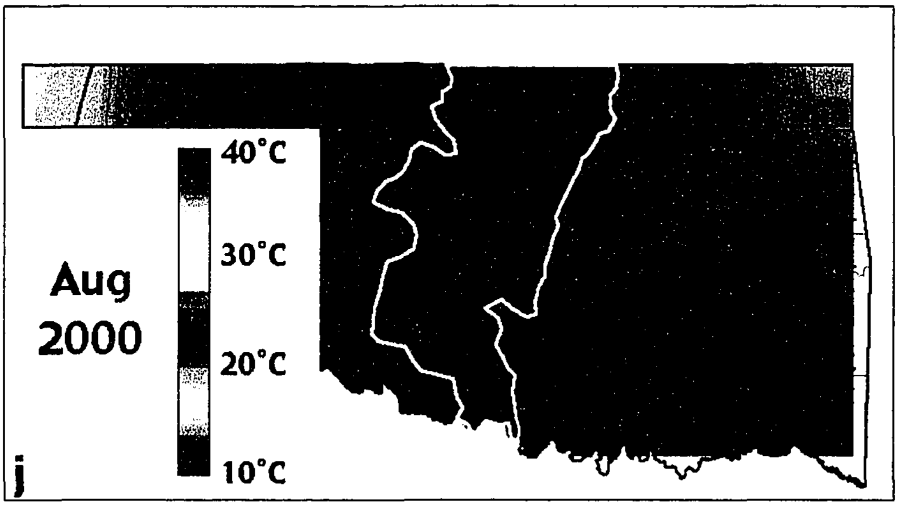

FIGURE 5.2*j*. Same as Fig. 5.2*a* except for August 2000.

The monthly averaged values of TMAX for the period November 1999 through April 2000 were consistent with previous studies that disclosed that an increase in living vegetation created cooler maximum temperatures (Anthes 1984). Analogous results indicating that increased foliage was associated with increased minimum temperatures were not apparent in the TMIN data for Crop Year 2000. Previous studies also noted an increase in relative and specific humidities over living vegetation (e.g., Schwartz 1992). HMAX (daily maximum relative humidity) values averaged using data from April 2000 (Fig. 5.3) seemed to confirm these findings. A comparison of the HMAX map with visual greenness for the week ending 18 April 2000 (Fig. 5.1*h*) illustrated that where vegetation was dense, relative humidities were maximized and where vegetation was sparse, dead, or senescent, relative humidities were minimized.

The relationship between the surface-level moisture field and the growth of winter wheat was observed using monthly averaged values of DMAX during Crop Year 2000. A slight moist bias existed over Oklahoma's wheat belt between November and April (Figs. 5.4*a–d*). During May (Fig. 5.4*e*), the statewide pattern began to be characterized by a predominantly east-west gradient, attained by July (Fig. 5.4*f*). This meridional pattern continued through September 2000 (not shown).

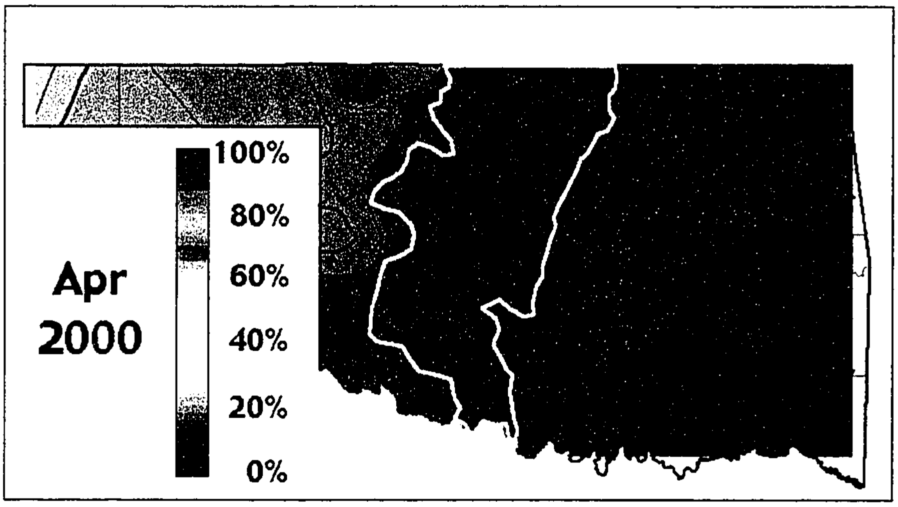


FIGURE 5.3. Map of the monthly averaged values of HMAX (maximum daily relative humidity) during April 2000. The white outline represents the boundary of Oklahoma's winter wheat belt.

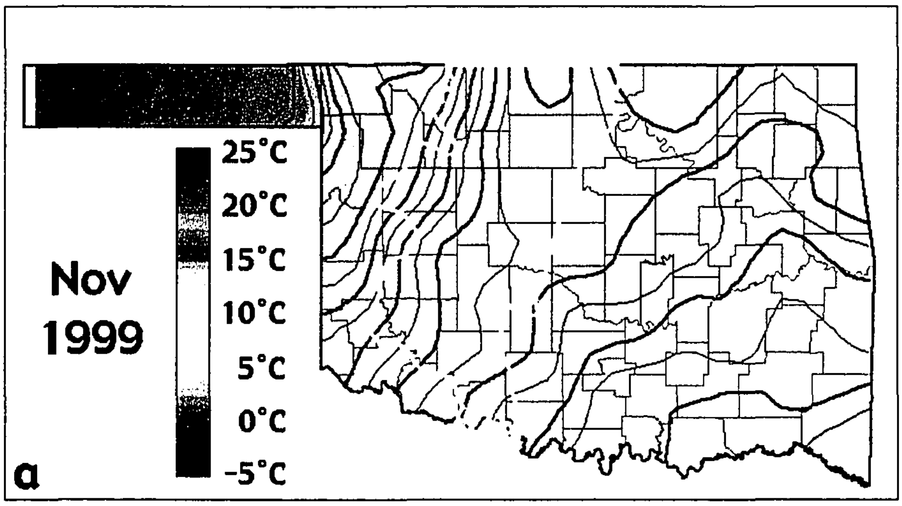

FIGURE 5.4*a*. Map of the monthly averaged values of DMAX (maximum daily dew point) during November 1999. The white outline represents the boundary of Oklahoma's wheat belt. Thick black lines denote isopleths at intervals of 1°C.

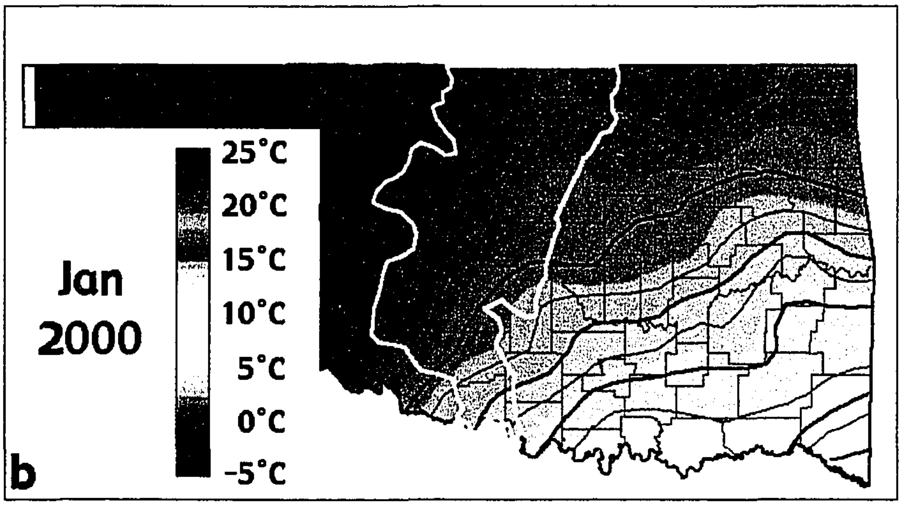

FIGURE 5.4*b*. Same as Fig. 5.4*a* except for January 2000.

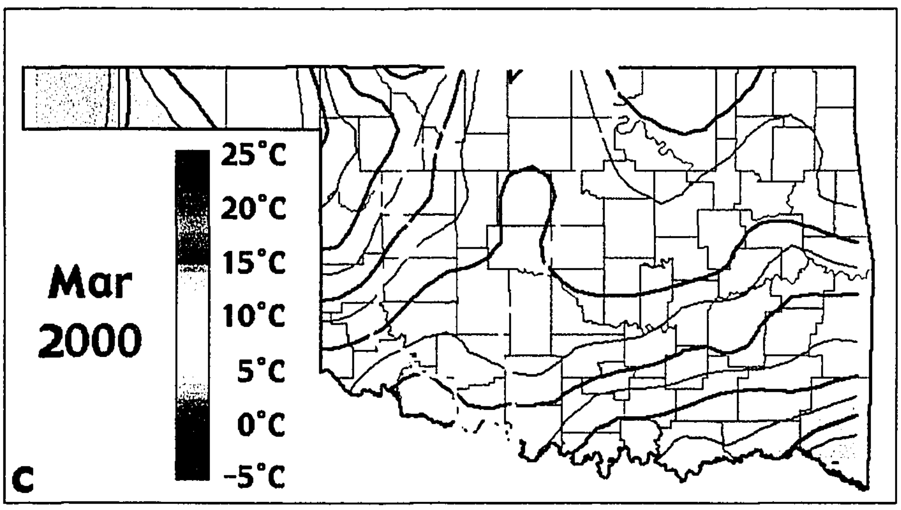

FIGURE 5.4*c*. Same as Fig. 5.4*a* except for March 2000.

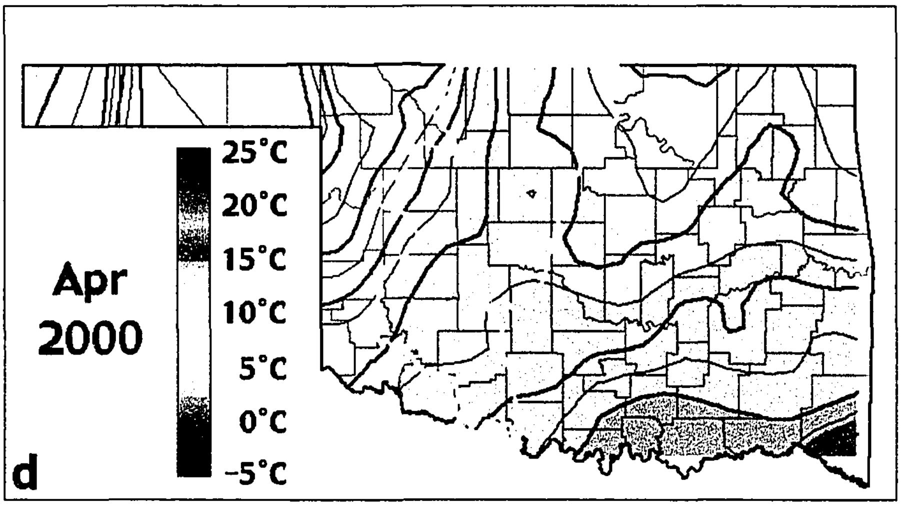

FIGURE 5.4*d*. Same as Fig. 5.4*a* except for April 2000. The white outline represents the boundary of Oklahoma's winter wheat belt.

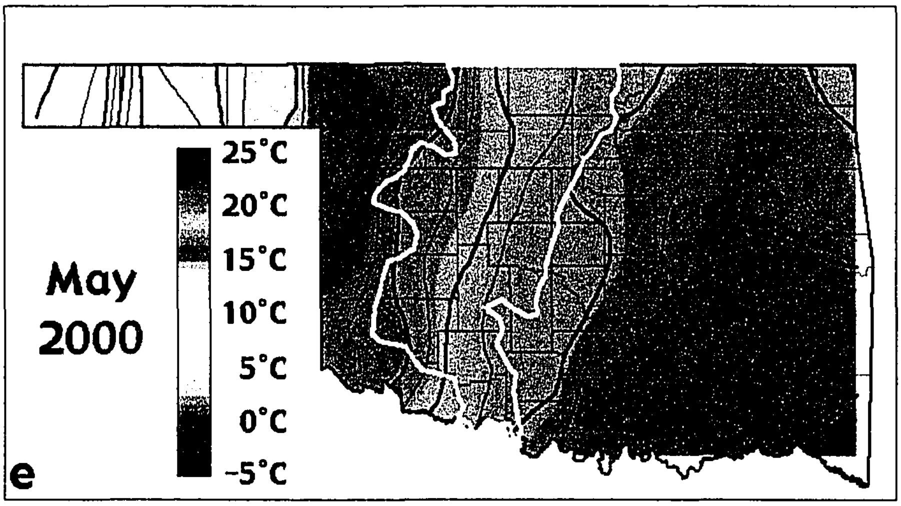

FIGURE 5.4*e*. Same as Fig. 5.4*a* except for May 2000.

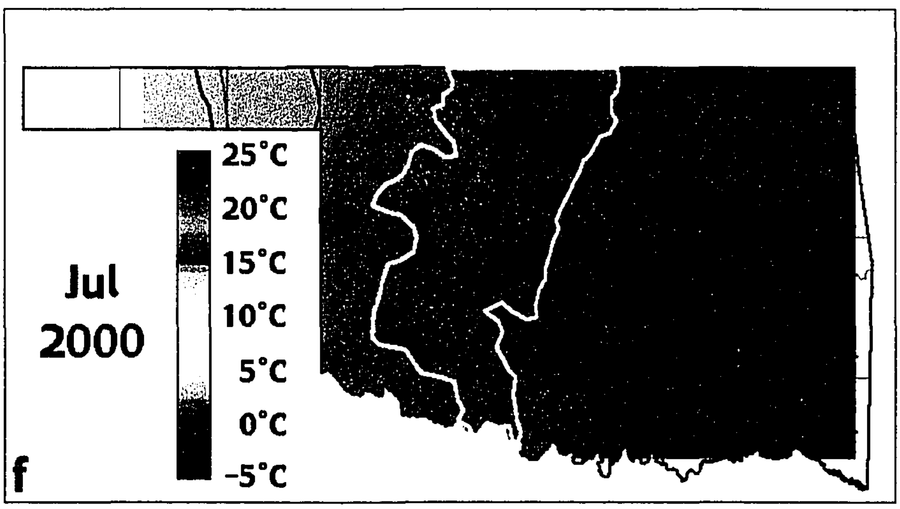

FIGURE 5.4*f*. Same as Fig. 5.4*a* except for July 2000.

An enhancement of DMAX values occurred across the wheat belt every year during April from 1995 to 2001 (Fig. 5.5). Although its intensity varied from year to year, the moist anomaly over the wheat belt was most evident across the northern half of the wheat belt. In addition, a relative minimum of DMAX existed east of the wheat belt along the Oklahoma-Kansas border and enhanced the appearance of the moist anomaly (e.g., Fig. 5.4*d*). Monthly averaged values of VDEF (daily average vapor deficit) for April 2000, April 1999, and April 1997 (Fig. 5.6) also exhibited a minimum over Oklahoma's winter wheat crop.

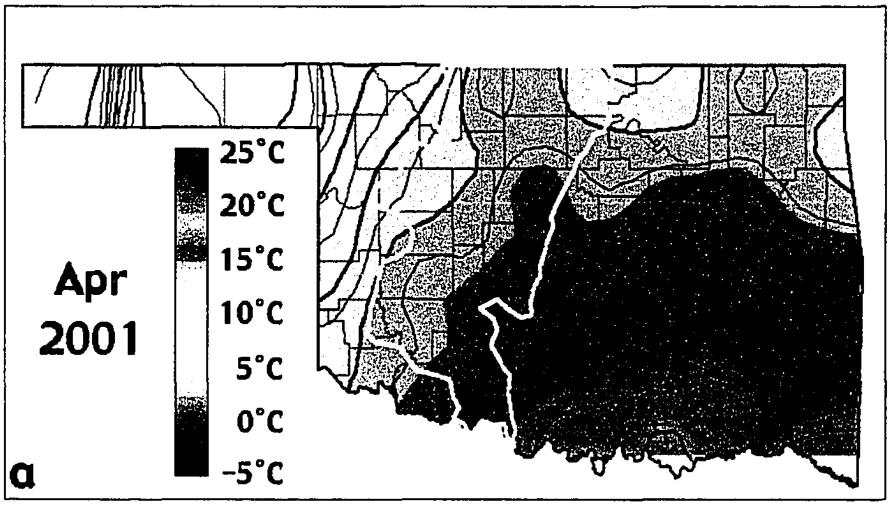


FIGURE 5.5*a*. Map of the monthly averaged values of DMAX (maximum daily dew point) during April 2001. The white outline represents the boundary of Oklahoma's winter wheat belt.

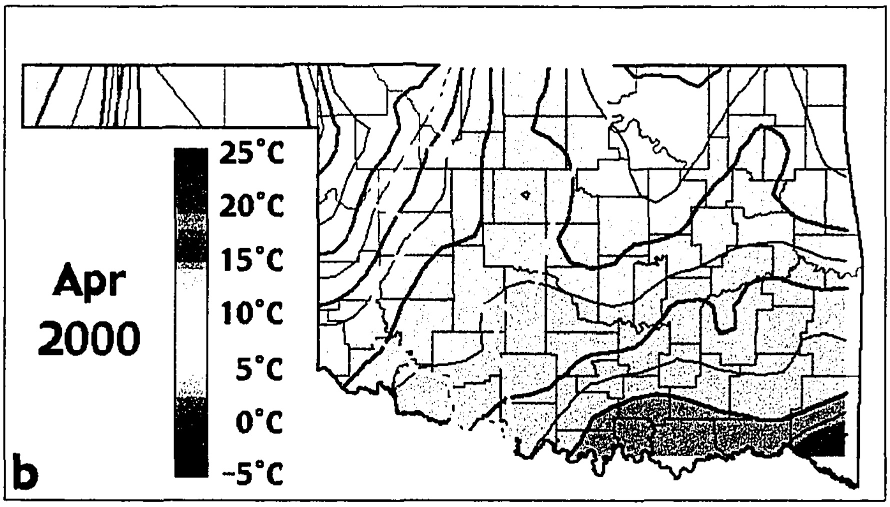


FIGURE 5.5*b*. Same as Fig. 5.5*a* except for April 2000.

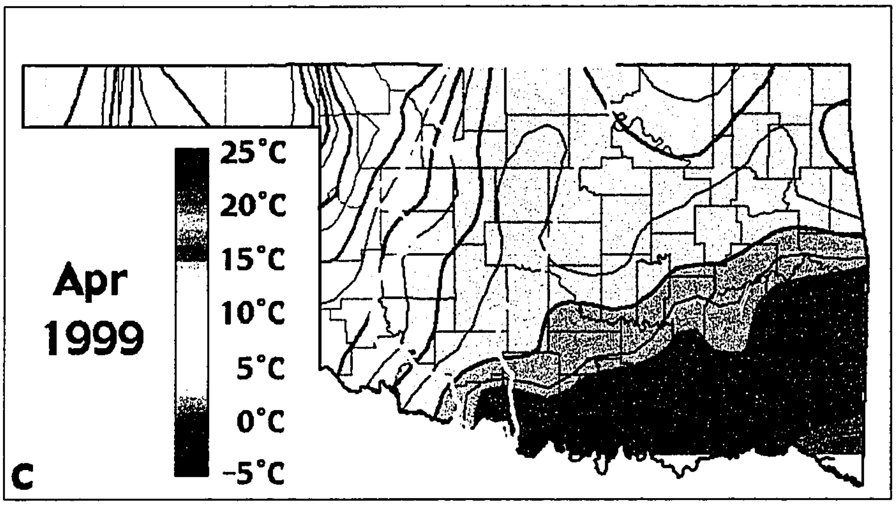


FIGURE 5.5*c*. Same as Fig. 5.5*a* except for April 1999. The white outline represents the boundary of Oklahoma's winter wheat belt.

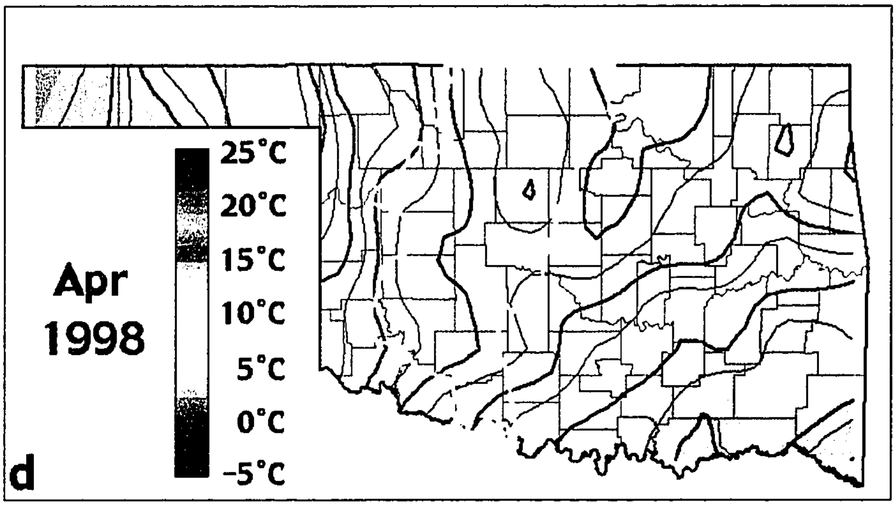


FIGURE 5.5*d*. Same as Fig. 5.5*a* except for April 1998.

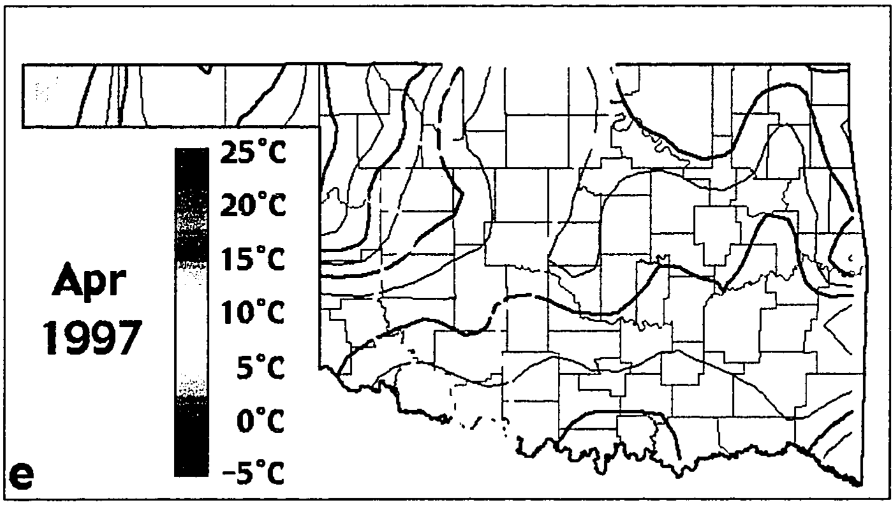


FIGURE 5.5*e*. Same as Fig. 5.5*a* except for April 1997.

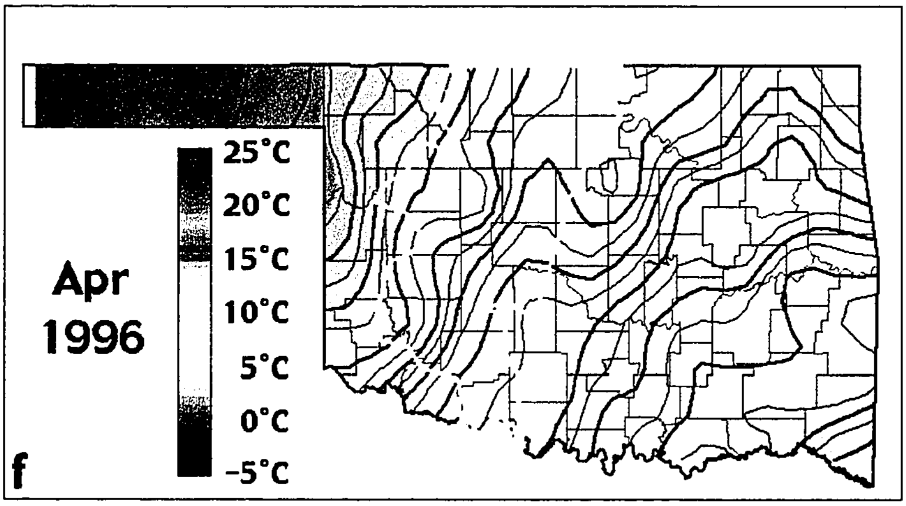


FIGURE 5.5*f*. Same as Fig. 5.5*a* except for April 1996. The white outline represents the boundary of Oklahoma's winter wheat belt.

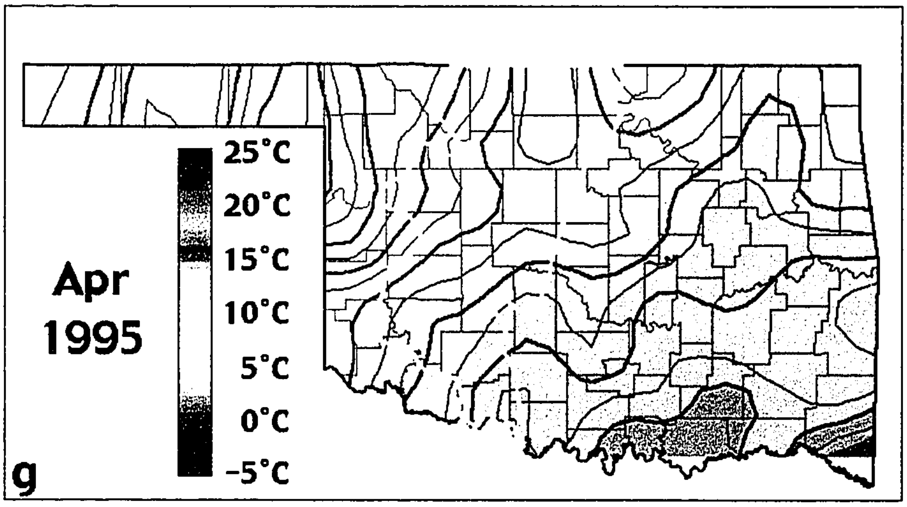


FIGURE 5.5*g*. Same as Fig. 5.5*a* except for April 1995.

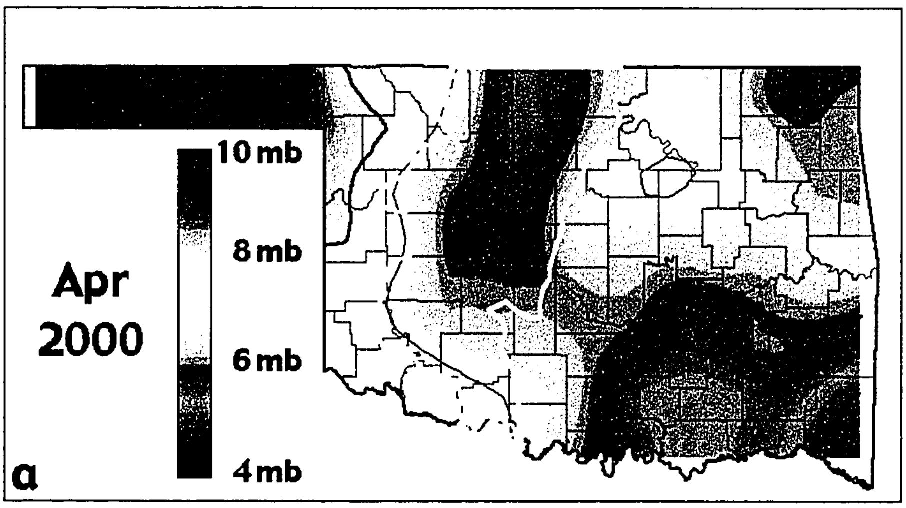


FIGURE 5.6*a*. Map of the monthly averaged values of VDEF (average vapor deficit) during April 2000. The white outline represents the boundary of Oklahoma's winter wheat belt.

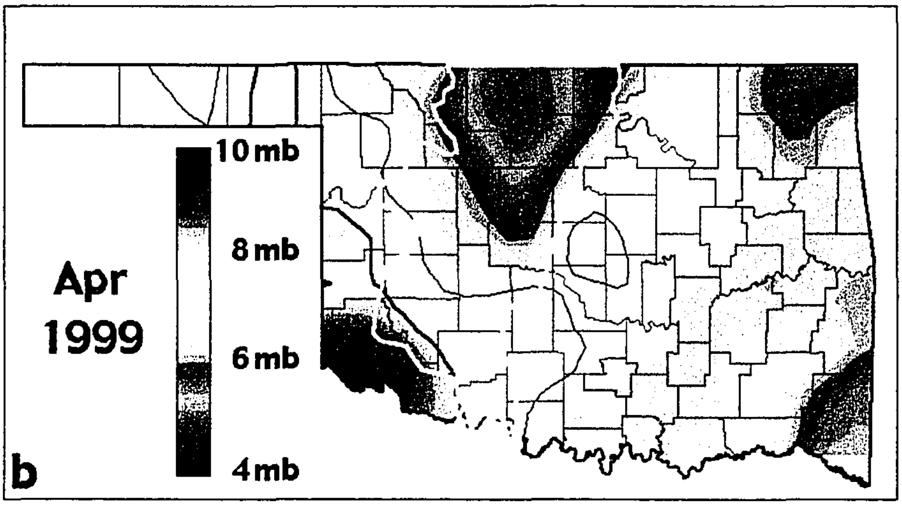

FIGURE 5.6*b*. Same as Fig. 5.6*a* except for April 1999. The white outline represents the boundary of Oklahoma's winter wheat belt.

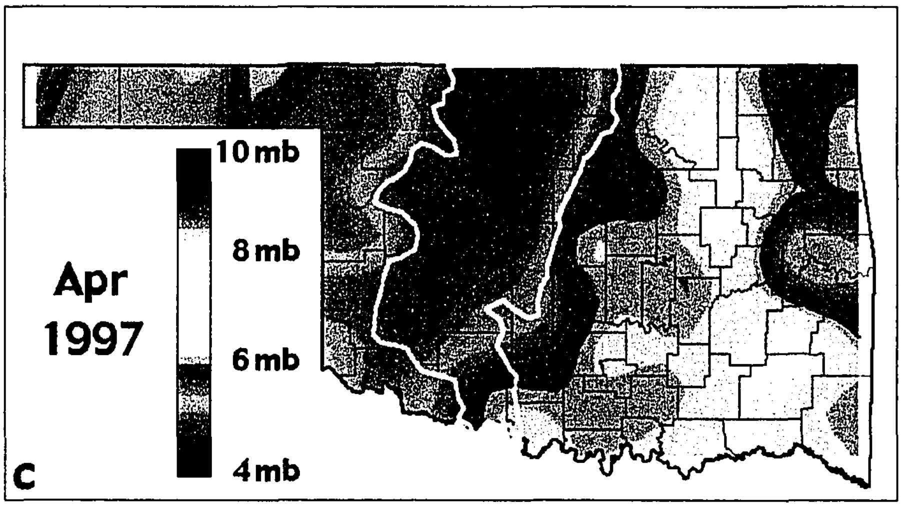

FIGURE 5.6*c*. Same as Fig. 5.6*a* except for April 1997.

### *5.3.2 Statistical Analysis for 1994–2001*

A statistical analysis was used to determine whether the patterns detected in the examination of the statewide maps (Section 5.2.1) were statistically significant. For this analysis, a west-to-east swath was defined from the eastern Panhandle to Osage County, encompassing the primary wheat-producing counties of the state. This swath was divided into three regions, and Mesonet stations within the swath were assigned to a region. From west to east, the regions were labeled "West", "Wheat", and "East" and represented Oklahoma's northwestern grasslands, northern wheat belt, and eastern mixture of grasslands and hardwood forest, respectively. Although care was taken to minimize numeric and latitudinal differences between each region, "West" contained only six sites at an average latitude of 36° 36′ N as compared to 11 sites averaging 36° 18′ N for "Wheat" and 11 sites averaging 36° 22′ N for "East". The average elevation was 626 m above sea level for "West", 402 m for "Wheat", and 301 m for "East". Table 5.2 lists the Mesonet sites assigned to each region, and Fig. 5.7 displays their locations.

Of the six "West" sites, four were located within the region defined as mixed-grass – eroded plains and two were sited within shortgrass – high plains (Fig. 3.6). Recall, also, that the Buffalo and Freedom Mesonet sites were situated near wheat fields (Section 3.3). Hence, the inclusion of these sites within "West" served to test the statistical significance of the results more stringently. Of the 11 "Wheat" sites, 10 were located in the region defined as tallgrass prairie and one was sited within mixed-grass – eroded plains. Of the 11 "East" sites, seven were located in the region defined as post oak – blackjack oak and four were sited within tallgrass prairie.

TABLE 5.2. Mesonet sites assigned to three regions for statistical analysis.

| *West* | *Wheat* | *East* |
|---|---|---|
| Arnett (ARNE) | Blackwell (BLAC) | Burbank (BURB) |
| Buffalo (BUFF) | Breckinridge (BREC) | Foraker (FORA) |
| Freedom (FREE) | Cherokee (CHER) | Guthrie (GUTH) |
| May Ranch (MAYR) | Fairview (FAIR) | Marena (MARE) |
| Slapout (SLAP) | Kingfisher (KING) | Newkirk (NEWK) |
| Woodward (WOOD) | Lahoma (LAHO) | Oilton (OILT) |
| | Marshall (MARS) | Pawnee (PAWN) |
| | Medford (MEDF) | Red Rock (REDR) |
| | Putnam (PUTN) | Skiatook (SKIA) |
| | Seiling (SEIL) | Stillwater (STIL) |
| | Watonga (WATO) | Wynona (WYNO) |

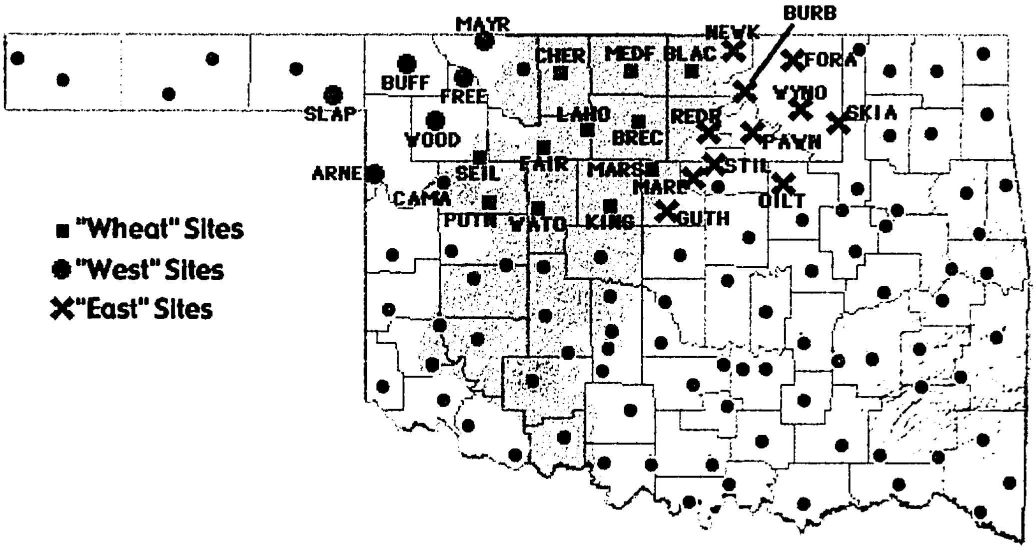


FIGURE 5.7. Location of Mesonet sites selected for statistical analysis. Sites belonging to "Wheat" are green squares. Those representing "West" and "East" are red circles and dark blue X's, respectively. The shaded region (violet) represents Oklahoma's winter wheat belt. Four-letter identifiers for selected Mesonet sites are displayed near the corresponding site location.

For this analysis, the null hypothesis stated that the wheat belt did not influence the near-surface conditions and, hence, the three regions represented the same population. To try the null hypothesis, the Wilcoxon signed-rank test was implemented. The Wilcoxon signed-rank test (Wilks 1995) does not assume that any probability distribution adequately represents the data. The test was executed individually for each month from November through August for nine variables: TMAX, TMIN, TAVG, DMAX, DMIN, DAVG, and VDEF as well as for total daily solar radiation and total daily rainfall. Mesonet data from 1994 through 2001 were used such that any extreme during a specific year (e.g., drought) was tempered by data from seven other years. As a result, the sample size $n$ equaled 224 for February, 240 for April, June, and November, and 248 for January, March, May, July, August, and December.

For month M and variable V, a daily mean was calculated for each region $r$ using V measured at the assigned sites. A set of differences, $\{\Delta V^{mean}\}$, was calculated from the set of daily means for each region, $\{V^{mean}(r)\}$. For example, using TMAX values for November, the set of differences between "West" and "Wheat" was obtained as follows:

$$\{\Delta TMAX^{mean}(West\ vs.\ Wheat)\} =$$
$$\{\Delta TMAX^{mean}{}_i = TMAX^{mean}(West)_i - TMAX^{mean}(Wheat)_i, \text{ for } i = 1,\ldots, n\}.$$

After obtaining $\{\Delta V^{mean}\}$ for each pair of regions (i.e., $\Delta V^{mean}$(*West vs. Wheat*), $\Delta V^{mean}$(*Wheat vs. East*), and $\Delta V^{mean}$(*West vs. East*)), a series was created for each pair from the absolute value of $\{\Delta V^{mean}\}$ ranked from the lowest value (i.e., rank = 1) to the highest value (i.e., rank = $n$). Summing the ranks associated with positive values of $\Delta V^{mean}{}_i$ and with negative values of $\Delta V^{mean}{}_i$ led directly to the computation of the probability that the two regional datasets represented different populations. For $n > 20$, the null distribution is theoretically Gaussian. Hence, the summation of ranks that corresponded to positive and negative differences would be comparable for the null distribution. If these sums were comparatively large and small, however, then a regional distinction existed in variable V.

Results from the significance testing of the total daily solar radiation and total daily rainfall indicated either a meridional gradient that was characteristic of Oklahoma's climatology or differences between regions that were not statistically significant. Thus, Oklahoma's wheat belt did not produce an evident signature in the statistical analysis of total daily solar radiation or total daily rainfall. Consequently, differences evident in the analysis of the other variables did not result from differences in incoming solar energy or rainfall. Results for TAVG and DAVG were similar to those of TMIN and DMIN, respectively. Hence, the following discussion will focus on TMAX, TMIN, DMAX, DMIN, and VDEF.

Table 5.3 displays the mean values of five variables, by month, for each of the three regions. An *anomalous monthly mean* was defined for this study as a monthly mean for "Wheat" that did not have a numerical value between the monthly mean values for "West" and "East". Values shaded in gray denote *anomalous monthly means* that cannot be explained by the climatology of Oklahoma (see Section 3.1) or by synoptic-scale patterns. In addition, observable trends that resulted from changes in elevation across the region were expected to either monotonically increase or monotonically decrease. Hence, neglecting land-air interactions, the monthly mean for "Wheat" was expected to have a numerical value between that for "West" and that for "East".

The anomalies suggested by examining maps of objectively analyzed data also were evident as anomalous monthly means (Table 5.3). First, as vegetation grew across the wheat belt, maximum daily temperatures were cooler than those measured across adjacent regions of dormant grasslands (November – April). Second, as green-up of grasslands occurred and wheat became senescent during May, the cool anomaly over the wheat belt disappeared. Third, after the wheat harvest, maximum and minimum daily temperature data revealed a warm anomaly across the wheat belt. Fourth, DMAX and DMIN mean values indicated a slight moist bias during the early spring across the wheat belt, particularly during March. Fifth, lower VDEF values were computed over the growing wheat as compared to the dormant grasslands that bordered the wheat belt.

TABLE 5.3. Mean values of TMAX (°C), TMIN (°C), DMAX (°C), DMIN (°C), and VDEF (hPa) for November through August using Mesonet data from 1994 – 2001. Shaded values are "anomalous monthly means", as defined for this study. The three regions are defined in Table 5.2.

| | TMAX | | | TMIN | | |
|---|---|---|---|---|---|---|
| | West | Wheat | East | West | Wheat | East |
| Nov | 15.88 | 15.33 | 15.86 | 1.63 | 2.84 | 3.33 |
| Dec | 9.44 | 9.06 | 9.61 | -3.73 | -2.51 | -1.99 |
| Jan | 8.81 | 8.03 | 8.37 | -4.54 | -3.69 | -3.40 |
| Feb | 12.69 | 12.35 | 13.03 | -1.85 | -1.03 | -0.53 |
| Mar | 15.33 | 15.02 | 15.66 | 1.07 | 2.06 | 2.76 |
| Apr | 21.23 | 20.92 | 21.51 | 6.27 | 6.93 | 8.17 |
| May | 26.76 | 26.69 | 26.12 | 12.99 | 13.71 | 14.34 |
| Jun | 31.31 | 31.65 | 30.05 | 17.84 | 18.66 | 18.68 |
| Jul | 35.05 | 35.36 | 33.54 | 20.87 | 21.75 | 21.57 |
| Aug | 34.52 | 34.83 | 33.97 | 20.44 | 21.19 | 20.89 |

| | DMAX | | | DMIN | | | VDEF | | |
|---|---|---|---|---|---|---|---|---|---|
| | West | Wheat | East | West | Wheat | East | West | Wheat | East |
| Nov | 4.10 | 6.74 | 6.98 | -3.41 | -0.64 | -0.34 | 5.27 | 4.03 | 4.38 |
| Dec | -0.64 | 1.61 | 1.78 | -7.88 | -5.64 | -5.34 | 3.27 | 2.49 | 2.79 |
| Jan | -1.72 | 0.08 | 0.58 | -8.83 | -7.07 | -6.77 | 3.24 | 2.53 | 2.65 |
| Feb | 0.75 | 2.96 | 3.00 | -7.28 | -5.11 | -5.11 | 4.69 | 3.83 | 4.30 |
| Mar | 3.64 | 5.97 | 5.48 | -4.27 | -1.78 | -2.19 | 5.61 | 4.47 | 5.39 |
| Apr | 8.03 | 10.80 | 10.79 | -0.74 | 2.63 | 3.11 | 8.73 | 6.76 | 7.62 |
| May | 15.38 | 17.34 | 17.64 | 8.13 | 10.80 | 11.52 | 10.16 | 8.35 | 7.67 |
| Jun | 19.08 | 20.38 | 21.42 | 12.45 | 14.52 | 15.98 | 13.58 | 12.72 | 9.46 |
| Jul | 20.26 | 21.63 | 23.09 | 14.56 | 16.31 | 18.31 | 18.84 | 18.09 | 13.10 |
| Aug | 19.27 | 20.59 | 21.88 | 13.89 | 15.32 | 16.92 | 18.50 | 17.94 | 14.40 |

Using the 95% confidence level to indicate statistical significance (i.e., $p$ value less than 0.05), the Wilcoxon signed-rank test indicated that all TMAX differences between the three regions were significant during June, July, and August ($0.0001 \leq p \leq 0.0012$). Based on eight years of daily data from 28 Mesonet sites, the maximum temperatures across the northern portion of Oklahoma's wheat belt averaged 1–2°C higher during the climatological summer than those across grasslands directly to the east and averaged about 0.3°C warmer than those across the grasslands directly to the west. During July and August, the warm bias represented by the TMIN values over the wheat also was statistically significant ($p = 0.0001$).

From November through April, TMAX differences between "West" and "East" were not statistically significant ($p$ values ranged from 0.0735 to 0.984). Variations between "Wheat" and "East", however, were significant during all of these months ($p = 0.0058$ for January; $p = 0.0001$ for remaining months). Statistical significance between "West" and "Wheat" during wheat growth was noted for November ($p = 0.0001$), December ($p = 0.0143$), January ($p = 0.0001$), February ($p = 0.0114$), and April ($p = 0.0032$). The null hypothesis was not rejected for March, though the $p$ value was only 0.0599. In summary, the data confirmed the existence of a significant cool anomaly over growing winter wheat as compared to adjacent, dormant grasslands; thus, the null hypothesis was rejected.

During May, TMAX data populations from "West" and "Wheat" were indistinguishable ($p = 0.5353$). Although differences between the three regions were statistically significant for TMIN, DMAX, DMIN, and VDEF during May, the means were not anomalous – they exhibited a meridional gradient. These results strengthened the argument that, as green-up commenced across western grasslands, differences between the wheat belt and adjacent lands that were forced by land use were minimized.

Historical rainfall climatologies and a map of potential natural vegetation (Duck and Fletcher 1943; Section 3.1) provided circumstantial evidence that, in the absence of anthropogenic forces, the amount of near-surface atmospheric moisture should decrease from east to west across the region of interest. Additional evidence of a monotonous decrease in moisture across the region could be found in Table 5.2. An examination of DMAX values for January and May – the months with the most uniform evapotranspiration across this region – demonstrated that DMAX averaged about 2.3°C higher across "East" than "West". For both months, the value of DMAX for "Wheat" was between those values observed in adjacent regions.

A principally uniform gradient of moisture was expected from east to west across the region of interest; hence, it was consequential that mean DMAX values for "Wheat" during March and April were larger than those for "East". Perhaps more interesting was how the values of DMAX and DMIN changed from February to March, when the wheat crop grew rapidly. The February mean values of both DMAX and DMIN for "Wheat" were within 0.05°C of those for "East". Appropriately, the Wilcoxon signed-rank test indicated that the values of DMAX ($p$ = 0.8259), DAVG ($p$ = 8808), and DMIN ($p$ = 0.8887) from "Wheat" and "East" were from the same population. Hence, during February, a month with minimal precipitation, the moisture content near the surface was indistinguishable between these two regions.

In contrast, during March, the Wilcoxon test computed *less than a 0.1% chance* that DMAX, DMIN, and DAVG for "West", "Wheat", and "East" represented similar populations. *These results were based on almost 21,000 daily statistics over* *eight unique years.* In addition, the computations showed that DMAX, DMIN, and DAVG for "Wheat" averaged 0.49°C, 0.41°C, and 0.42°C higher than the respective values for "East". DMAX, DMIN, and DAVG for "Wheat" also averaged 2.33°C, 2.49°C, and 2.35°C higher than the respective values for "West". These results were even more interesting when one considered that ~25 frontal passages occurred during the months of March between 1994 and 2001.

Monthly means of the average daily vapor pressure deficit, VDEF, across the three regions mirrored the monthly means of TMAX (Table 5.2) during the wheat's growing season. With lower TMAX values and, during some months, higher DMAX values, it was not surprising that VDEF was anomalously low over "Wheat" from November through April. Post-harvest values of VDEF were comparable to those of "West", but still within its expected range (i.e., a value between that of "West" and "East"). With the exception of March, the Wilcoxon test indicated that VDEF differences during the wheat's growing season *were* statistically significant ($p < 0.0025$). During March, VDEF differences between "West" and "East" were not significant ($p = 0.3472$), although those between "Wheat" and its neighbors were significant at the 99.99% confidence level.

Given these results, one might expect that the reported anomalies would be amplified during March and April when the wheat crop was bountiful and suppressed during those months when the wheat crop was poor. Year-to-year comparisons were conducted (data not shown) for monthly means of TMAX versus Crop Year wheat production (Oklahoma Agricultural Statistics Service 1999a–e; 2001; 2002). No relationship was found, indicating that the anomalies were *not* enhanced or suppressed based on the condition of the crop. This seemingly negative outcome might result from many factors. For example, when the wheat crop grew well, environmental conditions likely were favorable for other vegetative species to green-up earlier and to grow abundantly. Thus, differences between the wheat belt and its adjacent land would not be as distinct as those during an average crop season. Other events could occur just prior to or during harvest that damaged or destroyed otherwise outstanding crop production (e.g., widespread flooding). Hence, crop production statistics might not adequately reflect the differences between cropland and adjacent grasslands during every crop year.

## 5.4 Daily Impact of the Wheat Belt: Pre-Harvest

To better interpret how Oklahoma's wheat belt alters its environment, case-study days were examined during three of the eight years of available data. From the period 1999 to 2001, approximately 50 days between 15 March and 1 June revealed evidence of heightened DMAX values over Oklahoma's wheat belt compared to adjacent grasslands. By two-week periods, the number of days classified as showing evidence of these heightened DMAX values was 19 days between 15 March and 31 March, 12 days between 1 April and 15 April, 12 days between 16 April and 30 April, six days between 1 May and 15 May, and two days between 16 May and 1 June. More than half of these cases revealed a DMAX enhancement only across five or six counties in north-central Oklahoma. It was possible that the advection of moisture from the Gulf of Mexico masked some DMAX signatures from the wheat fields.

Figures 5.8, 5.9, and 5.10 display DMAX for 27 March 2000, 4 April 2000, and 5 April 2000, respectively. The evolution of the meteorological features near the surface on these three days typified spring days when Oklahoma's wheat crop most influenced its environment. Associated visual greenness maps are displayed in Figs. 5.11 and 5.12 for the weeks ending 30 March 2000 and 6 April 2000, respectively.

The blue area that consistently appears on the visual greenness maps in north-central Oklahoma (Alfalfa County) is Great Salt Plains Lake and Wildlife Refuge. To the north and northeast of this region, soil permeated with salt does not support agriculture and, as a result, a red or yellow region denoting minimal vegetation was apparent on the visual greenness images during the wheat season. Observations from the Cherokee Mesonet site, located west-northwest of Great Salt Plains Lake, might have been influenced by moisture advection from the lake. Yet, an examination of the winds measured at Cherokee indicated that moisture advection from the lake did not influence Cherokee's dew points during the three case-study days.

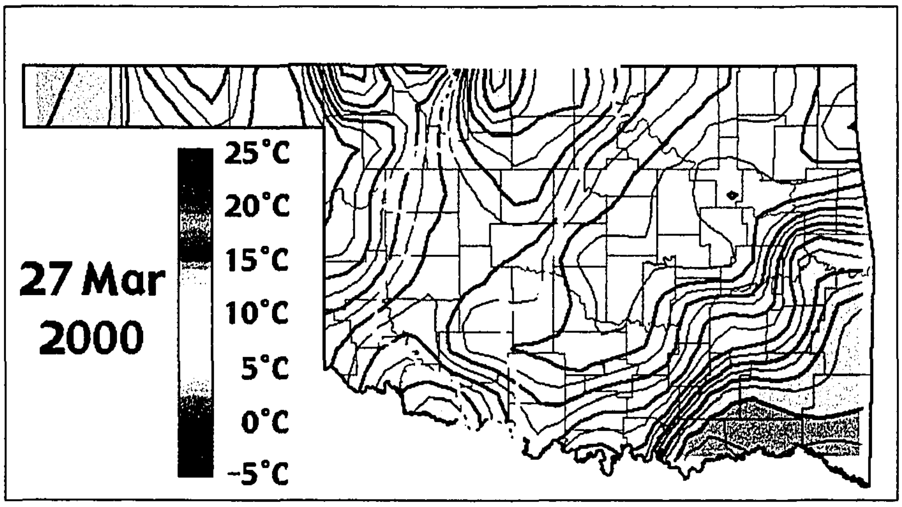


FIGURE 5.8. Map of the maximum dew points for 27 March 2000. The white outline represents the boundary of Oklahoma's winter wheat belt. Thick black lines denote isopleths at intervals of 1°C.

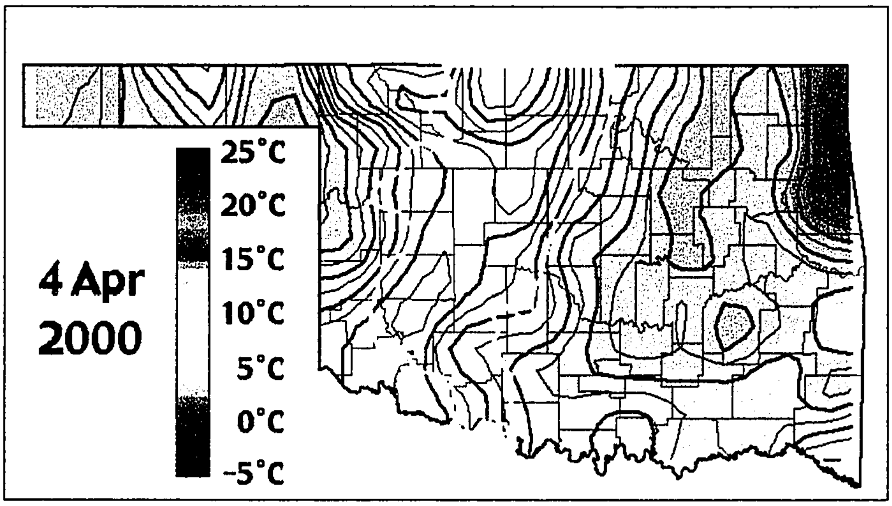


FIGURE 5.9. Same as Fig. 5.8 except for 4 April 2000. The white outline represents the boundary of Oklahoma's winter wheat belt.

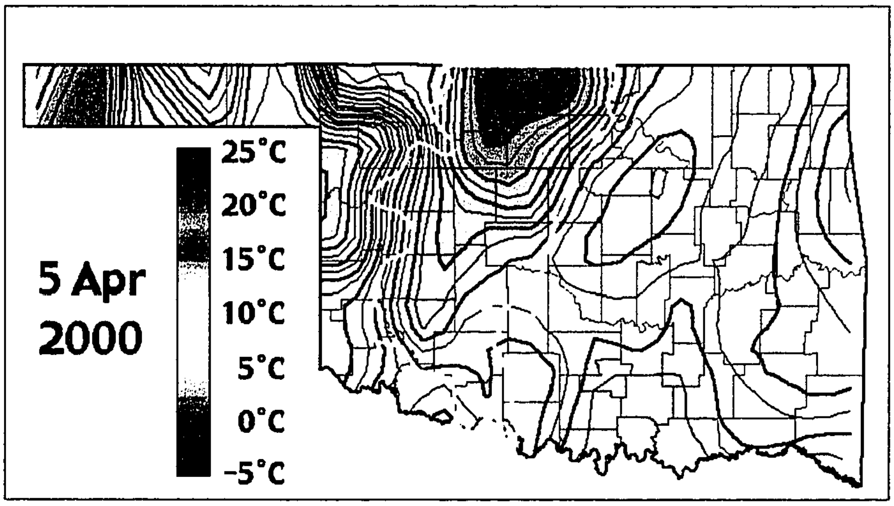


FIGURE 5.10. Same as Fig. 5.8 except for 5 April 2000.

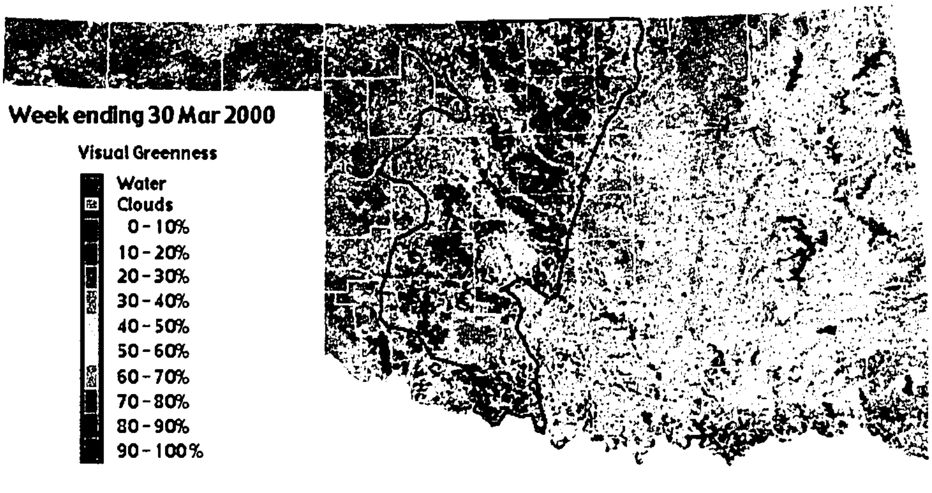


FIGURE 5.11. Visual greenness map for the week ending 30 March 2000. The black outline represents the boundary of Oklahoma's winter wheat belt.

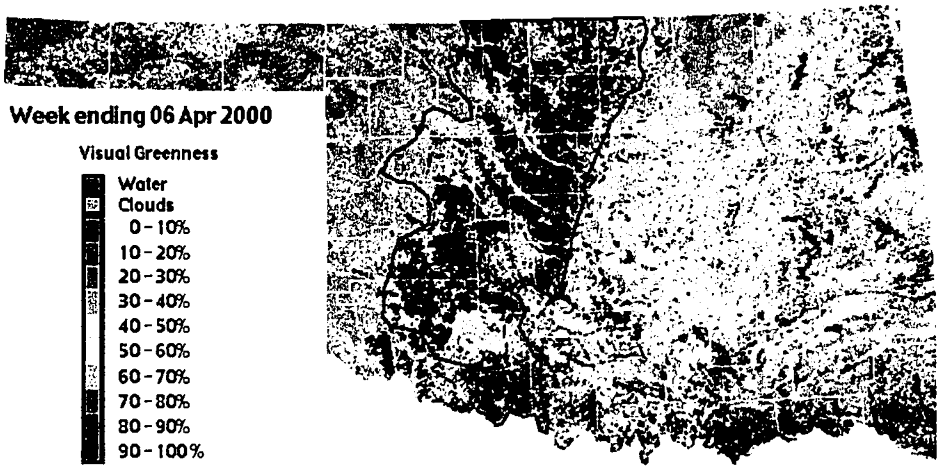


FIGURE 5.12. Visual greenness map for the week ending 6 April 2000. The black outline represents the boundary of Oklahoma's winter wheat belt.

*5.4.1 27 March 2000*

Clear skies and weak winds characterized the synoptic conditions across Oklahoma on 27 March 2000. Influenced by a large high pressure system over the western United States, surface winds across Oklahoma backed from light northerly in the morning to light westerly by noon. Statewide, the average wind speed was only 2.6 m $s^{-1}$. Rainfall totals of 5 to 10 cm had been recorded at many Mesonet sites across western Oklahoma during the week prior to 27 March in association with the passage of several weak frontal boundaries. The most significant events occurred on 22 March, when 1–2 cm of rain fell across the western two-thirds of the state, and on 23 March, when 2–6 cm fell across the western third of the state.

Mesonet soil moisture values at 5, 25, and 60 cm on 27 March 2000 indicated that water down to the root zone was available statewide. In fact, the pattern of DMAX (Fig. 5.8) more closely resembled the associated visual greenness map (Fig. 5.12) than it did the rainfall pattern of the previous week (not shown). Outside of the wheat belt, May Ranch (MAYR) received 8.6 cm of rain during the previous week; yet, its maximum dew point on 27 March was only 5.0°C. In contrast, nearby Cherokee (CHER), within the wheat belt, received 8.7 cm of rain during the previous week and its maximum dew point on 27 March was 14.2°C. Similarly, Woodward (WOOD) and its neighbor, Seiling (SEIL), recorded a total of 7.1 cm and 6.4 cm of rain, respectively, during the 21st, 22nd, and 23rd. Yet, the maximum dew point on the 27th at WOOD, outside of the wheat belt, was 5.0°C; at SEIL, within the wheat belt, DMAX was 9.0°C. Apparently, the cycling of water through the root zone of the growing winter wheat was more efficient at returning water to the atmosphere than was direct evaporation from either moist soil or dormant vegetation.

The dewpoint field across the region of interest evolved considerably from sunrise to sunset. From midnight to sunrise (about 0630 CST) on 27 March 2000, dew points decreased 2°C across "Wheat" and "East" and 1°C across "West" (Fig. 5.13). At 0600 CST, about 30 minutes prior to sunrise, near-surface air was the most moist (6 to 7°C) across the southwest and southeast corners of Oklahoma and the driest (1 to 2°C) across the northeast corner and the Panhandle (Fig. 5.14*a*). Dew points across the wheat belt were approximately the same as those observed over adjacent lands. Within an hour after sunrise, dew points increased 1 to 2°C statewide as a result of the evaporation of dew and transpiration. The nighttime drying of the surface layer and the rapid moisture return shortly after sunrise have been documented previously by Arndt (2001) for Oklahoma Mesonet sites.

The significant increase in low-level moisture after sunrise was aided by the existence of a nocturnal inversion. The inversion confined the surface flux of moisture to a shallow layer. At the ARM Central Facility near Lamont, OK, the morning sounding (0530 CST) indicated a nocturnal inversion in which the temperature increased by 6.4°C within the first 15 hPa above the ground

(~130 m). An analysis of Mesonet observations suggested that the inversion existed across a broad region, as dewpoint temperatures increased rapidly statewide by 0730 CST (Fig. 5.14*b*). Note the rapid increase of near-surface moisture between about 0700 and 0800 CST for "West", "Wheat", and "East" (Fig. 5.13). These composite observations provided additional evidence that, shortly after sunrise, an inversion confined the influx of moisture to a shallow atmospheric layer across all three regions.

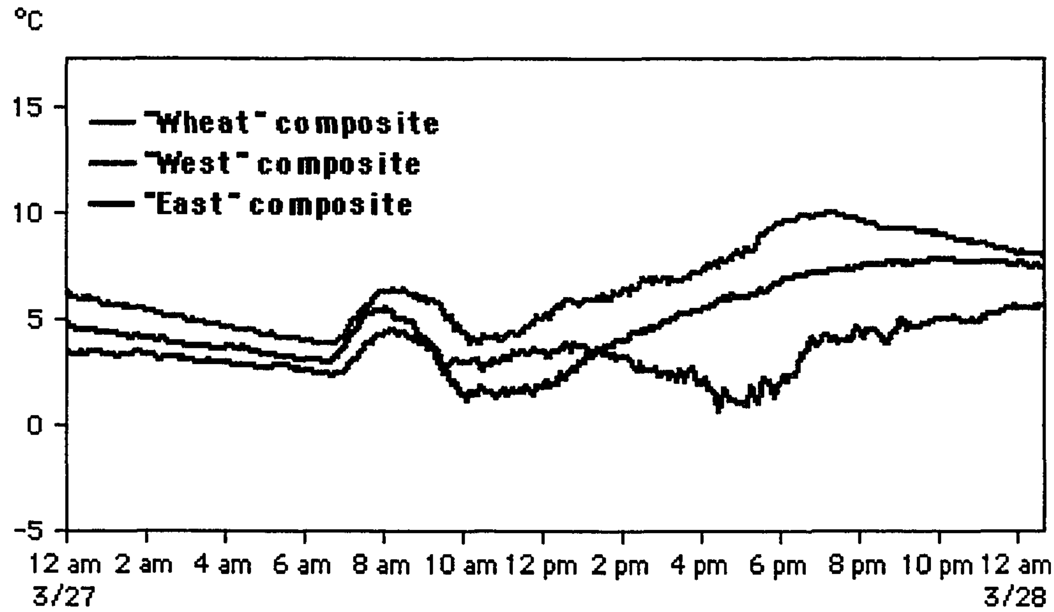


FIGURE 5.13. Graph of composite 5-minute observations of dew point for regions "West", "Wheat", and "East" between 0000 CST on 27 March 2000 and 0000 CST on 28 March. The green, red, and blue lines denote the composite dew point for "Wheat", "West", and "East", respectively (see Table 5.1). The composite data were constructed from the average of all observed values at a given time for the sites located with each region. The time series plot extends from midnight to midnight CST – the interval for computing DMAX.

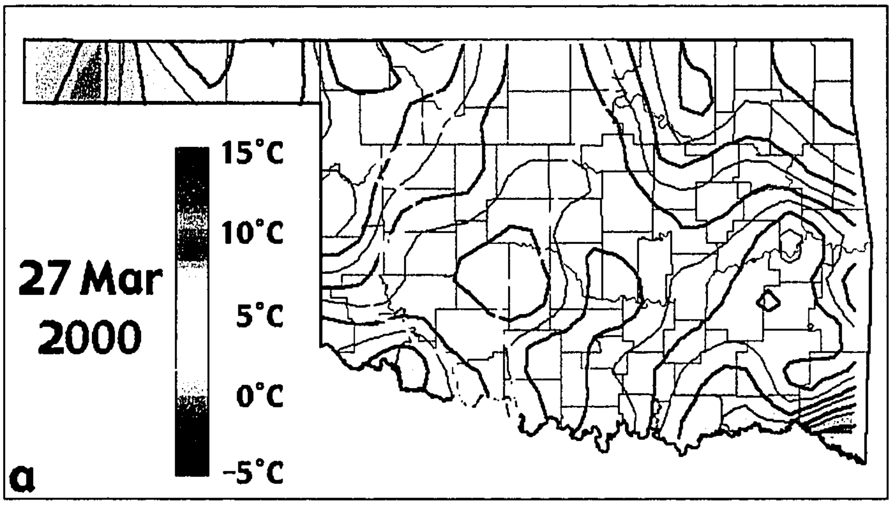


FIGURE 5.14*a*. Map of near-surface dew points at 0600 CST on 27 March 2000. A one-pass Barnes technique was used for the objective analysis. The white outline depicts the boundary of Oklahoma's wheat belt.

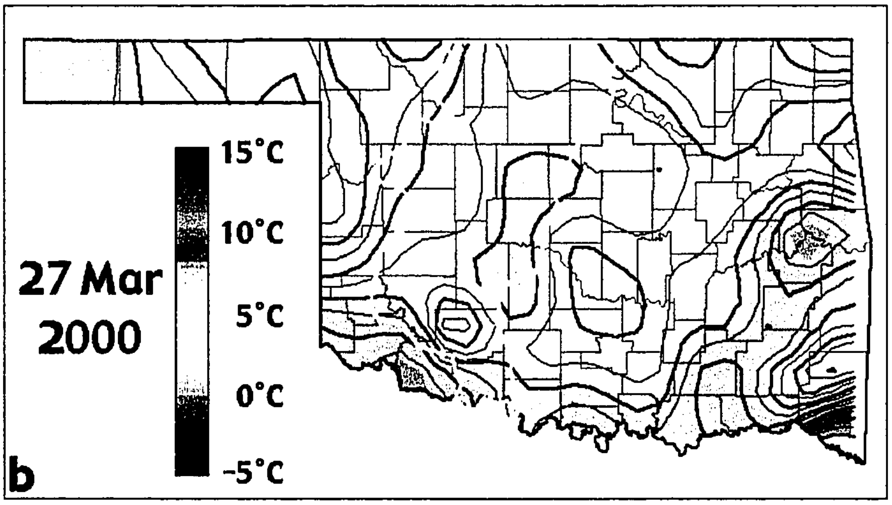


FIGURE 5.14*b*. Same as Fig. 5.13*a* except for 0730 CST on 27 March 2000.

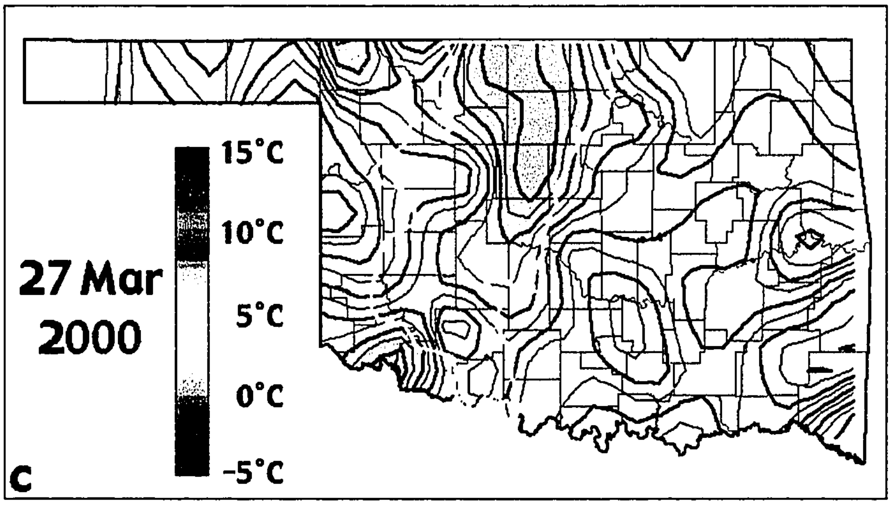


FIGURE 5.14*c*. Same as Fig. 5.13*a* except for 0900 CST on 27 March 2000.

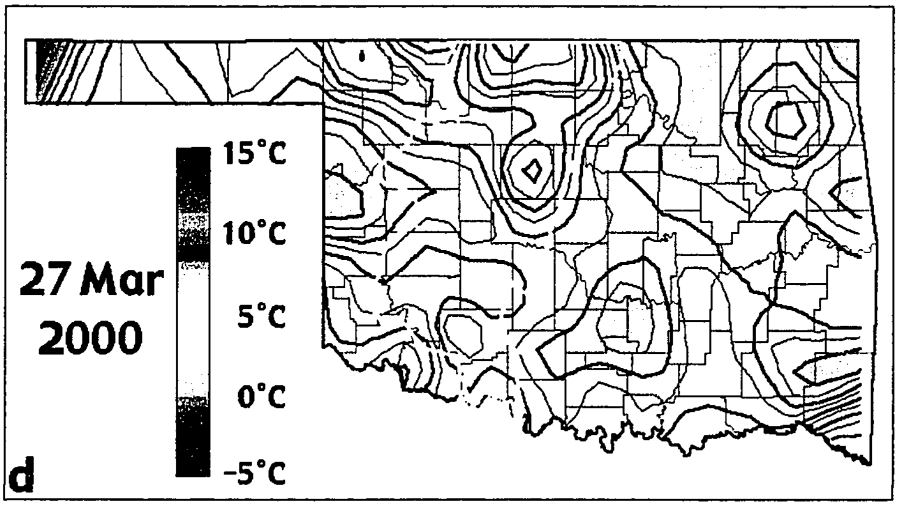


FIGURE 5.14*d*. Same as Fig. 5.13*a* except for 1000 CST on 27 March 2000. The white outline represents the boundary of Oklahoma's winter wheat belt.

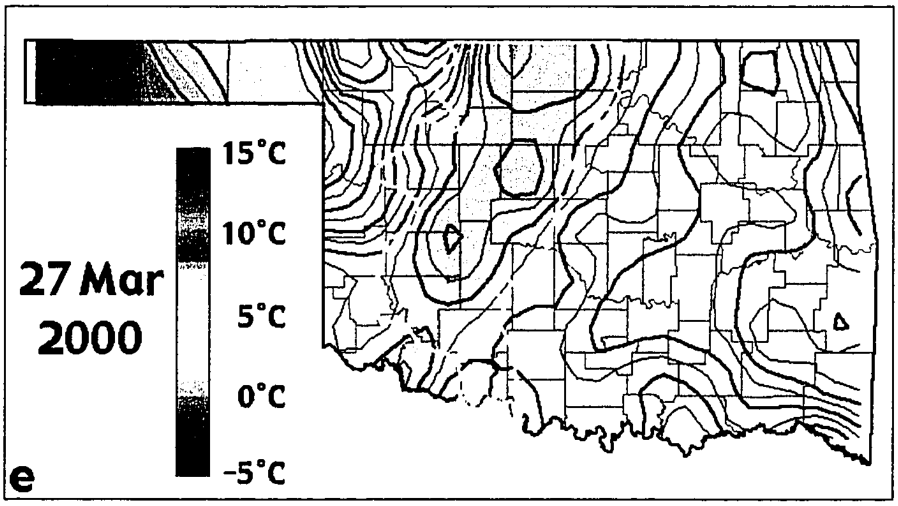


FIGURE 5.14*e*. Same as Fig. 5.13*a* except for 1500 CST on 27 March 2000.

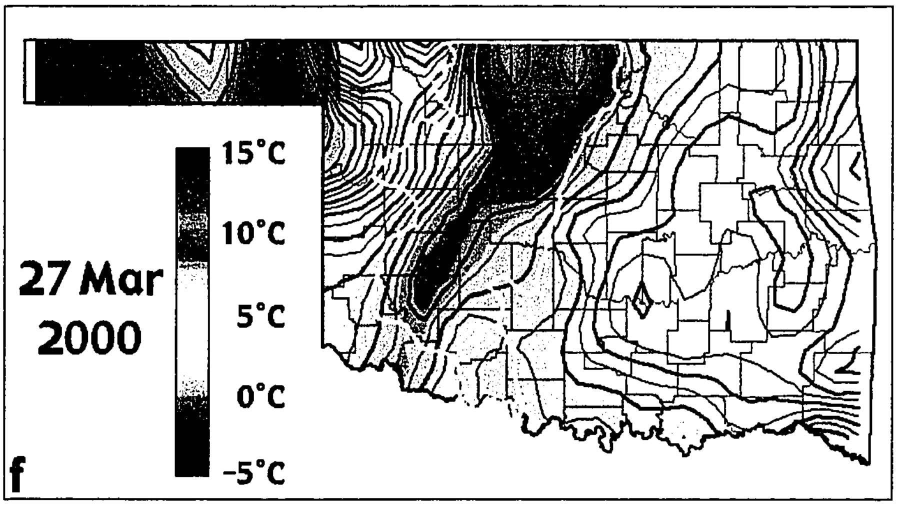


FIGURE 5.14*f*. Same as Fig. 5.13*a* except for 1730 CST on 27 March 2000.

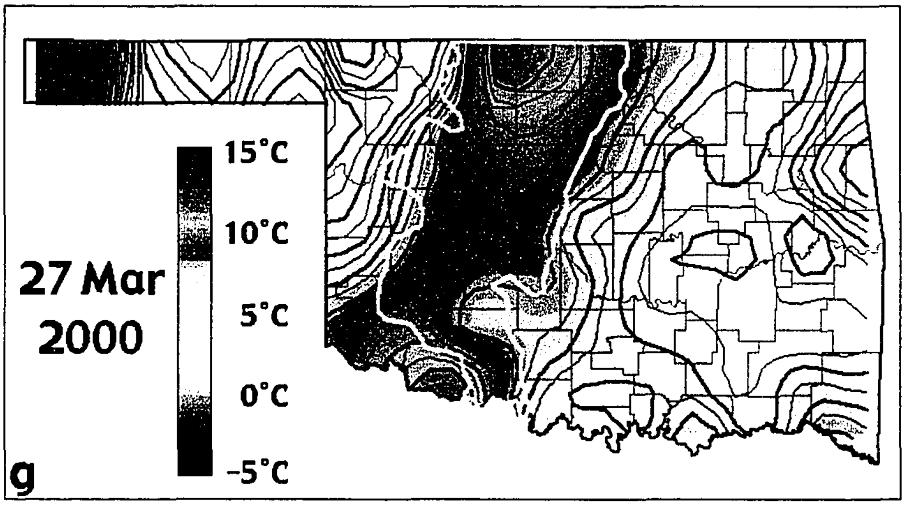

FIGURE 5.14*g*. Same as Fig. 5.13*a* except for 1915 CST on 27 March 2000. The white outline represents the boundary of Oklahoma's winter wheat belt.

By 0900 CST (Fig. 5.14*c*), it became evident that transpiration across the wheat belt supplied substantial moisture into the lower atmosphere, similar to the observations of Dirmeyer (1994). Dew points across the northern two-thirds of Oklahoma's wheat belt ranged from 5.5 to 8.5°C; several Mesonet sites across north-central Oklahoma experienced a four-degree increase during three hours. While transpiration influenced the dew point of several Mesonet sites within the wheat belt, dry-air entrainment appeared to cause a 1 to 2°C reduction in near-surface moisture elsewhere between 0800 and 0900 CST. By 1000 CST (Fig. 5.14*d*), surface heating eroded the inversion over most, if not all, of the Mesonet sites. Composite dew points for "West", "Wheat", and "East" identified 1000 CST as the time when a local minimum of surface moisture occurred (Fig. 5.13). At that time, dew points ranged from –1 to 4°C adjacent to the wheat belt and from 3 to 7°C within the wheat belt (Fig. 5.14*d*).

Interestingly, the magnitude of the morning increase of dew point was equal for "East" and "Wheat" (~2.5°C); however, the magnitude of the midmorning decline in moisture was 4°C for "East" but only 2.5°C for "Wheat". Hence, between sunrise and 1000 CST, the dewpoint difference between "Wheat" and "East" *increased* by 1.5°C. Evidence from modeling runs (Chapter 6) indicated that vertical mixing could occur through a deeper layer across "East" than across "Wheat". As a result, more dry air was entrained from aloft for "East" than for "Wheat", thus decreasing the near-surface dew points more for the "East" region.

Between 1000 and 1900 CST, an upward trend of dew points was evident for "Wheat" (Fig. 5.13). A similar increase was noted for "East" between 1200 and 2100 CST. Because the magnitudes of the increases for "Wheat" and "East" were nearly identical (6°C) yet set apart in time by 2 h, it was probable that the dewpoint enhancement for "East" resulted from advection from "Wheat" by the light westerly surface winds. In contrast, dew points decreased for "West" between 1300 and 1700 CST, as a turbulent boundary layer entrained dry air from aloft. After 1700 CST, dew points over "West" increased until sunset (or ~1900 CST), as surface heating diminished and the surface layer decoupled from the convective boundary layer (CBL) established during the day.

Data from an ARM radiosonde at Lamont provided evidence that moisture that transpired from the wheat fields was mixed rapidly into the CBL during the afternoon. At 1430 CST, when the mixed layer was approximately 130 hPa deep, the dew point increased by 5.5°C within the first 1.4 hPa above the ground. The steep vertical gradient of dew points also confirmed that a local source of moisture (i.e., transpiration from the wheat) existed nearby Lamont. Unfortunately, sounding data directly east of the wheat belt were not available. Such data could have provided insight as to whether the afternoon dewpoint increase also was generated locally or was advected from the wheat belt. If the former were true, an extremely shallow (~1 hPa) layer of moisture should have been detected, as measured by the Lamont sounding. If the latter were true, one would expect that moisture observations would have been more vertically uniform near the surface.

By 1200 CST (not shown), the axis of maximum dew points corresponded well with the axis of the wheat belt. A similar pattern (Fig. 5.14*e*) was evident throughout the remainder of the afternoon . Although moisture from Texas appeared to advect across southwest Oklahoma, it was clear from the westerly winds that the dewpoint maximum across north-central Oklahoma did not result from positive moisture advection from the south.

Dew points ranged from 9 to 12°C by 1730 CST across the northern third of the wheat belt (Fig. 5.14*f*), including 11°C at Lamont. At this time, the mixed layer over the ARM Central Facility extended to about 700 hPa. A surface-based source of moisture still was evident at Lamont (not shown), as the surface dew point of 10.7°C was about 3.5°C higher than the dew point just 5 hPa aloft.

One-half hour after sunset (5.14*g*), dew points across the northern half of Oklahoma ranged from 2 to 7°C greater than those measured 30 minutes before sunrise. Notably, the winter wheat belt not only altered its local area, but moisture advected downwind from the crop and greatly enhanced the dew points across several counties to the east.

On a much smaller scale, a microscale impact of moisture advection was evident in observations from the Freedom Mesonet site. Relative to FREE, wheat was grown to the immediate southwest of the site (Fig. 5.15). Hence, advection by winds from these highly localized wheat fields probably influenced Freedom's observations. Five-minute dew point and wind direction observations from the Freedom Mesonet site (Fig. 5.16) capably illustrated the advection of moisture from these local wheat fields. Aside from the evaporation associated with sunrise, when winds were from north of west (between 270° and 360°), dewpoint temperatures tended to decrease or remain steady. In contrast, winds between 180° and 270° were associated with rapid increases in dew point.

The impact was most evident between 1200 and 1630 CST, when the wind direction repeatedly shifted from just north of due west (>270°) to just south of due west (<270°). Interestingly, the dewpoint temperatures repeatedly decreased and increased by 1-3°C in association with these minor changes in the wind direction.

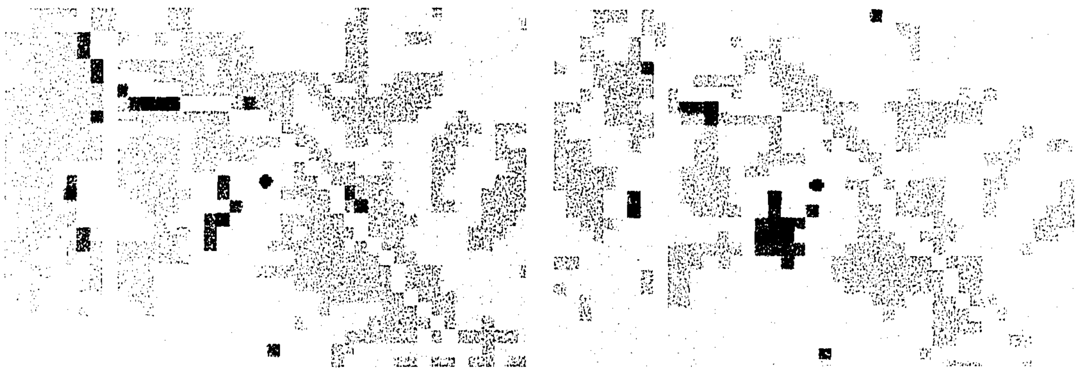

FIGURE 5.15. Zoomed maps of visual greenness for the week ending 30 March 2000 (left) and 6 April 2000 (right). The Freedom Mesonet site (FREE) is represented by the black dot in the center of each image. Note the region of growing vegetation southwest of Freedom.

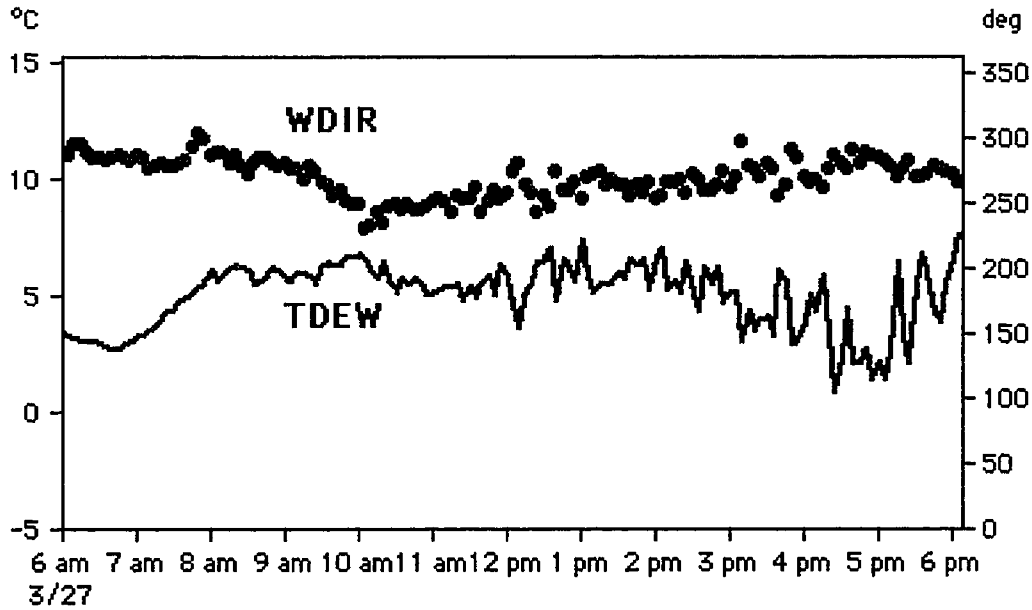


FIGURE 5.16. Graph of 5-minute measurements of dew point (green line, TDEW) and wind direction (blue dots, WDIR) at the Freedom Mesonet site between 0600 and 1800 CST on 27 March 2000.

*5.4.2 4 April 2000*

Throughout the day of 4 April 2000, winds across the main body of Oklahoma were light and southerly or southeasterly, with wind speeds strengthening slightly during the afternoon. Winds across the Panhandle were westerly until about 1700 Central Daylight Time (CDT; CDT = UTC – 5 h), when they began to veer to the north. Statewide-averaged wind speeds were 3.6 m $s^{-1}$. Rainfall events associated with frontal passages occurred on 28 March, 29 March, 31 March, and 1 April, with the most significant rainfall occurring across southwestern Oklahoma. Rain totals for the week prior to 4 April were significantly less than those prior to 27 March. Statewide, dew points were about 5°C lower on 4 April than on 27 March. Hence, this case study day illustrated how the wheat belt could modify a relatively dry air mass.

Patterns in the DMAX field were similar between 27 March (Fig. 5.8) and 4 April (Fig. 5.9); both mimicked the pattern in the visual greenness maps (Figs. 5.11 and 5.12) moreso than they did the rainfall pattern of the previous week. Similar to 27 March, May Ranch received 3.5 cm of rain from 27 March to 4 April and observed a maximum dew point of 5.5°C on 4 April; Cherokee, which recorded 0.8 cm of rain during the same week, observed a maximum dew point of 10.7°C on the same day. On the east side of the wheat belt, Newkirk (in northeastern Kay County) received 3.1 cm of rain during the previous week and measured a maximum dew point of 5.2°C on 4 April. In contrast, Medford (in central Grant County) recorded 1.7 cm of weekly rainfall and a DMAX of 9.7°C.

The diurnal cycle of dew points on 4 April 2000 (Fig. 5.17) was similar to that detailed for 27 March 2000. An increase in dew points occurred immediately after sunrise and was followed by a decrease at all sites during midmorning. As with the 27 March case, the midmorning decline in surface moisture was greater for

"East" than for "Wheat" – in this case, by 2.5°C. In contrast to 27 March, the magnitude of the post-sunrise moisture influx was 1.3°C greater for "Wheat" than for "East". One explanation for this difference between the two study days could be explained by a greater vapor deficit after sunrise on 4 April than on 27 March. Because unstressed wheat plants respond to a greater vapor deficit by increasing their transpiration, the wheat canopy could have injected more moisture on 4 April in response to drier synoptic conditions.

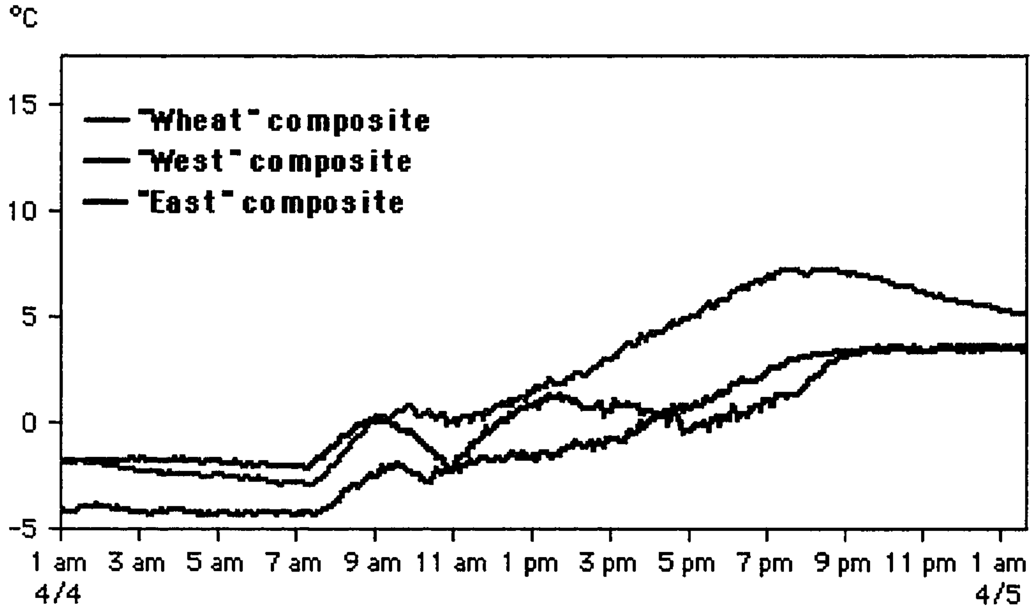


FIGURE 5.17. Graph of composite 5-minute observations of dew point for regions "West", "Wheat", and "East" between 0100 CDT on 4 April 2000 and 0100 CDT on 5 April. The green, red, and blue lines denote the composite dew point for "Wheat", "West", and "East", respectively (see Table 5.1). The composite data were constructed from the average of all observed values at a given time for the sites located with each region. The time series plot extends from midnight to midnight CST – the interval for computing DMAX.

As on 27 March, an overall increase in dew points occurred on 4 April between 1100 CDT and 2000 CDT over "Wheat" and "East" (Fig. 5.17). In contrast to 27 March, however, the magnitude of the increase on 4 April was about 1.5°C greater for "Wheat" than for "East". The different rate at which the dew point increased could have resulted from different wind directions between these two days. Figure 5.18 displays maps of dew point and wind direction for

1500 CST on 27 March and 1600 CDT on 4 April. On 27 March, surface winds across "Wheat" and "East" advected moisture directly from "Wheat" to "East". On 4 April, however, only a component of the winds across these regions advected moisture from the wheat belt toward the east.

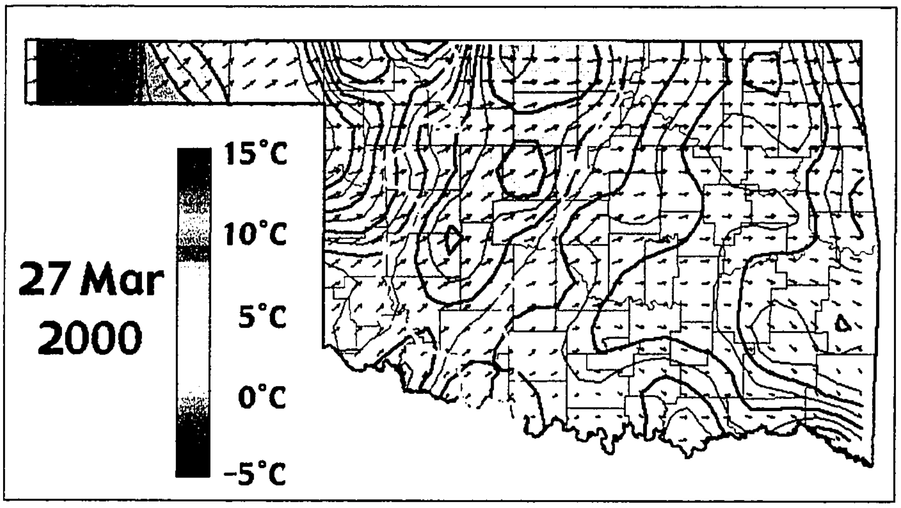


FIGURE 5.18*a*. Map of near-surface dew points at 1500 CST on 27 March 2000. A one-pass Barnes technique was used for the objective analysis. The white outline depicts the boundary of Oklahoma's wheat belt.

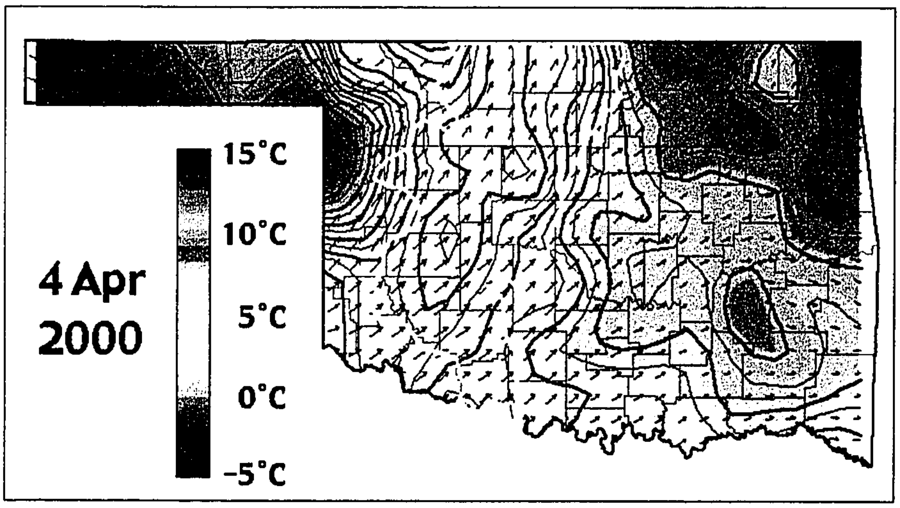


FIGURE 5.18*b*. Same as Fig. 5.18*a* except for 1600 CDT on 4 April 2000.

Although the composite graphs provided information regarding the different evolutions of the dewpoint field across "West", "Wheat", and "East", a synoptic map better illustrated the spatial relationship between the wheat belt and the daily moisture maximum. Figure 5.19 depicts the daily maximum dew point (DMAX) measured at Mesonet sites on 4 April. Values of DMAX overlay a visual greenness map for the week ending 6 April 2000. With the exception of Freedom, where moisture advection from its nearby wheat fields (see Section 5.3.1) increased DMAX to a value of 10.7°C, the values for DMAX on the wheat side of the wheat belt boundaries were greater than those adjacent to the wheat belt. In most cases, DMAX was about 2°C higher for sites within the wheat belt than for their neighbors outside of the belt. Skin temperature imagery from NOAA's GOES-8 satellite (Fig. 5.20) confirmed the existence of a corresponding region of cooler temperatures across the wheat belt.

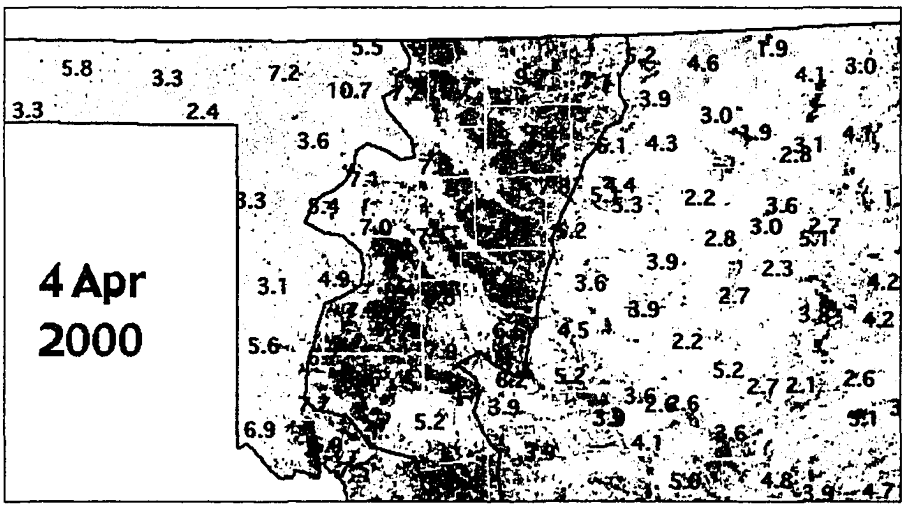


FIGURE 5.19. Zoomed map of visual greenness for the week ending 6 April 2000 with plotted observations of the daily maximum dew point (DMAX) in degrees Celsius for 4 April 2000. Wet or densely vegetated areas appear green, and dry or sparsely vegetated areas appear red to tan. The solid black line represents the boundary of Oklahoma's winter wheat belt, as defined for this study.

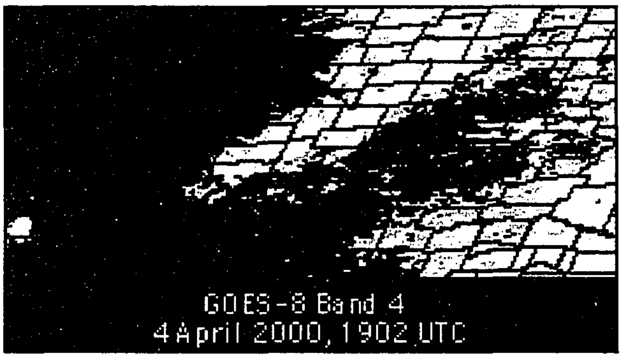


FIGURE 5.20. Surface temperature image (10.7 μm) at 1402 CDT on 4 April 2000 from the GOES–8 geostationary satellite. Note the relative minimum in skin temperature over the wheat belt of western Oklahoma. Data courtesy of the Space Science and Engineering Center at the University of Wisconsin.

With weak winds and a substantial moisture gradient across the boundary of the wheat belt on 4 April, conditions appeared favorable for detecting a landscape-induced mesoscale circulation (e.g., Chen and Avissar 1994). At 1700 CDT, a 4°C dew point difference existed between the Cherokee and Alva Mesonet sites (31 km apart), and a 9°C difference was observed between Cherokee and May Ranch (64 km apart). About 1700 CDT, the weather radar at Vance Air Force Base (KVNX), located near the border of Alfalfa and Grant counties, detected several isolated convective elements within 100 km of the radar. Movement of the convection was toward the east or northeast, corresponding to the 10-m wind directions (not shown). At 1830 CDT, KVNX detected the development of a southwest-to-northeast-oriented thin line in southeastern Woods County. Movement of the thin line was toward the northwest, *perpendicular* to the movement of surrounding echoes, including one echo that moved within 10 km of the thin line. By 1930 CDT, the thin line was undetectable.

The location of the thin line over time was coincident with changes in near-surface winds and dew points at the Alva Mesonet site in eastern Woods County (Fig. 5.21). Between 1700 and 1830 CDT, winds at the Alva site backed from 220°

to 165°, reflecting the passage of a surface boundary. During this 90-minute period, dew points increased by 3.3°C at Alva. The wind shift and subsequent moisture increase were not measured at surrounding Mesonet sites. Hence, it is possible that the thin line represented the boundary of a local vegetation breeze.

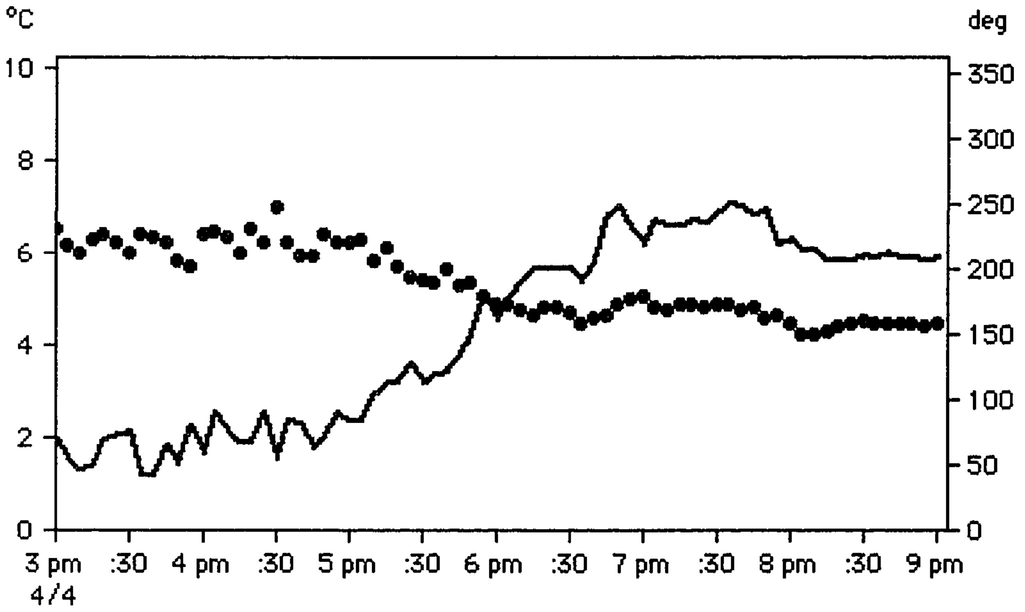


FIGURE 5.21. Graph of 5-minute measurements of dew point (green line, TDEW) and wind direction (blue dots, WDIR) at the Alva Mesonet site between 1500 and 2100 CDT on 4 April 2000.

*5.4.3 5 April 2000*

No rain fell during the clear days of 4 April and 5 April; however, wind speeds significantly increased from one day to the next in response to an approaching low pressure system. Winds were southerly or southwesterly across the state for most of the day on 5 April, with speeds averaging 6.4 m $s^{-1}$ statewide and gusting to about 15 m $s^{-1}$. Wind speeds across western Oklahoma were slightly higher than those across the eastern half of the state. Skies on 5 April were clear statewide.

A comparison of the DMAX fields on 4 April (Fig. 5.9) with those on 5 April (Fig. 5.10) demonstrated a considerable increase in near-surface moisture from one day to the next. The primary features evident on 5 April were: (1) a region of significantly elevated DMAX values over the wheat belt and (2) an associated intensification (as compared to 4 April) of the DMAX gradient across far western Oklahoma (Fig. 5.10). Daily maximum dew points within the wheat belt ranged from 11-17°C, whereas those just east of the wheat belt ranged from 9-11°C. DMAX values just west of the wheat belt ranged from 4-10°C, with two notable exceptions: 12.4°C at Buffalo and 12.0°C at Freedom. As noted earlier, dew points at FREE were enhanced by moisture advection from local wheat fields. By the same physical processes local wheat farms near Buffalo influenced dewpoint measurements given favorable wind directions.

Southwest winds at 1530 CDT on 5 April averaged 10 m $s^{-1}$ across the main body of Oklahoma; westerly surface winds prevailed across far northwest Oklahoma and the Panhandle (Fig. 5.22). Two regions of enhanced moisture were evident: (1) an area across south-central Oklahoma where dew points ranged from 9 to 12°C and (2) an extended region across the wheat belt where dew points ranged from 10 to 15°C (Fig. 5.22). An animation of the dew point field (not shown) revealed that the former area increased its low-level moisture as a result of positive moisture advection from North Texas and the Gulf of Mexico. Over the latter region, however, surface fluxes generated a local moisture maximum.

The daytime evolution of near-surface dew points during 5 April 2000 (Fig. 5.23) differed from those of the previous two cases (Figs. 5.13 and 5.17). From sunrise to about 1600 CDT, dew points for "Wheat" and "East" increased steadily. After 1600 CDT, dew points for both regions decreased into the nighttime hours as dew began to form. The observations on 5 April did not reflect a late morning maximum of low-level moisture over either "Wheat" or "East", as was apparent during both 27 March and 4 April. Composite data for "West" indicated that substantial drying of near-surface air occurred from ~1200 CDT to sunset. Unlike the previous two case-study days, a dewpoint maximum was not evident during the late morning.

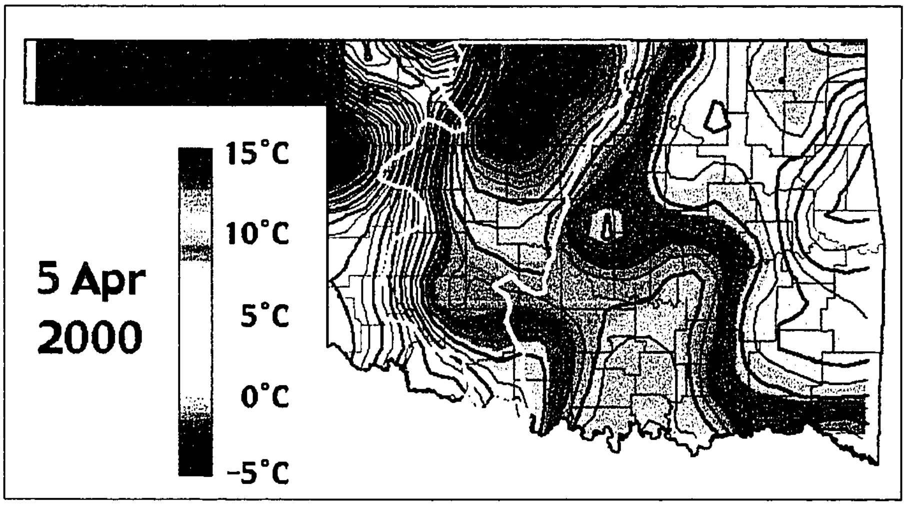


FIGURE 5.22. Map of near-surface dew points at 1530 CDT on 5 April 2000. A one-pass Barnes technique was used for the objective analysis. The black outline depicts the boundary of Oklahoma's wheat belt.

The thermodynamic profile from Lamont, OK (not shown) provided a vital clue as to why dew points for "Wheat" did not decrease during the late morning and exceeded 14°C by late afternoon at eight Mesonet sites within the wheat belt. At 0635 CDT, 40 minutes prior to sunrise, a substantial inversion, with a temperature increase of 10.7°C between the surface (970 hPa) and 860 hPa, was measured at the ARM Central Facility. Soundings at 1530 CDT and 1830 CDT indicated that the inversion never eroded fully over Lamont on 5 April. Hence, moisture added to the mixed layer by transpiration was confined to a layer about 100 hPa deep, and dry air above the inversion was not entrained significantly into the mixed layer. Surface dew points measured at the radiosonde site at 0635 CDT, 1530 CDT, and 1830 CDT were 2.9, 14.4, and 13.2°C, respectively. Presumably, the stronger winds on 5 April (as compared to the two previous cases) also enhanced transpiration from the wheat (Doran et al. 1995), with the resulting atmospheric moisture confined to the mixed layer.

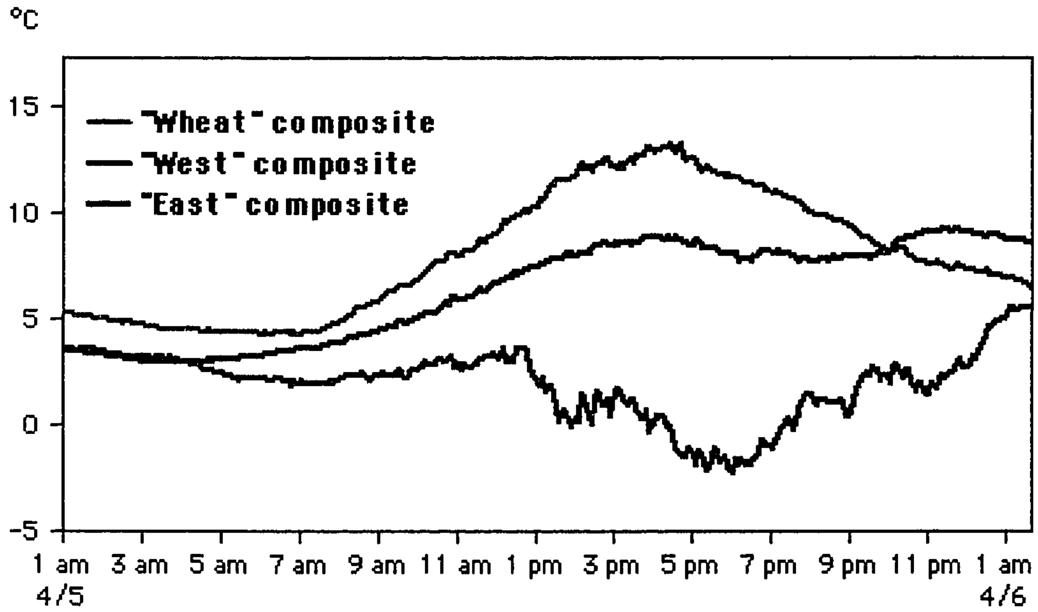


FIGURE 5.23. Graph of composite 5-minute observations of dew point for regions "West", "Wheat", and "East" between 0100 CDT on 5 April 2000 and 0100 CDT on 6 April. The green, red, and blue lines denote the composite dew point for "Wheat", "West", and "East", respectively (see Table 5.1). The composite data were constructed from the average of all observed values at a given time for the sites located with each region. The time series plot extends from midnight to midnight CST – the interval for computing DMAX.

In addition to the moist anomaly, a cool anomaly was evident in the near-surface temperature field across a portion of the wheat belt. Mesonet sites measured air temperatures between 27 and 30°C within the northern half of the wheat belt at 1530 CDT (Fig. 5.24). To the west of the wheat belt, temperatures ranged from 31 to 34°C. Along the eastern boundary of the wheat belt, the temperature gradient was less evident. On average, however, temperatures just east of the wheat belt were 1°C warmer than those measured at their closest neighbor sites within the wheat belt.

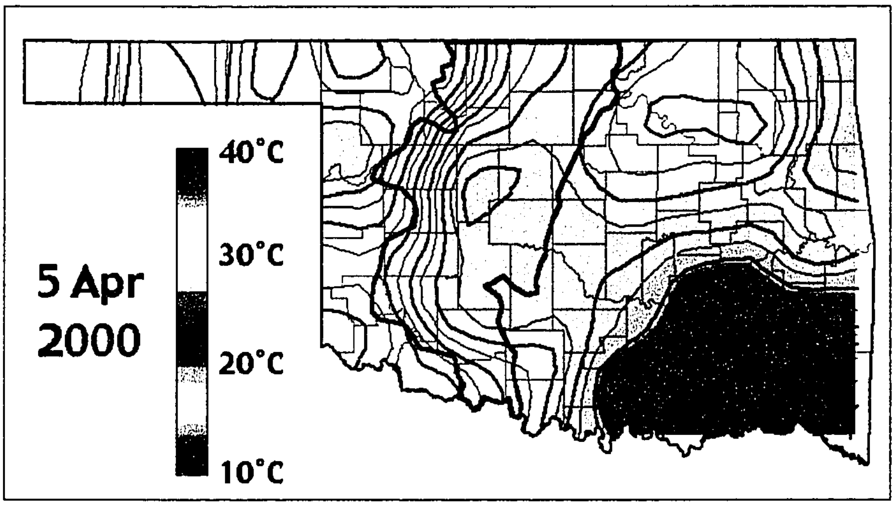

FIGURE 5.24. Same as Fig. 5.22 except for air temperatures (color contours).

As in the 4 April 2000 case, KVNX detected the development of a thin line that was oriented from southwest to northeast and was located in eastern Woods County (Fig. 5.25). At 1630 CDT on 5 April, the thin line was evident in an image acquired via the radar's precipitation mode. While other nearby echoes progressed toward the east, the thin line remained quasi-stationary until 1830 CDT, when it began to move northwest. As before, the thin line became undetectable by 1930 CDT. Winds at the Alva Mesonet site backed from 253° at 1620 CDT to 192° at 1625 CDT; a *corresponding dewpoint increase of 7.7°C was measured during this 5-minute period* (Fig. 5.26). Between 1630 and 1730 CDT, the wind direction at Alva varied between 178° and 216° and dew points remained greater than 10°C. From 1735 to 1800 CDT, winds shifted to westerly and the dewpoint values plunged to 1.6°C. After 1800 CDT, winds returned to southerly or south-southeasterly. The wind direction and dew point changes appeared to coincide with the movement of the thin line. The observations are consistent with the documented attributes of a vegetation breeze (e.g., Doran et al. 1995; Smith et al. 1994).

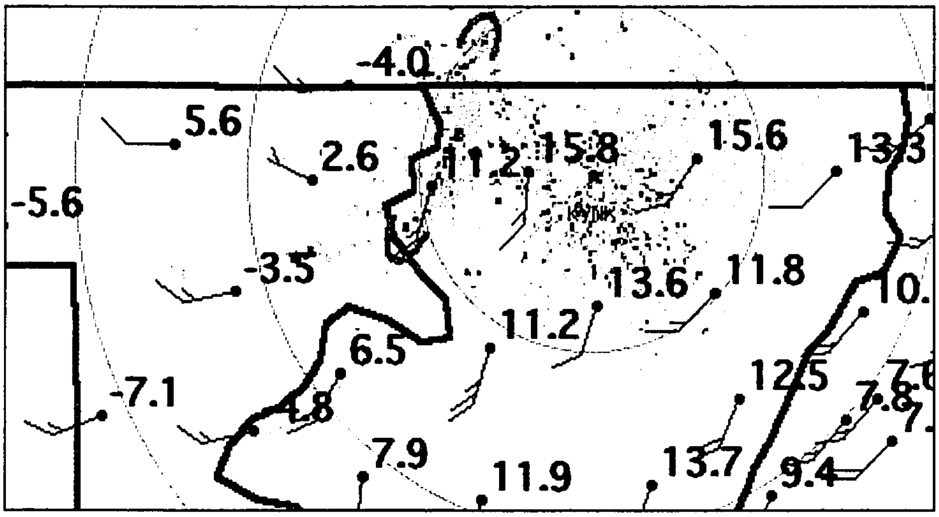


FIGURE 5.25. Base reflectivity at 1728 CDT on 5 April 2000 from the Vance Air Force radar (KVNX) in north-central Oklahoma. The red horseshoes depict the location of the ends of the thin line. Mesonet winds and dew points at 1725 CDT are identified by barbs and numbers, respectively. A full barb represents 5 m s$^{-1}$. The black outline portrays the boundary of Oklahoma's wheat belt. Radar data are courtesy of the Oklahoma Climatological Survey.

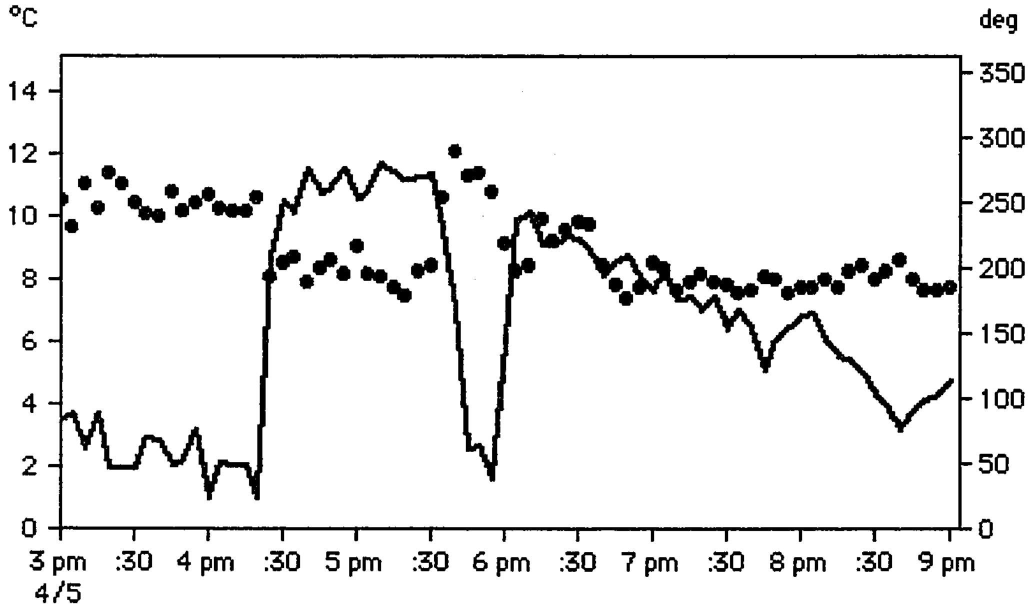


FIGURE 5.26. Graph of 5-minute measurements of dew point (green line, TDEW) and wind direction (blue dots, WDIR) at the Alva Mesonet site between 1500 and 2100 CDT on 5 April 2000.

## 5.5 Daily Impact of the Wheat Belt: Post-Harvest

As noted in Section 5.3, a warm anomaly commenced during June (Fig. 5.2*h*) as wheat growers completed the harvest. The warmer temperatures persisted through July (Fig. 5.2*i*) and August (Fig. 5.2*j*). In fact, for 92 (out of 183) days from June and July of 1999, 2000, and 2001, a distinct warm anomaly existed in the daily maximum temperature field over the wheat belt, particularly across north-central Oklahoma. It was possible that, during a number of these days, warm air advection from the Mexican Plateau into southwestern Oklahoma masked the TMAX signature from the wheat fields. By two-week periods, the number of days classified as showing evidence of warm anomalies was 19 days between 1 June and 15 June, 13 days between 16 June and 30 June, 30 days between 1 July and 15 July, and 30 days between 16 July and 31 July.

Strong solar forcing appeared to be the most evident factor related to the existence of a warm anomaly over the wheat belt. Using the same grouping of stations noted in Table 5.2, the average of the total daily solar radiation was computed for regions "West", "Wheat", and "East". The computed average for each of the three regions was greater than 26 $MJ/m^2$ on 72 days during June and July of 1999-2001. On 62 of those days, warm anomalies were evident over north-central Oklahoma. Of the 10 remaining days, four were marked by significant cloud cover elsewhere in the state, one was influenced by the passage of a weak cold front, and three exhibited a slight warm anomaly over the wheat belt.

Figures 5.27 and 5.28 display TMAX for 10 July 2000 and 14 July 2000, respectively. These two days typified those summer days when Oklahoma's harvested wheat belt most influenced its environment. The associated visual greenness map for the week ending 13 July 2000 is displayed in Fig. 5.29.

To better interpret the observations for 10 and 14 July 2000, three caveats are noted. First, because cattle ranching was a substantial industry across western and northwestern Oklahoma, grazing by livestock reduced the foliage of western grasslands from June to August. Hence, the vegetation gradient across the western boundary of the wheat belt was not as distinct during the summer of 2000 as during the early spring. Second, summer crops were grown across some of the farmland within Oklahoma's winter wheat belt. In particular, Caddo County produced 63 million pounds of peanuts on 25,500 acres during Summer 2000. In addition, hay grew across substantial acreages within Comanche, Caddo, and Grady counties. Third, the El Reno Mesonet site was situated on the Grazinglands Research Laboratory for the U.S. Department of Agriculture. The vegetation in this area was atypical of the wheat belt during the summer. On Fig. 5.30, the small region of dark green pixels in central Canadian County denotes where the El Reno site was located. Because of the dense vegetation in this region, TMAX values from El Reno were not representative of maximum temperatures above wheat stubble across other regions of Canadian County.

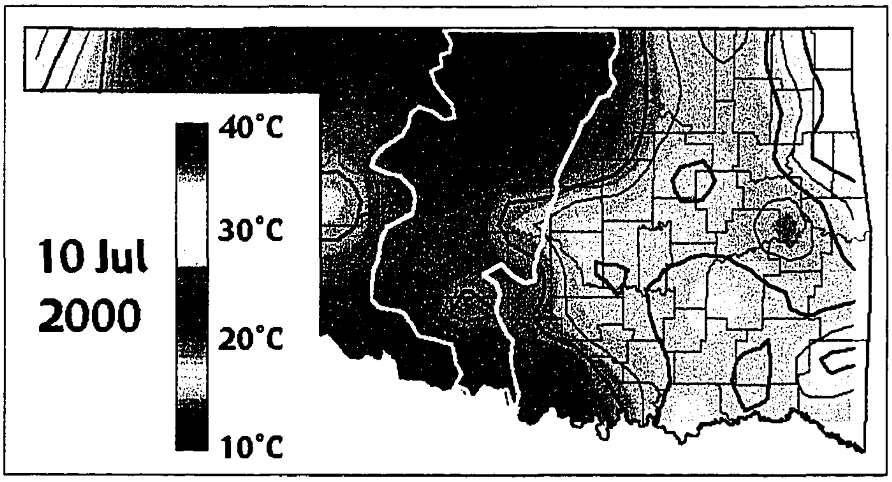

FIGURE 5.27. Map of the maximum air temperatures for 10 July 2000. A one-pass Barnes technique was used for the objective analysis. The white outline represents the boundary of Oklahoma's winter wheat belt.

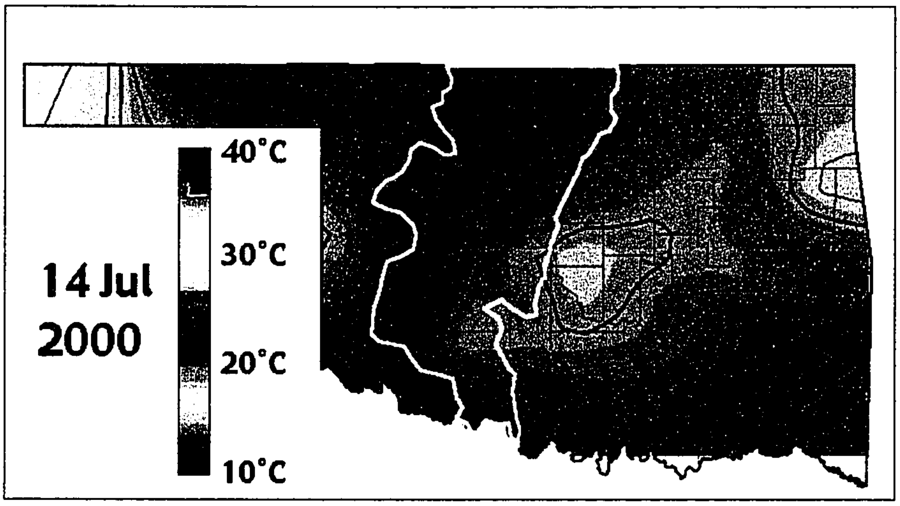


FIGURE 5.28. Map of the maximum air temperatures for 14 July 2000. A one-pass Barnes technique was used for the objective analysis. The white outline represents the boundary of Oklahoma's winter wheat belt.

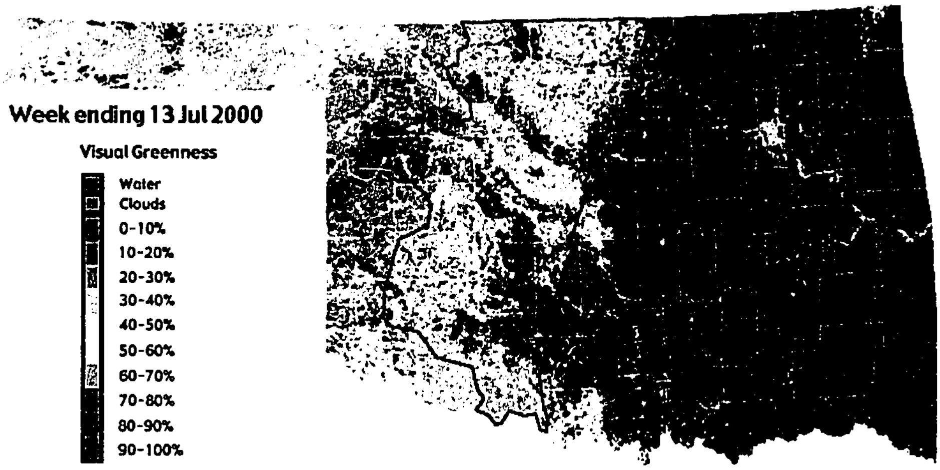


FIGURE 5.29. Visual greenness map for the week ending 13 July 2000. The black outline represents the boundary of Oklahoma's winter wheat belt.

*5.5.1 10 July 2000*

A high pressure system dominated Oklahoma's weather from 4 July to 10 July 2000. Consequently, no rainfall was measured during this period and skies were predominantly clear. Statewide, winds were from the south-southeast, south, or south-southwest at an average speed of 4.8 m $s^{-1}$. Values of TMAX (Fig. 5.21) across the northern third of Oklahoma's wheat belt ranged from 36.9°C at Marshall (MARS) to 39.4°C at Medford (MEDF). Directly east of and adjacent to this region, maximum temperatures varied from 34.9°C at

Marena (MARE) to 36.3°C at Red Rock (REDR). Across southwest Oklahoma, southerly winds advected air warmer than 38°C northward from north-central Texas. Despite the warm air advection, daytime temperatures were ~1°C warmer across north-central Oklahoma than across southwest Oklahoma.

The relative maximum in air temperatures across north-central Oklahoma extended southwest (Fig. 5.27) across the central third of Oklahoma's wheat belt (divided north to south). Within the harvested wheat belt, the value of TMAX at Weatherford (WEAT) was 36.1°C and at Hinton (HINT) was 36.3°C. In contrast, at the same latitude but outside of the wheat belt, the Cheyenne Mesonet site (CHEY) measured 34.7°C as the maximum air temperature. The value of TMAX was 37.3°C at Watonga (WATO), a site that was centrally located within the wheat belt. In comparison, at the western boundary of the wheat belt, the TMAX value at Camargo (CAMA) was 35.7°C . West of the wheat belt, the TMAX value at Arnett (ARNE) was 35.6°C.

The eastern side of the center portion of the wheat belt did not exhibit a distinct warm anomaly (Fig. 5.27), as was measured directly to the west. Cooler temperatures at several of the Mesonet sites across this swath influenced the one-pass Barnes analysis used to create the contour map. The local influence of vegetation on the maximum daily temperatures for 10 July became evident from a close inspection of Fig. 5.30. Although TMAX values ranged from 36.0°C to 36.9°C across the western side of the harvested wheat, maximum daily temperatures of only 34.5°C, 34.8°C, 35.4°C, and 34.9°C were measured at the El Reno (Canadian County), Minco (northern Grady County), Apache (southern Caddo County), and Medicine Park (Comanche County) Mesonet sites, respectively. By comparing these observations with a concurrent visual greenness map, one notes that these sites were characterized by growing vegetation. Recall that Medicine Park was situated in the grasslands of a wildlife refuge and El Reno resided on a grasslands research area. Furthermore, summer crops of peanuts, hay, watermelon, and corn were grown across portions of Grady and Caddo counties.

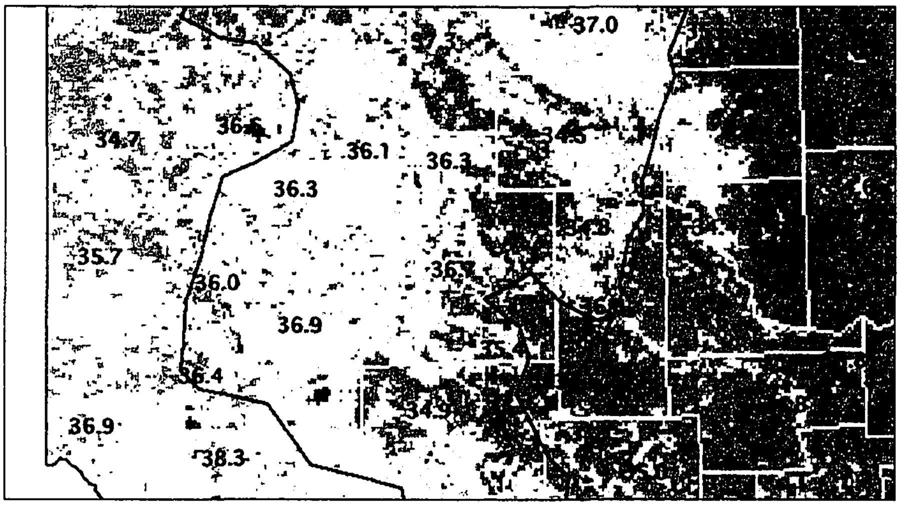


FIGURE 5.30. Zoomed map of visual greenness for the week ending 13 July 2000 with plotted observations of the daily maximum air temperature (TMAX) in degrees Celsius for 10 July 2000. The solid black line represents the boundary of Oklahoma's winter wheat belt.

A colorized animation of wind vectors and isotherms (not shown) provided evidence that the warm anomaly across the harvested wheat belt did not result from warm air advection. Instead, the temperatures increased locally across the wheat belt. The cause of the warming was an increase in the flux of sensible heat. Shortly before sunrise, an extremely weak gradient of air temperature existed across the wheat belt and adjacent lands. Within 75 minutes after sunrise, a warm anomaly became evident across portions of northern Oklahoma within the harvested wheat belt. Throughout the morning, the temperature maximum intensified and expanded in size outward from the wheat belt. Along an east-west line through central Oklahoma, the temperature gradient remained minimal until about 1315 CDT. By 1500 CDT, a warm anomaly was well-defined across north-central Oklahoma (Fig. 5.31). By 1700 CDT, temperatures began to decrease statewide. Shortly after 0100 CDT on 11 July, the temperature pattern ceased to resemble the vegetation pattern across the state.

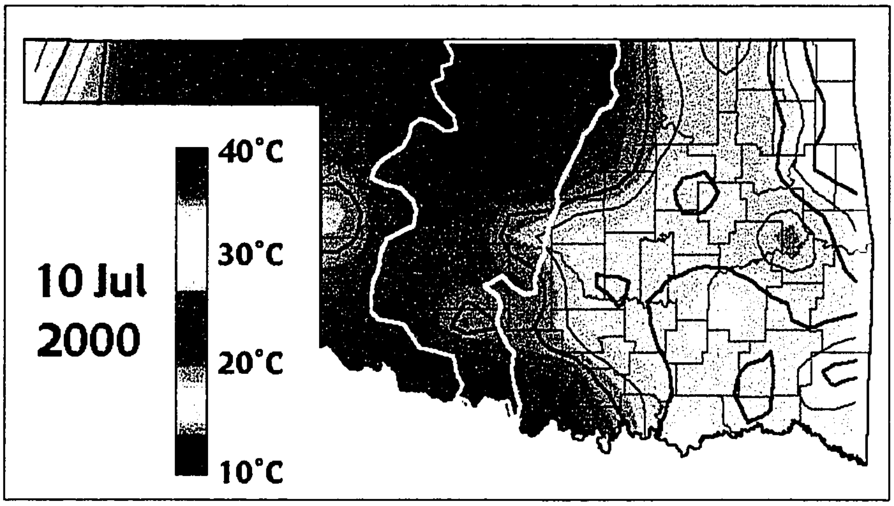

FIGURE 5.31. Map of near-surface air temperatures at 1500 CDT on 10 July 2000. A one-pass Barnes technique was used for the objective analysis. The white outline depicts the boundary of Oklahoma's wheat belt.

*5.5.2 14 July 2000*

A weak low pressure system crossed the Central Plains into the Ohio Valley between 11 July and 13 July 2000. The low pressure brought bands of cloud cover across portions of Oklahoma during those three days. By 14 July, high pressure again dominated Oklahoma's near-surface atmosphere, and the skies were clear except for sporadic cumulus clouds. Winds were calm statewide prior to sunrise on the 14th and remained so until 1200 CDT, with the exception of the Panhandle, where light south-southwest winds prevailed. Light easterly winds blew across the main body of Oklahoma during early afternoon. By 1600 CDT, the southerly winds across the Panhandle extended eastward across the harvested wheat in north-central Oklahoma. At sunset, winds became calm across the eastern third of Oklahoma, were light southeasterly across the Panhandle and northwestern quarter of Oklahoma, and were light easterly throughout the remainder of the state. Statewide, winds averaged 1.8 m $s^{-1}$ on 14 July.

Patterns in the TMAX field were similar between 10 July (Fig. 5.27) and 14 July (Fig. 5.28); both mimicked the pattern in the visual greenness map

(Fig. 5.29). The northern third of Oklahoma's wheat belt exhibited the largest TMAX values, which ranged from 36.7°C at Marshall to 39.3°C at Cherokee. Directly east of this region, maximum temperatures varied from 35.1°C at Marena to 36.1°C at Red Rock. To the west, Woodward (in western Woodward County) measured 35.6°C as its daily high temperature.

Stations within the central third of Oklahoma's harvested wheat belt (divided north to south), where the landscape included grassland and summer crops, observed maximum temperatures 1°-2°C cooler than those across the northern third of the wheat belt. Similar to 10 July, TMAX values across southwestern Oklahoma were larger than those across the central third of the wheat belt; yet, the maximum temperatures across southwestern Oklahoma were cooler than those across the northern third of the wheat belt.

Just before sunrise, temperatures across "Wheat" and "West" were about 1.5°C cooler than those across "East" (Fig. 5.32). By 1700 CDT, when temperatures attained their daily maximum, "Wheat" was 2.5°C warmer than "East" and 1.3°C warmer than "West". Hence, the diurnal temperature range on 14 July was larger across the harvested wheat than across adjacent lands with growing vegetation.

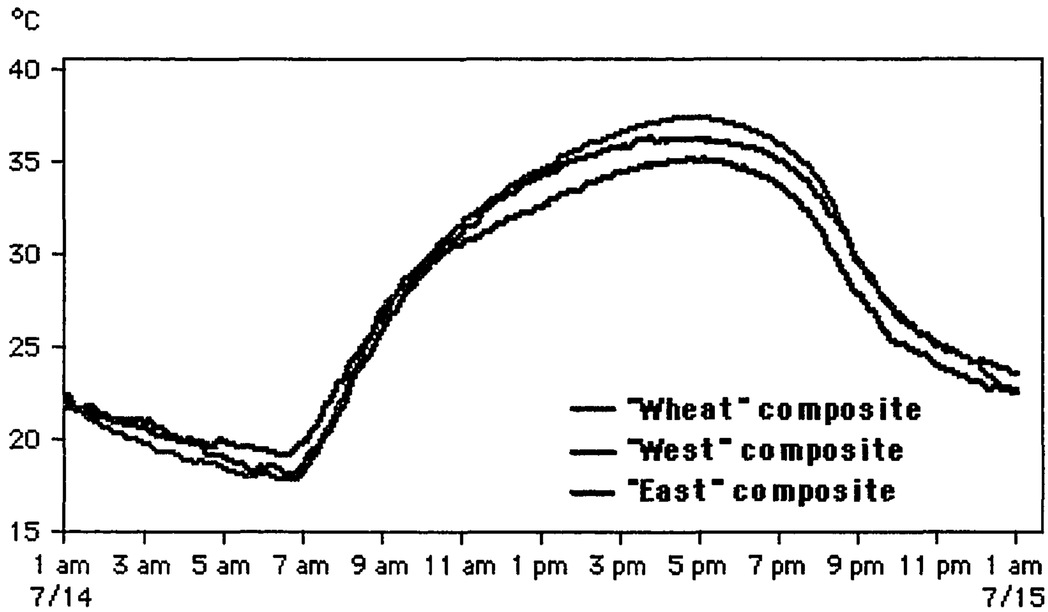


FIGURE 5.32. Graph of composite 5-minute observations of air temperature for regions "West", "Wheat", and "East" between 0100 CDT on 14 July 2000 and 0100 CDT on 15 July. The green, red, and blue lines denote the composite temperature for "Wheat", "West", and "East", respectively (see Table 5.1). The composite data were constructed from the average of all observed values at a given time for the sites located with each region. The time series plot extends from midnight to midnight CST – the interval for computing DMAX.

## 5.6 Overview of Observational Analyses

Analyses of many related observations demonstrated that Oklahoma's winter wheat belt had a significant impact on the near-surface temperature and moisture fields, both during the period when winter wheat was growing and during the period after harvest. In particular, the following results are noteworthy from this study:

1. As vegetation grew across the wheat belt, maximum daily temperatures were cooler than those measured over adjacent regions of dormant grasslands. Monthly averaged values of TMAX (maximum daily air temperature) for Crop Year 2000 displayed a cool anomaly over the growing wheat from November 1999 through April 2000. Using Mesonet data from 1994 through 2001, the cooler temperatures over the wheat belt

were shown to be statistically significant at the 95% confidence level for November, December, January, February, and April.

2. As green-up of grasslands occurred during May, the cool anomaly over the wheat belt disappeared. After the wheat was harvested, maximum and minimum daily temperature data revealed a warm anomaly across the wheat belt during June, July, and August. The warmer temperatures also were shown to be statistically significant for all three months.

3. Monthly averaged values of DMAX and DMIN (maximum and minimum daily dew points) indicated a slight moist bias during the early spring across the wheat belt, particularly during March. DMAX for Crop Year 2000 indicated a slight moist anomaly over the growing wheat from November 1999 through April 2000. Based upon 21,000 daily statistics over eight unique years, statistical computations indicated *less than a 0.1% chance* that the moist anomaly during March resulted from random chance.

4. During the period from 1999 to 2001, about 50 days between 15 March and 1 June showed evidence of heightened DMAX values over Oklahoma's winter wheat belt as compared to adjacent grasslands. On more than half of these days, the dew points were enhanced across only five or six counties in north-central Oklahoma, where the winter wheat production was the highest.

5. Case studies from the spring of 2000 indicated that the presence of growing wheat impacted the maximum daily dew points and the diurnal cycles of dew point on days with both weak and moderate winds, and in

both moist and dry air masses. Days with clear skies were examined so that uneven solar forcing across the state did not mask the results.

6. Examination of wind and dew point data from the Freedom Mesonet site demonstrated the impact that moisture advection from local wheat fields had on dew point measurements. On the mesoscale, moisture advection from the wheat belt enhanced both downstream dew points and the *rate* of increase of dew point during midday over lands adjacent to the wheat belt.

7. For the spring case studies, a comparison of the prior week's rainfall with values of dew point demonstrated that the growing wheat was more efficient at recirculating water back to the atmosphere than was dormant grassland in adjacent lands.

8. On two of the case study days (4 April and 5 April), evidence supported the existence of a vegetation breeze in Woods County.

9. During the period from 1999 to 2001, about 90 days between 1 June and 31 July revealed a distinct warm anomaly in daily maximum air temperatures over the wheat belt, particularly across north-central Oklahoma. Case studies from the summer of 2000 indicated that the warmer temperatures over the harvested wheat resulted from local heating rather than from warm air advection.

# CHAPTER 6: RESULTS FROM MODEL SIMULATIONS

## 6.1 Motivation

Observational evidence for the impact of the Oklahoma winter wheat belt on the mesoscale environment was discussed in Chapter 5. The observations, however, did not document fully the land surface's influence on the structure and evolution of the planetary boundary layer; nor did the observations reveal the physical processes that caused the reported surface anomalies of temperature and moisture. To better understand the observational results, a numerical modeling study was conducted.

Numerical model simulations also afforded the unique opportunity to examine how the natural environment might evolve from *identical* initial conditions in the *absence* of a wheat belt. Thus, the motivation for conducting numerical simulations was to provide additional insight into the physical mechanisms by which the regional wheat belt impacted the mesoscale atmosphere.

## 6.2 Simulation Design

Simplicity and realism were the guiding characteristics of the design of the numerical model studies. Previous authors had examined a variety of parameter spaces related to the impact of vegetation on the atmosphere. Rather than conduct an exhaustive set of simulations, this study simply compared numerical runs both with and without a simulated wheat belt. In this manner, the impact of the vegetation region could be identified directly and analyzed through difference fields. To link the simulations to reality, observations and Eta analyses were input into the model from three of the case study days discussed in Chapter 5. Modeled surface fields were compared to observed fields from the

Oklahoma Mesonet to verify that the model was simulating the near-surface atmosphere adequately.

Three case study days were selected: 27 March 2000, 5 April 2000, and 14 July 2000. For each case, two simulations were conducted: one with a simulated wheat belt – hereafter called a *wheat run* – and one with simulated natural grassland that substituted for the wheat belt – hereafter called a *natural vegetation run*. Hence, the numerical modeling study involved six simulations (Table 6.1). The spring cases – 27 March and 5 April – were selected as those that represented clear days with weak to moderate winds, respectively. Results in Chapter 5 already revealed a demonstrable impact on the surface environment by growing wheat. The July case represented a clear day during the summer when the harvested wheat belt influenced the lower atmosphere. Initial atmospheric and soil conditions were identical for both the wheat and natural vegetation runs on any given day.

TABLE 6.1. Overview of numerical model simulations conducted.

| | 27 Mar 2000 | 5 Apr 2000 | 14 Jul 2000 |
|---|---|---|---|
| **Wheat Run** | Wheat belt represented as growing crop | Wheat belt represented as growing crop | Wheat belt represented as bare soil or sparse vegetation |
| **Natural Vegetation Run** | Wheat belt represented as dormant grassland | Wheat belt represented as dormant grassland | Wheat belt represented as growing grassland |

The model was initiated at 1200 UTC for every simulation, and its equations were computed at time steps of 36 s and 12 s for the mother and nested domains, respectively. Although every model run extended through 12 hours of simulated time, the investigation focused on model hours 3, 6, and 9. At model hour 3, representing 1500 UTC, small differences between the wheat and natural vegetation runs became apparent. At model hour 6, representing 1800 UTC, incoming solar energy was near its daily maximum. By model hour 9, representing 2100 UTC, the maximum differences between the two runs were occurring.

A comparison of Figs. 3.1 and 4.5 highlights the limited capability of the 25-category USGS land use dataset (used in MM5) to delineate the wheat belt's region of mixed winter wheat and grassland (represented in Fig. 3.1 by light orange pixels). In addition, the physical parameters defined by the 25-category dataset (e.g., albedo, roughness length) were identical for winter wheat and corn, for example. Tsvetsinskaya et al. (2001), Xue et al. (1996), and others demonstrated the need to distinguish physical parameters adequately between substantially different crops to obtain representative simulation results in the lower atmosphere. Equally as restrictive for MM5, these parameters were not permitted to change throughout the growing season. As discussed in Chapter 2, physical characteristics of plants vary by vegetation type and stage of growth. Hence, for this study, the default vegetation parameters were deemed inadequate and were modified to obtain more representative results. Table 6.2 lists some of the parameters used to define the four most significant land use types in this study: mixed dryland/irrigated cropland/pasture (representing the wheat belt), grassland, savanna, and bare/sparse vegetation.

TABLE 6.2. Selected parameters used to define the vegetative state within the model.

| | Albedo (%) | Minimum Canopy Resistance (s m$^{-1}$) | | Roughness Length (m) |
|---|---|---|---|---|
| | | Spring | Summer | |
| Mixed Dryland/Irrigated Cropland and Pasture | 17 | 40 | N/A | .07 |
| Grassland | 19 | 300 | 40 | .08 |
| Barren or Sparsely Vegetated | 12 | N/A | 999 | .01 |
| Savanna | 20 | 300 | 300 | .86 |

Model results were sensitive to values of both soil moisture within the root zone and minimum stomatal conductance; these sensitivities were consistent with other modeling studies (e.g., Crawford et al. 2001; Chen and Dudhia 2001*a*; Collins and Avissar 1994). In most cases, these values were altered until the simulated near-surface temperatures and dew points aligned well with Mesonet observations. At that point, the author deemed that the chosen values were appropriate for the resulting simulations to be used to better understand the physical processes.

In addition to updating some of the default vegetation parameters, the extent of the winter wheat belt across Oklahoma, southern Kansas, and north-central Texas was redefined (Fig. 6.1*a*). The extensive but realistic expansion of the wheat region, originally limited to north-central Oklahoma and south-central Kansas, is evident from a comparison of Fig. 6.1*a* with Fig. 4.5. To obtain this expanded region, grid points that represented a mixture of winter wheat and grassland (light orange pixels on Fig. 3.1) were shifted from the "grassland" category in the model to the "mixed dry/irrigated cropland/pasture" category.

The reassignment of grid points to a different vegetation category was justified by the observational evidence presented in Chapter 5. More precisely, the Mesonet observations indicated that the atmosphere across the region of mixed winter wheat and grassland responded more like the winter wheat region than it did the grassland region. Hence, the USGS data set was modified to be more representative of the actual land use.

Because the simulated wheat belt was defined by 2438 selected grid points (on the nested domain), it was straightforward to swap those points to become bare/sparse vegetation for the summer wheat run (Fig. 6.1*b*) and grassland for all natural vegetation runs (Fig. 6.1*c*).

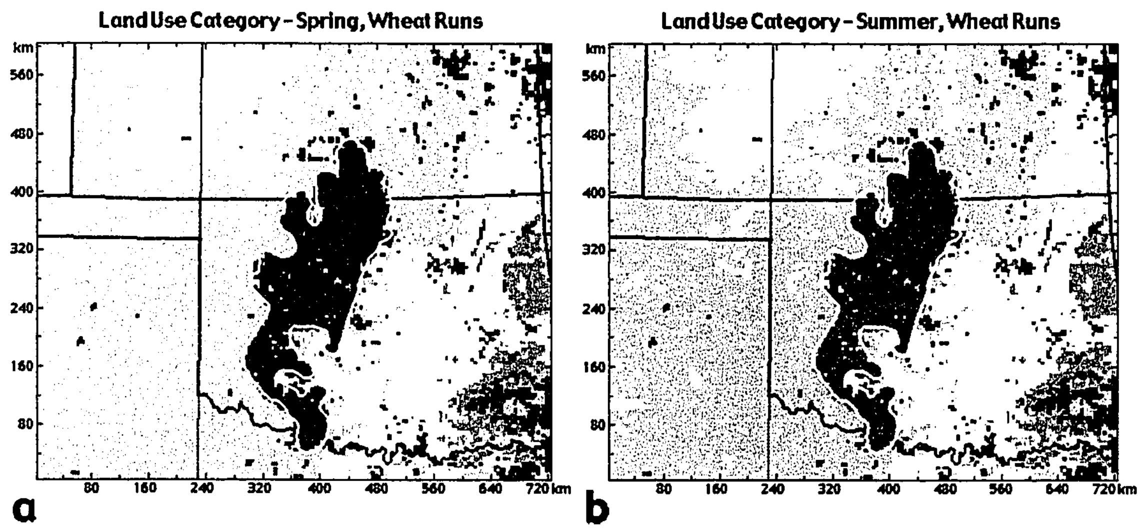


FIGURE 6.1. Redefined land use extent and categories employed in this study. The wheat belt was comprised of 2438 grid points defined as MM5 category (*a*) "mixed dry/irrigated cropland/pasture" (dark green) to represent growing wheat, (*b*) "bare/sparse vegetation" (dark orange) to represent harvested wheat, and (*c*) "grassland" (light green) to represent natural vegetation. Light yellow represents MM5 category "savanna". The white outline depicts the boundary of the wheat belt.

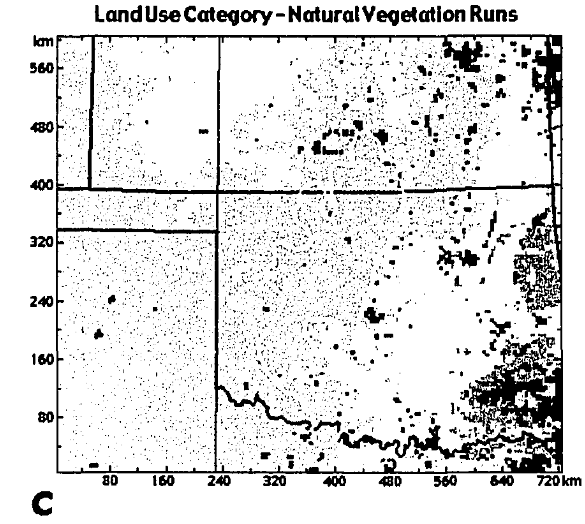


FIGURE 6.1. (Continued)

For the natural vegetation runs, the vegetation fraction was altered to better represent the lack of a wheat belt. In particular, for the spring simulations, the high values of vegetation fraction across north-central Oklahoma, where there was growing wheat in the wheat run, were reduced to values similar to those of the surrounding grassland or savannah. Similarly, for the summer simulation, the low values of vegetation fraction over this same region, where wheat was stubble in the wheat run, were increased to values more representative of growing grassland. Figures 6.2*a* and 6.2*b* display the spring vegetation fractions for the wheat and natural vegetation runs; Figs. 6.3*a* and 6.3*b* display the summer vegetation fractions for the wheat and natural vegetation runs.

Difference fields were computed for many of the simulation variables. For this study, a *difference field* was defined as a variable field from the natural vegetation run subtracted from that of the wheat run.

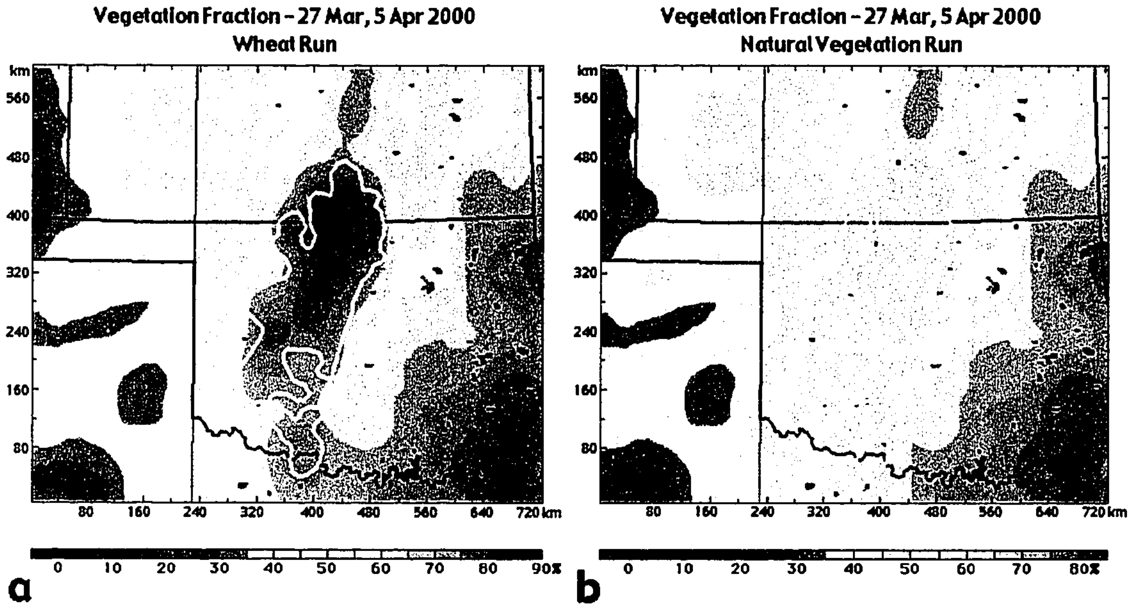


FIGURE 6.2. Vegetation fraction used for (*a*) the wheat run and (*b*) the natural vegetation run for both spring cases (27 March and 5 April 2000). Values shown for the wheat run were defined by the Oregon State University/ NCEP Eta Land-Surface Model as the monthly climatological vegetation fraction for April. Note the high percentage of vegetation (80-90%) through the heart of Oklahoma's winter wheat belt (across north-central and west-central Oklahoma) for the wheat run.

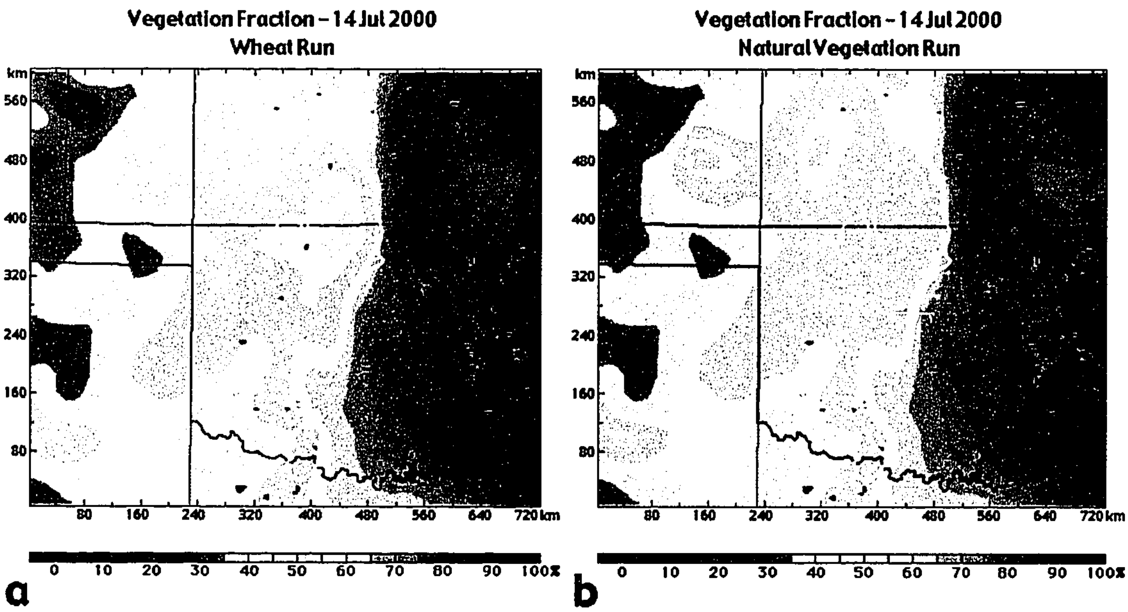


FIGURE 6.3. Same as Fig. 6.2 except for July. Note the low percentage of vegetation through Oklahoma's winter wheat belt for the wheat run.

## 6.3 Ability of the Model to Simulate Reality

To justify confidence in the model results, several fields from the wheat run were compared to observations at selected times. Recall that the modeled wheat belt did not distinguish cropland from a cropland/grassland mixture – the pervasive land use across the southern half of Oklahoma's wheat belt. As a result, the model was not expected to simulate the observations perfectly, rather to simulate overall patterns and relative amplitudes in near-surface atmospheric fields.

Figures 6.4 – 6.9 present the surface temperature and dew point fields for the 27 March, 5 April, and 14 July case studies at 1200, 1500, 1800 and 2100 UTC. The model evolution of the *patterns and amplitudes* of air temperature and dew point reflected those detected by observations during all three days (see Sections 5.4 and 5.5). Simulations of 27 March and 5 April demonstrated cooler temperatures and higher dew points over the wheat belt than over adjacent lands, most notably during midday through late afternoon. The 14 July simulation demonstrated warmer temperatures over the wheat belt than over adjacent lands during this same period of the day.

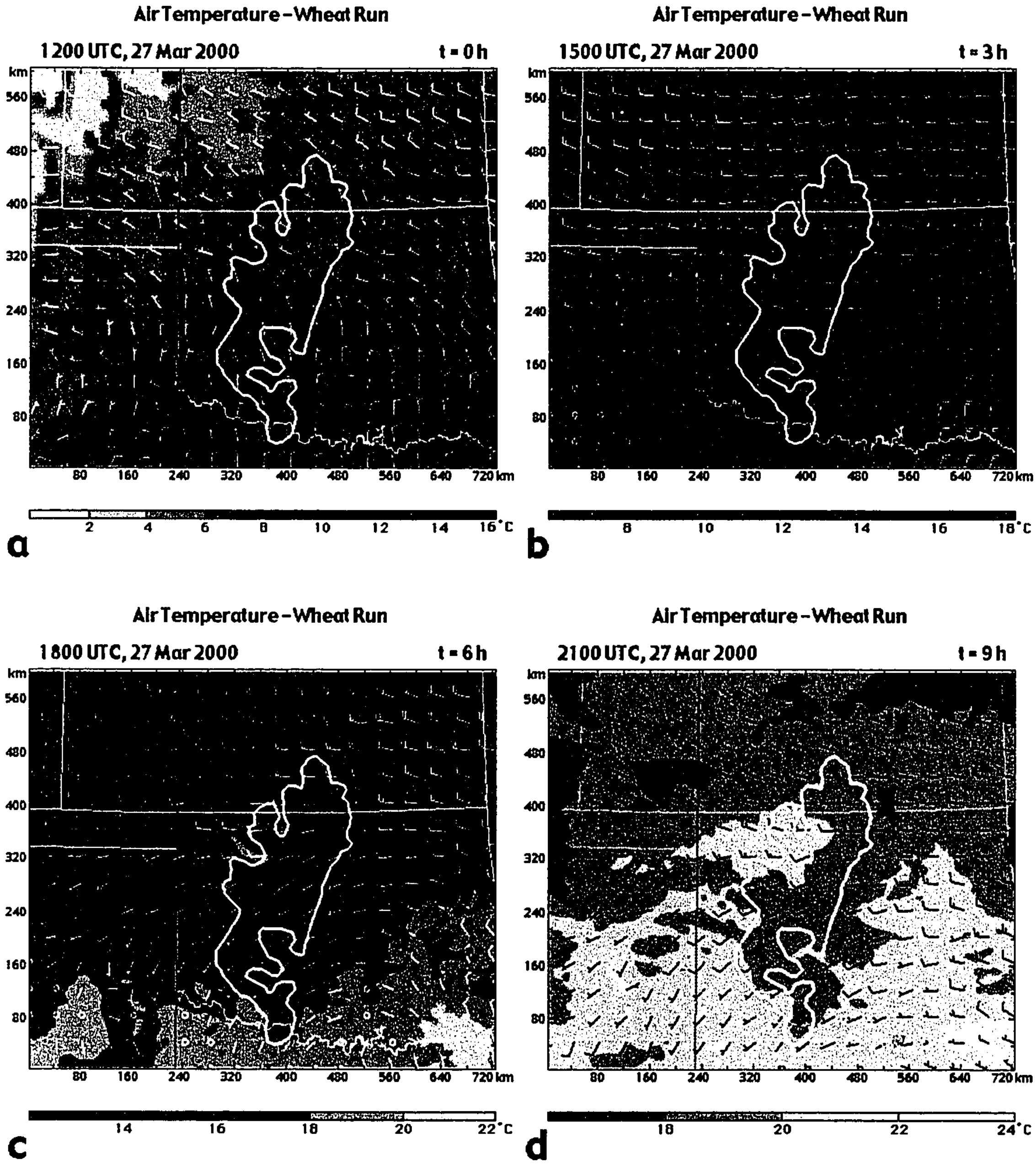


FIGURE 6.4. Air temperature (°C) and wind (m s$^{-1}$) fields at the lowest sigma level ($\sigma$ = 0.995) for the wheat run representing 27 March 2000 at (*a*) 1200 UTC (0600 CST), (*b*) 1500 UTC (0900 CST), (*c*) 1800 UTC (1200 CST), and (*d*) 2100 UTC (1500 CST). The white outline depicts the boundary of the wheat belt.

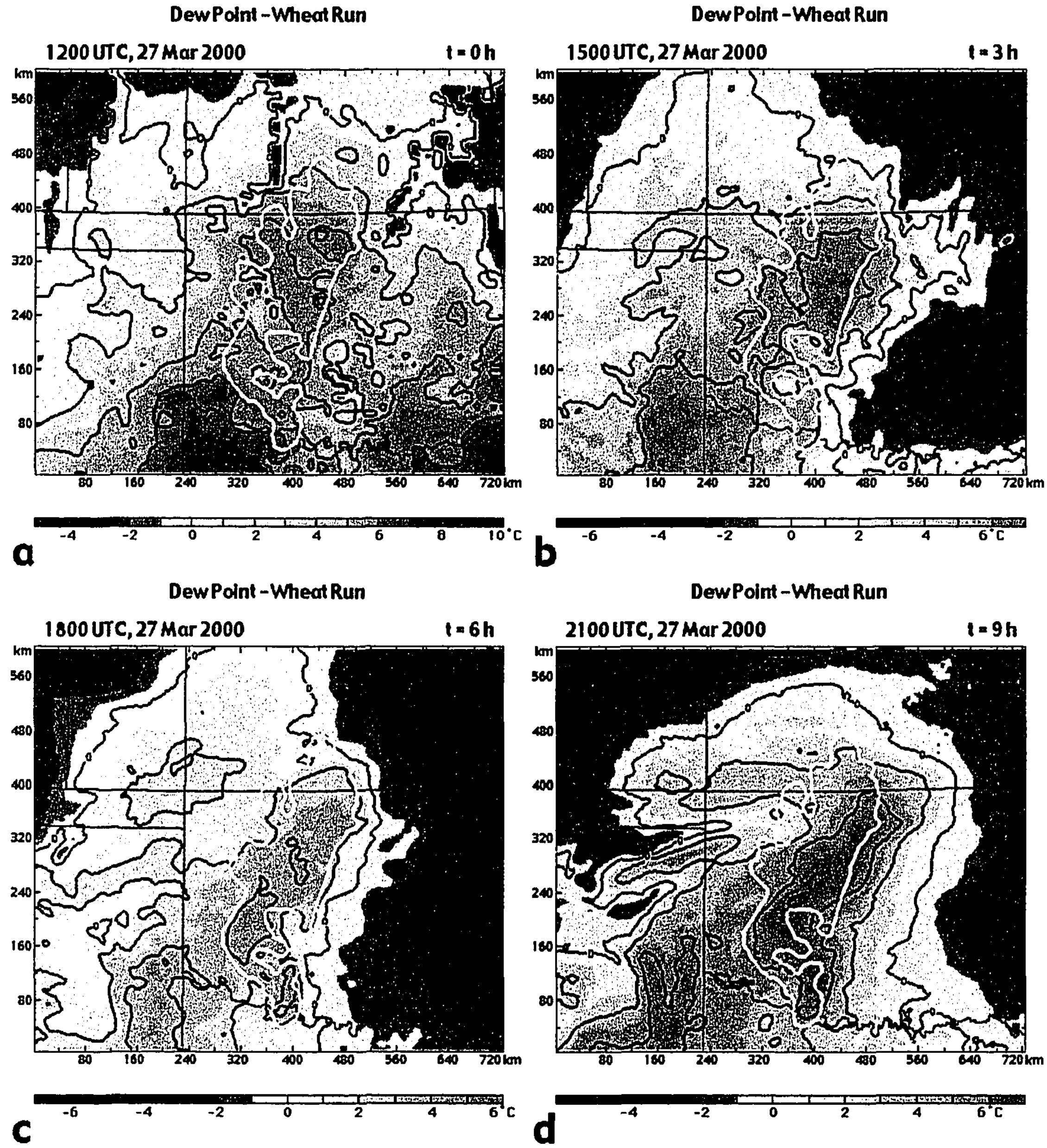


FIGURE 6.5. Dewpoint fields (°C) at the lowest sigma level ($\sigma$ = 0.995) for the wheat run representing 27 March 2000 at (*a*) 1200 UTC (0600 CST), (*b*) 1500 UTC (0900 CST), (*c*) 1800 UTC (1200 CST), and (*d*) 2100 UTC (1500 CST). The white outline depicts the boundary of the wheat belt.

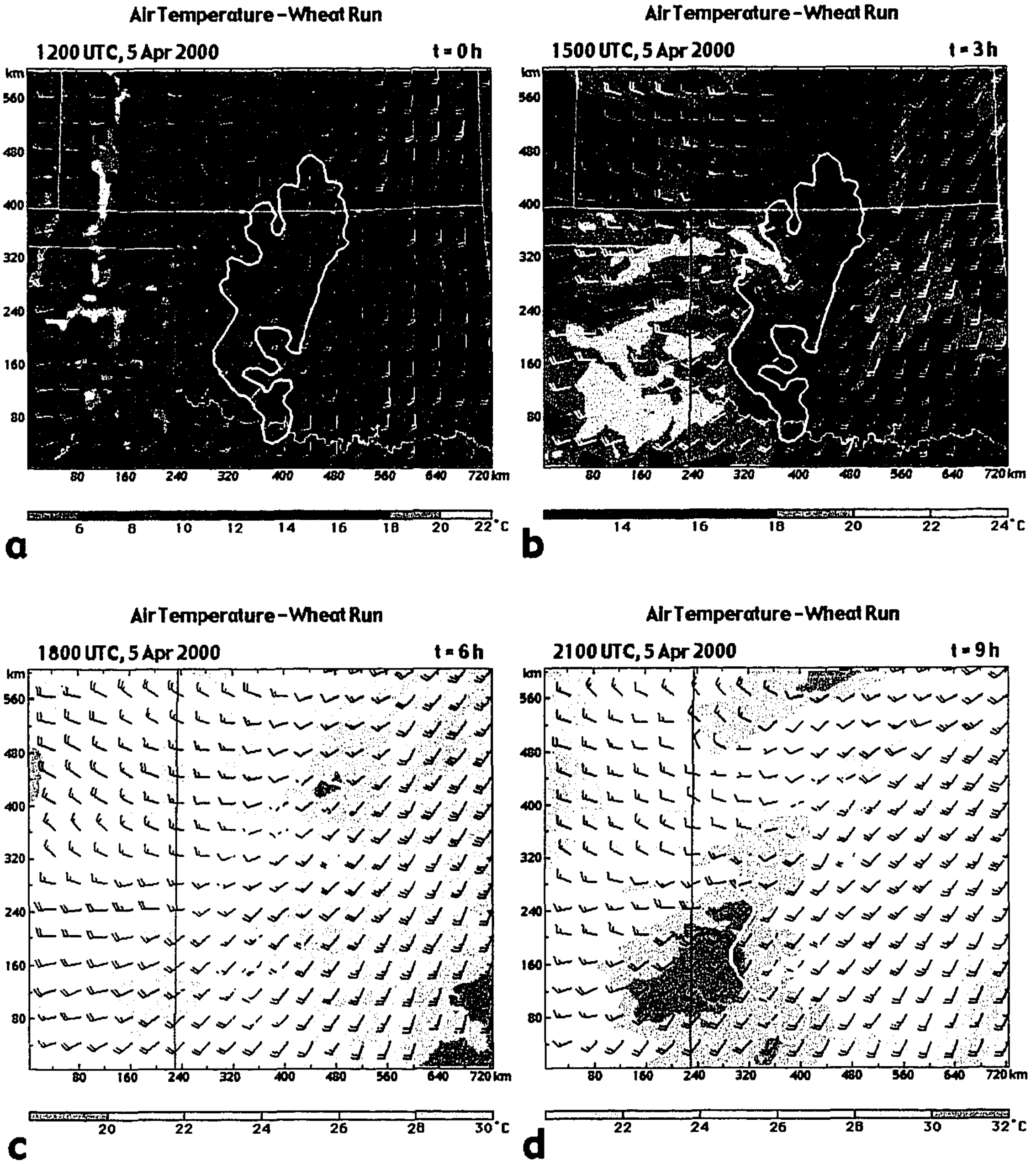


FIGURE 6.6. Air temperature (°C) and wind (m $s^{-1}$) fields at the lowest sigma level ($\sigma$ = 0.995) for the wheat run representing 5 April 2000 at (*a*) 1200 UTC (0700 CDT), (*b*) 1500 UTC (1000 CDT), (*c*) 1800 UTC (1300 CDT), and (*d*) 2100 UTC (1600 CDT). The white outline depicts the boundary of the wheat belt.

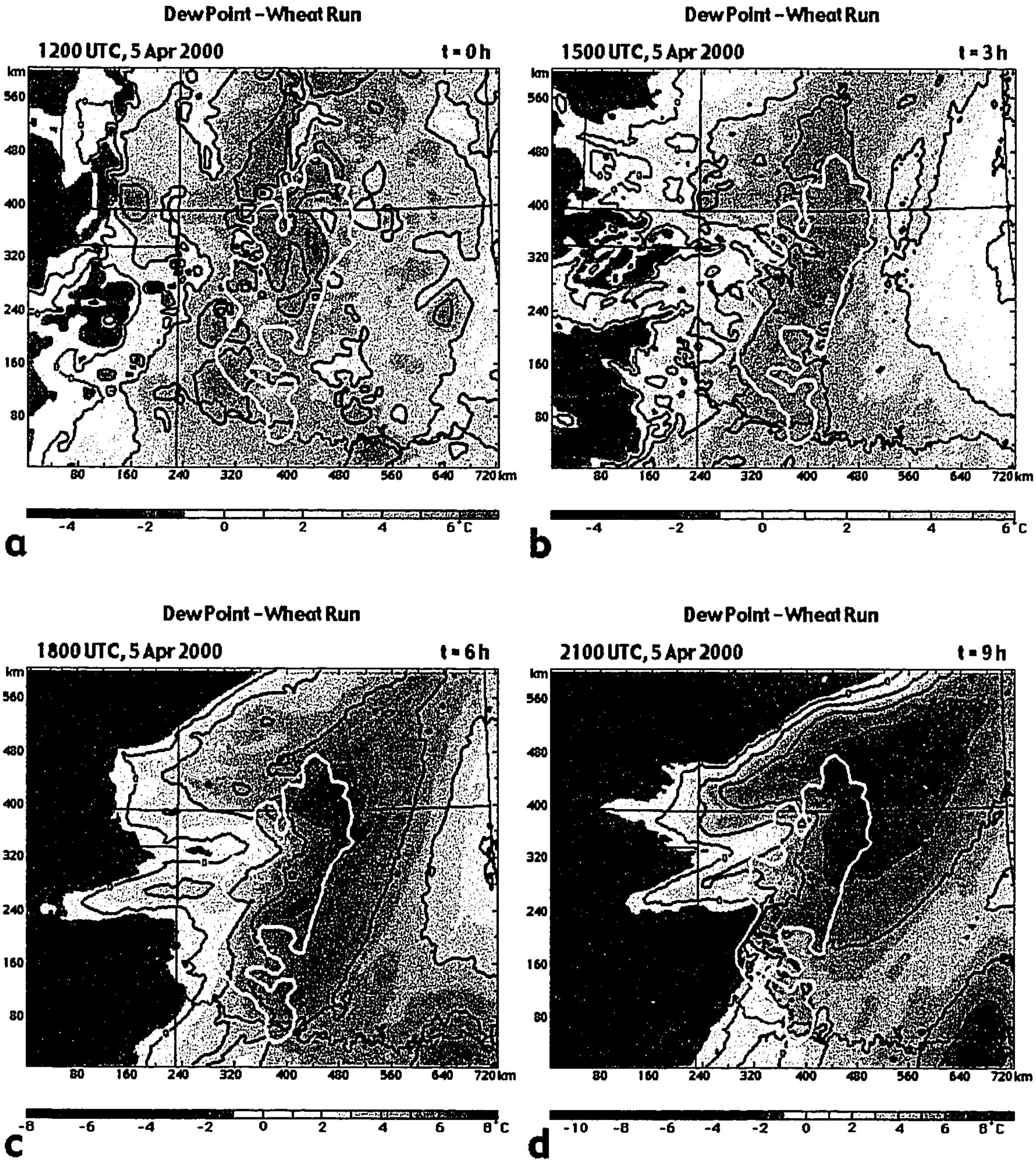


FIGURE 6.7. Dewpoint fields (°C) at the lowest sigma level ($\sigma$ = 0.995) for the wheat run representing 5 April 2000 at (*a*) 1200 UTC (0700 CDT), (*b*) 1500 UTC (1000 CDT), (*c*) 1800 UTC (1300 CDT), and (*d*) 2100 UTC (1600 CDT). The white outline depicts the boundary of the wheat belt.

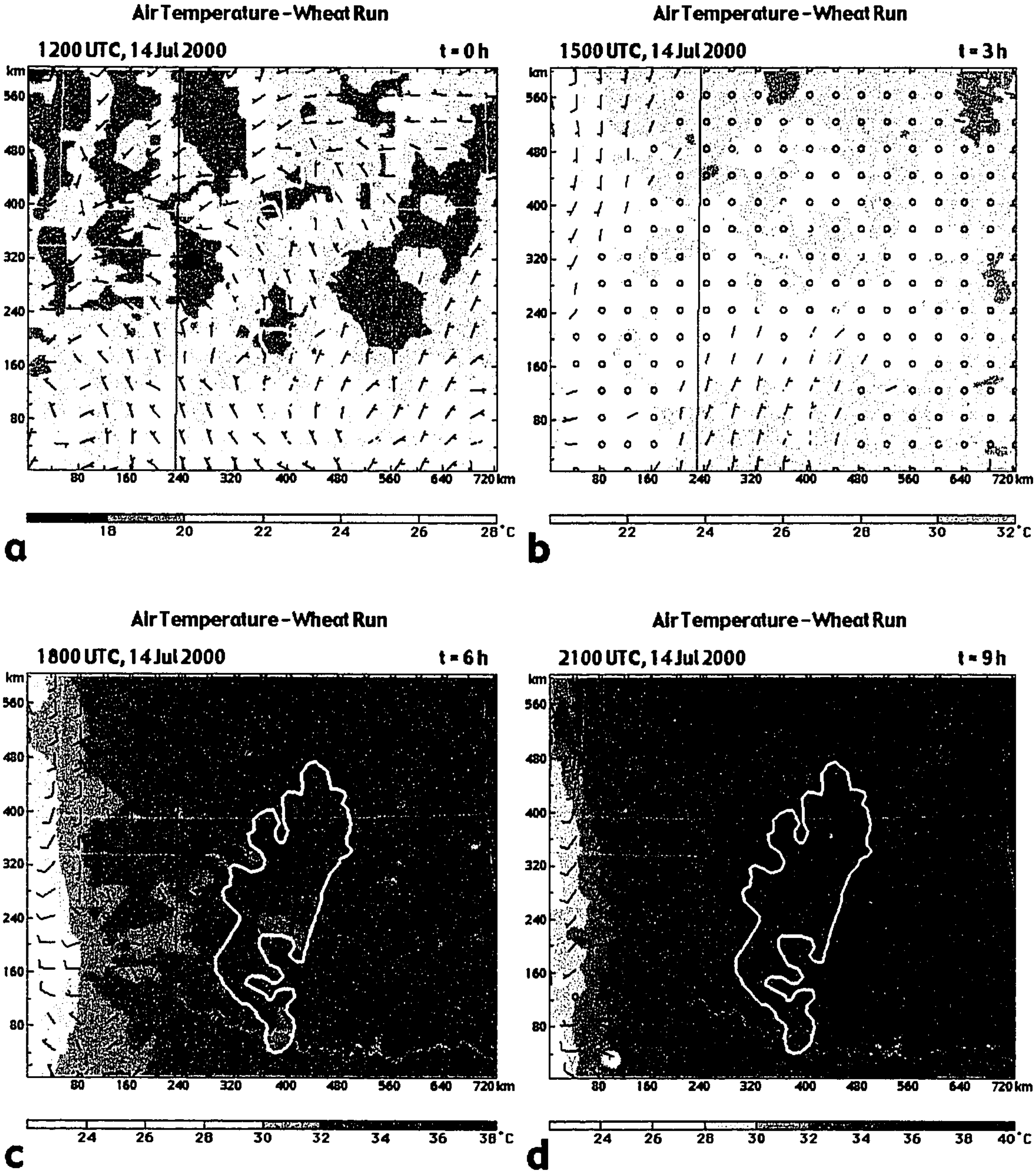


FIGURE 6.8. Same as Fig. 6.6 except for 14 July 2000.

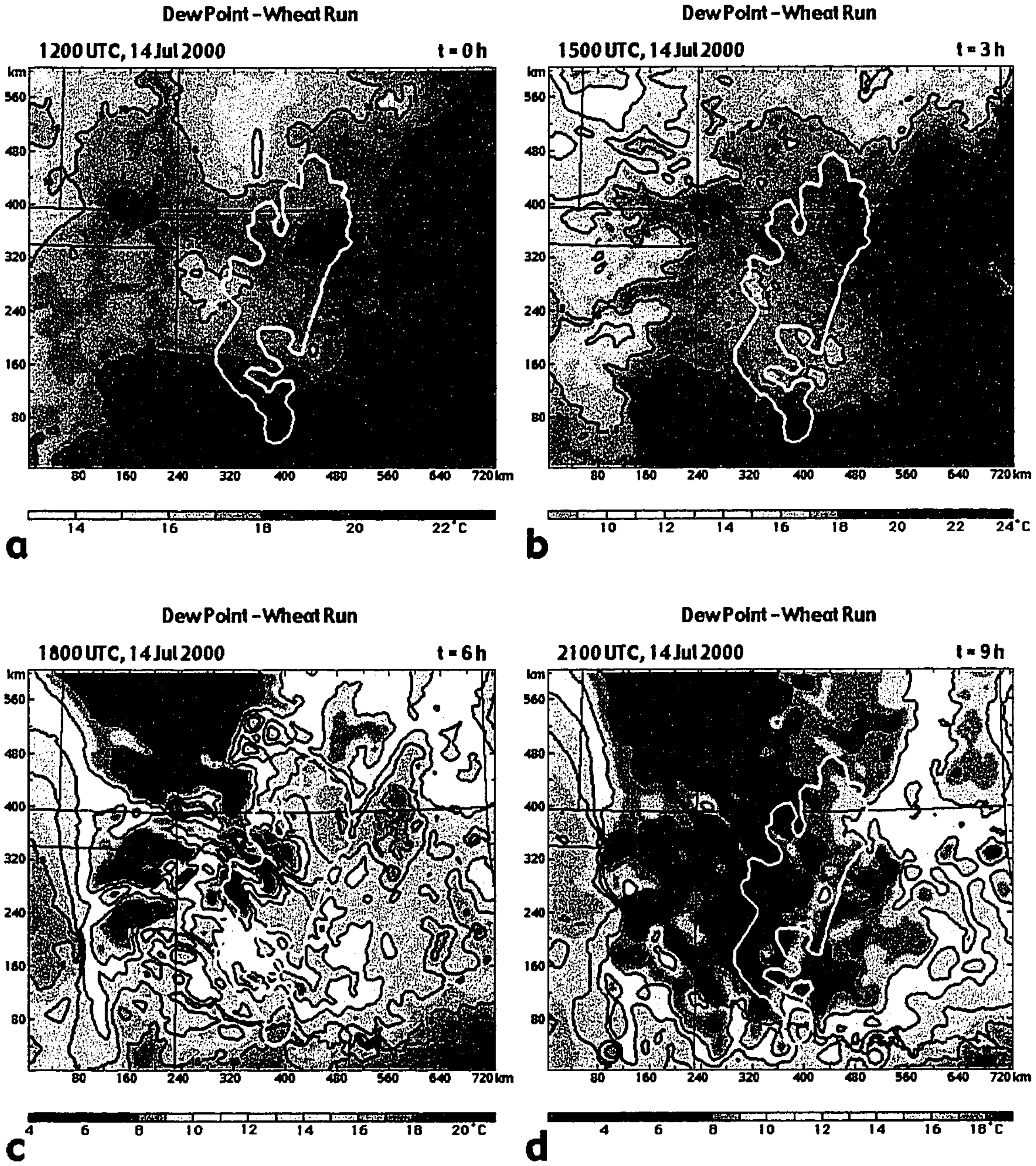


FIGURE 6.9. Same as Fig. 6.7 except for 14 July 2000.

## 6.4 Spring Cases: 27 March 2000 and 5 April 2000

Model simulations of 27 March 2000 and 5 April 2000 provided the basis for examining the impact of the wheat crop on the mesoscale environment during the growing season. The atmospheric conditions during 27 March and 5 April were typical of clear days during March or April. Recall that the primary differences between the near-surface synoptic conditions on 27 March versus 5 April were higher wind speeds and a stronger inversion on 5 April.

### *6.4.1 Simulation of 27 March 2000 conditions*

The near-surface field of atmospheric moisture for the 27 March simulation was initialized with the remnants of a moisture plume over the wheat belt. Near-surface dew points at 1200 UTC were 1 – 2°C higher over the wheat belt than about 30 km beyond the boundary of the wheat belt. Higher dew points also were evident across southeast Oklahoma, where moisture advection from the Gulf of Mexico during 26 March might have impacted the region.

Figure 6.10 displays examples of the initial thermodynamic profile over sites within, to the west of, and to the east of the wheat belt. At May Ranch (MAYR), west of the wheat belt, an inversion existed between the surface and 900 hPa (Fig. 6.10*a*). Within the wheat belt, the inversion was similarly deep at Cherokee (CHER) on the west side of the wheat belt (Fig. 6.10*b*). At Breckinridge (BREC), also within the wheat belt but on its east side, the inversion was about 50 hPa shallower (Fig. 6.10*c*). East of the wheat belt, over Pawnee (PAWN), the inversion depth was similar to that of BREC (Fig. 6.10*d*).

By 1500 UTC, winds had veered at all four sites (not shown) from westerly near the surface to northwesterly between 875 and 900 hPa. In addition, speed shear was evident between the surface (~2.5 m $s^{-1}$) and 700 hPa (20 – 25 m $s^{-1}$). This low-level shear became important to differences in vertical circulations between the wheat and natural vegetation runs (discussed later).

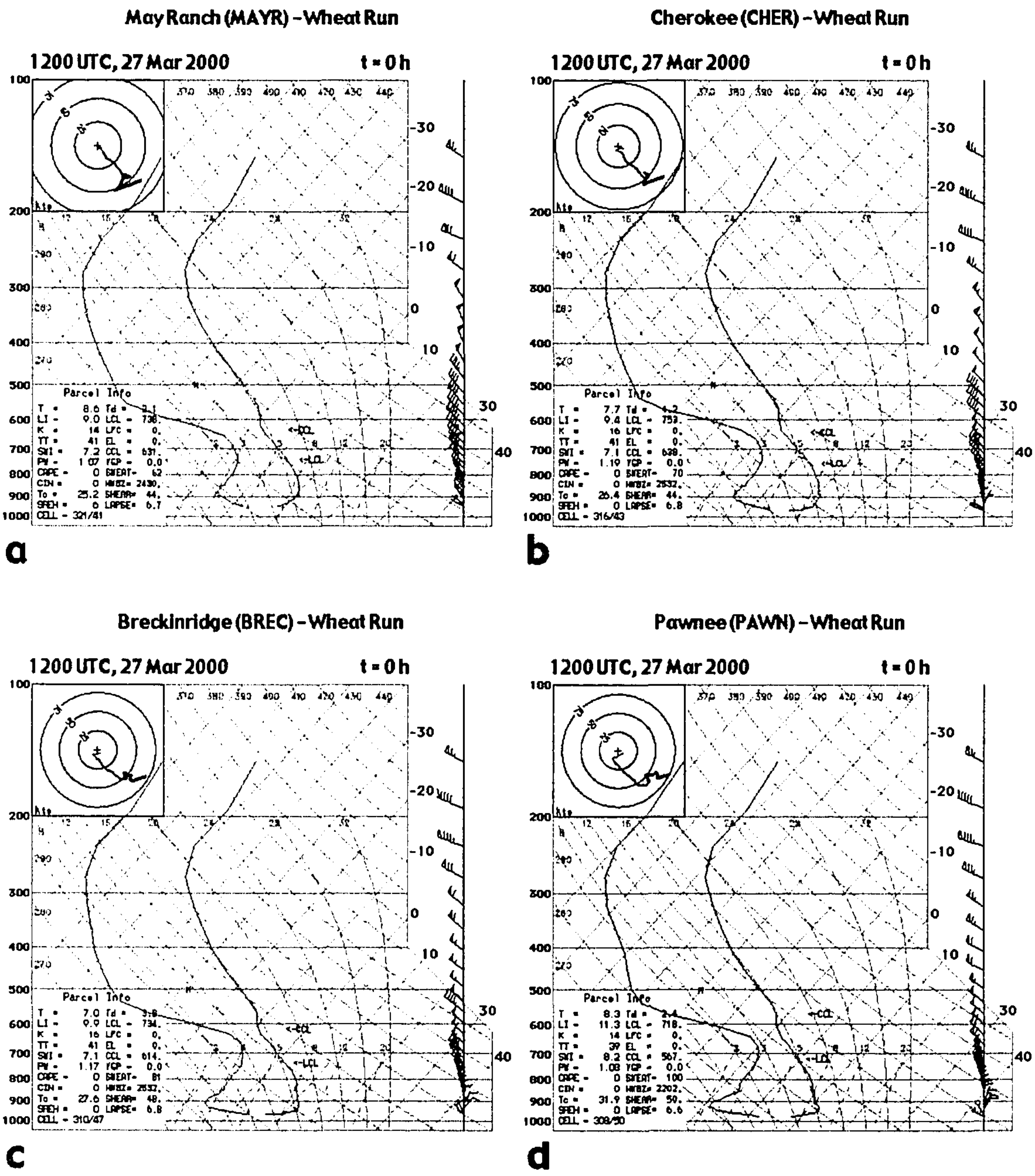


FIGURE 6.10. Initial thermodynamic profiles for model simulation of 27 March 2000. The profiles correspond to the locations of the following Mesonet sites: (*a*) May Ranch (MAYR), (*b*) Cherokee (CHER), (*c*) Breckinridge (BREC), and (*d*) Pawnee (PAWN).

Subsurface moisture measured by the Oklahoma Mesonet was abundant statewide from 5 to 75 cm below ground on 27 March. As a result of these measurements, soil moisture was set to field capacity in the deepest three (out of four) MM5 soil layers. Consequently, the simulated vegetation would have adequate water for transpiration; yet direct evaporation from the surface would not add unrealistic moisture to the model results.

Figure 6.11 displays the dewpoint field at the lowest sigma level at 1200, 1500, 1800, and 2100 UTC for both the wheat run (left side of Fig. 6.11) and the natural vegetation run (right side of Fig. 6.11). Dew points beyond the wheat belt were identical between the two runs. Within the wheat belt, however, dewpoint temperatures were 1–3°C higher for the wheat run than its natural vegetation counterpart. Indeed, by 2100 UTC, a swath of higher dew points appeared on the wheat run as a distorted image of the wheat belt itself (compare to Fig. 6.1*a*).

In agreement with observations, after an initial increase of near-surface dew points, substantial drying of the near-surface air occurred between 1300 and 1500 UTC for both runs, particularly across the eastern third of the nested domain. The only exception to this trend was a slight moistening near the surface over the wheat belt in the wheat run. Consequently, the moisture gradient between the wheat belt and its surrounding area increased. Values of near-surface dew points from the wheat run were approximately 1°C greater over central and southern sections of the wheat belt as compared to the same region for the natural vegetation run.

The results from the wheat run were consistent in patterns and amplitudes with measured changes in surface dew points from the Oklahoma Mesonet. Hence, the model adequately simulated the post-sunrise evaporation of dew followed by the drying of the mixed layer as a result of entrainment (Willis and Deardorff 1974; Tennekes 1973; Lilly 1968).

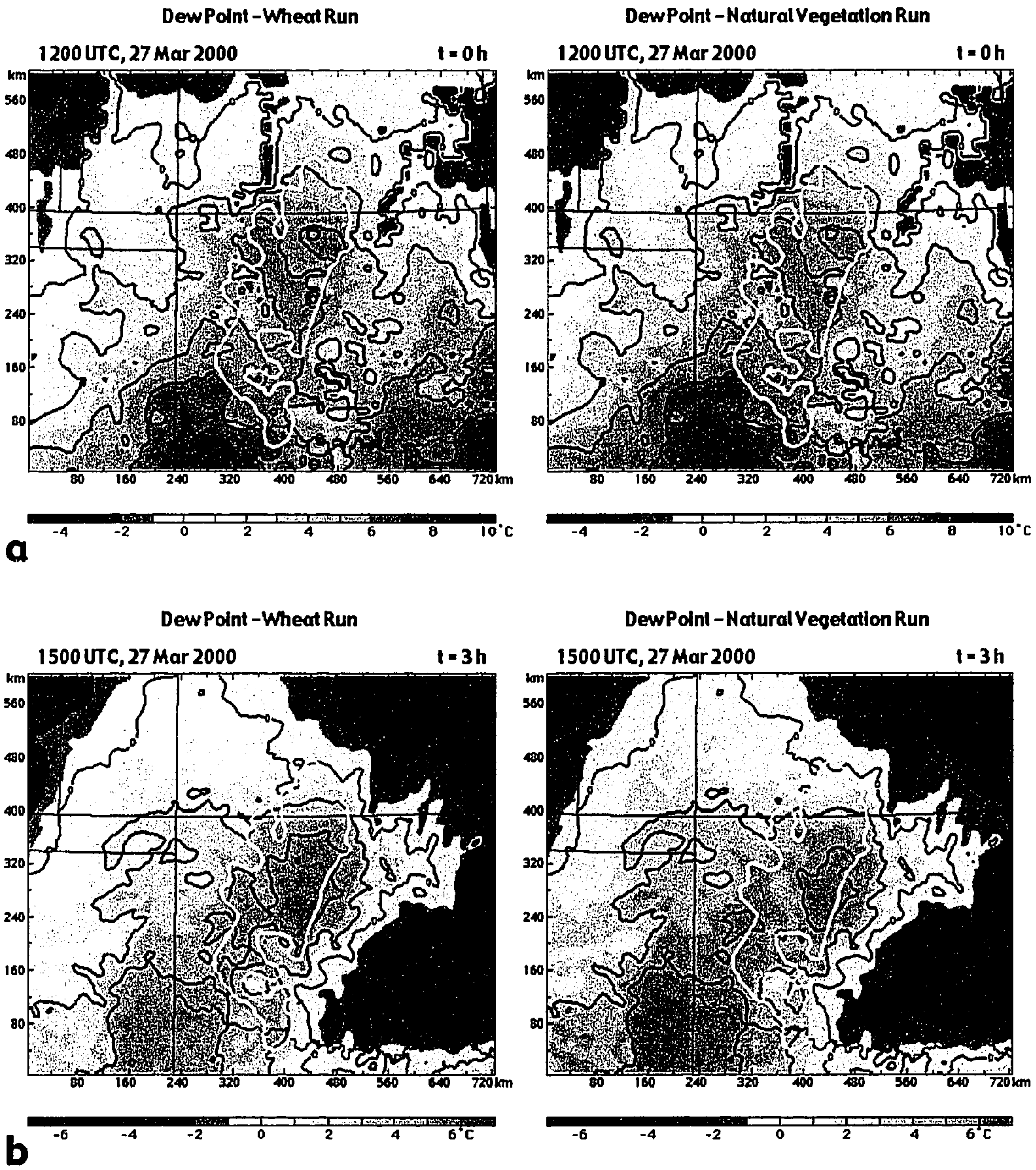


FIGURE 6.11. Dewpoint fields at the lowest sigma level for the wheat run (left) and the natural vegetation run (right) for 27 March 2000. The times displayed are (*a*) 1200 UTC on 27 March, (*b*) 1500 UTC, (*c*) 1800 UTC, (*d*) 2100 UTC, and (*e*) 0000 UTC on 28 March. The white outline depicts the boundary of the wheat belt.

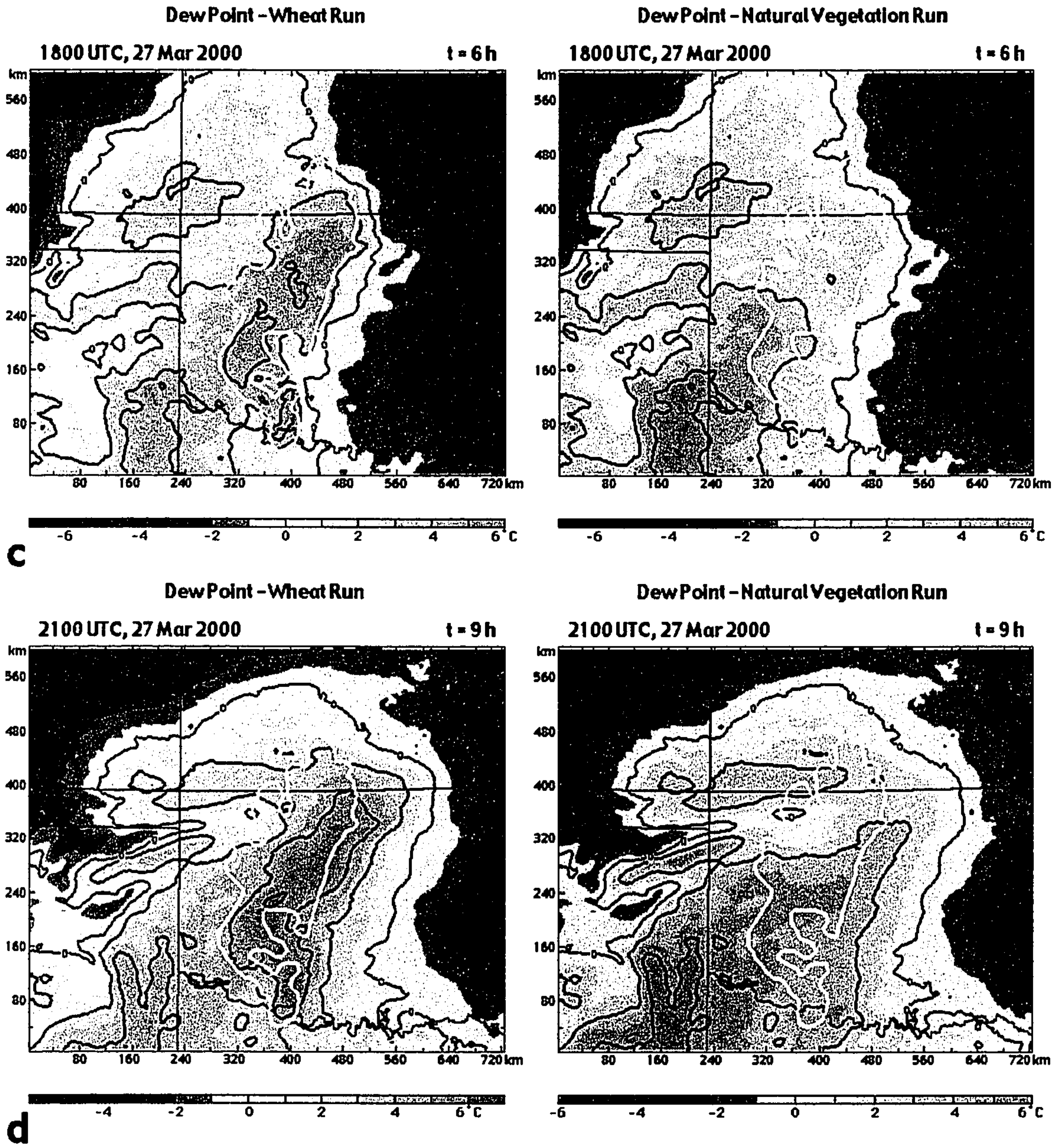


FIGURE 6.11. (Continued)

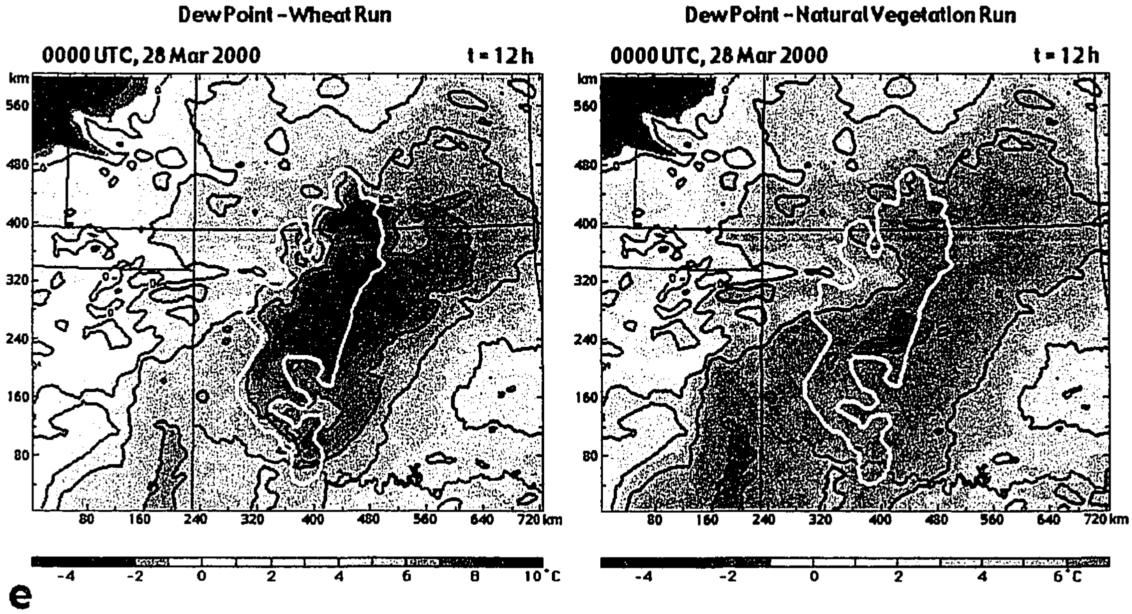


FIGURE 6.11. (Continued)

From 1500 to 1800 UTC, the surface continued to dry across the entire domain for the natural vegetation run. The trend was similar for the wheat run except across the wheat belt. Although the northern half of the wheat belt was less moist at 1800 UTC than at 1500 UTC for the wheat run, dewpoint values ranged 2 – 3°C higher across this region than those for the natural vegetation run. Moistening of the surface layer was most evident across the southern half of the wheat belt.

Between 1800 and 2100 UTC, dew points across all but the northern edge of the wheat belt increased a few degrees Celsius for the wheat run. At this time, the most significant difference between the wheat and the natural vegetation runs occurred across the wheat belt in both north-central and south-central Oklahoma. Over these two areas, dew points ranged from 4 – 5°C higher for the wheat run than for the natural vegetation run (Fig. 6.12*a*). Across the far western and far northern edges of the wheat belt, differences between the wheat and natural vegetation runs were minimal. This lack of appreciable dewpoint differences was attributed to dry-air advection by the low-level winds (Fig. 6.12*b*).

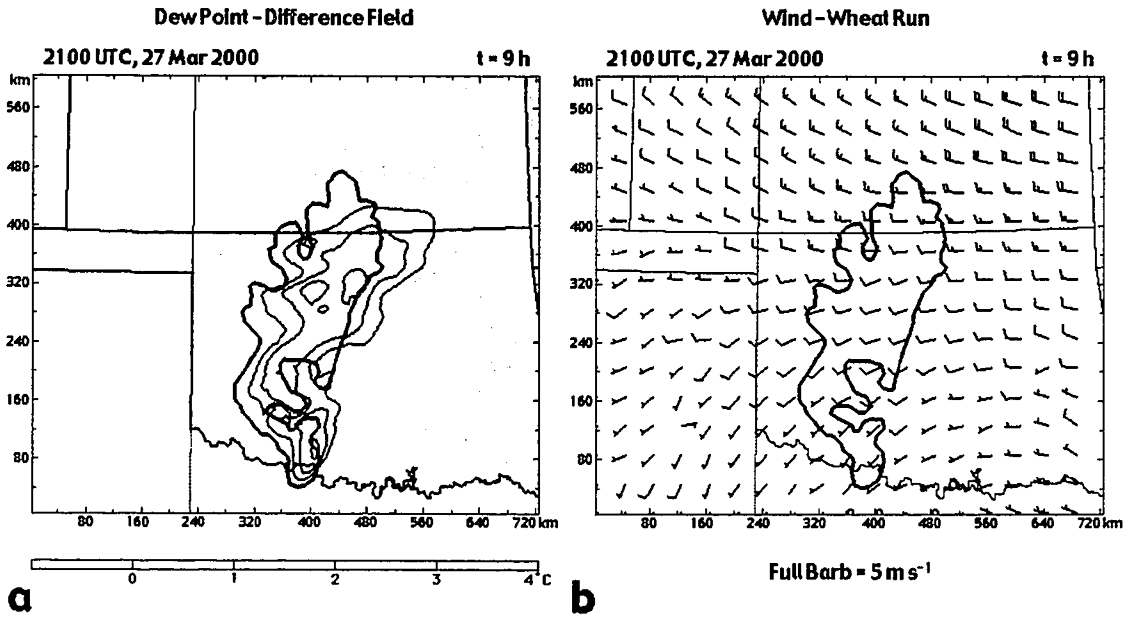


FIGURE 6.12. Model results for (*a*) the difference field of near-surface dew points and (*b*) the near-surface winds for the wheat run at 2100 UTC on 27 March 2000. The black outline depicts the boundary of the wheat belt. Positive values of the dewpoint difference field (shaded in gold) indicate locations where the wheat run was more moist than the natural vegetation run.

By 2300 UTC, surface sensible heat flux was minimal and the convective boundary layer collapsed. As a result, near-surface moisture was confined within a shallow layer (20 – 30 hPa in depth), causing surface dew points to increase domain-wide by 1°C over an hour. Between 2300 UTC on 27 March and 0000 UTC on 28 March, surface dew points continued to increase by about 2°C domain-wide. Similar to 2100 UTC, the largest differences between the wheat and natural vegetation runs occurred across the wheat belt, where dew points ranged to 5°C higher than in the natural vegetation run.

Higher dew points over the wheat belt for the wheat run resulted from the simulated transpiration of growing plants. Surface latent heat values, shown in Fig. 6.13, were larger across the wheat belt for the wheat run than for the natural vegetation run. By 2100 UTC, latent heat fluxes across the wheat belt ranged from 300 to 400 W m$^{-2}$ for the wheat run as compared to 200 to 275 W m$^{-2}$ for the natural vegetation run. Values of sensible heat flux ranged from 25 to 125 W $m^{-2}$ for the wheat run and from 100 to 200 W $m^{-2}$ for the natural vegetation run (Fig. 6.14). These results were consistent with values from observations during CASES/ABLE (LeMone 2000). During that May experiment, latent and sensible heat fluxes over winter wheat were approximately 400 W $m^{-2}$ and 150 W $m^{-2}$, respectively. Over grassland, latent and sensible heat fluxes both were measured to be about 200 W $m^{-2}$.

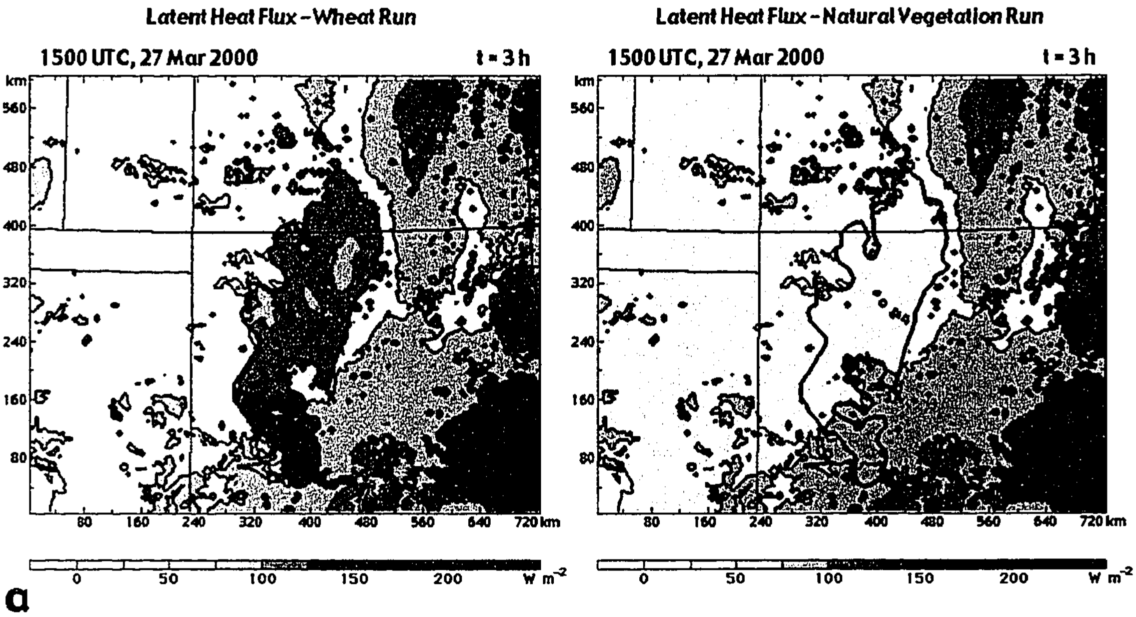


FIGURE 6.13. Fields of latent heat flux (W $m^{-2}$) for the wheat run (left) and the natural vegetation run (right) for 27 March 2000. The times displayed are (*a*) 1500 UTC, (*b*) 1800 UTC, and (*c*) 2100 UTC. The black outline depicts the boundary of the wheat belt.

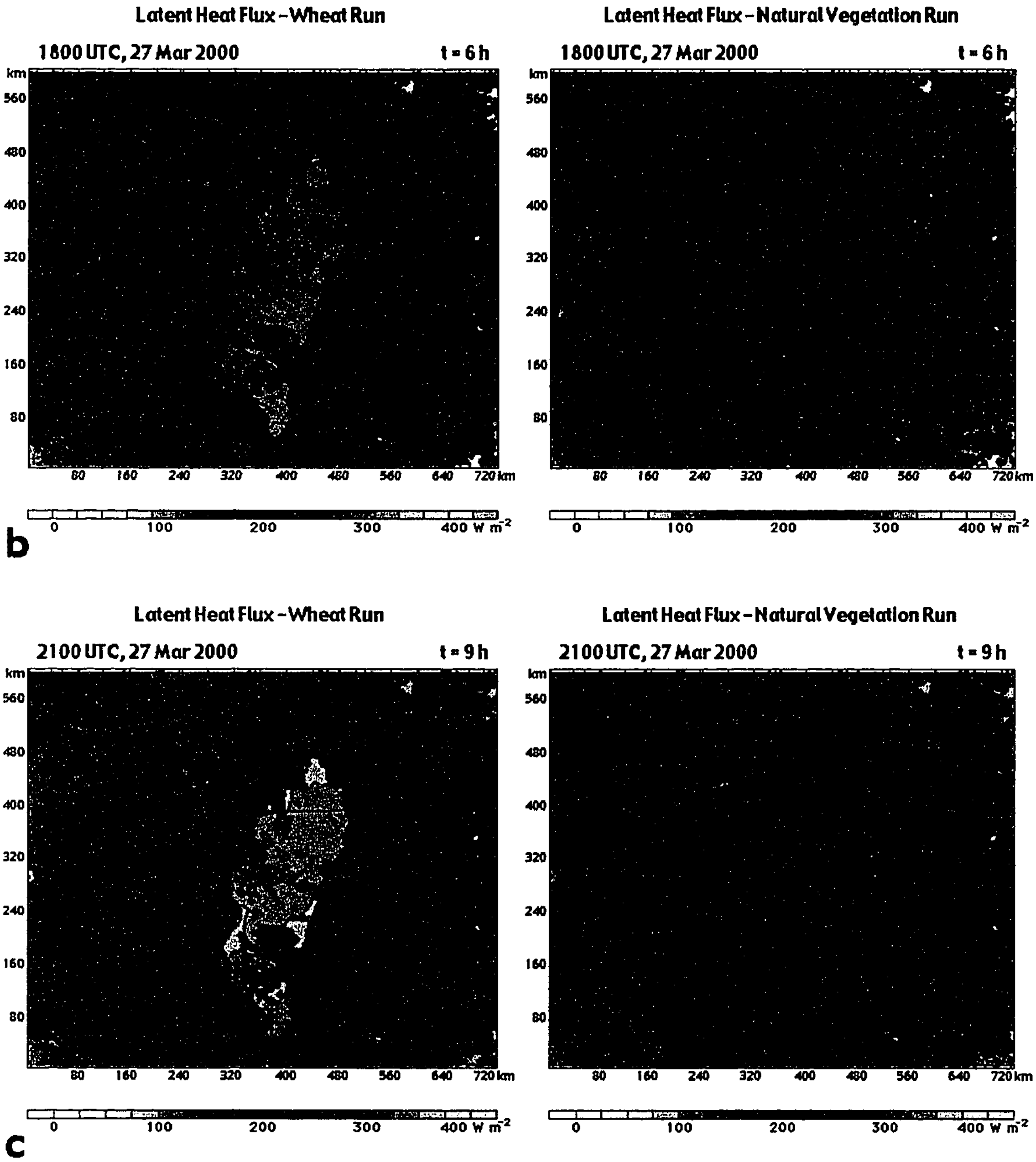


FIGURE 6.13. (Continued)

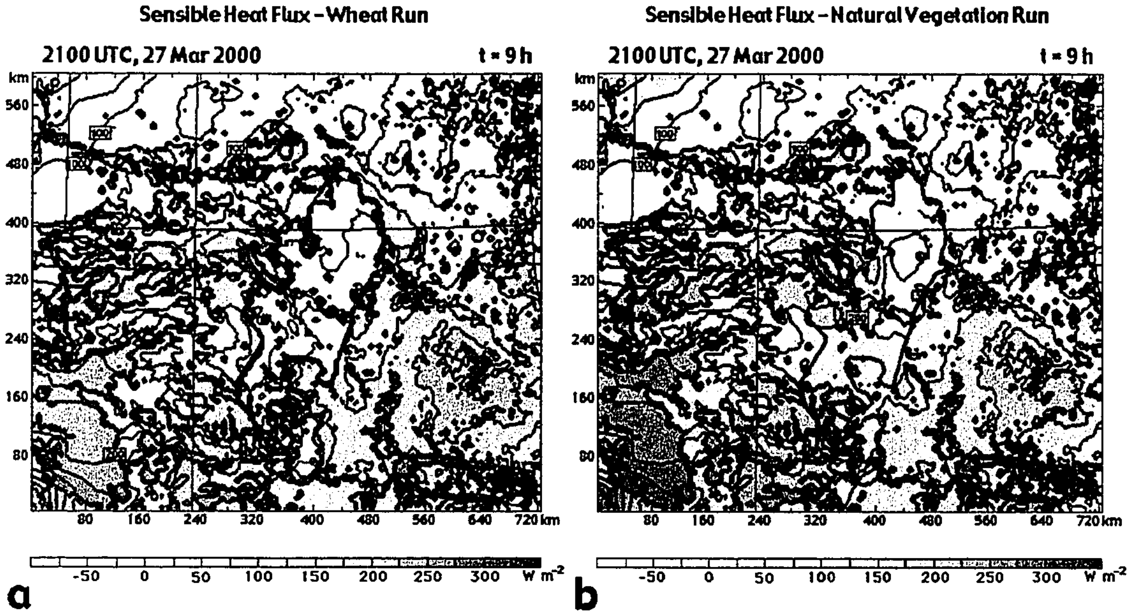


FIGURE 6.14. Fields of sensible heat flux (W $m^{-2}$) for the wheat run (left) and the natural vegetation run (right) for 2100 UTC on 27 March 2000. The black outline depicts the boundary of the wheat belt.

Simulated soundings at 2100 UTC (Fig. 6.15) were compared to the initial soundings over May Ranch, Cherokee, Breckinridge, and Pawnee (Fig. 6.10). As expected for an upwind location, the May Ranch sounding showed no detectable difference between the wheat and natural vegetation runs. In fact, the lifted condensation level (LCL) was identical between the two runs over MAYR. In contrast, the depth of the mixed layer was shallower over CHER by 21 hPa, over BREC by 45 hPa, and over PAWN by 20 hPa for the wheat run in comparison to the natural vegetation run. Over Cherokee and Breckinridge, the differences in LCL values between the two runs were consistent with the associated differences in the values of surface sensible heat flux. Over Pawnee, the shallower PBL was attributed to advection by westerlies within the mixed layer from the wheat belt toward the east. Doran et al. (1995) observed that the growth of the mixed layer could be modified significantly by upwind surface fluxes.

The model-calculated heights of the planetary boundary layer for both the wheat and natural vegetation simulations were between 1250 and 3000 m across the nested domain. Although the height patterns did not appear substantially different (not shown), the impact of the wheat belt was evident in the difference field of PBL heights (Fig. 6.16). Height differences ranged predominantly from 100 to 400 m, with a maximum difference of 600 m located above portions of north-central Oklahoma near the eastern boundary of the wheat belt.

As a result of both a shallower mixed layer over the wheat and advection from the wheat belt eastward, the convective boundary layer above Pawnee was about 0.5 g $kg^{-1}$ more moist for the wheat run than the natural vegetation run. Similarly, because of a shallower mixed layer and the increased latent heat flux for the wheat run, the atmosphere above Breckinridge was almost 1 g $kg^{-1}$ more moist throughout the convective boundary layer, as compared to the natural vegetation run. In addition, temperatures were about 2°C cooler within the mixed layer over Breckinridge for the wheat run than for the natural vegetation run. Over Cherokee, where the boundary layer could have been influenced by less evapotranspiration upstream, mixing ratios were about 0.5 g $kg^{-1}$ more moist for the wheat run than for the natural vegetation run.

Thus, according to the model simulations, the winter wheat belt significantly modified the characteristics of the convective boundary layer. The modification was not limited to the atmosphere directly over the wheat belt; it also extended up to 150 km downstream (Fig. 6.16).

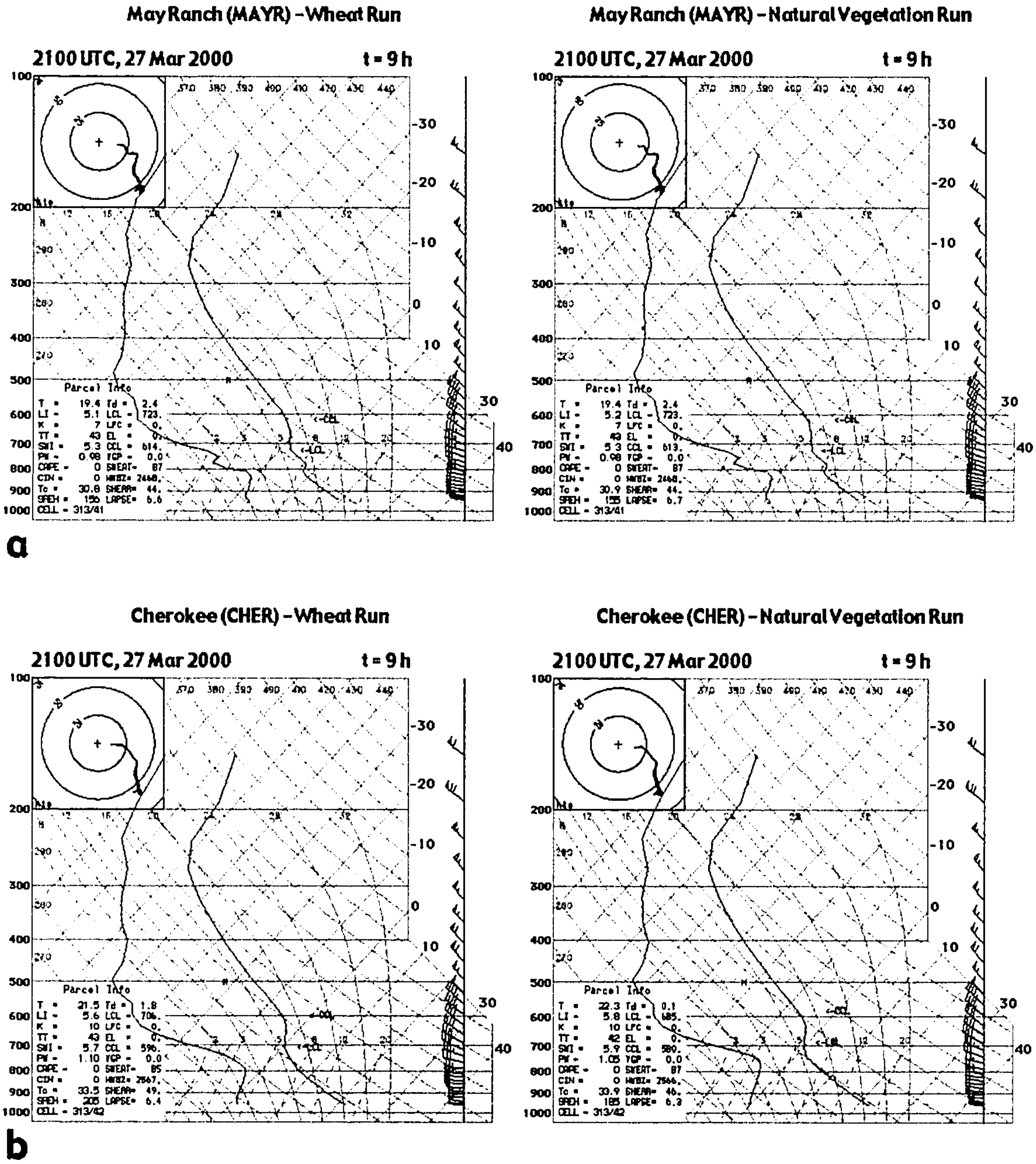


FIGURE 6.15. Simulated thermodynamic profiles at 2100 UTC on 27 March 2000 for the wheat run (left) and the natural vegetation run (right). The profiles correspond to the location of the following Mesonet sites: (*a*) May Ranch (MAYR), (*b*) Cherokee (CHER), (*c*) Breckinridge (BREC), and (*d*) Pawnee (PAWN).

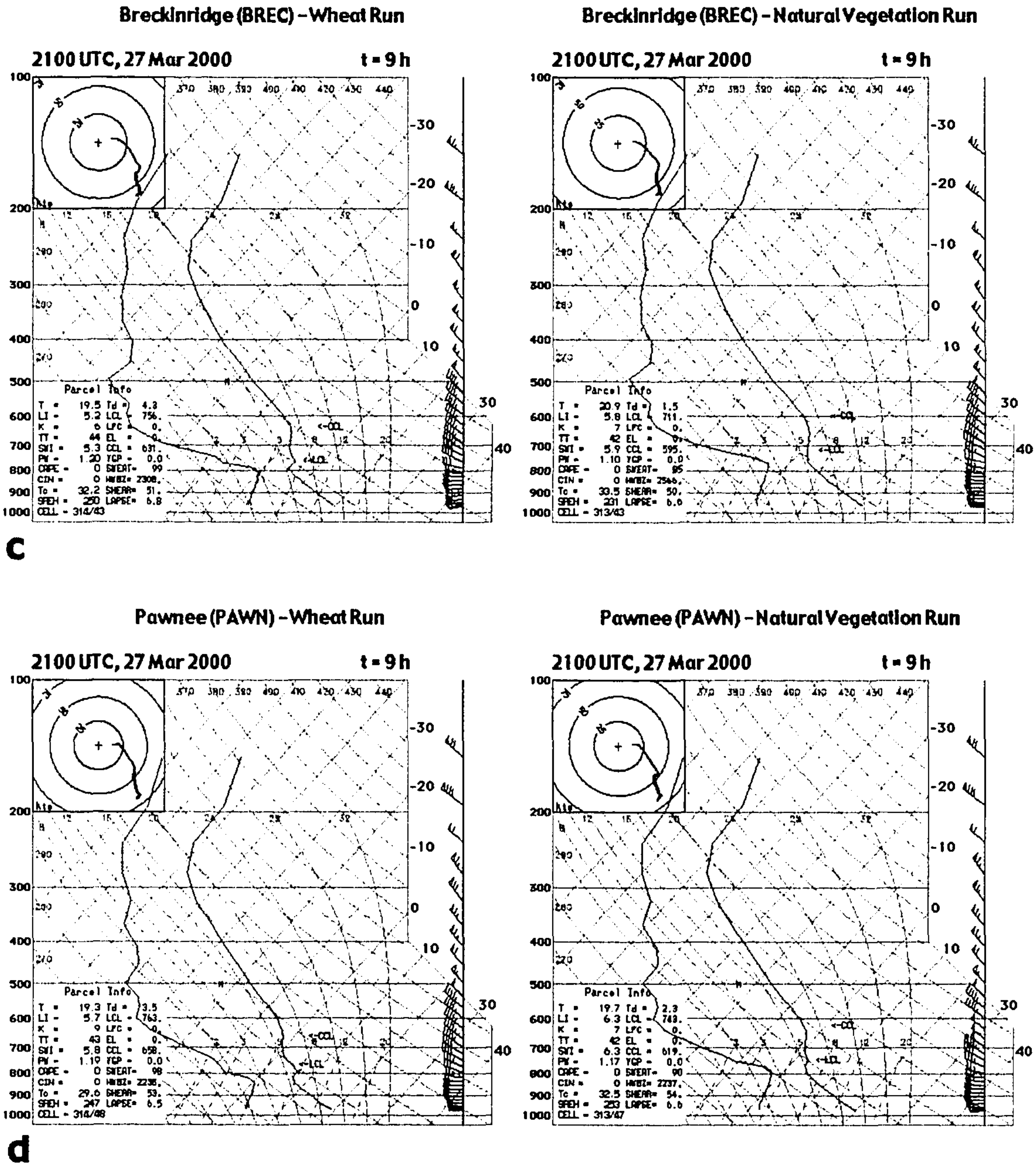


FIGURE 6.15. (Continued)

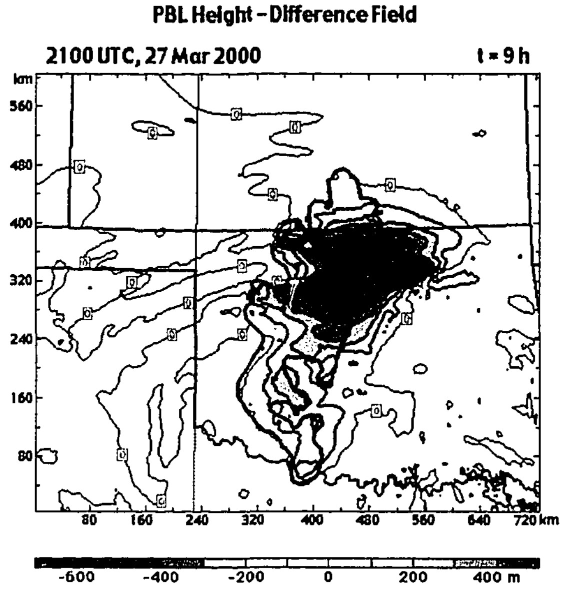


FIGURE 6.16. Difference field of the model-calculated PBL heights at 2100 UTC on 27 March 2000. Negative values (in blue) indicate PBL heights were lower for the wheat run than the natural vegetation run. The black outline depicts the boundary of the winter wheat belt.

The PBL height differences above and downstream from the wheat belt (Fig. 6.16) not only affected thermodynamic variables, but they directly influenced the transfer of momentum into the mixed layer. Recall that the initial wind profiles displayed low-level speed shear (Fig. 6.10). For the wheat run, a shallower mixed layer resulted in less entrainment of higher-momentum air into the mixed layer. It is important to note that because previous modeling studies of vegetation breeze circulations focused on environments without vertical wind shear, the results from the current study, with its sheared environment, appeared different than those discussed in the scientific literature.

Based on PBL height values across the wheat belt over north-central Oklahoma, winds at 1 km above sea level were selected to be representative of those throughout the mixed layer above this region. At 2100 UTC, across north-central Oklahoma, westerly winds dominated at 1 km (Fig. 6.17). Hence, east-west and north-south cross-sections (locations shown in Fig. 6.17) through the core of Oklahoma's wheat belt were selected to provide insight to the circulations parallel and perpendicular to the prevailing flow.

A shallower PBL for the wheat run as compared to the natural vegetation run was evident for both cross-sections (Figs. 6.18 and 6.19). Both runs exhibited a cooling of the PBL from west to east (Fig. 6.18), as expected. In addition, the height of the PBL, characterized by a tight vertical gradient of potential temperature, was lower to the south than to the north for both runs (Fig. 6.19). Circulation vectors displayed a predominantly west-to-east motion from the surface to 3 km above sea level.

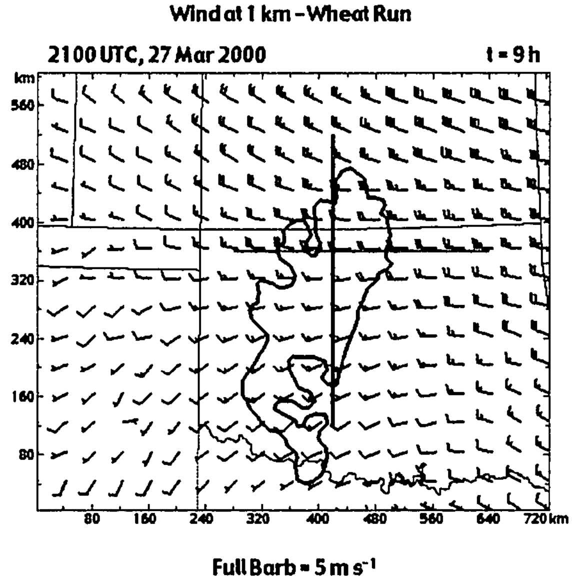


FIGURE 6.17. Wind field (barbs) from the wheat run at 1 km above sea level for 2100 UTC on 27 March 2000. The black outline depicts the boundary of the winter wheat belt. Note that winds across the wheat belt over north-central Oklahoma were westerly. The east-west and north-south lines mark the location of the axes of vertical cross-sections in Figs. 6.18 and 6.19, respectively. The east-west cross-section is parallel to the prevailing flow; the north-south cross-section is perpendicular to the prevailing flow.

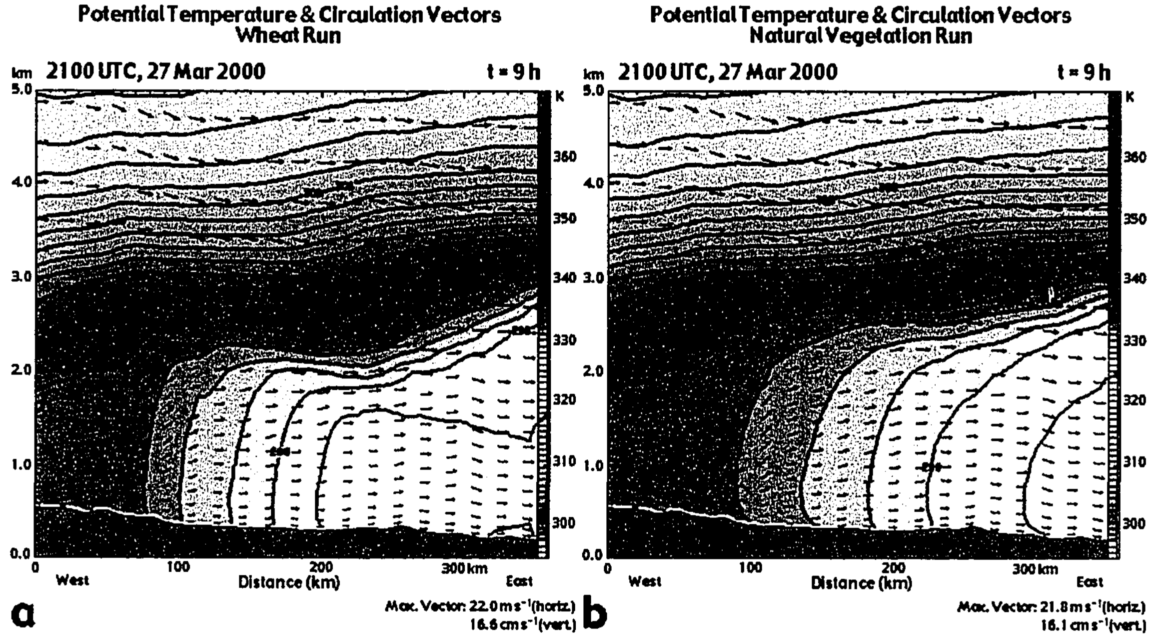


FIGURE 6.18. East-west vertical cross-sections of potential temperature (K) at 2100 UTC on 27 March 2000 for (*a*) the wheat run and (*b*) the natural vegetation run. The location of the cross-sections is shown in Fig. 6.17. Arrows represent circulation vectors parallel to the cross-section.

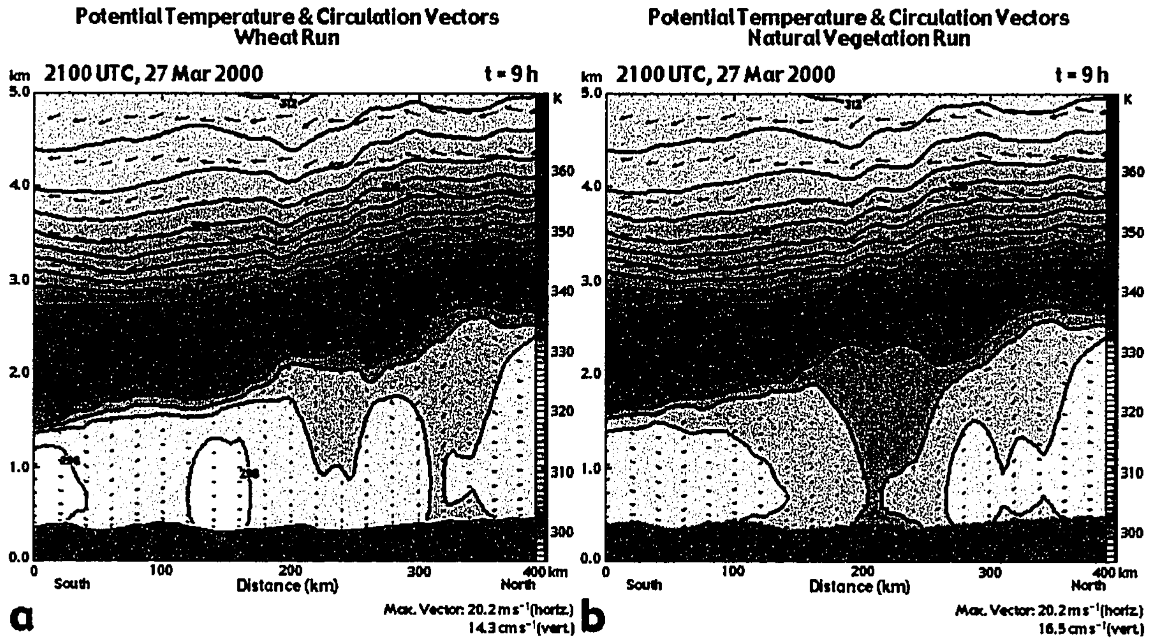


FIGURE 6.19. North-south vertical cross-sections of potential temperature (K) at 2100 UTC on 27 March 2000 for (*a*) the wheat run and (*b*) the natural vegetation run. The location of the cross-sections is shown in Fig. 6.17. Arrows represent circulation vectors parallel to the cross-section.

The difference fields of potential temperature and circulation vectors for these cross-sections are displayed in Fig. 6.20. Across north-central Oklahoma, potential temperatures ranged from 1.0 to 1.6°C cooler throughout the PBL for the wheat run across the eastern half of the wheat belt (Fig. 6.20*a*). These results were consistent with observations detailed in Segal et al. (1989). Although potential temperature differences between the two runs did not exist to the west of the wheat belt boundary, the boundary layer to the east of the wheat belt was modified by upwind conditions. The eastward advection of a shallower PBL also was evident on the north-south cross-section of the potential temperature difference field (Fig. 6.20*b*). The southernmost 40 to 50 km of this cross-section resided east of the wheat belt (Fig. 6.17). Yet the difference field clearly indicated that potential temperatures were as much as 0.8°C cooler across this region for the wheat run than the natural vegetation run. Apparently, the cooler boundary layer upwind (and over the southern leg of the wheat belt) was advected over this area just east of the wheat belt.

Of particular interest were the circulation vectors depicted on the east-west cross-section of Fig. 6.20*a*. Based on previous studies (discussed in Section 2.3.6), one would expect descending motion over the wheat belt, ascending motion to the west of and adjacent to the wheat belt, and, to a lesser intensity, rising motion to the east of and adjacent to the wheat belt. In this manner, two circulation cells would be established, with the descending branch of both cells occurring over the wheat belt. As a result, vegetation breezes near the surface would expand outward from the crop belt.

The model results, however, indicated that a single-cell circulation was established within the mixed layer (Fig. 6.20*a*), whereby the *difference circulation* was defined as a circulation that was evident in the difference field of the circulation vectors. The ascending branch of this circulation was along the western boundary of the wheat belt and the descending branch was along its eastern boundary. Although solenoidal circulations could exist across west and east boundaries of the wheat belt, another physical process apparently was dominating the difference circulation on the meso-β scale.

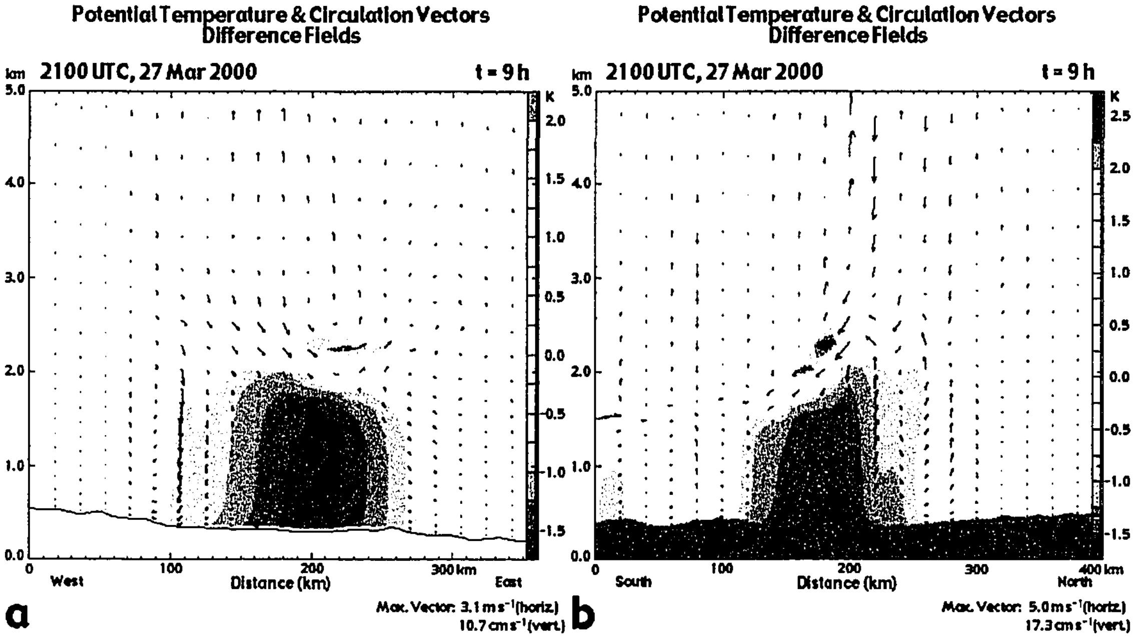


FIGURE 6.20. Vertical cross-sections of the potential temperature (K) and circulation vector (m $s^{-1}$) difference fields at 2100 UTC on 27 March 2000. The locations of the (*a*) east-west and (*b*) north-south cross-sections are displayed in Fig. 6.17. Negative values of potential temperature difference (shaded blue) indicate locations where the wheat run was cooler than the natural vegetation run. Positive values of potential temperature difference (shaded gold) indicate locations where the wheat run was warmer than its counterpart. Vectors display the circulation difference field resulting from velocities from the natural vegetation run subtracted from those from the wheat run.

The velocity and velocity difference fields at a height of 1 km above sea level (Fig. 6.21) provided insight into the difference circulation. Vertical velocities at 2100 UTC for the wheat run were weak on 27 March 2000, as expected on a synoptically benign day (Fig. 6.21*a*). It was evident that no intense circulation was generated by the wheat belt. However, examination of the vertical velocity difference field (Fig. 6.21*b*) revealed several weak velocity differences between the two runs. First, along the western boundary of the wheat belt, localized areas of ascending motion were evident as compared to the natural vegetation run. Second, along the eastern boundary, localized areas of descending motion were apparent as compared to the natural vegetation run. Finally, horizontal velocity differences extended 150 km downstream of the northern half of the wheat belt (Fig. 6.21*b*).

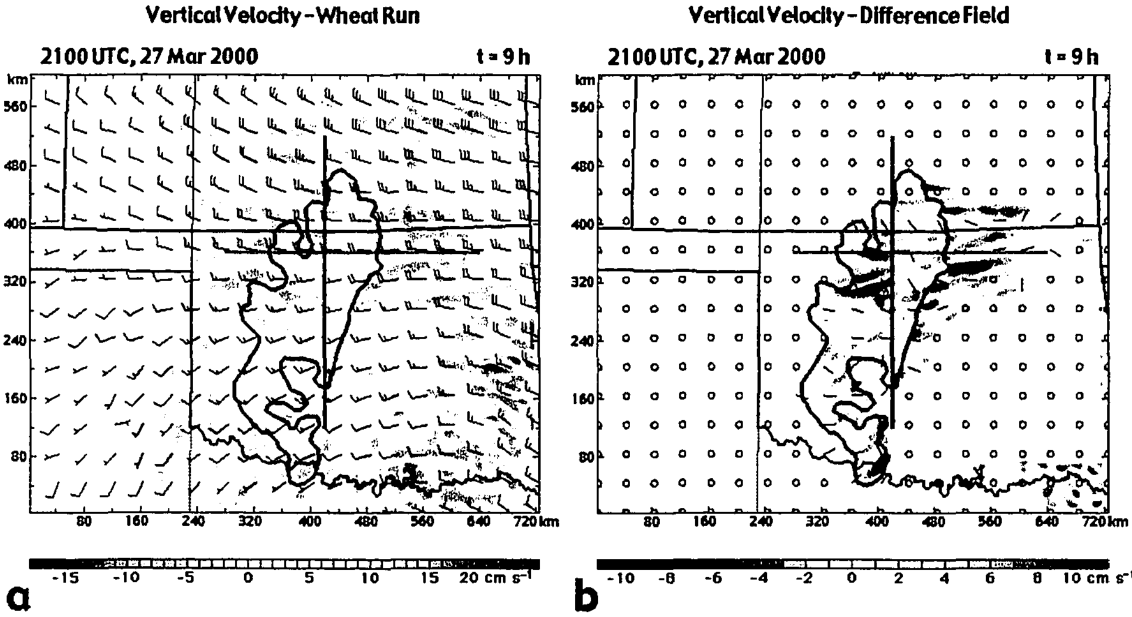


FIGURE 6.21. Horizontal plot of (*a*) the velocity field as simulated for the wheat run and (*b*) the velocity difference field at 2100 UTC. In the left figure (Fig. 6.21*a*), color-filled contours represent vertical velocities at 1 km above sea level; yellow represents upward motion and green represents downward motion. Horizontal velocities at a height of 1 km above sea level are plotted as barbs. In the right figure (Fig. 6.21*b*), color-filled contours represent vertical velocity differences at 1 km above sea level; orange represents positive differences and purple represents negative differences. Horizontal velocity differences at a height of 1 km above sea level are plotted as barbs. Horizontal speed differences less than 1.25 m $s^{-1}$ are displayed as open circles in the right figure (Fig. 6.21*b*). The black outline depicts the boundary of the winter wheat belt.

To examine the differences in horizontal velocities between the runs, the horizontal wind fields for the wheat run at heights of 1.8 and 2.2 km were compared (Fig. 6.22). Over north-central Oklahoma, winds at 1.8 km above sea level were *within* the mixed layer (see Fig. 6.18*a*); winds at 2.2 km were *above* the top of the convective boundary layer (see Fig. 6.18*a*). In the natural vegetation run, however, winds at 2.2 km were entrained into the mixed layer (see Fig. 6.18*b*). Hence, higher speed winds were entrained into the mixed layer of the natural vegetation run than into that of the wheat run. As a result, vectors representing the horizontal wind differences at 1 km (Fig. 6.21*b*) generally were oriented opposite to the flow at 2.2 km (Fig. 6.22*b*).

The locations of horizontal wind differences greater than 1.25 m $s^{-1}$ between the wheat and natural vegetation runs were well aligned with the locations of lower PBL heights for the wheat run (Fig. 6.23). These wind differences, however, were not as aligned with differences in either the surface fluxes of latent or sensible heat (Figs. 6.13 and 6.14) or differences in the near-surface dew points (Fig. 6.12). The largest differences in the vertical velocity fields for the wheat and natural vegetation runs (Fig. 6.21*b*) coincided with the tightest gradients in the PBL height difference field (Fig. 6.23). Hence, in this environment with low-level shear, the first-order difference of the mixed-layer winds between the wheat and natural vegetation runs resulted from the change in the PBL height and, consequently, the entrainment of different wind velocities within the mixed layer.

Differences in the vertical wind field within the mixed layer between the wheat and natural vegetation runs were attributed to mass continuity. The differences in horizontal wind velocity across the wheat belt (e.g., Figs. 6.20*a* and 6.21*b*) caused rising motion along the upstream boundary of the wheat belt and similarly caused sinking motion along or downwind from the downstream boundary of the wheat belt (Fig. 6.20*a*).

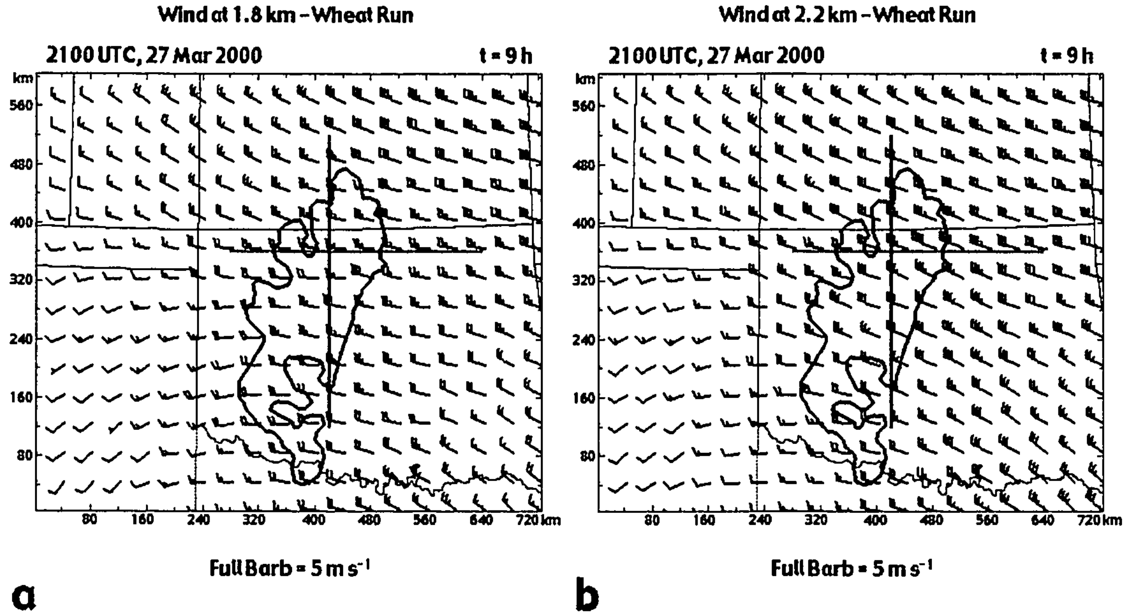


FIGURE 6.22. Plot of the horizontal velocity field at 2100 UTC on 27 March 2000 for the wheat run. The plots represent heights of (*a*) 1.8 km above sea level and (*b*) 2.2 km above sea level. The black outline depicts the boundary of the winter wheat belt.

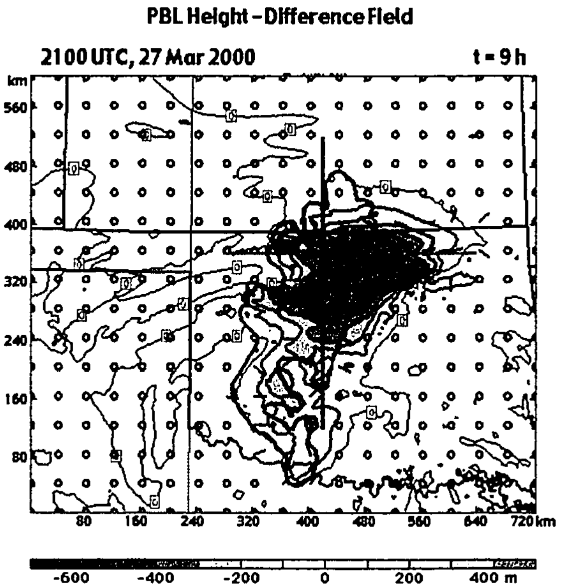


FIGURE 6.23. Plot of the horizontal difference fields of PBL heights (contours) and horizontal winds at 1 km (barbs) between the wheat run and the natural vegetation run at 2100 UTC on 27 March 2000. Horizontal speed differences less than 1.25 m $s^{-1}$ are displayed as open circles. The black outline depicts the boundary of the wheat belt.

*6.4.2 Simulation of 5 April 2000 conditions*

Initial dew points at 1200 UTC on 5 April 2000 were higher across the winter wheat belt than adjoining lands (Fig. 6.24*a*). Initial thermodynamic profiles identified a strong inversion over the region, as temperatures at 850 hPa ranged from 11 to 14°C warmer than those at the lowest model level (Fig. 6.25). Low-level winds veered from southwesterly to westerly between the surface and 900 hPa at CHER, between the surface and 850 hPa at BREC, and between the surface and 800 hPa at PAWN. Wind speeds increased from about 5 m $s^{-1}$ at the surface for these three sites to about 20 m $s^{-1}$ at 850 hPa.

By 1500 UTC, dew points were distinctly different over the wheat belt between the wheat and natural vegetation runs (Fig. 6.24*b*). By 1800 UTC, for the natural vegetation run, moderate southeast winds (not shown) advected drier air (dew points less than 3°C) over most of the wheat belt except for the section across southern Kansas (Fig. 6.24*c*). For the wheat run, dry air advection also occurred by 1800 UTC, but the eastern half of the wheat belt experienced dew points in excess of 4°C. Similar to the 27 March simulation, added moisture for the wheat run resulted from increased transpiration from the simulated winter wheat as compared to the grassland.

From 1800 to 2100 UTC, latent heat flux values across the wheat belt (not shown) ranged from about 100 to 200 W $m^{-2}$ higher for the wheat run than for the natural vegetation run. As a result, near-surface dew points were 2-3°C higher at 1800 UTC and 2-5°C higher at 2100 UTC over about half of the wheat belt in the wheat run as compared to the natural vegetation run. Values of sensible heat flux over the wheat belt were negligible for the wheat run and ranged from 50 to 125 W $m^{-2}$ for the natural vegetation run. Latent heat values over the wheat ranged from 350 to 425 W $m^{-2}$ for the wheat run, about 25 W $m^{-2}$

higher than those for the 27 March simulation. These results were consistent with observational findings of Doran et al. (1995) whereby latent heat fluxes over wheat and steppe increased with increased surface winds.

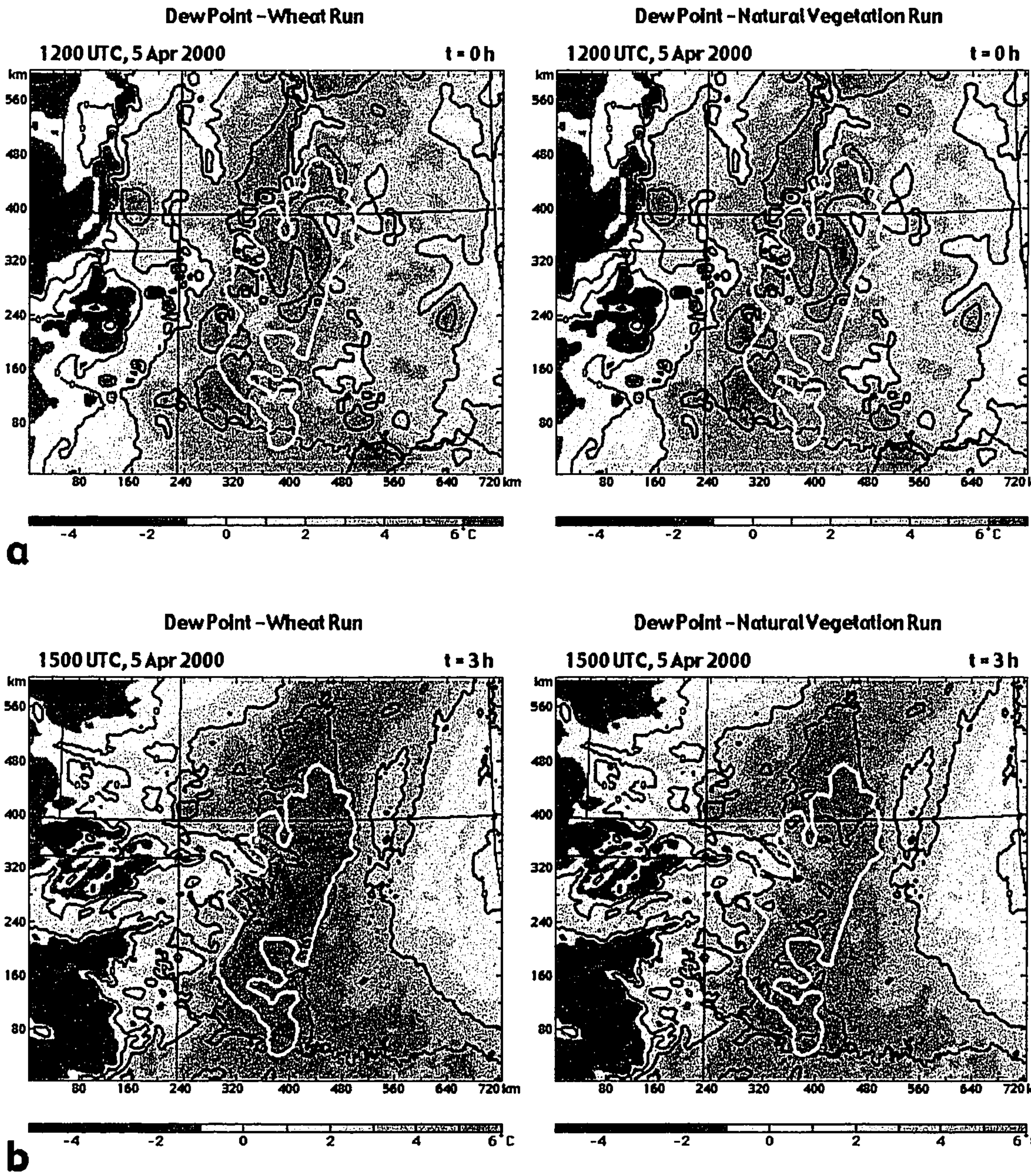


FIGURE 6.24. Dewpoint fields at the lowest sigma level for the wheat run (left) and the natural vegetation run (right) for 5 April 2000. The times displayed are (*a*) 1200 UTC on 5 April, (*b*) 1500 UTC, (*c*) 1800 UTC, (*d*) 2100 UTC, and (*e*) 0000 UTC on 6 April. The white outline depicts the boundary of the wheat belt.

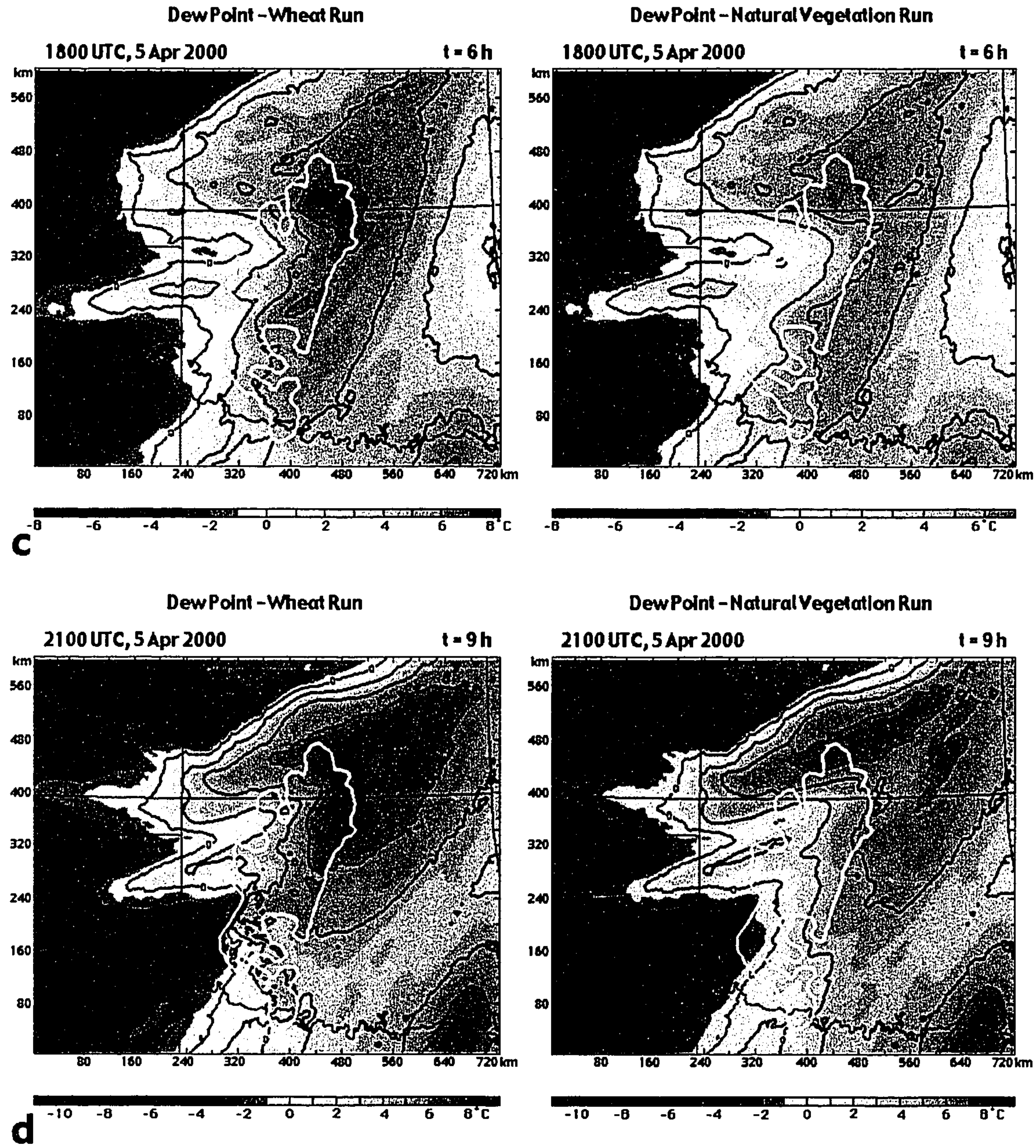


FIGURE 6.24. (Continued)

The boundary layer over the wheat field did not deepen as quickly during the wheat run for 5 April as it did for 27 March. By 2100 UTC, the mixed layer was about 1 km shallower for 5 April than it was on 27 March. However, similar to the 27 March case, boundary layer heights above and downwind of the wheat belt (not shown) were lower for the wheat run than they were for the natural vegetation run. Height differences of the PBL for 5 April ranged from 50 to 150 m over the wheat belt at 1800 UTC (Fig. 6.26*a*) and from 100 to 350 m at

2100 UTC (Fig. 6.26*b*). In comparison, height differences over the wheat belt on 27 March generally ranged from 75 to 250 m at 1800 UTC and from 100 to 600 m at 2100 UTC (Fig. 6.16). Although the low-level wind shear was greater on 5 April than on 27 March, the stronger inversion on 5 April suppressed the vertical development of the PBL.

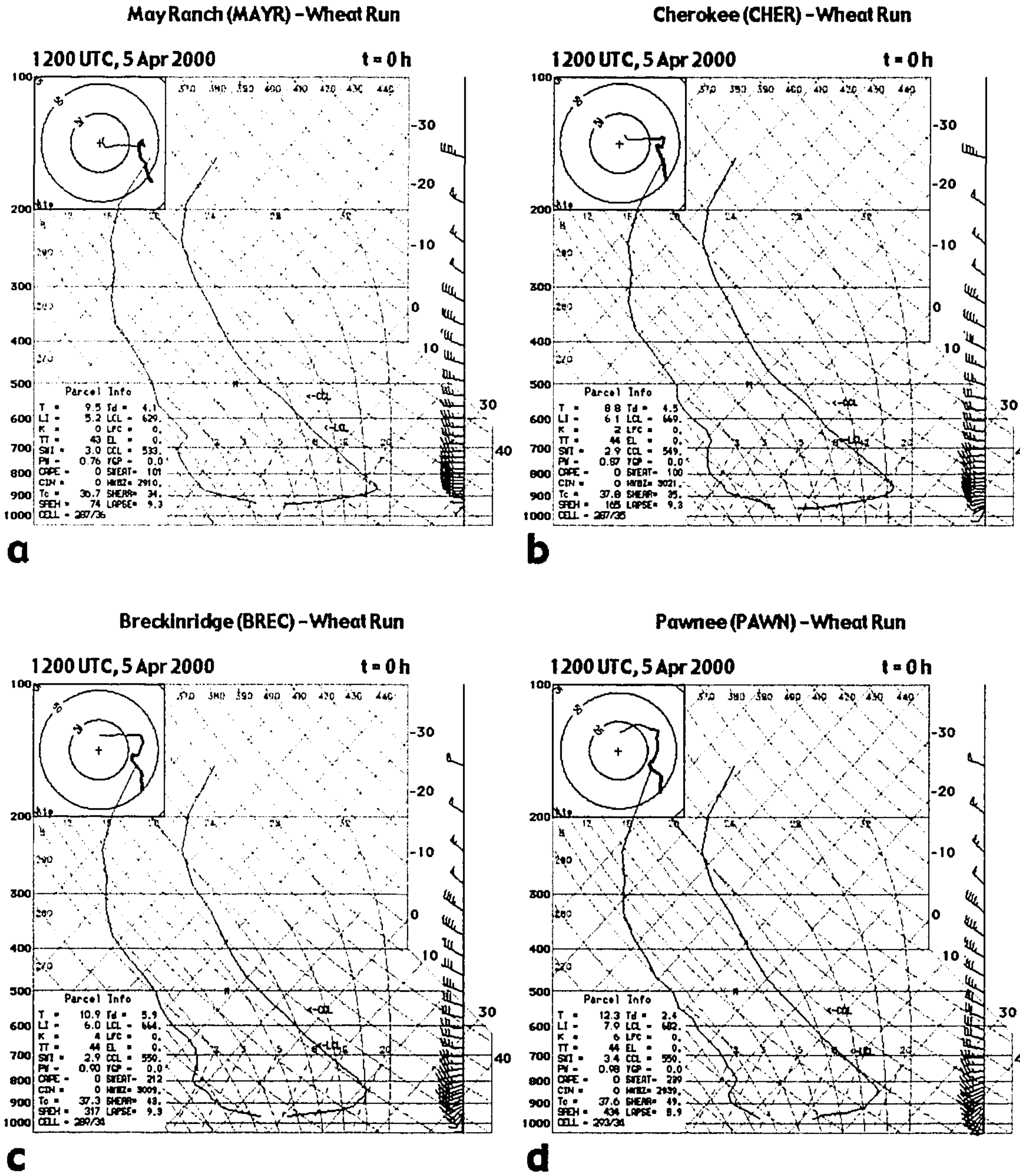


FIGURE 6.25. Initial thermodynamic profiles for simulation of 5 April at (*a*) May Ranch (MAYR), (b) Cherokee (CHER), (c) Breckinridge (BREC), and (d) Pawnee (PAWN).

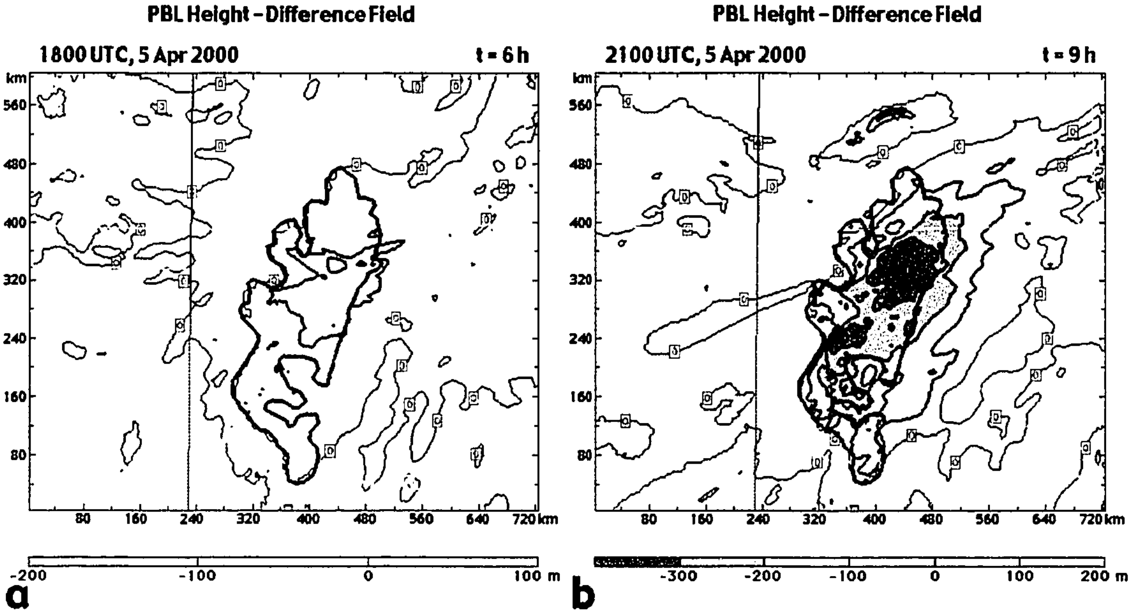


FIGURE 6.26. Difference fields of the model-calculated PBL heights at (*a*) 1800 UTC and (*b*) 2100 UTC on 5 April 2000. Negative values (in blue) indicate PBL heights were lower for the wheat run than the natural vegetation run. The black outline depicts the boundary of the winter wheat belt.

Because PBL height differences were substantially less at 2100 UTC on 5 April than on 27 March, the entrainment of air above the PBL was more uniform between the wheat and natural vegetation runs on 5 April, as demonstrated by the difference field of the circulation vectors (Fig. 6.27). Unlike 27 March, a difference circulation on the meso-β scale was not evident. In addition, differences in the horizontal wind field between the two runs were weak. Nevertheless, in the wheat run, vertical velocities on the western boundary of the wheat belt suggested that a solenoidal circulation was imposed on the background wind field (Figs. 6.27 and 6.28). For the natural vegetation run, two relative maxima of vertical velocities were apparent between 1 and 2 km above sea level on the western half of the cross section (Fig. 6.28*b*). Upward motion generally was 6 – 9 cm $s^{-1}$ within these maxima. For the wheat run, vertical velocities were stronger (in comparison to the natural vegetation run) for the western maximum (9 – 12 cm $s^{-1}$) but weaker for the eastern maximum (3 – 6 cm $s^{-1}$). These differences were accentuated in the difference field of the circulation vectors along this same cross-section (Fig. 6.27); a narrow (10 – 20 km wide) difference circulation was evident near the western boundary of the wheat belt. Thus, the simulations suggested that, at 2100 UTC on 5 April 2000, a solenoidal circulation could have been embedded within the background wind field. This result coincided with Mesonet and radar observations around this same time that indicated the possibility of a vegetation breeze (Figs. 5.25 and 5.26).

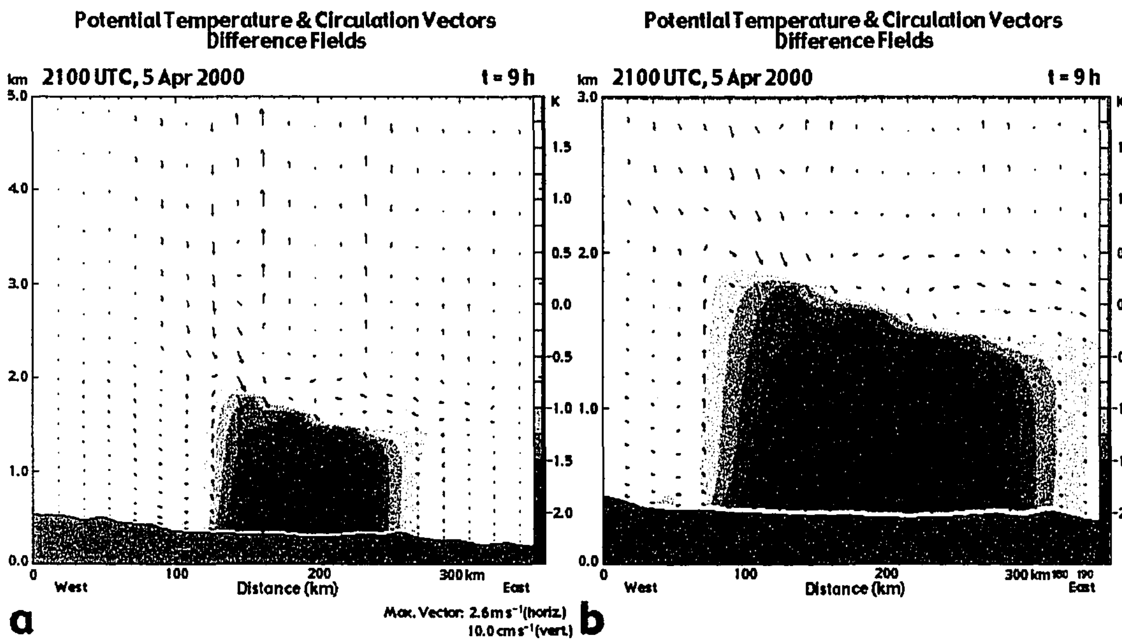


FIGURE 6.27. Vertical cross-sections of the difference fields for potential temperature (K) and circulation vector (m s$^{-1}$) at 2100 UTC on 5 April 2000. The location of the east-west cross-section for the left figure is displayed in Fig. 6.26. The right figure is identical to the left figure except that it is zoomed into the region of interest. Negative values of potential temperature difference (shaded purple) indicate locations where the wheat run was cooler than the natural vegetation run. Positive values of potential temperature difference (shaded orange) indicate locations where the wheat run was warmer than its counterpart. Vectors display the circulation difference field that resulted from velocities from the natural vegetation run subtracted from those from the wheat run.

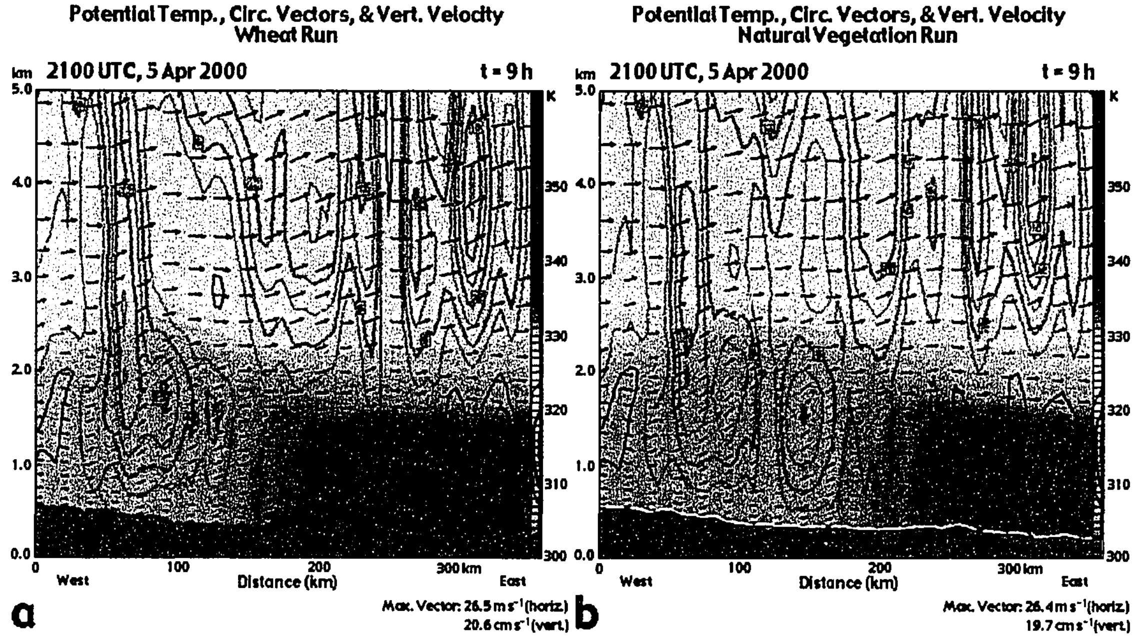


FIGURE 6.28. East-west vertical cross-sections of potential temperature (K) at 2100 UTC on 5 April 2000 for (*a*) the wheat run and (*b*) the natural vegetation run. The location of the cross-sections is shown in Fig. 6.26. Arrows represent circulation vectors parallel to the cross-section. Red contours represent positive vertical velocities (m $s^{-1}$; ascent); blue contours represent negative vertical velocities (m $s^{-1}$; descent).

## 6.5 Summer Case: 14 July 2000

In contrast to the previous two case-study days, 14 July 2000 represented a day with harvested wheat adjacent to a growing prairie (to the west) or mixed prairie and forest (to the east). Although non-wheat crops influenced the Mesonet observations across a portion of the wheat belt (predominantly in the central third and southern third), the model run did not attempt to simulate growing summer crops. As a result, the *wheat run* represented a harvested wheat belt, with sparse vegetation or bare soil (Fig. 6.1*b*), surrounded by growing grassland; the *natural vegetation run* represented natural grassland, with growing vegetation (Fig. 6.1*c*).

The thermodynamic profiles across northern Oklahoma at 1200 UTC revealed conditions typical of summer days when the atmosphere was dominated by high pressure. A nocturnal inversion between the surface and 850 hPa was evident at both CHER and PAWN (Fig. 6.29), as well as at MAYR and BREC (not shown). Winds above the inversion to about 600 hPa were light (2.5 to 10 m $s^{-1}$) and east to northeast. At CHER, winds below the inversion were westerly and less than 2.5 m $s^{-1}$; at PAWN, winds below the inversion were light and variable.

Air temperatures across Oklahoma at 1200 UTC ranged from about 18 to 24°C. No impact of the wheat belt was evident in the temperature field at model initialization (Fig 6.30). Near-surface winds across the Oklahoma Panhandle and far northwestern Oklahoma were weak and westerly or northwesterly; winds across the remainder of Oklahoma were light northerly.

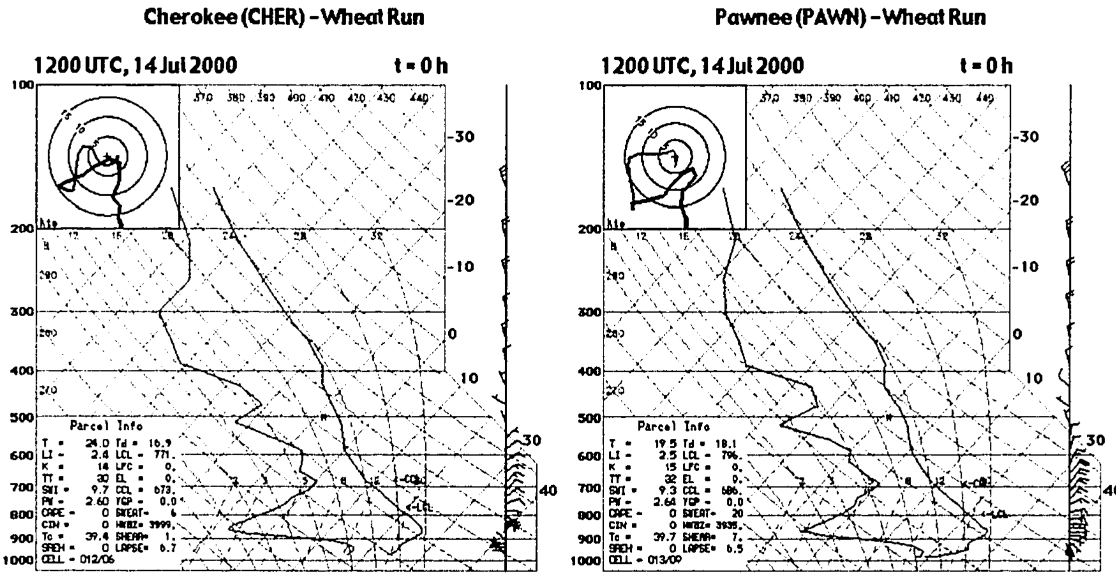


**a** **b**

FIGURE 6.29. Initial thermodynamic profiles for model simulation of 14 July 2000 above (*a*) Cherokee (CHER) and (*b*) Pawnee (PAWN).

On 14 July, Mesonet observations indicated that subsurface moisture at 5 cm was limited statewide for vegetation growth; subsurface moisture from 25 to 75 cm was adequate or limited. Despite these measurements, MM5 soil moisture values were initialized with estimated values from the Eta analysis input to demonstrate the importance of accurate soil moisture content to PBL development over the harvested wheat belt. As a result, adequate moisture was available within the model's top soil layer for direct evaporation across the northern and southern portions of the wheat belt (Fig. 6.31). Soil moisture was limited across the central half of the wheat belt; minimal moisture was available across the western half of the wheat belt in northern Oklahoma. This gradient of near-surface soil moisture in the model's initialization was shown to contribute greatly to surface temperature differences across the harvested wheat belt between the wheat and natural vegetation runs.

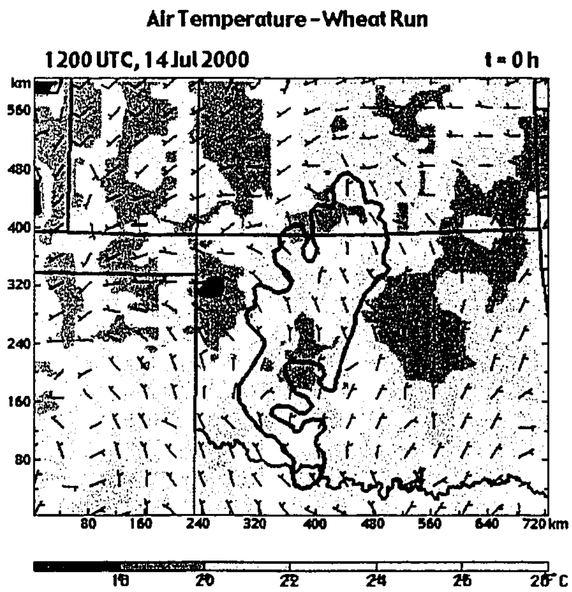


FIGURE 6.30. Initial air temperature (°C) for the wheat run at 1200 UTC on 14 July 2000. The black outline depicts the boundary of the wheat belt.

For the wheat run, values of latent and sensible heat flux at 2100 UTC (Fig. 6.32) demonstrated that more incoming energy was used for latent heating across far northern and far southern sections of the wheat belt than across the region between. Soils were more moist at the northern and southern extremities of the wheat belt, allowing energy to be directed into evaporation from the barren surface. In contrast, a relative maximum of sensible heat flux occurred over the region of the wheat belt with the driest soil. The difference fields for latent and sensible heat flux (Fig. 6.33) indicated that the amplitudes of these relative maxima of latent and sensible heat fluxes in the wheat run were decreased in the natural vegetation run. Hence, in agreement with Clark and Arritt (1995), the grassland of the natural vegetation run moderated the impact of the gradients in soil moisture.

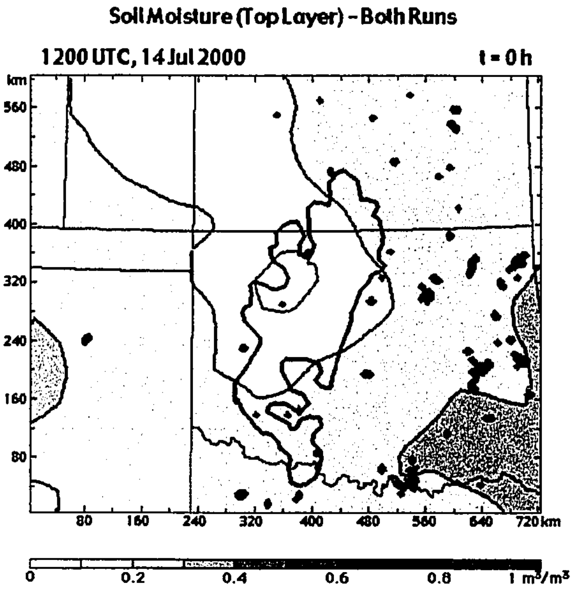


FIGURE 6.31. Initial soil moisture within the top soil layer for the wheat run on 14 July 2000. The black outline depicts the boundary of the wheat belt.

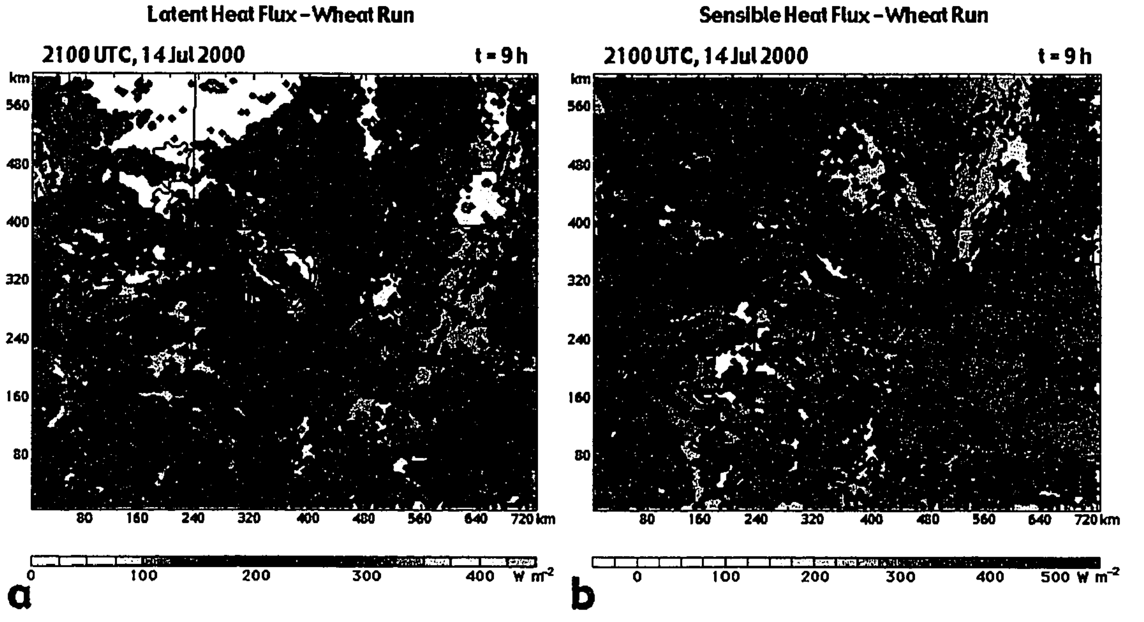


FIGURE 6.32. Fields of (*a*) latent heat flux and (*b*) sensible heat flux (W $m^{-2}$) for the wheat run at 2100 UTC on 14 July 2000. The black outline depicts the boundary of the wheat belt.

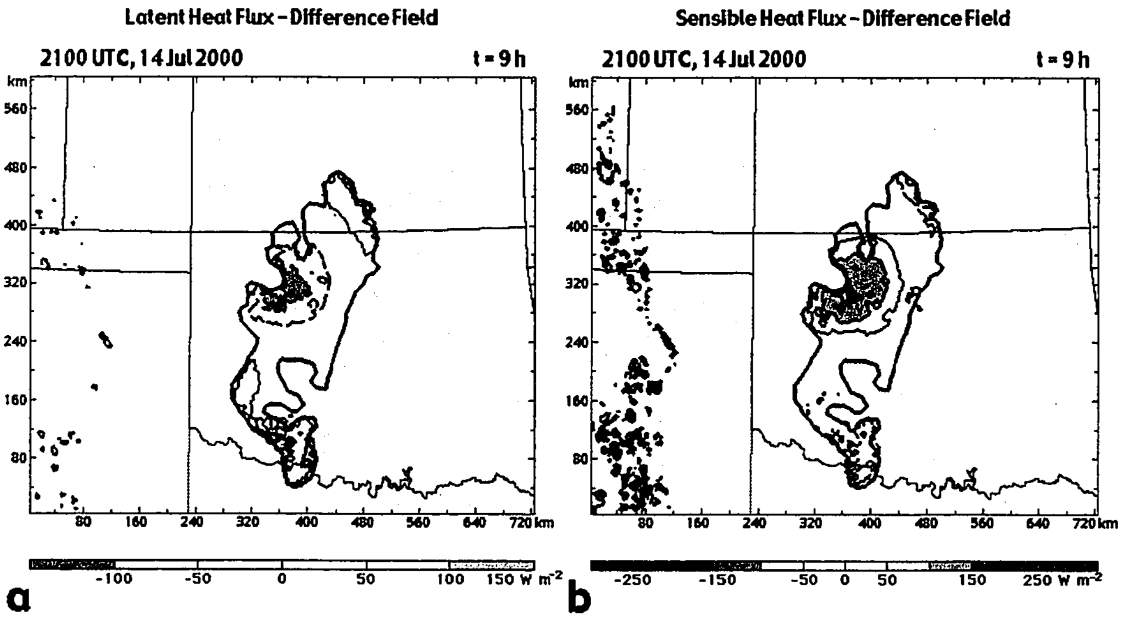


FIGURE 6.33. Difference fields of (*a*) latent heat flux and (*b*) sensible heat flux (W $m^{-2}$) between the wheat and natural vegetation runs at 2100 UTC on 14 July. The black outline depicts the boundary of the wheat belt. Negative values of heat flux difference indicate locations where heat fluxes were less for the wheat run than for the natural vegetation run. Positive values of heat flux difference indicate locations where heat fluxes were greater for the wheat run than for its counterpart.

At 2100 UTC, the warmest temperatures across the wheat belt were located over north-central Oklahoma (Fig. 6.34*a*), particularly over the area marked by the driest near-surface soil (Fig. 6.31). The difference field of air temperatures (Fig. 6.34*b*) mirrored the difference field of sensible heat flux (Fig. 6.33*b*) such that areas with increased (decreased) sensible heat flux in the wheat run (as compared to the natural vegetation run) corresponded to areas with increased (decreased) near-surface temperatures in the wheat run. As expected from these results, the depth of the PBL for the wheat run (Fig. 6.35*a*) was greater than that of the natural vegetation run above and downstream of the relative maximum in surface sensible heating (Fig. 6.33*b*). (Recall that near-surface winds (Fig. 6.8) had shifted from the north at 1200 UTC to the east or southeast at 2100 UTC.) Similarly, the PBL was shallower for the wheat run than the natural vegetation run above and downstream from the relative maxima in latent heat flux (Fig. 6.34*a*).

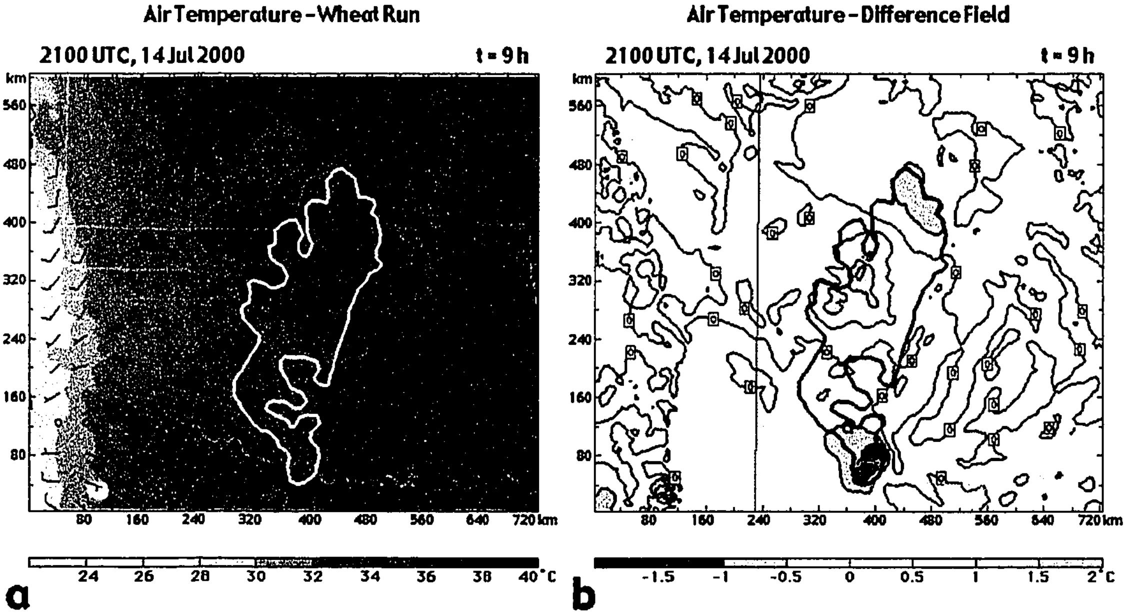


FIGURE 6.34. Air temperature fields (°C) at the lowest sigma level ($\sigma = 0.995$) for the wheat run representing 14 July 2000 at 2100 UTC (left) and the corresponding difference field between the wheat and the natural vegetation runs (right). Positive values of temperature difference (in orange) indicate locations where near-surface temperatures were warmer for the wheat run than for its counterpart. Negative values of temperature difference (in purple) indicate locations where near-surface temperatures were cooler for the wheat run than for the natural vegetation run.

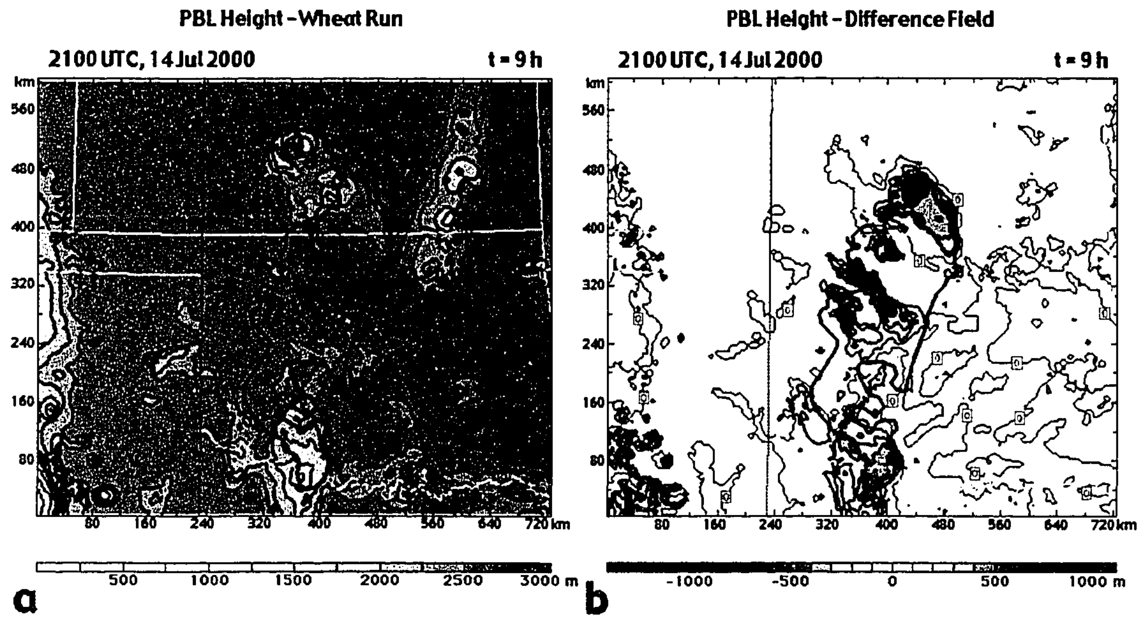


FIGURE 6.35. Model-calculated heights of the planetary boundary layer for the wheat run (left) and horizontal difference fields of PBL heights between the wheat run and the natural vegetation run (right). The fields represent 2100 UTC on 14 July 2000. Negative values (in blue) indicate that the PBL was shallower for the wheat run than the natural vegetation run. Positive values (in red) indicate that the PBL was deeper for the wheat run than the natural vegetation run. The black outline denotes the boundary of the winter wheat belt.

The case study of 14 July 2000 demonstrated that unrealistic gradients of soil moisture over sparse vegetation could cause an inadequate representation of the near-surface field of air temperature, a point of concern that should be critically important to the modeling community. In this case, the model was initialized with an Eta analysis that depicted moister soils across portions of the wheat belt than were verified by the Oklahoma Mesonet. The increased soil moisture in these regions resulted in a gradient of latent heat flux across the wheat belt that, in turn, altered the near-surface temperature field. Many previous studies have discussed the need for correct initialization of soil moisture (e.g., Crawford et al. 2001; Basara 2001). This case study provided a further accent on this requirement, particularly when land usage was included accurately as a substantial region of bare soil or sparse vegetation.

## 6.6 Overview of Numerical Model Analyses

The numerical model results generally confirmed observations for the case studies of 27 March 2000, 5 April 2000, and 14 July 2000. Moreover, the simulations provided additional insight into the physical processes involved and, in particular, into the changes that occurred throughout the depth of the planetary boundary layer. The study was strengthened by the comparisons of model runs that were initiated identically but incorporated different land uses (i.e., anthropogenically modified or natural coverage) over the defined wheat belt. The key results from the modeling study are as follows:

1. With proper adjustment of vegetation parameters, land use type, and fractional vegetation coverage, numerical simulations were able to capture the overall patterns measured near the surface across a growing wheat belt during benign springtime conditions in Oklahoma.

2. The impacts of the mesoscale belt of growing wheat included increased values of latent heat flux and decreased values of sensible heat flux over the wheat, increased values of atmospheric moisture near the surface above and downstream of the wheat, and a shallower PBL above and downstream of the wheat.

3. In the sheared environments that were examined, a shallower PBL that resulted from growing wheat (rather than natural vegetation) led to reduced entrainment of higher momentum air into the PBL and, thus, weaker winds within the PBL over and downwind from the growing wheat.

4. For the cases studied, gradients in sensible heat were insufficient to establish an unambiguous vegetation breeze or its corresponding mesoscale circulation.

5. The initialization of soil moisture within the root zone aided latent heat fluxes from growing vegetation, while the soil moisture near the surface altered sensible heat fluxes from bare soil or sparse vegetation.

# CHAPTER 7: SUMMARY AND CONCLUSION

## 7.1 Summary

During early spring, a mature winter wheat crop forms a swath about 150 km wide that extends from southwest Oklahoma into north-central Oklahoma and southern Kansas. On either side of this band is sparse or dormant vegetation, especially across extreme western Oklahoma and the Panhandle. During the late spring or early summer, after growers harvest the wheat, previously dormant grassland grows. The result is a band of short stubble and bare soil surrounded by mature prairie grasses. Thus, Oklahoma is an optimal real-world environment for examination of mesoscale vegetative impacts on the atmosphere.

The research documented in this dissertation examined the impact of Oklahoma's winter wheat belt on the mesoscale environment using a combination of observational and numerical analyses. Based on knowledge obtained from past studies, three hypotheses were set forth and examined in this study:

1. *Monthly averaged, daily averaged, and instantaneous surface temperature and moisture fields are affected by the evolution (e.g., during growth and after harvest) of Oklahoma's winter wheat crop.*

2. *The impact of Oklahoma's winter wheat belt on monthly climatic patterns is statistically significant.*

3. *Surface fluxes from Oklahoma's winter wheat belt modify the depth of the planetary boundary layer.*

The *winter wheat belt* was defined as the swath of land across Oklahoma and Kansas that was characterized by either winter wheat or a winter wheat/grassland mix as the land use type designated by the U.S. Geological Survey. Most of the land area of the current wheat belt originally was tallgrass prairie, as surveyed by Duck and Fletcher (1943) prior to the "dust bowl" years of the 1930's. They remarked that "climatic peculiarities do not characterize the Tallgrass Prairie Game Type insofar as Oklahoma is concerned." Thus, *substantial anomalies in the atmospheric measurements across this region were not expected, and results to the contrary found in this study were considered significant.*

The boundary of Oklahoma's winter wheat belt, as defined for this research, was designated using a land cover data base, aerial photographs, and Mesonet field technician reports. The primary sources of observational data were the Oklahoma Mesonet (Brock et al. 1995) and the Atmospheric Radiation Measurement (ARM) Program (Ackerman and Stokes 2003; Stokes and Schwartz 1994). The extent and maturity of the winter wheat crop was monitored with a NDVI-derived product called visual greenness, as defined by the Forest Service Intermountain Fire Sciences Lab of the U.S. Department of Agriculture (Burgan and Hartford 1993). The evolution of a typical crop year (i.e., Crop Year 2000) was overviewed to provide a basis for understanding the observational and numerical results.

Monthly means of several variables were calculated using data from all Mesonet sites and were objectively analyzed to a grid for contour maps. A statistical analysis based on the Wilcoxon signed-rank test (Wilks 1995) was conducted using data from 28 Mesonet sites to determine if anomalous monthly means were statistically significant. The following results are noteworthy from the observational study:

1. As vegetation grew across the wheat belt, maximum daily temperatures were cooler than those measured over adjacent regions of dormant grasslands. Monthly averaged values of TMAX (maximum daily air temperature) for Crop Year 2000 displayed a cool anomaly over the growing wheat from November 1999 through April 2000. Using Mesonet data from 1994 through 2001, the cooler temperatures over the wheat belt were shown to be statistically significant at the 95% confidence level for November, December, January, February, and April.

2. As green-up of grasslands occurred during May, the cool anomaly over the wheat belt disappeared. After the wheat was harvested, maximum and minimum daily temperature data revealed a warm anomaly across the wheat belt during June, July, and August. The warmer temperatures also were shown to be statistically significant for all three months.

3. Monthly averaged values of DMAX and DMIN (maximum and minimum daily dew points) indicated a slight moist bias during the early spring across the wheat belt, particularly during March. DMAX for Crop Year 2000 indicated a slight moist anomaly over the growing wheat from November 1999 through April 2000. Based upon 21,000 daily statistics over eight unique years, statistical computations indicated *less than a 0.1% chance* that the moist anomaly during March resulted from random chance.

4. During the period from 1999 to 2001, about 50 days between 15 March and 1 June showed evidence of heightened DMAX values over Oklahoma's winter wheat belt as compared to adjacent grasslands. On more than half of these days, the dew points were enhanced across only

five or six counties in north-central Oklahoma, where the winter wheat production was the highest.

5. Case studies from the spring of 2000 indicated that the presence of growing wheat impacted the maximum daily dew points and the diurnal cycles of dew point on days with both weak and moderate winds, and in both moist and dry air masses. Days with clear skies were examined so that uneven solar forcing across the state did not mask the results.

6. Examination of wind and dew point data from the Freedom Mesonet site demonstrated the impact that moisture advection from local wheat fields had on dew point measurements. On the mesoscale, moisture advection from the wheat belt enhanced both downstream dew points and the *rate* of increase of dew point during midday over lands adjacent to the wheat belt.

7. For the spring case studies, a comparison of the prior week's rainfall with values of dew point demonstrated that the growing wheat was more efficient at recirculating water back to the atmosphere than was dormant grassland in adjacent lands.

8. On two of the case study days (4 April and 5 April), evidence supported the existence of a vegetation breeze in Woods County during the afternoon.

9. During the period from 1999 to 2001, about 90 days between 1 June and 31 July revealed a distinct warm anomaly in daily maximum air temperatures over the wheat belt, particularly across north-central

Oklahoma. Case studies from the summer of 2000 indicated that the warmer temperatures over the harvested wheat resulted from local heating rather than from warm air advection.

The observational analysis demonstrated that Oklahoma's winter wheat belt had a significant impact on the near-surface temperature and moisture fields, both during the period when winter wheat was growing and during the period after harvest. The first two hypotheses of this study were as follows:

1. *Monthly averaged, daily averaged, and instantaneous surface temperature and moisture fields are affected by the evolution (e.g., during growth and after harvest) of Oklahoma's winter wheat crop.*

2. *The impact of Oklahoma's winter wheat belt on monthly climatic patterns is statistically significant.*

Based on the results of the observational analysis, neither of these hypotheses could be rejected.

Measurements of the evolution of the planetary boundary layer (PBL), however, were inadequate to examine the third hypothesis of this research without the aid of a numerical model. The National Center for Atmospheric Research (NCAR) – Pennsylvania State University (PSU) mesoscale model (MM5) was used because of its well established history, its incorporation of land surface parameterizations, and its documented ability to simulate both mesoscale phenomena and land-atmosphere interactions. MM5 is a three-dimensional, limited-area, nonhydrostatic model devised to simulate atmospheric circulations on the mesoscale and regional-scale.

The NCEP Eta model analyses were interpolated to model levels to serve as initial and boundary conditions for the mother (175 x 250 grid points; 12 km resolution) and nested (181 x 151 grid points; 4 km resolution) domains. NWS surface and upper air observations and hourly Oklahoma Mesonet data were assimilated into the model to enhance the gridded, first-guess field. MM5's version of the Eta Land-Surface Model (LSM) (Chen and Dudhia 2001a,b) from Oregon State University and NCEP was activated for all simulations. Initial soil moisture (at 10 and 200 cm) and soil temperature (at 10, 200, and 400 cm) fields from the NCEP Eta model analyses were input into the LSM.

Three case study days were selected: 27 March 2000, 5 April 2000, and 14 July 2000. For each case, two simulations were conducted: one with a simulated wheat belt (called a *wheat run*) and one with simulated natural grassland that substituted for the wheat belt (called a *natural vegetation run*). The default vegetation parameters of MM5 were deemed inadequate and were modified to obtain more representative results. In addition, the extent of the winter wheat belt across Oklahoma, southern Kansas, and north-central Texas was redefined. For the natural vegetation runs, the vegetation fraction was altered to better represent the lack of a wheat belt.

The numerical model results generally confirmed observations for the case studies of 27 March 2000, 5 April 2000, and 14 July 2000. Moreover, the simulations provided additional insight into the physical processes involved and, in particular, into the changes that occurred throughout the depth of the planetary boundary layer. The study was strengthened by the comparisons of model runs that were initiated identically but incorporated different land uses (i.e., anthropogenically modified or natural coverage) over the defined wheat belt. The key results from the numerical model study are as follows:

1. With proper adjustment of vegetation parameters, land use type, and fractional vegetation coverage, numerical simulations were able to capture the overall patterns measured near the surface across a growing wheat belt during benign springtime conditions in Oklahoma.

2. The impacts of the mesoscale belt of growing wheat included increased values of latent heat flux and decreased values of sensible heat flux over the wheat, increased values of atmospheric moisture near the surface above and downstream of the wheat, and a shallower PBL above and downstream of the wheat.

3. In the sheared environments that were examined, a shallower PBL that resulted from growing wheat (rather than natural vegetation) led to reduced entrainment of higher momentum air into the PBL and, thus, weaker winds within the PBL over and downwind from the growing wheat.

4. For the cases studied, gradients in sensible heat were insufficient to establish an evident vegetation breeze or its corresponding mesoscale circulation.

5. The initialization of soil moisture within the root zone aided latent heat fluxes from growing vegetation, while the soil moisture near the surface altered sensible heat fluxes from bare soil or sparse vegetation.

The third hypothesis for this study was as follows: *Surface fluxes from Oklahoma's winter wheat belt modify the depth of the planetary boundary layer.* Based on the results of the numerical modeling study, this hypothesis could not be rejected.

## 7.2 Conclusion

The research documented in this dissertation demonstrated that Oklahoma's winter wheat belt had a significant impact on the near-surface, mesoscale environment during growth and after harvest. Consequently, it is imperative that mesoscale forecasts, whether produced objectively or subjectively, account for the vegetation-air interactions that occur across western Oklahoma and, presumably, across other crop regions in the U.S. and around the globe.

Differences in near-surface atmospheric variables across the wheat belt and its adjacent lands were documented using the following methods: (1) observational analyses of monthly averaged daily statistics (e.g., daily maximum or minimum) during Crop Year 2000, (2) observational analyses of daily averages and instantaneous measurements for several case study days during Crop Year 2000, (3) statistical analyses of daily statistics from 1994 through 2001, and (4) numerical simulations of case study days during Crop Year 2000 that applied two different land uses over the wheat belt region for comparison. Analysis results from these different methods were consistent and established a convincing case that the crop belt modified the mesoscale climatology of Oklahoma. In addition, observational results from case studies provided evidence that, across the boundary of the wheat belt during the early spring, gradients in near-surface moisture could be as large as those expected from synoptic-scale discontinuities.

The observational portion of this study differed from previous research primarily because of the extensive, quality-assured data set that was employed. In particular, the statistical analysis used eight years of Oklahoma Mesonet data from 28 sites within or adjacent to the wheat belt. Additionally, the results of this analysis coincided with patterns detected in maps that used more than 110

Mesonet locations statewide during a single crop year. The numerical modeling portion of this study differed from previous research by exploring case study days when the environment exhibited moderate speed shear within the lowest 2 km above the surface. As a result, this research represents a substantial contribution to the fundamental understanding of vegetation-land-air interactions and provides a foundation for future research.

# BIBLIOGRAPHY


Aase, J. K., and F. H. Siddoway, 1982: Evaporative flux from wheat and fallow in semiarid climate. *Soil Sci. Amer. J.*, **46**, 619-626.

Ackerman, T. P., and G. M. Stokes, 2003: The Atmospheric Radiation Measurement Program. *Phys. Today*, 38 - 44.

Alpert, P., and M. Mandel, 1986: Wind variability – an indicator for a mesoclimate change in Israel. *J. Climate Appl. Meteor.*, **25**, 1568-1576.

André, J.-C., J.-P. Goutorbe, and A. Perrier, 1986: HAPEX-MOBILHY: A hydrological atmospheric experiment for the study of water budget and evaporation flux at the climatic scale. *Bull. Amer. Meteor. Soc.*, **67**, 138-144.

André, J.-C., J.-P. Goutorbe, A. Perrier, F. Becker, P. Bessemoulin, P. Bougeault, Y. Brunet, W. Brutsaert, T. Carlson, R. Cuenca, J. Gash, J. Gelpe, P. Hildebrand, P. Lagouarde, C. Lloyd, L. Mahrt, P. Mascart, C. Mazaudier, J. Noilhan, C. Ottlé, M. Payen, T. Phulpin, R. Stull, J. Shuttleworth, T. Schmugge, O. Taconet, C. Tarrieu, R. M. Thépenier, C. Valencogne, D. Vidal-Madjar, and A. Weill, 1988: HAPEX-MOBILHY: First results from the special observing period. *Ann. Geofis.*, **6**, 477-492.

Anthes, R. A., 1984: Enhancement of convective precipitation by mesoscale variations in vegetative covering in semiarid regions. *J. Clim. Appl. Meteor.*, **23**, 541-554.

Anthes, R. A., and T. T. Warner, 1978: Development of hydrodynamic models suitable for air pollution and other mesometeorological studies. *Mon. Wea. Rev.*, **106**, 1045-1078.

Arakawa, A., and V. R. Lamb, 1977: Computational design of the basic dynamical process of the UCLA general circulation model. *Methods in Computational Physics*, **17**, 173-265.

Arndt, D. S., 2001: The lasting effects of mesoscale convective systems over eastern Oklahoma during August 1994. M.S. thesis, School of Meteorology, University of Oklahoma, Norman, 73 pp.

Avissar, R., and F. Chen, 1993: Development and analysis of prognostic equations for mesoscale kinetic energy and mesoscale (subgrid-scale) fluxes for large-scale atmospheric models. *J. Atmos. Sci.*, **50**, 3751-3774.

Avissar, R., and R. A. Pielke, 1989: A parameterization of heterogeneous land surfaces for atmospheric numerical models and its impact on regional meteorology. *Mon. Wea. Rev.*, **117**, 2113–2136.

Barnes, S. L., 1964: A technique for maximizing details in numerical weather map analysis. *J. Appl. Meteor.*, **3**, 396-409.

Barnston, S. G., and P. T. Schickedanz, 1984: The effect of irrigation on warm season precipitation in the southern Great Plains. *J. Climate Appl. Meteor.*, **23**, 865-888.

Basara, J. B., 2001: The value of point-scale measurements of soil moisture in planetary boundary layer simulations. Ph.D. dissertation, School of Meteorology, University of Oklahoma, Norman, 225 pp.

Bechtold, P., J.-P. Pinty, and F. Mascart, 1991: A numerical investigation of the influence of large-scale winds on sea-breeze- and inland-breeze-type circulations. *J. Appl. Meteor.*, **9**, 1268–1279.

Beebe, R. C., 1974: Large scale irrigation and severe storm enhancement. *Preprints, Symp. on Atmospheric Diffusion and Air Pollution*. Santa Barbara, Amer. Meteor. Soc., 392–295.

Betts, A. K., and J. H. Ball, 1997: Albedo over the boreal forest. *J. Geophys. Res.*, **102** (D24), 28,901 - 28,909.

Betts, A. K., J. H. Ball, A. C. M. Beljaars, M. J. Miller, and P. A. Viterbo, 1996: The land surface-atmosphere interaction: A review based on observational and global modeling perspectives. *J. Geophys. Res.*, **101** (D3), 7209 - 7225.

Betts, A. K., P. Viterbo, and A. C. M. Beljaars, 1998: Comparison of the land-surface interaction in the ECMWF reanalysis model with the 1987 FIFE data. *Mon. Wea. Rev.*, **126**, 186-198.

Blyth, E. M., A. J. Dolman, and J. Noilhan, 1994: The effect of forest on mesoscale rainfall: An example from HAPEX–MOBILHY. *J. Appl. Meteor.*, **33**, 445-454.

Bonan, G. B., 2001: Observational evidence for reduction of daily maximum temperatures by croplands in the Midwest United States. *J. Climate*, **14**, 2430-2442.

Brock, F. V., K. C. Crawford, R. L. Elliott, G. W. Cuperus, S. J. Stadler, H. L. Johnson and M. D. Eilts, 1995: The Oklahoma Mesonet: a technical overview. *J. Atmos. Oceanic Tech.*, **12**, 5-19.

Brotzge, J. A., and K. C. Crawford, 2000: Estimating sensible heat flux from the Oklahoma Mesonet. *J. Appl. Meteor.*, **39**, 102-116.

Burgan, R. E., and R. A. Hartford, 1993: Monitoring vegetation greenness with satellite data. Gen. Tech. Rep. INT-297. Ogden, UT: U.S. Department of Agriculture, Forest Service, Intermountain Research Station. 13 pp.

Burman, R. D., J. L. Wright, and M. E. Jensen, 1975: Changes in climate and estimated evaporation across a large irrigated area in Idaho. *Trans. ASAE*, **18**, 1089-1093.

Carleton, A., D. Travis, D. Arnold, R. Brinegar, D. E. Jelinski, and D. R. Easterling, 1994: Climatic-scale vegetation–cloud interactions during drought using satellite data. *Int. J. Climatol.*, **14**, 593-623.

Carlson, J. D., R. E. Burgan, D. M. Engle, and J. R. Greenfield, 2002: The Oklahoma Fire Danger Model: An operational tool for mesoscale fire danger rating in Oklahoma. *Intl J. Wildland Fire*, **11**, 183-191.

Chang, J. T., and P. J. Wetzel, 1991: Effects of spatial variations of soil moisture and vegetation on the evolution of a prestorm environment: a numerical case study. *Mon. Wea. Rev.*, **119**, 1368-1390.

Changnon, S. A., 1973: Weather modification in 1972: Up or down? *Bull. Amer. Meteor. Soc.*, **54**, 642-646.

Chen, F., and R. Avissar, 1994: Impact of land-surface moisture variability on local shallow convective cumulus and precipitation in large-scale models. *J. Appl. Meteor.*, **33**, 1382-1401.

Chen, F., and J. Dudhia, 2001a: Coupling an advanced land-surface/hydrology model with the Penn State/NCAR MM5 modeling system. Part I: Model description and implementation. *Mon. Wea. Rev.*, **129**, 569–585.

Chen, F., and J. Dudhia, 2001b: Coupling an advanced land-surface/hydrology model with the Penn State/NCAR MM5 modeling system. Part II: Preliminary model validation. *Mon. Wea. Rev.*, **129**, 587–604.

Cihlar, J., P. H. Caramori, P. H. Schuepp, R. L. Desjardins, and J. I. MacPherson, 1992: Relationship between satellite-derived vegetation indices and aircraft-based $CO_2$ measurements. *J. Geophys. Res.*, **97** (D17), 18,515–18,521.

Clark, C. A., and R. W. Arritt, 1995: Numerical simulations of the effect of soil moisture and vegetation cover on the development of deep convection. *J. Appl. Meteor.*, **34**, 2029–2045.

Collins, D., and R. Avissar, 1994: An evaluation with the Fourier amplitude sensitivity test (FAST) of which land-surface parameters are of greatest importance for atmospheric modelling. *J. Climate*, **7**, 681-703.

Crawford, T. M., and H. B. Bluestein, 1996: The relationship between sensible and latent heat fluxes and the location of initial convective storm development along the dryline. *7th Conference on Mesoscale Processes;* Amer. Meteor. Soc., Reading, United Kingdom, pp. 538-541.

Crawford, T. M., D. J. Stensrud, F. Mora, J. W. Merchant, and P. J. Wetzel, 2001: Value of incorporating satellite-derived land cover data in MM5/PLACE for simulating surface temperatures. *J. Hydrometeor.*, **2**, 453-468.

Cutrim, E., D. W. Martin, and R. Rabin, 1995: Enhancement of cumulus clouds over deforested lands in Amazonia. *Bull. Amer. Meteor. Soc.*, **76**, 1801-1805.

Dai, A., A. D. Del Genio, and I. Y. Fung, 1997: Clouds, precipitation, and temperature range. *Nature*, **386**, 665-666.

Davenport, D. C., and J. P. Hudson, 1967: Meteorological observations and Penman estimates along a 17 km transect in the Sudan Gezira. *Agric. Meteor.*, **4**, 405-414.

Deering, D. W., E. M. Middleton, J. R. Irons, B. L. Blad, E. A. Walter-Shea, C. J. Hays, C. Walthall, T. F. Eck, S. P. Ahmad, and B. P. Banerjee, 1992: Prairie grassland bidirectional reflectances measured by different instruments at the FIFE site. *J. Geophys. Res.*, **97** (D17), 18,887–18,903.

De Vries, D. A., and J. W. Birch, 1961: The modification of climate near the ground by irrigation for pastures on the Riverine Plain. *Aust. J. Agric. Res.*, **12**, 260-272.

Dirmeyer, P. A., 1994: Vegetation stress as a feedback mechanism in midlatitude drought. *J. Climate*, **7**, 1463-1483.

Doran, J. C. , J. M. Hubbe, R. R. Kirkham, W. J. Shaw, C. D. Whiteman, F. J. Barnes, D. Cooper, W. Porch, R. L. Coutler, D. R. Cook, R. L. Hart, W. Gao, T. J. Martin, J. D. Shannon, T. L. Crawford, D. D. Baldocchi, R. J. Dobosy, T. P. Meyers, L. Balick, W. A. Dugas, R. Hicks, L. Fritschen, L. Hipps, E. Swiatek, and K. E. Kunkel, 1992: The Boardman Regional Flux Experiment. *Bull. Amer. Meteor. Soc.*, **73**, 1785–1796.

Doran, J. C., W. J. Shaw, and J. M. Hubbe, 1995: Boundary layer characteristics over areas of inhomogeneous surface fluxes. *J. Appl. Meteor.*, **34**, 559-571.

Duck, J. G., and J. B. Fletcher, 1943: A survey of the game and furbearing animals of Oklahoma. Oklahoma Game and Fish Commission, Division of Wildlife Restoration and Research, Oklahoma City. Retrieved in digital format from http://www.biosurvey.ou.edu/duckflt/dfhome.html.

Durre, I., and J. M. Wallace, 2001: The warm season dip in diurnal temperature range over the eastern United States. *J. Climate*, **14**, 354-360.

Dzerdzeevskii, B. L., 1963: Meteorological parameters of the surface air layer over humid and dry sectors of the Trans-Volga Steppe. *Sukhoveis and Drought Control*, B. L. Dzerdzeevskii, Ed., Israel Program for Scientific Translations, Jerusalem, 162-180.

Easterling, D. R., T. R. Karl, E. H. Mason, P. Y. Hughes, and D. P. Bowman, 1996: United States Historical Climatology Network (U.S. HCN) monthly temperature and precipitation data. Oak Ridge National Laboratory ORNL/CDIAC-87, NDP-019/R3, Carbon Dioxide Information Analysis Center, 280 pp.

Eaton, A. K., W. R. Rouse, P. M. Lafleur, P. Marsh, and P. D. Blanken, 2001: Surface energy balance of the western and central Canadian subarctic: Variations in the energy balance among five major terrain types. *J. Climate*, **14**, 3692-3703.

Emanuel, K., D. Raymond, A. K. Betts, L. Bosart, C. Bretherton, K. Droegemeier, B. Farrell, J. M. Fritsch, R. Houze, M. LeMone, D. Lilly, R. Rotunno, M. Shapiro, R. Smith, and A. Thorpe, 1995: Report of the first prospectus development team of the U.S. Weather Research Program to NOAA and the NSF. *Bull. Amer. Meteor. Soc.*, **76**, 1194-1208.

Fiebrich, C. A., and K. C. Crawford, 2001: The impact of unique meteorological phenomena detected by the Oklahoma Mesonet and ARS Micronet on automated quality control. *Bull. Amer. Meteor. Soc.*, **82**, 2173-2187.

Fitzjarrald, D. R., O. C. Acevedo, and K. E. Moore, 2001: Climatic consequences of leaf presence in the eastern United States. *J. Clim.*, **14**, 598–614.

Freedman, J. M., D. R. Fitzjarrald, K. E. Moore, and R. K. Sakai, 2001: Boundary layer clouds and vegetation–atmosphere feedbacks. *J. Clim.*, **14**, 180-197.

Fowler, D. B., 1993: Winter Wheat Production Manual. Crop Development Centre, University of Saskatchewan, Saskatoon, Canada. Retrieved from http://www.usask.ca/agriculture/plantsci/winter_wheat/contents.htm.

Fowler, W. B., and J. D. Helvey, 1974: Effect of large-scale irrigation on climate in the Columbia Basin. *Science*, **84**, 121-127.

Garrett, A. J., 1982: A parameter study of interactions between convective clouds, the convective boundary layer, and forested surface. *Mon. Wea. Rev.*, **110**, 1041-1059.

Grell, G. A., J. Dudhia, and D. R. Stauffer, 1994: A description of the fifth-generation Penn State/ NCAR mesoscale model (MM5). *NCAR Technical Note*, NCAR/TN-398+STR, 117 pp.

Heim, J. E., 1993: Surface properties and their effect on deep cumulus convection over uniform terrain. M.S. Thesis, Department of Physics and Astronomy, University of Kansas, Lawrence, 95 pp.

Henderson, T. J., and S. A. Changnon, 1972: Results from an application program of hail suppression in Texas. *Preprints, 3rd Conf. on Weather Modification*, Rapid City, Amer. Meteor. Soc., 260–267.

Hong, S.-Y., and H.-L. Pan, 1996: Nonlocal boundary layer vertical diffusion in a medium-range forecast model. *Mon. Wea. Rev.*, **124**, 2322-2339.

Hong, X., M. J. Leach, and S. Raman, 1995: A sensitivity study of convective cloud formation by vegetation forcing with different atmospheric conditions. *J. Appl. Meteor.*, **34**, 2008–2028.

Huang, C. Y., 1990: A mesoscale planetary boundary layer model for simulations of topographically induced circulations. Ph. D. Dissertation. North Carolina State University, Raleigh, 253 pp.

Huang, C. Y., and S. Raman, 1991a: Numerical simulation of January 28 cold air outbreak during GALE. Part I: The model and sensitivity tests of turbulence closures. *Bound.-Layer Meteor.*, **55**, 381-407.

Huang, C. Y., and S. Raman, 1991b: Numerical simulation of January 28 cold air outbreak during GALE. Part II: The mesoscale circulation and marine boundary layer. *Bound.-Layer Meteor.*, **56**, 51-81.

Jacquemin, B., and J. Noilhan, 1990: Sensitivity study and validation of a land surface parameterization using the HAPEX-MOBILHY data set. *Bound.-Layer Meteor.*, **52**, 93–134.

Jarvis, P. G., R. S. Miranda, and R. I Meutzelfeldt, 1985: Modeling canopy exchanges of water vapor and carbon dioxide in coniferous forest plantations. *The Forest–Atmosphere Interaction*, B. A. Hutchison and B. B. Hicks, Eds. Reidel, 521-542.

Johnson, H. J., and C. E. Duchon, 1995: Atlas of Oklahoma climate. University of Oklahoma, Oklahoma Climatological Survey, Norman, OK, 32 pp.

Joos, A., 1969: Recent rainfall patterns in the Great Plains. Informal publication at AMS Symposium, Madison, WI, October 21, 1969.

Lakhtakia, M. N., and T. T. Warner, 1994: A comparison of simple and complex treatments of surface hydrology and thermodynamics suitable for mesoscale atmospheric models. *Mon. Wea. Rev.*, **122**, 880–896.

Lanicci, J. M., T. N. Carlson, and T. T. Warner, 1987: Sensitivity of the Great Plains severe-storm environment to soil-moisture distribution. *Mon. Wea. Rev.*, **115**, 2660–2673.

Lee, S. T., and F. Kimura, 2001: Comparative studies in the local circulations induced by land-use and by topography. *Bound.-Layer Meteor.*, **101**, 157-182.

Lee, T. J., 1992: The impact of vegetation on the atmospheric boundary layer and convective storms. Ph. D. Dissertation, Colorado State University, Fort Collins, CO, 137 pp.

LeMone, M. A., R. L. Grossman, R. L. Coulter, M. L. Wesley, G. E. Klazura, G. S. Poulos, W. Blumen, J. K. Lundquist, R. H. Cuenca, S. F. Kelly, E. A. Brandes, S. P. Oncley, R. T. McMillen, B. B. Hicks, 2000: Land–atmosphere interaction research, early results, and opportunities in the Walnut River Watershed in Southeast Kansas: CASES and ABLE. *Bull. Amer. Meteor. Soc.*, **81**, 757–780.

Lilly, D. K., 1968: Models of cloud-topped mixed layers under a strong inversion. *Quart. J. Roy. Meteor. Soc.*, **94**, 292-309.

Loveland, T. R., Z. Zhu, D. O. Ohlen, J. F. Brown, B. C. Reed, and L. Yang, 1999: An analysis of the IGBP global land-cover characterization process. *Photogrammetric Engineering and Remote Sensing*, **65**, 1021-1032.

Lu, L., R. A. Pielke, G. E. Liston, W. J. Parton, D. Ojima, and M. Hartman, 2001: Implementation of a two-way interactive atmospheric and ecological model and its application to the central United States. *J. Climate*, **14**, 900-919.

Lynn, B. H., D. Rind, and R. Avissar, 1995: The importance of mesoscale circulations generated by subgrid-scale landscape-heterogeneities in general circulation models. *J. Climate*, **8**, 191–205.

Lynn, B. H., W.-K. Tao, and P. J. Wetzel, 1998: A study of landscape-generated deep moist convection. *Mon. Wea. Rev.*, **126**, 928-942.

Mahfouf, J.-F., E. Richard, and P. Mascart, 1987: The influence of soil and vegetation on the development of mesoscale circulations. *J. Clim. Appl. Meteor.*, **26**, 1483-1495.

Mahrt, L., and M. Ek, 1984: The influence of atmospheric stability on potential evaporation. *J. Climate Appl. Meteor.*, **23**, 222–234.

Mahrt, L., and H. L. Pan, 1984: A two-layer model of soil hydrology. *Bound.-Layer Meteor.*, **29**, 1–20.

Mahrt, L., J. S. Sun, D. Vickers, J. I. MacPherson, J. R. Pederson, and R. L. Desjardins, 1994: Observations of fluxes and inland breezes over a heterogeneous surface. *J. Atmos. Sci.*, **51**, 2484–2499.

Markowski, P. M., and D. J. Stensrud, 1998: Mean monthly diurnal cycles observed with PRE-STORM surface data. *J. Climate*, **11**, 2995-3009.

Matthews, E., and W. B. Rossow, 1987: Regional and seasonal variations of surface reflectance from satellite observations at 0.6μm. *J. Clim. Appl. Meteor.*, **26**, 170–202.

McCumber, M. C., 1980: A numerical simulation of the influence of heat and moisture fluxes upon mesoscale circulations. Ph.D. Dissertation, Department of Environmental Science, University of Virginia, Charlottesville, 255 pp.

Mintz, Y., 1984: The sensitivity of numerically simulated climates to land-surface boundary conditions. *The Global Climate*, J. T. Houghton, Ed., Cambridge University Press, 79-105.

Moore, K. E., D. R. Fitzjarrald, R. K. Sakai, M. L. Goulden, J. W. Munger, and S. C. Wofsy, 1996: Seasonal variation in radiative and turbulent exchange at a deciduous forest in Central Massachusetts. *J. Appl. Meteor.*, **35**, 122–134.

Moore, N., and S. Rojstaczer, 2001: Irrigation-induced rainfall and the Great Plains. *J. Appl. Meteor.*, **40**, 1297-1309.

Musick, J. T., and K. B. Porter, 1990: Chapter 20: Wheat. *Irrigation of Agricultural Lands*. Agronomy Monograph #30. B. A. Stewart and D. R. Nielsen, Eds. Amer. Soc. of Agronomy, Crop Science Soc. of Amer., and Soil Science Soc. of Amer.

Nagai, H., 2002: Validation and sensitivity analysis of a new atmosphere – soil – vegetation model. *J. Appl. Meteor.*, **41**, 160-176.

National Climatic Data Center (NCDC), cited 1999: Summary of the day – First Order: TD-3210 online data format documentation. [Available online at ftp.ncdc.noaa.gov.]

National Oceanic and Atmospheric Administration (NOAA), 1977: Reprint of the June 1968 "Climatic Atlas of the United States". U.S. Department of Commerce, Environmental Science Services Administration, Environmental Data Service.

National Research Council, 1998: The Atmospheric Sciences Entering the Twenty-First Century. Board on Atmospheric Sciences and Climate, Commission on Geosciences, Environment, and Resources, National Academy Press, Washington, D.C., 384 pp.

NCEP, 2000: GCIP NCEP Eta model output. National Centers for Environmental Prediction. [Available online at http://dss.ucar.edu/datasets/ds609.2/.]

Nickerson, E. C., E. Richard, R. Rosset, and D. R. Smith, 1986: The numerical simulation of clouds, rain, and airflow over the Vosges and Black Forest mountains: A meso-β model with parameterized microphysics. *Mon. Wea. Rev.*, **114**, 398-414.

Noilhan, J., and S. Planton, 1989: A simple parameterization of land surface processes for meteorological models. *Mon. Wea. Rev.*, **117**, 536–549.

Oklahoma Agricultural Statistics Service, 1999a: Oklahoma Wheat County Estimates for Crop Year 1995. http://www.nass.usda.gov/ok/wheat95.htm, Okla. Dept. of Agriculture, reissued July, 1999.

Oklahoma Agricultural Statistics Service, 1999b: Oklahoma Wheat County Estimates for Crop Year 1996. http://www.nass.usda.gov/ok/wheat96.htm, Okla. Dept. of Agriculture, reissued July, 1999.

Oklahoma Agricultural Statistics Service, 1999c: Oklahoma Wheat County Estimates for Crop Year 1997. http://www.nass.usda.gov/ok/wheat97.htm, Okla. Dept. of Agriculture, reissued February 16, 1999.

Oklahoma Agricultural Statistics Service, 1999d: Oklahoma Wheat County Estimates for Crop Year 1998. http://www.nass.usda.gov/ok/wheat98.htm, Okla. Dept. of Agriculture, February 16, 1999.

Oklahoma Agricultural Statistics Service, 1999e: Oklahoma Wheat County Estimates for Crop Year 1999. http://www.nass.usda.gov/ok/wheat99.htm, Okla. Dept. of Agriculture, November 29, 1999.

Oklahoma Agricultural Statistics Service, 2001: Oklahoma Wheat County Estimates for Crop Year 2000. http://www.nass.usda.gov/ok/wheat00.htm, Okla. Dept. of Agriculture, reissued November, 2001.

Oklahoma Agricultural Statistics Service, 2002: Oklahoma Wheat County Estimates for Crop Year 2001. http://www.nass.usda.gov/ok/wheat01.htm, Okla. Dept. of Agriculture, reissued February, 2002.

Ookouchi, Y., M. Segal, R. C. Kessler, and R. A. Pielke, 1984: Evaluation of soil moisture effects on generation and modification of mesoscale circulations. *Mon. Wea. Rev.*, **11**, 2281-2292.

Orlanski, I., 1975: Rational subdivision of scales for atmospheric processes. *Bull. Amer. Meteor. Soc.*, **56**, 527-530.

Otterman, J., 1976: Reply. *Science*, **194**, 748-749.

Otterman, J., 1981: Satellite and field studies of man's impact on the surface in arid regions. *Tellus*, **33**, 68-77.

Pan, H.-L., and L. Mahrt, 1987: Interaction between soil hydrology and boundary-layer development. *Bound.-Layer Meteor.*, **38**, 185–202.

Paulsen, G. M., 2000: International contributions to improvement and marketing of Kansas wheat. Kansas Agricultural Extension Station, Kansas State University, 6 pp. Retrieved from http://www.kswheat.com/education/facts/history.htm.

Pielke, R. A., 1984: *Mesoscale Meteorological Modeling.* Academic Press, 612 pp.

Pielke, R. A., G. A. Dalu, J. S. Snook, T. J. Lee, and T. G. F Kittel, 1991: Nonlinear influence of mesoscale land use on weather and climate. *J. Climate*, **4**, 1053-1069.

Pinty, J.-P., P. Mascart, E. Richard, and R. Rosset, 1989: An investigation of mesoscale flows induced by vegetation inhomogeneities using an evapotranspiration model calibrated against HAPEX-MOBILHY data. *J. Appl. Meteor.*, **28**, 976-992.

Pleim, J. E., and A. Xiu, 1995: Development and testing of a surface flux and planetary boundary layer model for application in mesoscale models. *J. Appl. Meteor.*, **34**, 16-32.

Pugh, B. R., 1999: A study of springtime convection and hail using the WSR-88D at Twin Lakes, Oklahoma. M.S. thesis, School of Meteorology, University of Oklahoma, Norman, 70 pp.

Purdom, J. F. W., and J. J. Gurka, 1974: The effect of early morning cloud on afternoon thunderstorm development. *Preprints, 5th Conf. on Wea. Anal. and Forecasting*, St. Louis, Amer. Meteor. Soc., 58-60.

Rabin, R. M., 1977: The surface energy budget of a summer convective period. M. S. Thesis, McGill University, Montreal, Canada, 125 pp.

Rabin, R. M., S. Stadler, P. J. Wetzel, D. J. Stensrud, and M. Gregory, 1990: Observed effects of landscape variability on convective clouds. *Bull. Amer. Meteor. Soc.*, **71**, 272–280.

Reddy, S. J., 1983: A simple method of estimating the soil water balance. *Agric. Meteor.*, **28** 1-17.

Rind, D., 1982: The influence of ground moisture conditions in North America on summer climate as modeled in the GISS GCM. *Mon. Wea. Rev.*, **110**, 1487-1494.

Rogerson, T. L., 1976: Soil water deficits under forested and cleared areas in northern Arkansas. *Soil Sci. Soc. Amer. J.*, **40**, 802-805.

Rosenan, N., 1963: Changes of climate. *Proc. Rome Symp.*, UNESCO, WMO, 67-73.

Schadler, G., 1990: Triggering of atmospheric circulations by moisture inhomogeneities of the earth's surface. *Bound.-Layer Meteor.*, **51**, 1-30.

Schickedanz, P. T., 1976: The effect of irrigation on precipitation in the Great Plains. NSF-RANN, Grant GI-43871, Final Rep., Atmospheric Sciences Section, Illinois State Water Survey, Urbanna, IL, 105 pp.

Schmidt, J. M., and W. R. Cotton, 1990: Interactions between upper and lower tropospheric gravity waves on squall line structure and maintenance. *J. Atmos. Sci.*, **47**, 1205-1222.

Schultz, J.-P., L. Dümenil, J. Polcher, C. A. Schlosser, and Y. Xue, 1998: Land surface energy and moisture fluxes: comparing three models. *J. Appl. Meteor.*, **37**, 288-307.

Schwartz, M. D., 1992: Phenology and springtime surface-layer change. *Mon. Wea. Rev.*, **120**, 2570-2578.

Segal, M., and R. W. Arritt, 1992: Nonclassical mesoscale circulations caused by surface sensible heat-flux gradients. *Bull. Amer. Meteor. Soc.*, **73**, 1593-1604.

Segal, M., R. W. Arritt, and C. Clark, 1995: Scaling evaluation of the effect of surface characteristics on potential for deep convection over uniform terrain. *Mon. Wea. Rev.*, **123**, 383-400.

Segal, M., R. Avissar, M. C. McCumber, R. A. Pielke, 1988: Evaluation of vegetation effects on the generation and modification of mesoscale circulations. *J. Atmos. Sci.*, **45**, 2268–2292.

Segal, M., W. E. Schreiber, G. Kallos, J. R. Garratt, A. Rodi, J. Weaver, and R. A. Pielke, 1989: The impact of crop areas in northeast Colorado on midsummer mesoscale thermal circulations. *Mon. Wea. Rev.*, **117**, 809-825.

Sellers, P. J., Y. Mintz, Y. C. Sud, and A. Dalcher, 1986: Simple biosphere model (SiB) for use within general circulation models. *J. Atmos. Sci.*, **43**, 505-531.

Shafer, M. A., C. A. Fiebrich, D. Arndt, S. E. Fredrickson, and T. W. Hughes, 2000: Quality assurance procedures in the Oklahoma Mesonetwork. *J. Atmos. Ocean. Tech.*, **17**, 474–494.

Shaw, W. J., and J. C. Doran, 2001: Observations of systematic boundary layer divergence patterns and their relationship to land use and topography. *J. Clim.*, **14**, 1753-1764.

Smith, E. A., M. M.-K. Wai, H. J. Cooper, and M. T. Rubes, 1994: Linking boundary-layer circulations and surface processes during FIFE 89. Part I: observational analysis. *J. Atmos. Sci.*, **51**, 1497-1529.

Stidd, C. K., 1967: Local moisture and precipitation. Preprint Series No. 45, Desert Research Institute, University of Nevada, Reno, NV, 34 pp.

Stokes, G. M., and S. E. Schwartz, 1994: The Atmospheric Radiation Measurement (ARM) Program: Programmatic background and design of the Cloud and Radiation Testbed. *Bull. Amer. Meteor. Soc.*, **75**, 1201-1221.

Sud, Y. C., D. M. Mocko, and G. K. Walker, 2001: Influence of land surface fluxes on precipitation: Inferences from simulations forced with four ARM-CART SCM datasets. *J. Climate*, **14**, 3666-3691.

Sun, W. Y., and Y. Ogura, 1979: Boundary-layer forcing as a possible trigger to a squall-line formation. *J. Atmos. Sci.*, **36**, 235–254.

Taylor, C. M., and T. Lebel, 1998: Observational evidence of persistent convective-scale rainfall patterns. *Mon. Wea. Rev.*, **126**, 1597-1607.

Tennekes, H., 1973: A model for the dynamics of the inversion above a convective boundary layer. *J. Atmos. Sci.*, **30**, 558-567.

Tremback, C. J., G. Tripoli, R. W. Arritt, W. R. Cotton, and R. A. Pielke, 1986: The regional atmospheric modeling system. *Envirosoft 86 Conf., Proc. of the Int. Conf. on Development and Application of Computer Techniques to Environmental Studies*, Los Angeles, 601-608.

Trenberth, K. E., 1999: Atmospheric moisture recycling: Role of advection and local evaporation. *J. Climate*, **12**, 1368-1381.

Trenberth, K. E., and C. J. Guillemot, 1996: Physical processes involved in the 1988 drought and 1993 floods in North America. *J. Climate*, **9**, 1288-1298.

Tsvetsinskaya, E. A., L. O. Mearns, and W. E. Easterling, 2001: Investigating the effect of seasonal plant growth and development in three-dimensional atmospheric simulations. Part II: Atmospheric response to crop growth and development. *J. Climate*, **14**, 711-729.

Tucker, C. J., 1979: Red and photographic infrared linear combinations for monitoring vegetation. *Remote Sens. Environ.*, **8**, 127-150.

Turner, C. L., T. R. Seastedt, M. I. Dyer, T. G. F. Kittel, and D. S. Schimel, 1992: Effects of management and topography on the radiometric response of a tallgrass prairie, *J. Geophys. Res.*, **97** (D17), 18,855 - 18,866.

Voronstov, P. A., 1963: Local air circulations in regions with ameliorated climate. *Sukhoveis and Drought Control*, B. L. Dzerdzeevskii, Ed., Israel Program for Scientific Translations, Jerusalem, 287-294.

Wai, M. M.-K., and E. A. Smith, 1998: Linking boundary layer circulations and surface processes during FIFE 89. Part II: maintenance of secondary circulations.

Walter-Shea, E. A., B. L. Blad, C. J. Hays, M. A. Mesarch, D. W. Deering, and E. M. Middleton, 1992: Biophysical properties affecting vegetative canopy reflectance and absorbed photosynthetically active radiation at the FIFE site. *J. Geophys. Res.*, **97** (D17), 18,925 - 18,934.

Walthall, C. L., and E. M. Middleton, 1992: Assessing spatial and seasonal variations in grasslands with spectral reflectances from a helicopter platform. *J. Geophys. Res.*, **97** (D17), 18,905 - 18,912.

Wetzel, P. J., and R. H. Woodward, 1987: Soil moisture estimation using GOES-VISSR infrared data: A case study with simple statistical method. *J. Climate Appl. Meteor.*, **26**, 107-117.

Wilks, D. S., 1995: *Statistical Methods in the Atmospheric Sciences.* Academic Press, 467 pp.

Willis, G. E., and J. W. Deardorff, 1974: A laboratory model of the unstable planetary boundary layer. *J. Atmos. Sci.*, **31**, 1297-1307.

Woodcock, D. W., 1992: The rain on the plain: Are there vegetation–climate feedbacks? *Global Planet. Change*, **5**, 191-202.

Xue, Y., M. J. Fennessy, and P. J. Sellers, 1996: Impact of vegetation properties on U.S. summer weather prediction. *J. Geophys. Res.*, **101**, 7419-7430.

Xue, Y., P. J. Sellers, J. L. Kinter, and J. Shukla, 1991: A simplified biosphere model for global climate studies. *J. Climate*, **4**, 345-364.

Yates, D. N., F. Chen, M. A. LeMone, R. Qualls, S. P. Oncley, R. L. Grossman, and E. A. Brandes, 2001: A Cooperative Atmosphere-Surface Exchange Study (CASES) dataset for analyzing and parameterizing the effects of land surface heterogeneity on area-averaged surface heat fluxes. *J. Appl. Meteor.*, **40**, 921-937.

Yi, C., K. J. Davis, B. W. Berger, and P. S. Bakwin, 2001: Long-term observations of the dynamics of the continental planetary boundary layer. *J. Atmos. Sci.*, **58**, 1288-1299.

Zhang, D., and R. A. Anthes, 1982: A high-resolution model of the planetary boundary layer – sensitivity tests and comparisons with SESAME-79 data. *J. Appl. Meteor.*, **21**, 1594-1609.